Structural and Functional Studies on the Role of Noc3p for Large Ribosomal Subunit Maturation in *Saccharomyces cerevisiae*

DISSERTATION

ZUR ERLANGUNG DES

DOKTORGRADES DER NATURWISSENSCHAFTEN (DR. RER. NAT.)

DER FAKULTÄT FÜR BIOLOGIE UND VORKLINISCHE MEDIZIN

DER UNIVERSITÄT REGENSBURG

vorgelegt von

Fabian Teubl

aus Wörth an der Donau

Im August 2020

Das Promotionsgesuch wurde eingereicht am:

06. August 2020

Die Arbeit wurde angeleitet von:

Prof. Dr. Joachim Griesenbeck

Unterschrift:

_____

Fabian Teubl

Contents

1 Summary

Ribosomes are macromolecular ribonucleoprotein (RNP) particles that catalyze the translation of mRNA into proteins in all living cells in all kingdoms of life. The ongoing production of ribosomes ensures the availability of a sufficient amount of proteins, which are required for various cellular processes. Ribosome biogenesis represents a highly energy consuming and complex process. Starting in the nucleolus, RNA polymerase I and III transcribe the ribosomal RNA (rRNA) encoding genes to generate precursor rRNAs, which undergo a series of processing, folding, modifying and assembly events in the course of maturation. In the yeast *Saccharomyces cerevisiae*, 79 ribosomal proteins (RPs), four rRNAs, several snoRNAs and more than 150 transiently acting biogenesis factors operate in a concerted and highly dynamic network to generate the mature ribosomal subunits.

During the past decades, a lot of effort has been made to elucidate and further understand the synthesis of ribosomes as paradigm of RNP biogenesis. Extensive research on this field has produced detailed characterization of ribosome biogenesis factors like the maturation step for which they are crucial for or the molecular function they exert. Nevertheless, the role of many factors remains further and requires extensive further investigation.

The “Noc-proteins” belong to the broad group of biogenesis factors, which have been identified essential for large ribosomal subunit (LSU) maturation (Noc1p/2p/3p). Accompanying studies have indicated the existence of the dimeric complexes Noc1p/Noc2p and Noc2p/Noc3p, which possibly associate with early and intermediate LSU precursor particles, respectively.

In this study, focus was laid on the role of Noc3p. Single molecule cryo-EM revealed the association of Noc3p with subsets of different pre-ribosomal populations of intermediate maturation states. Thereby, a time interval for the association of Noc3p with pre-LSU particles could be deduced within a series of nuclear maturation steps. Simultaneously, first structural characterization could be obtained for the position of Noc2p, the Noc3p binding partner.

Furthermore, the basis of the time window, in which association of Noc3p with pre-ribosomes has been observed and the prerequisites for its recruitment and release to and off pre-LSUs has been explored. The results revealed that both recruitment and release of Noc3p depends on the pre-ribosomal assembly state. The varying impact of the single ribosomal proteins (r-proteins) has been discussed in regard to their known binding sites in LSU particles.

Applying a versatile tethered tertiary structure probing approach allowed investigation of possible structural alterations that impact or postpone the timely related release of Noc3p. Indeed, an impeded release could be backtracked to an altered conformational state of pre-LSU domain III upon knock-down of particular r-proteins.

Finally, structure-based mutagenesis of Noc3p helped to reveal sites within the protein that are essential for the formation of the heterodimer with Noc2p as well as for the association with the pre-LSU.

Further studies will be necessary to figure out the binding mode of Noc3p to pre-ribosomes and to which extent it might as well rely on the presence of Noc2p. For this, structural information on Noc2p as whole would greatly help to further address this issue. Altogether, the results presented in this work allow to hypothesize towards a role of Noc3p as sensor for LSU biogenesis and provide a solid base for further investigation.

2 Zusammenfassung

Ribosomen sind makromolekulare Ribonukleoprotein- (RNP) Partikel, die in allen lebenden Zellen und in allen Bereichen des Lebens vorkommen. Sie katalysieren die Translation von mRNA zu Proteinen. Die kontinuierliche Produktion von Ribosomen stellt letztlich die Verfügbarkeit von Proteinen in ausreichend hohen Mengen für verschiedene zelluläre Prozesse sicher. Bei der Ribosomenbiogenese handelt es sich um einen komplexen Prozess, der mit hohem Energiebedarf verbunden ist. Die Synthese von Ribosomen beginnt im Nukleolus, in dem die RNA Polymerasen I und III die ribosomalen RNA (rRNA) kodierenden Gene transkribieren und so Vorläufer-rRNAs generieren. Diese durchlaufen während ihres Reifungsverfahrens eine Vielzahl an Prozessierungs-, Faltungs-, Modifizierungs- und Assemblierungsschritten. In der Hefe *Saccharomyces cerevisiae* wirken 79 ribosomale Proteine (RPs), vier rRNAs, einige snoRNAs und mehr als 150 Biogenesefaktoren in einem abgestimmten und hochdynamischen Netzwerk zusammen, um die reifen ribosomal Untereinheiten zu erzeugen. Die Biogenesefaktoren interagieren dabei transient in einem definierten Zeitfenster mit den prä-ribosomalen Partikeln. Im Laufe der vergangenen Jahrzehnte wurde viel Aufwand betrieben, um dieses Paradigma der RNP-Biogenese weiter aufzuklären und zu verstehen. Umfangreiche Forschung auf diesem Feld hat dazu beigetragen, das Detailwissen zu ribosomalen Biogenesefaktoren zu erweitern. Dies schließt beispielsweise den Reifungsschritt ein, für welchen sie benötigt werden oder ihre molekulare Funktion. Nichtsdestotrotz bleibt die Rolle vieler dieser Faktoren bis dato schwer definierbar, was weitere intensive Untersuchungen erfordert.

Die „Noc-Proteine“ gehören als solche zu dieser großen Gruppe der Biogenesefaktoren. Sie wurden ursprünglich als essentielle Faktoren für die Reifung der großen ribosomalen Untereinheit (LSU) identifiziert (Noc1p/2p/3p). Begleitende Studien haben die Existenz eines Noc1p/Noc2p- und eines Noc2p/Noc3p- Dimers aufgedeckt, welche möglicherweise jeweils mit frühen und intermediären LSU-Partikeln assoziiert sind.

In der vorliegenden Arbeit wurde der Fokus auf die Rolle von Noc3p gelegt. Ergebnisse aus Kryo-Elektronenmikroskopie auf Einzelmolekülebene deuten auf die Assoziation von Noc3p mit einer Teilmenge an verschiedenen prä-ribosomalen Populationen eines intermediären Reifungszustandes hin. Dadurch konnte ein Zeitintervall über den Verlauf einiger nukleären Reifungsschritte definiert werden, für diese eine Assoziation mit Noc3p beobachtet werden konnte. Gleichzeitig gab es erste strukturelle Hinweise auf die Position von Noc2p, dem Bindungspartner von Noc3p.

Um die Basis, die dieses Zeitfenster definiert, weiter zu verstehen, wurden die Voraussetzungen für die Rekrutierung und die Freisetzung von Noc3p im Kontext von prä-LSU Partikel genauer untersucht. Die Ergebnisse deuten darauf hin, dass sowohl die Rekrutierung als auch die Freisetzung von Noc3p vom prä-ribosomalen Assemblierungszustand abhängig sind. Die unterschiedlichen Einflüsse der

einzelnen ribosomalen Proteine (r-Proteine) wurden in Bezug auf deren bekannte Bindungsstellen in LSU-Partikeln diskutiert.

Die Anwendung eines vielseitig einsetzbaren Ansatzes zur Strukturanalyse ermöglichte die Untersuchung etwaiger struktureller Veränderungen, die die zeitlich gesteuerte Freisetzung von Noc3p beeinflussen oder gar verzögern. Tatsächlich konnte dabei eine beeinträchtigte Freisetzung von Noc3p beobachtet werden, welche sich auf konformationelle Änderungen in der prä-LSU Domäne III als Konsequenz der Abwesenheit bestimmter r-Proteine zurückverfolgen ließ.

Letztlich konnten durch strukturbasierte Mutagenese von Noc3p Bereiche innerhalb dieses Proteins identifiziert werden, die unabdingbar für die Bildung des Heterodimers mit Noc2p und für die Assoziation mit prä-Ribosomen sind.

Weitere Studien werden nötig sein, um die Bindung von Noc3p an prä-Ribosomen genauer aufzuklären, insbesondere zu welchem Ausmaß hierfür Noc2p erforderlich ist. Hierfür wären strukturelle Daten zu Noc2p als Ganzes sehr hilfreich. Insgesamt erlauben die in der vorliegenden Arbeit präsentierten Ergebnisse eine Hypothese über die Rolle von Noc3p als Sensor für die LSU Biogenese. Dies bietet eine solide Basis für zukünftige Untersuchungen.

3 Introduction

3.1 The eukaryotic ribosome – Structure and function

3.1.1 Overview

Ribosomes are macromolecular ribonucleoproteins complexes that fulfill the same function in all growing cells in all domains of life – the translation of mRNA into proteins. They constitute a complex and essential element within the cell that has been highly conserved throughout evolution (Woolford and Baserga 2013).

The term "ribosome" was initially proposed by Richard B. Roberts in 1958 in the course of the 1st symposium of the Biophysical Society on "Microsomal Particles and Protein Synthesis" at the Massachusetts Institute of Technology (MIT) (Richard B. Roberts 1958). This expression helped to designate the RNPs of the microsome fraction that have been already described by several scientists at that time. Initially, Siekevitz and colleagues showed, that microsomal fractions contain indispensable elements that help to incorporate amino acids into proteins (Siekevitz 1952).

Ribosomes can generally be classified in prokaryotic 70S and eukaryotic 80S particles, whereas the unit "S" (short for "Svedberg") stands for the sedimentation coefficient. Since it considers the point, at which sedimentation and diffusion reach a state of equilibrium during centrifugation, the sedimentation coefficient does not only consider the pure molecular weight of proteins but as well their size and spatial structure in a native solution (Svedberg and Fåhraeus 1926).

All ribosomes are composed of a large and a small ribosomal subunit (LSU and SSU, respectively), whereas the eukaryotic 80S ribosome is larger in size compared to its prokaryotic 70S counterpart. Nevertheless, the general functions of the ribosomal subunits are identical across different organisms, respectively. In this work, all following statements refer to the situation encountered in the eukaryotic unicellular organism *Saccharomyces cerevisiae* unless stated otherwise. The large, 60S ribosomal subunit incorporates three RNA molecules (rRNAs), the 25S, 5.8S and 18S RNA (3396, 158 and 121 nucleotides (nt), respectively) and 46 ribosomal proteins (r-proteins). The small 40S subunit harbors solely one 18S rRNA (1800 nt) and 33 r-proteins (Klinge and Woolford 2019; Kressler et al. 2017). In brief, an important function of the SSU is to decode the sequence information on the mRNA template, which encodes for a certain protein. Binding sites for the tRNAs are contiguously located, thus facilitating codon-anticodon recognition between mRNAs and tRNAs loaded with amino acids. The LSU contains the peptidyl transferase center (PTC) that catalyzes the formation of a peptide bond between two amino acids (Schmeing and Ramakrishnan 2009). Notably, due to the fact that the PTC is nearly completely deprived of proteins, this reaction is predominantly mediated by the RNA components (Nissen et al. 2000), thus classifying the ribosome as ribozyme (Cech 2000). Together, both SSU and LSU build up the mature 80S ribosome (DELEY 1964) through interactions at their subunit interfaces.

Notably, the emergence of high resolution structures has strengthen the knowledge that not only the interaction between the subunits, but as well mechanistic processes for instance the binding of mRNA and tRNA and especially the formation of peptide bonds rely on the RNA components of the ribosome (Ban et al. 2000; Nissen et al. 2000; Carter et al. 2000; Harms et al. 2001; Yusupov et al. 2001; Ben-Shem et al. 2010; Ben-Shem et al. 2011).

3.1.2 Cryo-EM as state of the art for addressing ribosomal structure

To understand the processes underlying ribosome biogenesis has been an ambitious goal since their discovery. Throughout the last decades a lot of effort has been made to develop and refine new technologies to further enlighten ribosome assembly. In order to fully understand the mechanisms and processes that underlie the formation of ribosomes, it is necessary to know the exact structure of the respective particles.

Therefore, imaging techniques gained enormous importance for direct visualization of (pre-) ribosomes. X-ray crystallography has been used by structural biologists for decades. Especially around the turn of the millennium, a series of high-resolution crystal structures of bacterial and archaeal ribosomes were described (see 3.1.1). However, the main challenge in crystallographic studies is to figure out the right conditions for well-diffracting crystals. It is therefore of great importance to ensure that the isolated samples of ribosomes are highly homogeneous and can form well-ordered crystals. Unfortunately, for some proteins it can take months or years to crystallize them, whereas others never crystallize at all. In addition, several further problems have complicated the work with crystallography, for instance the stability of the resulting crystals or phasing problems.

Nowadays, single molecule cryogenic electron microscopy (cryo-EM) has largely superseded X-ray crystallography, especially for structure determination of macromolecular complexes (Carroni and Saibil 2016). Importantly, cryo-EM does not require crystals, but ribosomes can be directly observed after freezing, *ex vivo*. Additionally, cryo-EM requires a much smaller amount and a less concentration of samples for analysis and can tolerate impurities as well as structural heterogeneity of the sample. In fact, different sub-states of ribosomes or of their precursors can be deduced which allows an insight into the dynamic behavior of these particles (see for instance Kater et al. 2017; Sanghai et al. 2018b). An important step in the improvement of cryo-EM was the invention of direct-electron detectors enabling to achieve near atomic resolutions (Kühlbrandt 2014). Due to the constant further development of both soft- and hardware related with cryo-EM, this technique provides a powerful tool for receiving high resolution structure of mature ribosomes and ribosomal intermediates. Even though the evaluation of cryo-EM data is more complex and requires higher computing power it represents the method of choice for studying the structure and function of (pre-) ribosomes that is routinely used in laboratories over the whole globe.

3.1.3 Structure and components of the small ribosomal subunit

The 40S or small ribosomal subunit adopts, compared to the large subunit, a relatively simple structural conformation. The RNA component of the small subunit, the 18S rRNA, is subdivided in four phylogenetically conserved secondary structure domains: the 5´-, central-, 3´-minor and the 3´-major domain. These fold into tertiary structures, interacting with 33 r-proteins, thereby forming the head, beak, platform and the body (Figure 1, left side). These constitute characteristic architectural landmarks of the mature small ribosomal subunit (Klinge and Woolford 2019).

The 3´ major domain is almost exclusively located in the upper part of the SSU which forms the head and the beak, a protrusion of the 18S rRNA surrounded by proteins. The 3´minor domain is located at the subunit interface, vertically oriented to the head and surrounded by the 5´- and the central domain. The latter one connects the head and the body (Figure 1, right side).

The central pseudoknot represents a key feature of the small ribosomal subunit that brings together all of the four secondary structure subdomains of the 18S rRNA. This interface regions is important for the overall architecture of the 18S rRNA and the decoding center, which is located in close vicinity in the middle of the small subunit (Ben-Shem et al. 2011).

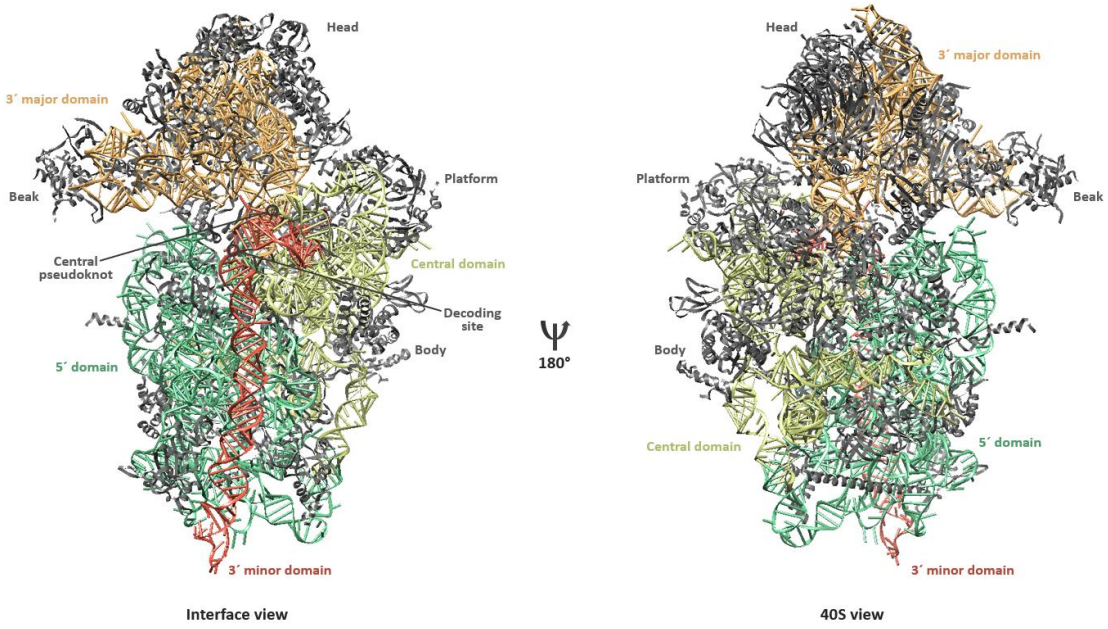

Figure 1: Overall structure of the mature small ribosomal subunit from *Saccharomyces cerevisiae*.
Cartoon representation of the small ribosomal subunit shown from an interface view (left side) and from an 40S- or solvent side view (right side) (PDB 4V88). The 18S rRNA subdomains are color-coded and indicated. Ribosomal proteins are shown in grey. Positions of structural landmarks (head, beak, platform, body, central pseudoknot) and of functional sites (decoding center) are annotated.

The mRNA passes the small subunit through a channel between the beak and body and exists between the platform and head. A series of high resolving crystal structures of different prokaryotic ribosomes have allowed to track the path of the mRNA through the small subunit (Yusupova et al. 2001). As

bacterial and eukaryotic ribosomes share an evolutionarily conserved core which attributes their intrinsic functions, the course of mRNA trough the SSU in eukaryotic organisms is the same. Structural data obtained by X-ray crystallography and cryo-EM have completed these findings (Melnikov et al. 2012). The initial entry of mRNA to the small subunit however shows substantial differences between pro- and eukaryotes. In prokaryotic, but not archaeal organisms, the shine Dalgarno sequence initializes binding of the SSU onto mRNA (Gualerzi and Pon 2015), whereas in eukaryotes the mechanism of mRNA recognition and recruitment appears to be more sophisticated involving the 5´-cap structure of mRNA and additional factors, ultimately forming the pre-initiation complex (Jackson et al. 2010; Fraser 2015).

3.1.4 Structure and components of the large ribosomal subunit

The 60S or large ribosomal subunit adopts a more condensed, crown-like conformation including several characteristic landmarks and functional centers. The large subunit harbors three RNA molecules – the 25S, the 5.8S and the 5S rRNAs. The former one is subdivided in six phylogenetically conserved secondary structures – domains I-VI – which form its defined tertiary structure, together with the interaction of 46 r-proteins. In general, the subdomains of the LSU are more intertwined with each other than are the 18S rRNA subdomains of the SSU.

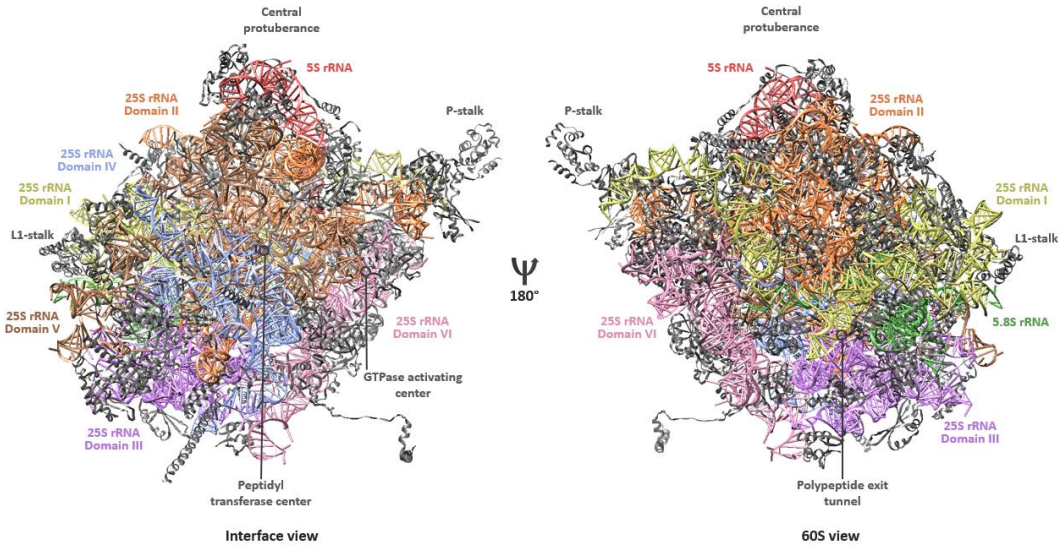

Figure 2: Overall structure of the mature large ribosomal subunit from *Saccharomyces cerevisiae*.
Cartoon representation of the large ribosomal subunit shown from an interface view (left side) and from an 60S- or solvent side view (right side) (PDB 4V88). The 25S rRNA subdomains as well as the 5.8S and the 5S rRNAs are color-coded and indicated. Ribosomal proteins are shown in grey. Positions of structural landmarks (P-stalk, L1-stalk, central protuberance) and of functional sites (peptidyl transferase center, polypeptide exit tunnel, GTPase activating center ("SRL" in Figure 3) are annotated.

The solvent side is largely structured both by the 25S rRNA domains I, II and by the 5.8S rRNA (Figure 2, right side), whereas domains IV and V form the subunit interface. The 5.8S rRNA base-pairs with

domain I and is sandwiched between domains I and III. The latter one is located at the bottom of the subunit, linking domains localized there. Domains III and VI bridge the subunit interface with the solvent exposed side. The 5S rRNA is assembled on top of the LSU, contacting domains II and V (Ben-Shem et al. 2011; Klinge and Woolford 2019).

Functional sites are mostly localized at or near the subunit interface (Figure 3) (Konikkat and Woolford 2017). The P-stalk is shown on the right side of the LSU (Figure 3, blue). At its basis lies the sarcin ricin loop (SRL) which has obtained its name by the cytotoxins α-sarcin and ricin that target this structural motif and completely abolish translation (Endo and Wool 1982; Endo et al. 1987). Both the P-stalk and the SRL form the GTPase-associated center (GAC). The P-stalk recruits and activates translation factors and the SRL triggers GTP hydrolysis to GDP of these factors (Santos and Ballesta 2005; Diaconu et al. 2005; Voorhees et al. 2010).

The tRNA accommodation corridor begins with helices of 25S rRNA domain V that form the tRNA entry tunnel (Figure 3, yellow) and continues with the A-, P- and E- (Aminoacyl-, Peptidyl- and Exit-) sites for tRNA binding. In the middle of this corridor, at the P-site, localizes the polypeptide transfer center (PTC) formed by domains IV and V and nearly completely deprived of proteins. At this site, the peptide bond formation between two amino acids and the hydrolysis of peptidyl-tRNA bonds are catalyzed. The PTC is adjacent to the entrance of a tunnel, the polypeptide exit tunnel (PET). Nascent proteins pass through the tunnel before they are released from the ribosome at the opposite, solvent exposed site. The exit of the PET is surrounded by the 25S rRNA domain III.

The central protuberance (CP) of the mature LSU is located atop of the particle comprising the 5S rRNA and the LSU r-proteins rpL5 and rpL11 (Figure 3, “CP”). It is involved in inter-subunit interactions with domains II and V and assembled r-proteins, respectively (Ben-Shem et al. 2011). A plethora of studies on the 5S rRNA has been performed throughout the decades and several functions have been attributed (for review see Gongadze 2011). Importantly, it has been shown to enhance translational fidelity. However, translation involves all functional centers of the ribosome since this process constitutes its dedicated function. Therefore, the central protuberance is supposed to operate as signal transducer between the functional centers of the large subunit through physical connections, thus helping to coordinate translation events (Smith et al. 2001; Dinman 2005; Kiparisov et al. 2005).

The L1 stalk (Figure 3, left side) is suggested to facilitate opening of the E-site by moving to a different conformation, thereby contributing to the efficient release of the tRNA (Andersen et al. 2006).

The A-site finger (ASF), which is as well highlighted in the structure protrudes to the inter-subunit space, located in close proximity to the A-site. It has been shown to attenuate the motion of the A-site tRNA, acting as translocation attenuator that helps to maintain the reading frame (Komoda et al. 2006).

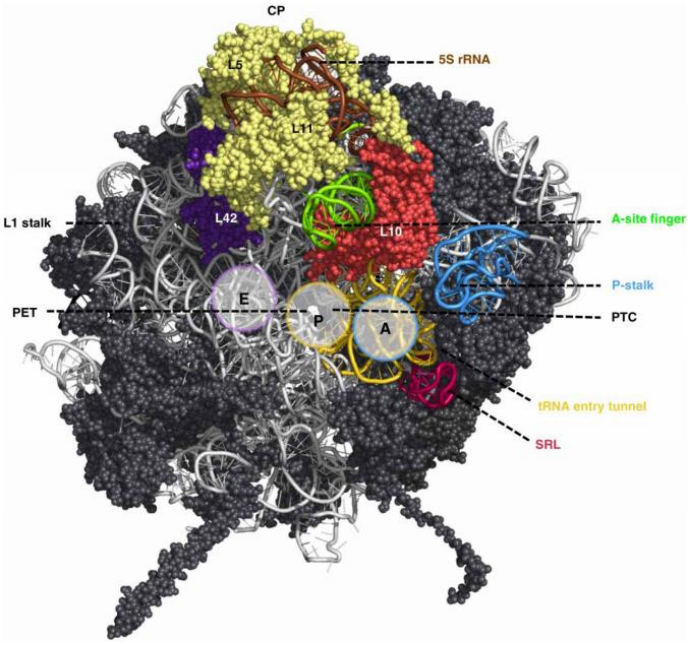

Figure 3: Functional centers of the large ribosomal subunit of *Saccharomyces cerevisiae*.
Cartoon representation of the 60S ribosomal subunit from an interface side view in order to primarily visualize its functional centers. At the top, the 5S rRNA and associated LSU r-proteins L5/L11 are shown. Two further characteristic landmarks, the P-stalk (on the right, blue) and the L1-stalk (on the left) are indicated. The SRL-loop is shown in red and the tRNA entry tunnel in yellow which depicts the beginning of the tRNA accommodation corridor that continues with the A- and P-sites for tRNAs and ends with rpL42 (purple) at the tRNA E-site. The PTC is indicated in the middle of the tRNA accommodation corridor at the P-site, the PET emerges to the solvent side and is indicated as well. The A-site finger (green) and the adjacent rpL10 (red) are shown as well. Adopted from (Konikkat and Woolford 2017).

3.1.5 Structure and function of the 80S or mature ribosome

Both the small as well as the large ribosomal subunit contain an evolutionarily conserved core that assigns the main functions of the ribosome. However, eukaryotic ribosomes are at least 40 % larger in size compared to their prokaryotic counterparts, which is due to additional elements present in the subunits. Eukaryote specific additives are extra ribosomal proteins and insertions/extensions into existing r-proteins, which could be visualized by the availability of the first high resolution crystal structures of *Saccharomyces cerevisiae* and *Tetrahymena thermophila* (Ben-Shem et al. 2010; Ben-Shem et al. 2011; Klinge et al. 2011; Rabl et al. 2011). A further eukaryote specific feature are blocks of additional rRNA, termed “expansion segments” (ES) (Gerbi 1996), which emerge from the conserved secondary structure core of the mature rRNAs and are mainly located on the solvent exposed peripheral surface of the subunits (Hsiao et al. 2009; Melnikov et al. 2012). Notably, these ES are not fully eukaryote specific elements, as ES were found in several archaeal organisms (see for instance Armache et al. 2013). Some archaea contain even supersized ES that are longer than eukaryotic ones (Penev et al. 2019).

The two subunits of *Saccharomyces cerevisiae* differ significantly from each other regarding the distribution of expansion segments and of r-proteins. In the small subunit, most rRNA is concentrated at the bottom, whereas the r-proteins are scattered all over its surface, mostly on the solvent exposed site. Conversely, the expansion segments of the large subunit form a nearly continuous ring around the PET, spanning from the P-stalk to the L1-stalk (for detailed description of the subunits see 3.1.3 and 3.1.4). The LSU r-proteins are mostly associated with this ring-structure, which results in the same characteristic distribution. Moreover, it has been shown that eukaryote specific r-proteins are often contacted by eukaryote specific ESs (Ben-Shem et al. 2011).

Information concerning the detailed roles of most expansion segments remains sparse although several properties and functions could already be attributed. For instance, deletion of ES27L of *tetrahymena* was lethal and lead to an accumulation of pre-rRNA. This indicated, that this ES might play a role in either pre-rRNA processing or the stability of mature rRNAs (Sweeney et al. 1994). Furthermore, replacement of the ES with unrelated sequences of similar size or a homologous sequence from another organism in incorrect orientation was lethal as well, suggesting that the ES are not simply spacers that can be replaced by any sequences of corresponding size (Sweeney et al. 1994). Similar observations in yeast corroborated these findings (Jeeninga et al. 1997). Recent studies revealed the association of the methionine amino peptidase (MetAP) with ES27L, which indicates a function in translation fidelity. Deletions at specific sites within the ES27 lead to increased amino acid misincorporation, read-through- and frameshifting-errors (Fujii et al. 2018).

In general, the deletion of ES mostly interferes with the correct production of mature rRNAs an hence impedes the proper biogenesis of ribosomes (Ramesh and Woolford 2016). Moreover, increased rRNAs of more complex organisms than prokaryotic ones could confer increased functionality to the ribosome. For instance, characterization of the binding partners of ES7 revealed, amongst others, the association of several aminoacyl tRNA synthetases with the ES. This connection is supposed to maintain a close interaction of the synthetases with each other and with the translation machinery (Gómez Ramos et al. 2016). Therefore, the increased complexity of eukaryotic translation, especially regarding initiation and elongation might also explain their presence (for selected reviews describing the current knowledge of the translation process see Wilson and Doudna Cate 2012; Voorhees and Ramakrishnan 2013; Hinnebusch 2014; Rodnina 2016; Dever et al. 2016; Hinnebusch 2017; Schuller and Green 2018; Shirokikh and Preiss 2018).

During translation initiation, the small ribosomal subunit joins the large ribosomal subunit to form an asymmetric assembly. Thereby, the head of the SSU interacts with the CP of the LSU (Figure 4). Importantly, the integrity of the two subunits to each other within the mature ribosome is strengthened by the formation of inter-subunit bridges.

Figure 4: Overall structure of the mature 80S ribosome from *Saccharomyces cerevisiae*.
Cartoon representation of the mature 80S ribosome from an A-site view, consisting of the small 40S subunit (rRNA chain in light green, r-proteins in dark green) and of the large 60S ribosomal subunit (rRNA in orange, r-proteins in brown) (PDB 4V88). Positions of the head, beak, body and the mRNA entry site of the SSU as well as the central protuberance (CP) and the polypeptide exit tunnel (PET) of the LSU are annotated.

In fact, the translation process is not static but highly dynamic. During elongation, when seen form the solvent side of the small subunit, the SSU rotates a few degrees counterclockwise in a ratcheting motion relatively to the large subunit (Frank and Agrawal 2000). Additionally, the head domain of the SSU swivels relatively to the body (Zhang et al. 2009a; Spahn et al. 2004). These movements are important for mRNA- and tRNA- translocation, termination and other processes. The inter-subunit interactions change with each rearrangement and are dynamic in composition. Therefore, inter-subunit bridges are indispensable to maintain the communication between the subunits during protein synthesis. The crystal structure of the yeast ribosome reveals 17 inter-subunit bridges which are, in contrast to the prokaryotic counterpart, mainly formed by the protein components of the subunits (Spahn et al. 2001; Yusupov et al. 2001; Ben-Shem et al. 2011).

3.2 Transcription of the genes encoding for the ribosomal RNAs in the nucleolus

The nucleolus defines a substructure within the nucleus that can be observed as dark spot by light microscopy. In 1781 Felice Fontana was the first to figure the nucleolus in the nucleus which he described as an egg-formed body occupied by a spot in the middle. Further, more explicit descriptions of the nucleolus emerged during the 18th century (for a historical review see Montgomery 1898).

According to the current state of knowledge, the nucleolus represents a functional intra-nuclear, membrane less organelle, which is present in all eukaryotic cells analyzed so far. It constitutes the ribosome factory of the cell where rDNA transcription, initial pre-rRNA processing and first assembly events of the earliest pre-ribosomal particles take place (Raška et al. 2006; Hernandez-Verdun et al. 2010). The structure of the nucleolus is not homogenous. In fact, three morphological compartments defined by their texture and contrast were observed in electron microscopy analyses of eukaryotes – fibrillar centers (FC), a dense fibrillar component (DFC) and a granular component (GC), which are functionally assigned to processes in ribosome biogenesis (Léger-Silvestre et al. 1999; Trumtel et al. 2000). However, the differentiation and organization of the nucleolar sub-components among different organism is challenging (discussed in the review of Thiry and Lafontaine 2005).

The nucleolus forms around the nucleolar organizer region (NOR), sites where multiple rDNA copies cluster in arrays. In the yeast *Saccharomyces cerevisiae* ~150 copies of the genes encoding the ribosomal RNAs, referred to as "rDNA repeats" are localized on chromosome XII as tandem array (Petes and Botstein 1977; Petes 1979; Long and Dawid 1980). Each rDNA repeat has a size of ~9.1 kb and is arranged in two transcriptional units (Figure 5, A). The first unit encodes an operon-like gene that produces a 35S pre-rRNA transcript containing the sequences for mature 18S, 5.8S and 25S rRNAs with a total size of ~6.6 kb. As indicated in Figure 5 (A), the sequences for the mature rRNAs are flanked by spacers (ETS/ITS), which have to be removed during pre-rRNA processing (see 3.3). The 35S precursor rRNA molecule is transcribed by RNA polymerase I (Pol I). The second unit encodes for the 5S rRNA, arranged in reverse direction, which is flanked on both sides by non-coding intergenic spacers (IGS), thereby separated from the first unit (Philippsen et al. 1978). The 5S rRNA is transcribed by RNA polymerase III (Pol III) (Weinmann and Roeder 1974).

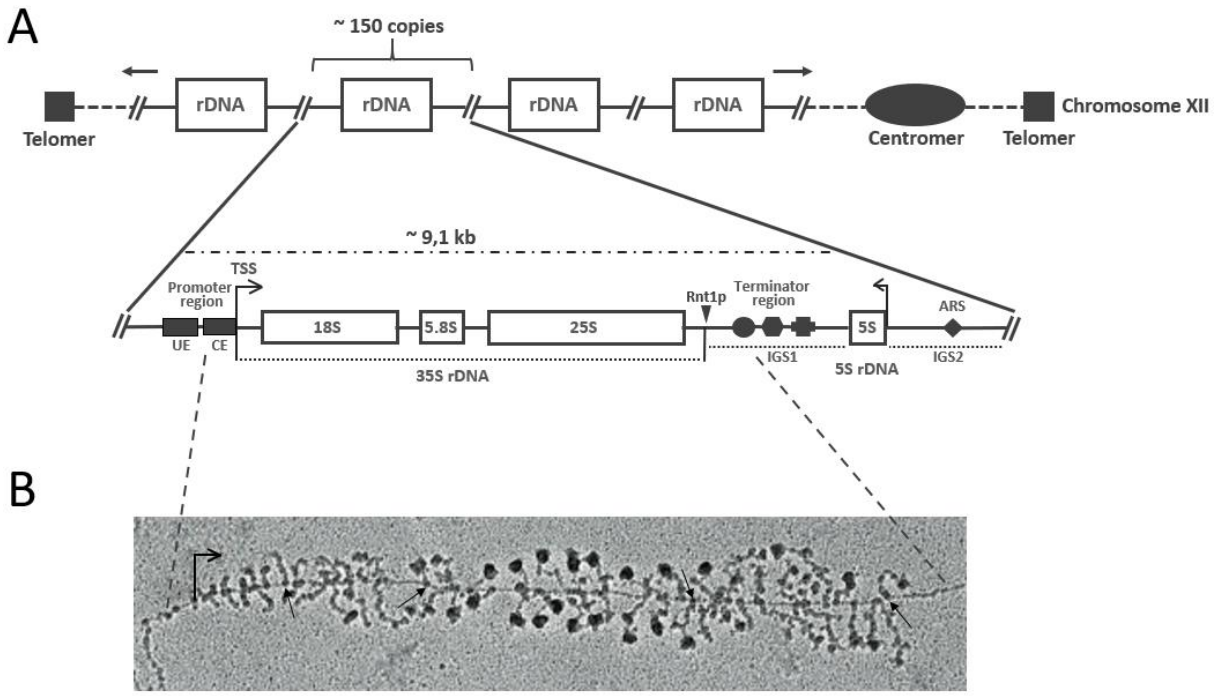

Figure 5: Organization of the rDNA locus in Saccharomyces cerevisiae and visualization of "Miller spreads".
(A) Organization of the rDNA encoding genes, arranged in a cluster of arrays (~ 150 copies) located on chromosome XII. The composition of one rDNA repeat which has a length of approximately 9,1 kb is illustrated in more detail. The 25S, 5.8S and the 18S rDNA sequences which make up the 35S rDNA are arranged in an operon-like structure, separated by internal transcribed sequences and flanked by external sequences (not annotated here, for illustration see Figure 6). The 5S rDNA is separated by the intergenic spacer 1, the region separating the 35S rDNA repeats from neighboring by the intergenic spacer 2 (IGS1/IGS2). The transcription directions of the 35S rDNA by Pol I and of the 5S rDNA by Pol III in opposite directions are indicated by arrows. The positions of relevant DNA elements are marked: The upstream element (UE) and the core element (CE) which are part of the rDNA promoter, the cleavage site of Rnt1p (triangle), the IGS1 including the T-rich element (circle), the Reb1p-binding site (trapeze) and the replication fork barrier (cross), and the IGS2 which contains an autonomous replicating sequence (ARS, diamond). (B) Electron micrograph of a Miller chromatin spread which shows actively a transcribed rDNA repeat. Pol I molecules are marked by arrows. Adapted from (Osheim et al. 2004).

The 14 subunit Pol I is an outstanding polymerase, as it is solely dedicated to transcribe the 35S pre-rRNA. In contrast, Pol III transcribes, besides the 5S rRNA, the tRNA genes and several other non-coding RNAs (ncRNAs) including the RNA component of the signal recognition particle and different small nucleolar RNAs (snoRNAs) (for review see Dieci et al. 2007). The requirements for an efficient initiation of Pol I transcription are well studied. It requires the action of the four proteins or protein modules, the core factor (CF), TATA box binding protein (TBP), upstream activating factor (UAF) and Rrn3p. Moreover, two regulatory *cis* elements in the Pol I promotor region, the core element (CE) ranging from -28 to +8 relative to the transcription start site (TSS) and the upstream element (UE) located around bases -146 to -51, are necessary (Musters et al. 1989; Kulkens et al. 1991; Choe et al. 1992). The Pol I specific initiation factor Rrn3p associates directly with the A43 subunit of Pol I and is strictly required to render Pol I competent for initiation (Yamamoto et al. 1996; Milkereit and Tschochner 1998; Peyroche et al. 2000). The heterotrimeric CF consisting of Rrn6p, Rrn7p and Rrn11p (Keys et al. 1994; Lin et al. 1996; Lalo et al. 1996) binds to the CE in the promoter region and can recruit the

initiation competent Rrn3p-Pol I to the rDNA, possibly via interaction between Rrn6p and Rrn3p (Peyroche et al. 2000). Notably, Pol I, Rrn3p and CF bound to the CE are sufficient for a very basal transcription *in vitro*. However, the transcription rate tremendously enhances upon binding and interaction with UAF and TBP (Keener et al. 1998). UAF consists of Rrn5p, Rrn9p, Rrn10p, Uaf30p and the two histones H3 and H4, which are suggested to mediate efficient binding to the UAE (Keys et al. 1996; Keener et al. 1997; Siddiqi et al. 2001). TBP binds, accordingly to UAF, to the UE and interacts both with components of the UAF and the CF namely Rrn9p and Rrn6p, respectively. The interaction with Rrn9p was shown to be more strong than with Rrn6p, which indicates a CF dependent recruitment by UAF, bridged through TBP (Steffan et al. 1996; Steffan et al. 1998; Keener et al. 1998). Therefore, the current model of Pol I initiation proposes UAF and TBP bound to the rDNA promoter region. Thereby, UAF and TBP recruiting CF, which provides a platform for binding of initiation competent Rrn3p-Pol I through CF recruitment to form the pre-initiation complex (PIC) that ultimately results in a high-level transcription of 35S pre-rRNA.

Once transcription is initiated, Pol I maintains a high elongation rate, transcribing at a speed of ~ 40-60 nts per second (Kos and Tollervey 2010). Regarding Pol I transcription termination, the exact mechanism is not clarified in detail. It depends on *cis*-elements downstream of the 35S rDNA region (T-rich sequence, Reb1-binding site, replication fork barrier) and on *trans*-acting factors that bind to these elements (Reb1p, Nsi1p, Fob1p). Moreover, endonucleolytic cleavage by Rnt1p followed by exonucleolytic trimming of the nascent rRNA could also contribute to the release of Pol I from the rDNA (for review see Németh et al. 2013). Previously, the availability of high-resolution structures of Pol I at different states, in association with Rrn3p, as well as initiation complexes have contributed to the understanding on how the transcription process and its regulation might occur (e.g. see Engel et al. 2013; Fernández-Tornero et al. 2013; Neyer et al. 2016; Tafur et al. 2016; Sadian et al. 2017; Sadian et al. 2019; Pilsl and Engel 2020).

Both transcription initiation and elongation of Pol I are regulated steps in rRNA synthesis (French et al. 2003; Zhang et al. 2010). During elongation, several protein factors have been found to influence Pol I activity, for instance Spt4p, Spt5p or the Paf1 complex (Paf1C). Importantly, these trans-acting factors exert their function upstream of pre-rRNA processing at the level of rDNA transcription. Due to their manipulation of the Pol I elongation properties, they influence the temporarily abundance of pre-rRNA transcripts and may therefore exert an impact on the organization of pre-rRNA processing (Schneider et al. 2006; Schneider et al. 2007; Zhang et al. 2009b; Zhang et al. 2010; Anderson et al. 2011). Another level of regulation is represented by the HMG protein Hmo1p which was found to bind on nucleosome free rDNA, thereby maintaining accessible rDNA structure (Gadal et al. 2002; Hall et al. 2006; Merz et al. 2008).

Finally, the synthesis of rRNA can be regulated at a very initial level through the abundance of rDNA copies that are accessible for transcription. Even in exponentially growing yeast cells, only ~ 50% of the 35S rDNA repeats are actively transcribed. In contrast, the other half is packaged into nucleosomes which seems to be important for the integrity of the rDNA locus (Ide et al. 2010).

One possibility to observe and quantitate actively transcribing Pol I complexes is the direct visualization of chromatin spreads by electron microscopy, a method that has been developed by Oscar L. Miller at the end of the 60s (Miller and Beatty 1969). Thereby, the numerous Pol I complexes, occupying a single rDNA repeat, can be observed at different positions within a single rDNA gene, having transcribed the 35S rDNA to a different degree. The emerging nascent rRNAs form the branches of the chromatin fiber, which are occupied with terminal knobs giving the "Miller-spreads" its characteristic "Christmas tree" like appearance (Figure 5, B). Notably, the terminal knobs represent the first ribosomal precursor particles, as initial steps of pre-RNA processing and ribosome assembly occur co-transcriptionally (see 3.3.1 and 3.5.1.1).

3.3 Processing and modification of ribosomal RNAs

As mentioned above, RNA polymerase I is dedicated to the transcription of the rDNA locus, except for the 5S rRNA. Thereby, the initial 35S pre-rRNA, which contains the mature sequences for the 18S, 5.8S and 25S rRNAs is generated. Embedded in this precursor transcript, the mature rRNAs are separated by two internal transcribed spacers (ITS1 and ITS2) and flanked by external transcribed spacers (5´-ETS and 3´-ETS). These additional blocks of RNA are not present in the mature ribosomal subunits and have therefore to be removed. This involves successive series of both endonucleolytic and exonucleolytic processing events (Venema and Tollervey 1995).

3.3.1 Co-transcriptional processing

Originally, it was assumed that pre-rRNA processing in eukaryotes occurs exclusively after transcription of the rDNA by RNA polymerase I. In this situation, the 35S pre-rRNA transcript is cleaved at processing site B_0 in the 3´-ETS (Figure 6) at an imperfect stem-loop by the endonuclease Rnt1p, a bacterial homologue to RNase III (Elela et al. 1996; Kufel et al. 1999). Subsequent processing steps, starting with successive cleavages within the 5´-ETS would occur after Rnt1p has performed its actions.

First evidence for co-transcriptional processing events comes from observations made by pulse-chase labelling experiments of synthesized rRNAs. The outcome of these analyses lead to the suggestion, that the introduction of base modifications followed by separating cleavage events on 35S pre-rRNA were not completely post-transcriptional (Udem and Warner 1972). In the late 80´s, further evidence for co-transcriptional processing of the 5´-ETS in *Saccharomyces cerevisiae* has been received. At that time, Veinot-Drebot and colleagues estimated half-lives of pre-rRNA molecules that contain ETS versus

the time period that is necessary to fully transcribe the 35S pre-rRNA by quantitative hybridization techniques. The results suggested that ETS removal takes place before the transcription is completed (Veinot-Drebot et al. 1988). Later, electron microscopy analysis of yeast cells in log phase helped to visualize the terminal knobs at the end of branches that appear in miller spreads, which represent the nascent RNPs. Transcripts of different lengths have been observed, dependent on the current position of Pol I within the rDNA gene. It was concluded that processing events of approximately 40-80 % occur on the nascent transcripts in the ITS1 (Osheim et al. 2004). More recently, these findings were confirmed by metabolic labelling experiments of exponentially growing yeast cells and mathematical modelling. The respective analyses demonstrated a co-transcriptional cleavage activity of pre-rRNA at a level of 70 % (Kos and Tollervey 2010).

The terminal knobs observed in miller spreads were supposed to form prior to possible processing events. In fact, compositional analysis revealed the integrity of components that are required for pre-18S processing. Thus, the knobs have been termed small subunit processome (SSU processome) (Dragon et al. 2002). This indicates that co-transcriptional processing involves endonucleolytic cleavage events at the processing sites A_0, A_1, A_2 and B_0. However, the molecular mechanisms underlying the decision for co- or post-transcriptional processing have not been clarified yet. 5´-ETS processing starts with cleavages at site A_0 and A_1, resulting in 33S and 32S pre-rRNAs, respectively. The exact position of processing at site A_1 is defined by evolutionarily conserved nucleotides upstream of this site in the 5´-ETS and by a stem-loop structure downstream of A_1 within the 5´-region of the 18S rRNA (Venema et al. 1995; Sharma et al. 1999). Cleavage at site A_2 splits the two maturing small and large subunits incorporating 20S and 27S pre-rRNA, respectively, from each other which leads to independent maturation routes. The A_2 processing site is as well defined by 3´- evolutionarily conserved nucleotides that form a stable hairpin structure, similar as observed for the 3´-region of 18S rRNA (Allmang et al. 1996). However, cleavage at site A_2 cannot be undoubtedly designated to one putative endonuclease. The involvement of Utp24 in cleavage at both positions A_1 and A_2 has been reported by some authors (Bleichert et al. 2006; Wells et al. 2016), whereas others attribute processing at site A_2 to Rcl1p (Billy et al. 2000; Horn et al. 2011; Delprato et al. 2014). Finally, processing at position B_0 in the 3´ETS terminates co-transcriptional processing, as this cleavage step releases the emerging pre-rRNA transcript. Interestingly, this has been found to impede processing at site A_3 within the ITS1, probably depicting a quality control checkpoint (Allmang and Tollervey 1998).

Growth of the yeast cells in an environment facing stress conditions, for instance nutrient limitation may, however, lead to increased post-transcriptional processing at the expense of co-transcriptional processing. In 2017 Kos-Braun and co-workers revealed the TOR1 and CK2 kinases as responsible key-players in regulating pre-rRNA processing at a post-transcriptional level. The Tor 1 complex (TORC1) is sensitive to growth conditions as nutrient availability and environmental stress. TORC1 depicts a

central signaling hub in response to environmental cues mediating a variety of intracellular signaling branches (González and Hall 2017) and citations therein). Thereby, TORC1 controls the transcriptional activity of all three RNA polymerases and therefore the availability of rRNA and r-proteins for ribosome biogenesis. Among them is the downstream activation of the CK2 kinase, a prerequisite for pre-rRNA processing at site A_2 along the A2-pathway (Kos-Braun et al. 2017). Inhibition of either TOR1 or CK2 leads to identical pre-rRNA processing abnormalities. As consequence, large amounts of 23S pre-rRNA resulting from a non-productive processing pathway through direct cleavage at A_3 in the ITS1 prior to 5´-ETS processing were observed. As processing at site A_3 is coupled to B_0 processing (Allmang and Tollervey 1998), the course of these events is per definition derived to post-transcriptional processing. Notably, experimental evidence that 23S pre-RNA is aberrant and ribosomes incorporating this pre-rRNA species are degraded is missing. Further evidence for diminishment of co-transcriptional processing activity could be obtained regarding the terminal knobs of the EM-analysis described above. Upon heat-shock at 37 °C the resulting transcripts failed to show transcript-cleavage in contrast to the untreated control (Osheim et al. 2004). In addition further mechanisms exist that serve for fine-tuning the balance between co- and post-transcriptional processing (for review see La Cruz et al. 2018). Therefore, co-transcriptional processing is preferred in favorable growth conditions controlled by a variety of intra- and extracellular signals.

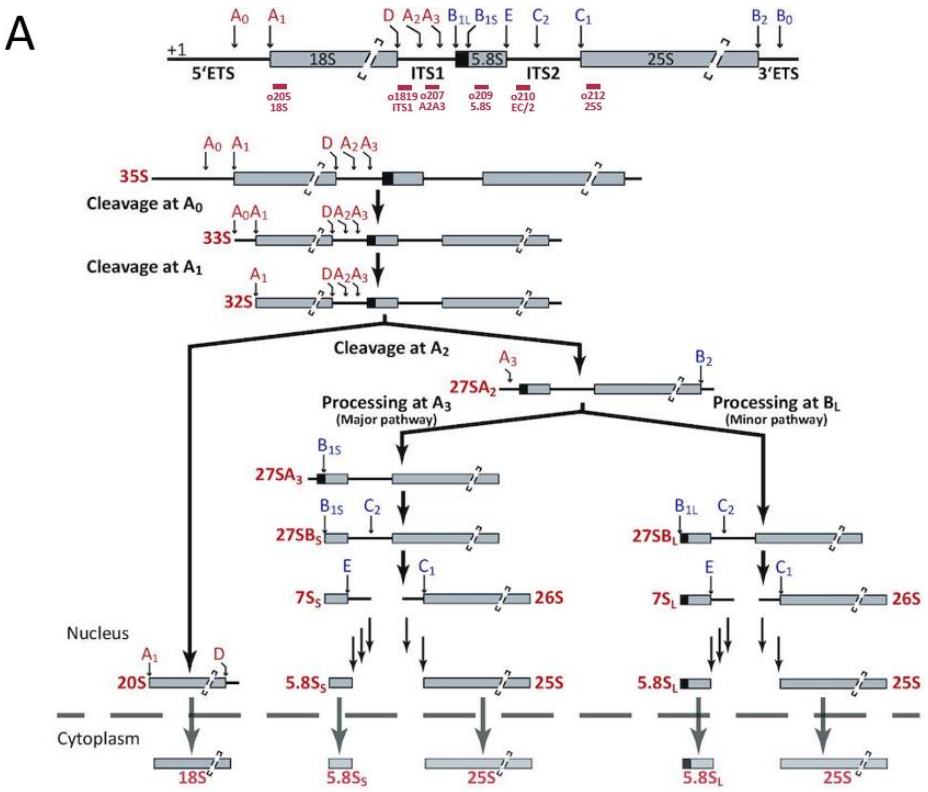

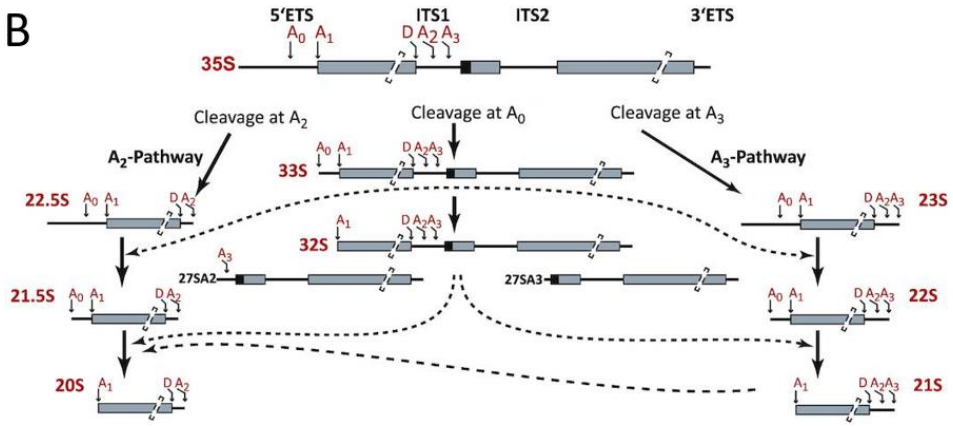

Figure 6: Pre-rRNA processing in the yeast *Saccharomyces cerevisiae*.
(A) Schematic representation of one 25S pre-rRNA molecule. The sequences of mature 18S, 5.8S$_{S/L}$ and 25S rRNA are separated by two internal transcribed spacers (ITS1/ITS2) and flanked by two external transcribed spacer regions (5´-ETS/3´-ETS). The positions of the individual processing which correspond to 5´- or 3´-end of rRNA (precursors) are indicated. The positions, numbers and designation of the DNA oligo probes used for detection of the different rRNA (precursors) by northern blotting are illustrated. Note that the lengths of rRNAs and spacer sequences are not in proportion to their real lengths. Processing site for generation of 18S rRNA are depicted in red, those for generation of 5.8S$_{S/L}$ and 25S rRNA are depicted in blue. (B) Alternative pathways of 27SA$_2$ pre-rRNA processing. See text for more detailed explanation. Adopted and modified (Braun et al. 2020).

3.3.2 Post-transcriptional processing

At least the further maturation steps of both the small and the large subunit occur as post-transcriptional processing events. The 20S pre-rRNA incorporated in SSU-precursor particles are exported to the cytoplasm where the final maturation to 18S rRNA occurs (Udem and Warner 1973). Therefore, the endonuclease Nob1p performs cleavage at the single stranded processing site D in the ITS1 (Fatica et al. 2003a; Lamanna and Karbstein 2009; Pertschy et al. 2009).

The precursor of the large subunit incorporating 27SA$_2$ pre-rRNA represents the second product from cleavage at site A$_2$. Further processing splits in two possible pathways both ultimately resulting in the same 25S rRNA sequence but yielding alternative forms of 5.8S rRNA that differ in length of 7 nucleotides at their 5´-ends (5.8S$_S$/5.8S$_L$). In the vast majority, site A$_3$ within the ITS1 is cleaved by the endonuclease MRP (Lindahl et al. 1992; Chu et al. 1994a). Notably, in 1991 the group of Jonathan R. Warner already isolated a temperature sensitive strain carrying a mutation in the gene designated as *RRP2*. This mutant strain accumulated this, at that time novel, pre-rRNA species containing sequences of the ITS1 (Shuai and Warner 1991). One year later, this phenotype was referred to a mutation in the endonuclease MRP (Lindahl et al. 1992).

In any case, cleavage at site A$_3$ provides the entry site for 5´-3´ exonucleolytic ITS1 trimming to the B$_{1S}$ site, the mature 5´-end of 27SB$_S$ pre-rRNA involving the exonucleases Rat1p, Xrn1p and Rrp17 (Henry et al. 1994; Oeffinger et al. 2009). Alternatively, in approximately 10 % of the cases, cleavage at B$_{1L}$ by an so far unknown endonucleolytic processing event, generates the mature 5´-end of 5.8S$_L$ (Faber et al. 2006). This alternative processing pathway results in the production of 27SA$_3$ pre-rRNA which

subsequently undergoes normal maturation as well as 23S pre-rRNA which are stepwise processed at sites A_0, A_1 and A_2 yielding 22S, 21S and 20S pre-rRNA, respectively (see Figure 6), detected in lower amounts. Interestingly, inhibition of nuclease MRP results exclusively in the generation of the prolonged processing variant $27SB_L$ (Schmitt and Clayton 1993; Chu et al. 1994a; Lygerou et al. 1996). Absence of the factors Dbp3 or Rrp5 involved in the major pathway following processing at A_2, has as well shown to cause an imbalance of $5.8S_S$ and $5.8S_L$, shifting the ratio to an increased production of the latter rRNA species (Venema and Tollervey 1996; Weaver et al. 1997; Eppens et al. 1999; Lebaron et al. 2013).

Independently of producing the mature 5´-end of $5.8S_{S/L}$, the next steps in the route of pre-rRNA processing are dedicated to removal of the ITS2. This constitutes a surprisingly complex succession of exonucleolytic trimming events yielding the mature 3´-end of $5.8S_{S/L}$ rRNA and the mature 5´-end of 25S rRNA. ITS2 processing is initiated by a single cleavage event at the C_2 processing site executed by the endonuclease Las1p (Gasse et al. 2015). The C_2 site is located in the ITS2 within a strongly conserved region, directly adjacent to a G-C base pairing (Geerlings et al. 2000; Granneman et al. 2011).

Two secondary structure models were initially predicted for the ITS2 termed the “hairpin-model” (Yeh and Lee 1990) and the “ring-model” (Joseph et al. 1999). Later, a dynamic conformational model in which the both previous suggested secondary structure predictions transit into one another, depending on the pre-ribosomal assembly and processing status, has been suggested (Côté et al. 2002). In the 2010s, a third model that comprises a proximal ring structure, continued with a hairpin structure, was introduced (Coleman 2015). Later, cryo-EM analyses in which a proximal stem could be resolved at intermediate pre-ribosomes put emphasis on this model prediction (Wu et al. 2016). Moreover, tethered tertiary structure probing approaches have as well indicated, that the “ring-pin” model, presented in 2015, likely reflects the *in vivo* situation (Pöll et al. 2017). Cleavage at site C_2 creates a free hydroxyl group at the 5´-end of the 26S pre-rRNA which is being phosphorylated by Grc3p (Gasse et al. 2015). This provides a starting point for a set of exonucleases: Rrp17, Xrn1p as well as Rat1p and its co-factor Rai1p successively process the ITS2, forming the mature end of 25S rRNA (Geerlings et al. 2000; Oeffinger et al. 2009). Concomitantly with the formation of the 5´-end of 25S rRNA, its 3´-end is generated by a so far unknown nuclease. Trimming of the remaining ~140 nucleotides from the 7S pre-rRNA to form the mature 3´-end of $5.8S_{S/L}$ requires in a first instance the nuclear exosome which includes several 3´-5´ exonucleases. The 7S substrate is first trimmed to a precursor intermediate of $5.8S_{S/L}$ pre-rRNA that is prolonged at its 3´-end by 30 nts which is further processed to the 8 nts extended 6S pre-rRNA, involving the action of the exosome associated nucleases Rrp44p and Rrp6p (Mitchell et al. 1996; Briggs et al. 1998; Allmang and Tollervey 1998; Liu et al. 2006; Lebreton et al. 2008b). Besides, the ATP dependent helicase Mtr4p as well plays an indispensable role

to successively perform the indicated processing steps, probably by unwinding secondary structure motifs of the ITS2 and by guiding the exosome to the pre-rRNA (La Cruz et al. 1998; Fromm et al. 2017). The final 3´-end maturation of $5.8S_{S/L}$ occurs in the cytoplasm after nuclear export of the pre-ribosomes (Thomson and Tollervey 2010). The 3´-5´exonucleases Rex1/Rex2/Rex3, members of the RNase D family, further shorten the 6S pre-rRNA. However, solely the former two were described to exhibit nuclease activity on the 6S pre-rRNA substrate (van Hoof et al. 2000). Finally, the mature 3´-end of $5.8S_{S/L}$ rRNA is created by the putative, non-essential nuclease Ngl2p (Faber et al. 2002).

Besides the formation of mature rRNAs derived from the 35S pre-rRNA transcript, the 5S rRNA is separately transcribed and processed. As mentioned in 3.2, RNA polymerase III transcribes the 5S rDNA which includes a short 3´-extension. The conversion of the pre-rRNA transcript to mature 5S rRNA occurs kinetically much faster than the formation of 18S, $5.8S_{S/L}$ and 25S rRNA. Its processing involves a single 3´-5´ exonucleolytic trimming event performed by the exonuclease Rex1p (van Hoof et al. 2000). However, mutant analyses have indicated, that 3´-end processing of 5S rRNA constitutes a non-essential step, as 3´-extended versions of 5S rRNA have been found to assemble in fully functional 60S ribosomal subunits (Nariai et al. 2005).

To ensure that only functional ribosomes are produced, pre-ribosomal biogenesis breakdowns along the route to mature subunits have to be instantly detected and according particles have to be efficiently degraded. Unless, defects during pre-ribosomal maturation can result in aberrant precursor populations. These incorporate mis- or non-processed pre-rRNA species and hence accumulate pre-rRNAs over one another, which would trigger a massive accumulation of pre-ribosomal intermediates. This in turn would interfere with the abundance of assembly factors and snoRNAs required for ribosome biosynthesis through sequestration of these components in dead-end products (Houseley and Tollervey 2009).

The major pathway involved in quality control and degradation of pre-rRNA incorporated in defective pre-ribosomes involves the nuclear exosome and the TRAMP complex. Notably, as described above, the exosome is as well involved in the 3´-end formation of the $5.8S_{S/L}$ rRNA. The TRAMP complex contains the putative RNA helicase Mtr4p, the zinc knuckle RNA binding protein Air1p or Air2p and the poly(A) polymerase Trf4p orTrf5p (Vanácová et al. 2005; LaCava et al. 2005). The latter ones polyadenylate aberrant pre-rRNAs, which serves as signal for subsequent degradation by the nuclear exosome, whose recruitment is mediated by Mtr4p (Bernstein et al. 2008). Interestingly, it has been shown, that the poly(A) polymerase Trf4p stimulates the helicase activity of Mtr4p and, in turn, Mtr4p modulates Trf4p activity to slow down the polyadenylation after introduction of only 3-4 adenosines to the RNA (Jia et al. 2011; Jia et al. 2012). However, it has not been confirmed yet if these *in vitro* findings reflect the *in vivo* situation. Moreover, it has not been completely clarified how the

TRAMP complex differentiates between aberrant and functional pre-rRNA species. However, current analyses seem to confer substrate specificity on Trf4p and Trf5p (Delan-Forino et al. 2020).
A further example for degradation of aberrant pre-rRNAs is the 5´-3´ exonuclease Rat1p (FANG et al. 2005), which is also involved in formation of the 5´-ends of both $5.8S_S$ and 25S rRNA (see above). This raises the question for mechanisms that prevent "over-trimming" by exonucleases which could lead to non-functional pre-rRNAs and to defects in ribosome biogenesis. For Rat1p it is supposed, that binding of rpL17 located immediately downstream of the B_{1S} site (Ben-Shem et al. 2011) might serve as a roadblock for Rat1p, preventing it from trimming of mature 5.8S rRNA sequences through this rRNA-protein interaction (Henry et al. 1994; Pöll et al. 2009; Sahasranaman et al. 2011).
In general, both functional as well as aberrant pre-rRNAs are at any time a potential substrate for a plenty of intracellular exonucleases. Those seem to not exhibit a pronounced sequence specificity for their targets, representatively shown for Rat1p. Therefore, access of nucleases to pre-rRNA targets has to be strictly controlled. This could be achieved by different mechanisms for instance occupancy of free rRNA ends with proteins or incorporation into the core of pre-ribosomes resulting in steric inaccessibility.

3.4 Modification of ribosomal RNAs

In addition to processing, pre-rRNA is extensively modified at specific sites. In general, ribosomal RNAs are intensively modified RNA species within eukaryotic cells – up to 2% of the bases are modified in *Saccharomyces cerevisiae,* that often cluster in mechanistically important sites, for example the decoding center, the tRNA binding sites of the subunit interface (for reviews see Watkins and Bohnsack 2012; Sloan et al. 2017, and citations therein). Modifications are most frequently referred to 2´-O-methylations and uridine isomerization into pseudouridine which are introduced at an early stage of ribosome biogenesis, probably co-transcriptionally (Retèl et al. 1969; Brand et al. 1977; Kos and Tollervey 2010). For a vast majority, these modifications are introduced by two families of snoRNPs – box C/D and box H/ACA. Both snoRNP families contain a set of individual proteins that confer structural stability and catalytic activity which his necessary to introduce the base modifications. The enzyme for introducing 2´-O-methylations by box C/D snoRNPs is represented by Nop1 (Tollervey et al. 1993; Galardi et al. 2002), whereas pseudouridines are introduced by box H/ACA-snoRNPs through the catalytic activity of Cbf5p (Lafontaine et al. 1998; Zebarjadian et al. 1999). By reason, that each rRNA nucleotide depicts a potential target for these base modifications, a plethora of variable snoRNAs incorporated into these complexes confer substrate specificity and lead the modification machineries to their distinct RNA targets for both box C/D- (Cavaillé et al. 1996; Kiss-László et al. 1996) as well as for box H/ACA snoRNPs (Ni et al. 1997; Ganot et al. 1997) snoRNPs.

Besides the protein-snoRNA complexes that introduce a myriad of 2´-O-methylations and pseudouridines to rRNA, single proteins with catalytic activity are as well known to introduce base modifications, acting as stand-alone enzymes. These attach 8 different types of modifications to nucleotides at specific positions within the large and small ribosomal subunit, whereof most of them are methylations and acetylations, except one complex hypermodification (for review see Sloan et al. 2017). The definite function of single base modifications is mostly not clear. The current opinion describes the presence of sub-clusters of modifications, which act cooperatively to optimize ribosomal structure and function. This could be advantageous for instance for ribosome biogenesis or translational fidelity and processivity (King et al. 2003; Baxter-Roshek et al. 2007; Liang et al. 2007, 2009; Baudin-Baillieu et al. 2009; Sharma and Lafontaine 2015)

3.5 Assembly of the ribosomal subunits

The synthesis of ribosomes is one of the most demanding cellular activities that appears to be a process of extraordinary complexity, involving a vast majority of cellular resources and spanning over various cellular compartments. Under favorable growth conditions, the assembly lines of the ribosome production machinery are in continuous operation. A single rapidly growing yeast cell is equipped with approximately 200,000 ribosomes. To cope with the demand of this massive quantity, each cell has to produce more than 2,000 ribosomes per minute. To do so, 60 % of total transcription is devoted to rRNA and additionally 50 % of RNA polymerase II transcription as well as 90 % of mRNA splicing are devoted to the production of ribosomal proteins (Warner 1999).

In addition to structural components of the subunits (rRNAs, r-proteins), these processes require the function of more than 70 snoRNAs and approximately 200 ribosome biogenesis factors which transiently interact with the maturing pre-ribosomes at different maturation states (Klinge and Woolford 2019). These biogenesis factors (BFs) or assembly factors (AFs) are involved in maturation events of pre-ribosomes during their maturation pathway (see 3.5.1 and 3.5.2). Many of them have been assigned to be important for a distinct maturation event since their depletion often leads to a specific phenotype. Most our knowledge about eukaryotic ribosome biogenesis factors is derived from investigation of the model organism *Saccharomyces cerevisiae*. This organism is easily accessible for genetic manipulations, cell biological techniques and biochemical approaches. However, the detailed molecular function for most of them remains unclear. Some of them are predicted or proved to include enzymatic activity and are therefore depicted as GTPases, ATPases, RNA helicases, Kinases or phosphatases that act during subunit maturation.

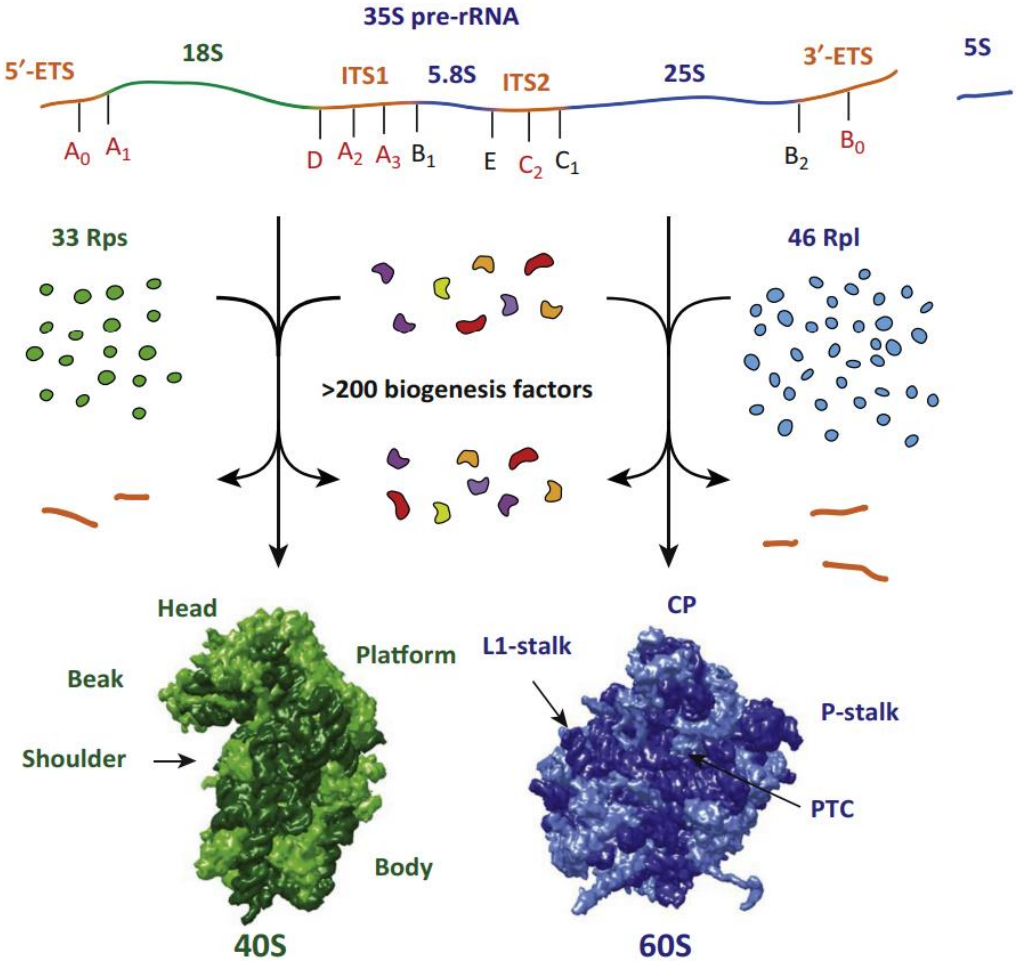

Figure 7: Schematic representation of ribosome biogenesis in the yeast *Saccharomyces cerevisiae*.
Ribosome biogenesis requires the coordination and catalyzation of approximately 200 biogenesis factors (various colors) which are necessary to form the mature subunits. R-proteins of the small 40S (light green) and of the large 60S (light blue) ribosomal subunit are synthesized from mRNA transcribed by RNA polymerase II (Pol II). The 35S pre-rRNA (dark blue) and the 5S rRNA (dark green) are transcribed by Pol I and Pol III, respectively. External and internal transcribed spacer regions (5´-ETS, ITS1, ITS2, 3´-ETS) are removed by endo- and exonucleolytic processing events during ribosome biogenesis (indicated in orange and black on the 35S pre-rRNA transcript) to obtain the mature 18S, 25S and 5.8S rRNAs. Maturation of the subunits is finalized in the cytoplasm which ultimately contain 33 or 46 r-proteins in the small or the large subunit, respectively. Architectural hallmarks of both the subunits are annotated: The head, beak, platform, shoulder and body of the 40S- as well as the central protuberance (CP), the L1-stalk and the P-stalk of the 60S subunit. Adopted from (Kressler et al. 2017).

Biogenesis factors that bind to the earliest, nascent pre-ribosomal particles are supposed to protect the pre-rRNA from degradation, to scaffold the pre-ribosomal subunits to enhance the establishment of proper sub-structures, and to compact the earliest assembly intermediates (see 3.5.2.1). Others are endo- and exonucleases which process pre-rRNA at specifically prescribed sites (see 3.3). Energy consuming ATPases and GTPases might induce structural rearrangements and/or the release of proteins (see 3.5.1 and 3.5.2). Some factors were described to monitor the correct assembly and maturation events, providing a quality control checkpoint for the further biogenesis (Matsuo et al. 2014). Others in turn bind to mechanistically functional sites of the pre-ribosomal subunits to shield them from translation factors and to prevent a premature entry into the translation cycle. The spectrum of functions that can be assigned to biogenesis factors is large. Often, binding and release of

biogenesis factors to and off pre-ribosomes are linked to certain maturation events like stable incorporation of r-proteins, structural rearrangements, pre-rRNA processing or nuclear export. The following chapters focus on the processes that ensure a proper production of functional ribosomal subunits, starting with the transcription of the ribosomal RNAs, co-transcriptional assembly and processing events in the nucleolus (see further chapters 3.5.1 and 3.5.2 for details).

3.5.1 Assembly of the SSU

3.5.1.1 Formation and assembly of the small subunit processome - the initial precursor for both ribosomal subunits

This chapter describes the formation of the SSU processome. A short overview on the description of the terminal knobs, observed in Miller spreads, which represent the SSU processome will be given. Furthermore, the formation of the 5´-ETS particle and the successive assembly of proteins and protein modules to the nascent transcript will be outlined. The formation and incorporation of the four small subunit domains, ultimately yielding the SSU-processome will be addressed in more detail.

The development of the tandem affinity purification (TAP) method depicts a milestone in molecular technologies which allows purification of a single bait protein from its native environment without overexpression (Rigaut et al. 1999). In combination with mass spectrometry all directly or indirectly interacting components can be identified in a single experiment. The TAP-tag technique has been intensively used over the last three decades to study the composition of SSU and LSU precursor intermediates. By using this approach, the SSU/LSU maturation pathway can be surmised by the purification of a plethora of pre-ribosomal particles with differing bait proteins.

In order to study ribosome biogenesis, it is important to deduce the starting point at which the first pre-ribosomal intermediates assemble. Pioneering experiments in this regard have been performed in the 1970s. It was described that 90S pre-ribosomes containing 35S pre-rRNA are processed to 43S and 66S particles which depict the precursors of the small and the large ribosomal subunit, respectively (Udem and Warner 1972; Trapman and Planta 1975). However, deeper analysis of these very early arising ribosomal precursors remained very challenging for several reasons. In 2002, the group of Susan Baserga characterized the terminal knobs present at the 5´-ends of nascent pre-rRNAs (Dragon et al. 2002) which have been initially observed in amphibian oocytes (Miller and Beatty 1969). In fact, nearly one decade earlier, these terminal knobs were already suggested to constitute ultrastructural visualizations of an 5´-ETS processing complex (Mougey et al. 1993).

For the Baserga group it appeared, that both size of the knobs deduced by electron microscopy and their sedimentation coefficient were similar to mature ribosomes. Moreover, purification and

compositional analysis of these macromolecular structures revealed the integrity of the U3 snoRNA as well as SSU r-proteins and components of snoRNPs. Additionally, 17 yet undescribed proteins were identified and named Utp 1-17 (“U three proteins). Due to its composition found in these analyses by the group of Susan Baserga (Dragon et al. 2002), it is described as “SSU-processome”. Notably, term “processome” for ribosome biogenesis has been proposed earlier by the description of U3 associated components (Fournier and Maxwell 1993).

At the same time, experiments of an independent research group provided the purification of pre-ribosomes via epitope tagged factors, that sedimented at 90S and co-precipitated both the 35S pre-rRNA containing 5´-ETS sequence and the U3 snoRNA. Additionally thirty five non-ribosomal proteins, amongst others factors that are required for 18S synthesis were detected, whereas most pre-60S factors were lacking (Grandi et al. 2002). The identification of a related but not identical complex was suggested to reflect the terminal knobs. This underlined the assumption that these terminal knobs of rDNA chromatin spreads represent initial processing machineries of maturing pre-ribosomes. Notably, the non-ribosomal proteins were later classified as components of the SSU processome as they co-purify SSU components, localize to the nucleolus and affect 18S rRNA maturation (Bernstein et al. 2004).

Notably, the following steps described in this chapter concerning the formation of the SSU processome occur co-transcriptionally. Evidence therefore has been obtained since depletion of the U3 snoRNA or other components of the SSU processome as well as mutations of 5´-ETS elements leads to the absence of terminal knobs at the nascent pre-rRNAs (Mougey et al. 1993; Dragon et al. 2002; Osheim et al. 2004).

The first step of the SSU processome formation is the assembly of the heptameric tUTP/UTP-A complex to the nascent pre-rRNA (Gallagher et al. 2004; Pérez-Fernández et al. 2007). The tUTP-complex is formed by the proteins Utp4, Utp5, Utp8, Utp9, Utp10, Utp15 and Nan1/Utp17. The complex was further described to link transcription and pre-rRNA processing, which is stimulated by binding to rDNA chromatin. Therefore, this subset of the SSU processome was termed t-UTP complex (U3 proteins required for transcription) (Gallagher et al. 2004). The initial characterization of this protein module as one out of three 90S-associated subcomplexes by high-throughput proteomic studies has detected Pol5p instead of Utp5 and therefore termed “UTP-A” (Krogan et al. 2004). However, due to inconsistent nomenclature throughout the literature, in the following the tUTP and the UTP-A complex are referred to two different complexes containing either Utp5 or Pol5, respectively. The tUTP/UTP-A complex does not depend on other subunits or r-proteins for binding which indicates a very early and autonomous event (Gallagher et al. 2004; Pérez-Fernández et al. 2007; Jakob et al. 2012). Supporting this finding, the tUTP/UTP-A complex was co-purified by a proximal part of the 5´-ETS (Zhang et al. 2016; Gallagher 2019).

The subsequent further assembly of SSU components divides into two mutually independent assembly branches. In the first branch, the Pwp2p/UTP-B complex consisting of Pwp2p/Utp1, Dip2p/Utp12, Utp6, Utp13, Utp18 and Utp21 (Krogan et al. 2004), as well as the U3 snoRNP containing the U3 snoRNA, Nop1, Nop56, Nop58, Snu13p and Rrp9 associate with the tUTP/UTP-A primed 5´-ETS (Watkins et al. 2000; Dosil and Bustelo 2004; Pérez-Fernández et al. 2007). These assembly events ultimately lead to the formation of the 5´-ETS particle (Figure 8) (Chaker-Margot et al. 2015). The assembly of UTP-B is mediated via Pwp2p, and Nan1p of the tUTP/UTP-A complex (Pérez-Fernández et al. 2007; Boissier et al. 2017).

The U3, which depicts the most intensively studied snoRNA belongs to the box C/D family of snoRNAs which acts as a guide for 2´-O-methylation. Notably, there is no modification associated to U3. However, this special snoRNA plays an essential role in 90S assembly. The U3 has several binding sites within the 5´-ETS and the 18S rRNA sequence which contributes to the scaffolding and organization of the nascent pre-ribosomes and hence the 90S structure, thereby promoting early cleavage and folding events (Beltrame and Tollervey 1992, 1995; Hughes 1996; Méreau et al. 1997; Sharma and Tollervey 1999; Dutca et al. 2011; Marmier-Gourrier et al. 2011; Kudla et al. 2011). Moreover, binding of U3 to regions where the central pseudoknot is formed (see Figure 1) during later biogenesis might prevent its premature folding. The U3 snoRNP and especially binding of tUTP/UTP-A- and UTP-B to the nascent pre-rRNA and to the U3 snoRNA act as chaperoning complexes which initiate eukaryotic ribosome assembly (Hunziker et al. 2016). Binding of the Mpp10-complex consisting of Im3p, Imp4p and Mpp10p (Lee and Baserga 1999; Granneman et al. 2003) which might occur as single heterotrimeric protein complex downstream of UTP-B and U3 snoRNP association (Pérez-Fernández et al. 2011), further expands the protein/RNA network through interactions with the U3 snoRNA (Wehner et al. 2002; Gérczei and Correll 2004; Gérczei et al. 2009).

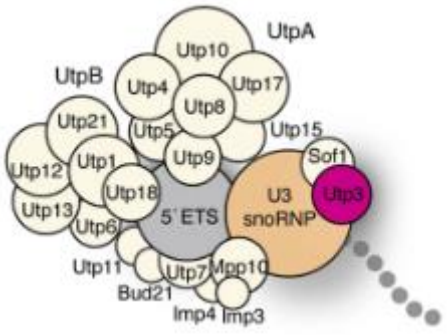

Figure 8: Protein components of the 5´-ETS.
Schematic representation of the RNA and protein component of the 5´-ETS particle obtained by mass spectrometry analysis. The 5´-ETS is colored in grey, the U3 snoRNP in orange. Further proteins belonging to the tUTP/UTP-A- or the UTP-B-complex (for more specific definition see the continuous text) as well as additional proteins of the 5´-ETS particle are colored in beige. Utp3 is colored in pink. Adapted from (Chaker-Margot et al. 2015).

The binding of additional 5´-ETS proteins like Utp3/Sas10p, Utp7, Utp11, Utp16/Bud21p, Fcf2p, Sof1 and later the proposed A1 site nuclease Fcf1p/Utp24 (Wells et al. 2016) completes the formation of the 5´-ETS particle (Figure 8). This indicates that the 5´-ETS can nucleate a large particle with an approximate weight of 2 MDa that likely corresponds to the small terminal knobs on early rRNA transcripts (Chaker-Margot et al. 2015; Zhang et al. 2016). In total, the assembly events forming the 5´-ETS particle generates a very dense structure stabilized by various protein-protein, protein-RNA and RNA/RNA interactions, which maintain the fold of the rRNAs. In total, this provides a platform for the further association of assembly factors and SSU r-proteins that promote the further maturation of the pre-ribosomal particle (Chaker-Margot et al. 2015; Zhang et al. 2016; Chaker-Margot et al. 2017; Barandun et al. 2017; Sun et al. 2017). Once the 5´-ETS particle is formed, the formation of the 5´-, central-, 3´-major- and 3´-minor domain occurs in sequential, stage-specific events (Chaker-Margot et al. 2015).

The four subdomains form the mature 40S subunit, including all architectural landmarks (see 3.1.3). Notably, whereas the 5´-ETS particle incorporates no r-proteins, the 5´-domain is decorated with Rps4, Rps6, Rps8, Rps9, Rps11, Rps23 and Rps24 (Sun et al. 2017). It should however be noted that the binding of r-proteins mentioned here and, in the following, represents their appearance in cryo-EM analyses. This does not necessarily reflect the real situation, as solely the thorough assembly of proteins reveals their presence in EM. Proteins might already interact with the maturing pre-ribosome but are not resolved due to high structural flexibilities. To further address the association of r-proteins, functional biochemical studies, for instance depetion analyses are indistinguishable (see for example Jakob et al. 2012).

During successive formation of the 5´- domain, the U14 snoRNP associates, introducing a 2´-O-methylation to 18S rRNA nucleotide C415 (Liang and Fournier 1995). Besides, a further set of assembly factors is recruited to the nascent pre-rRNA (Figure 10). However, the detailed function for most of them is not yet further defined. Among these factors are Bfr2p and Enp2p which are supposed to recruit the DEAD-box RNA helicase Hca4/Dbp4 to the pre-ribosome (Soltanieh et al. 2014), which is in turn required for the release of the U14 snoRNA at a later step of the biogenesis process (Kos and Tollervey 2005). The assembly factor Lcp5p, which was found to interact with Bfr2p (Uetz et al. 2000), might as well play a role for efficient recruitment of Hca4/Dbp4.

The central domain includes the SSU r-proteins Rps1, Rps7, Rps13, Rps14, Rps22, Rps26 and Rps27 (Sun et al. 2017). Concurrently the H/ACA box snoRNAs snR30 and snR10 associate. In combination with the U3 and U14 snoRNAs, this set of RNA molecules is required for pre-rRNA processing at sites A_0, A_1 and A_2 (position of the processing sites indicated in Figure 6) (Li et al. 1990; Hughes and Ares 1991; Morrissey and Tollervey 1993; Beltrame and Tollervey 1995; Liang and Fournier 1995; Fayet-Lebaron et al. 2009). Further, Rrp5p is associated to the central domain, which as well binds rRNA

sequences of the large subunits. It is therefore described to play a role for the maturation of both ribosomal subunits (Lebaron et al. 2013). At next, association of UTP-C consisting of Utp22, Rrp7p and four subunit of casein kinase II occurs (Cka1p, Cka2p, Ckb1p and Ckb2p) (Krogan et al. 2004; Pérez-Fernández et al. 2007; Lin et al. 2013). Importantly, the binding of UTP-C is dependent on the preceding association of Rrp5p (Vos et al. 2004; Pérez-Fernández et al. 2007). Binding of Rrp5p and subsequent association of the UTP-C complex depicts the second independent assembly branch in a partial hierarchical order after association of tUTP/UTP-A as described above. Notably, the binding partners of Rrp5p, Noc1p and Noc2p associate as well at this state forming a heterotrimeric complex which plays an essential role for the maturation of the large ribosomal subunit (Hierlmeier et al. 2012). It should be noted, that the association of Noc1p/Noc2p was not found by the Ye- but by the Klinge-group which may be due to different experimental techniques (Chaker-Margot et al. 2015; Zhang et al. 2016). In addition, Rok1p which assembles one step earlier than Rrp5p (Zhang et al. 2016) and a series of additional assembly factors appear to be present upon finishing the central domain of the 18S rRNA (Figure 10).

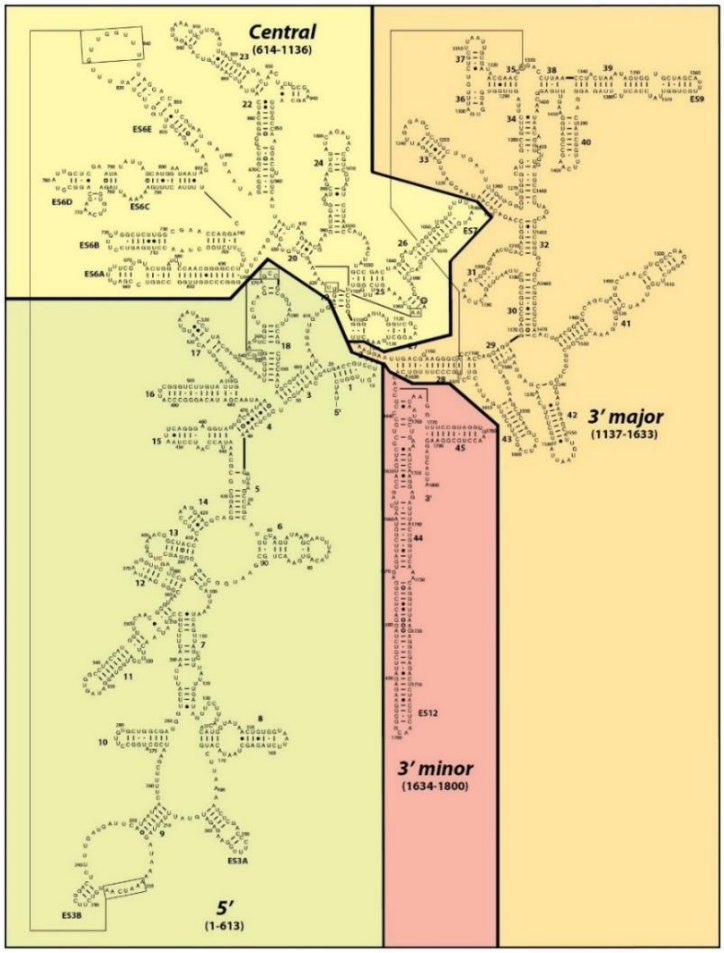

Figure 9: Secondary structure domains of the 18S rRNA from *Saccharomyces cerevisiae*.
The 18S secondary structure domains are annotated and colored as follows: 5´-domain in green, central domain in yellow, 3´-major domain in orange, 3´-minor domain in red. Corresponding nucleotide numbers are annotated. Base pairings which are involved in the formation of tertiary structures are indicated: Lines correspond to canonical base-pairs, filled and empty dots to non-canonical ones. Adopted from (Chaker-Margot et al. 2015).

The building of the 3´-major domain, which forms the head in the mature small subunit is accompanied by the association of only few assembly factors and the r-proteins Rps5, Rps12, Rps16, Rps28 and Rps31 (Chaker-Margot et al. 2015; Zhang et al. 2016; Sun et al. 2017). In contrast to the 5´-domain, which adopts a near-mature conformation upon its assembly, the shape of the central and the two 3´-domains remain rather unstructured in the SSU-processome (Chaker-Margot et al. 2017; Barandun et al. 2017; Sun et al. 2017).

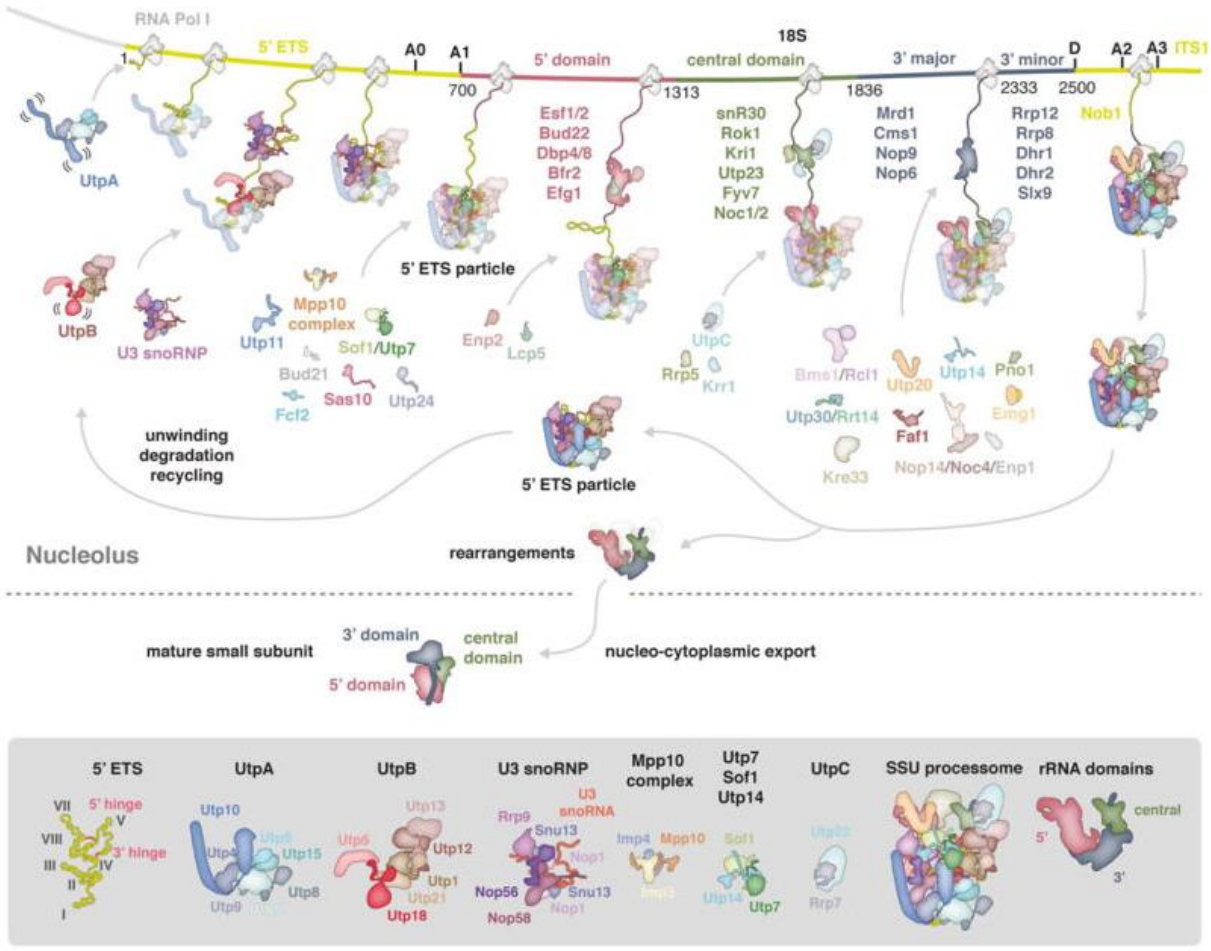

Figure 10: Co-transcriptional assembly of the small subunit processome in *Saccharomyces cerevisae*.

Schematic representation of assembly events that contribute to the formation of the SSU processome in the nucleolus and subsequent maturation to the SSU in the cytoplasm. A section of a rDNA repeat is shown: The 5´-ETS and the ITS1 are yellow and the 18S in various colors according to secondary structure domains (5´-domain in red, central domain in green, 3´-major and 3´-minor domains in slate). Factors of the assembled SSU processome are shown as schematic outline, whereas transient protein component are colored according to the rRNA domain they are associated with. In the lower part, the major components of the SSU processome are shown in more detail. Adopted from (Barandun et al. 2018).

The formation of the 3´-minor domain is accompanied with the association and the release of a large subset of assembly factors, several of them are further characterized in the following. To current knowledge, the finishing of the 3´-minor domain leads to the association of 12 assembly factors and to the dissociation of 14 (Chaker-Margot et al. 2015; Zhang et al. 2016; Sun et al. 2017).

Several biogenesis factors associated with the 3´-minor domain were found to stabilize the overall fold of the SSU processome through bridging interactions between the secondary structure subunits (Chaker-Margot et al. 2017). Bms1p is the only GTPase present in the 90S pre-ribosome (Gelperin et al. 2001), which forms a heterodimer with Rcl1p, both being important for pre-rRNA processing (Billy et al. 2000; Wegierski et al. 2001; Delprato et al. 2014). The Rcl1p/Bms1p complex bridges the 3´-major and the 5´-domains (Chaker-Margot et al. 2017). Besides, the GTP hydrolysis of Bms1p might induce a mechanical force within the pre-ribosomal particle that contributes to a structural rearrangement which facilitates cleavage at site A_2 (Delprato et al. 2014) and the further association of assembly factors, attributing Bms1p a role as second-order nucleator (Pérez-Fernández et al. 2011). The acetyltransferase Kree33p, which sits atop of the Rcl1p/Bms1p dimer, connects both the 5´- with the 3´-domains and Bms1p with Enp2, located at the 5´-domain (Chaker-Margot et al. 2017; Sun et al. 2017; Barandun et al. 2017). Utp20, connects the 5´- with the 3´-minor domain and with parts of the 5´-ETS (Chaker-Margot et al. 2017). Noc4p, which forms a stable complex with Nop14 (Milkereit et al. 2003); Kühn et al. 2009) associates with the pre-ribosomes once the head structure is formed and bridges the 5´-ETS with the central and the 5´-domain through various interactions, amongst others with components of the tUTP/UTP-A complex (via Utp4) and the Rcl1p/Bms1p dimer (Barandun et al. 2017; Chaker-Margot et al. 2017). Therefore, the Noc4p/Nop14p complex can be regarded as large architectural factor module. The recruitment of Noc4p to pre-ribosomes is however dependent on a certain assembly state which in turn influences the assembly of further r-proteins (Jakob et al. 2012). Altogether, the short- and long range connections formed within the SSU-processome contribute to its shape and functionality (Figure 11).

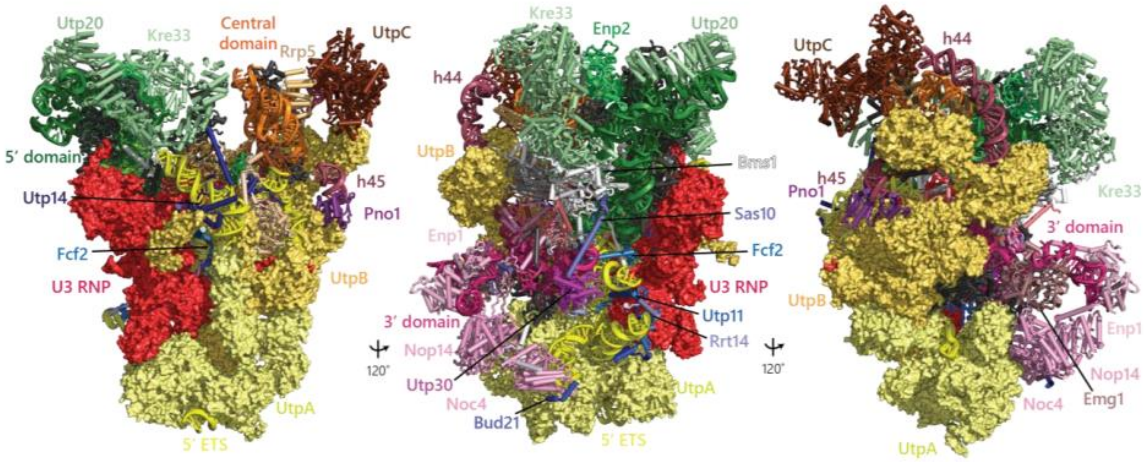

Figure 11: Structure of the SSU processome from *Saccharomyces cerevisiae*.
Three views on the fully assembly SSU processome, each rotated by 120 degrees. The 5´-ETS rRNA is shown in yellow. Associated tUTP/UTP-A (yellow), UTP-B (orange yellow) and the U3 snoRNP (red) are annotated. The secondary structure domains of the 18S rRNA are labeled and colored in green (5´-domain), orange (central), pink (3´-major) and purple (3´-minor). Associated proteins are shown in similar colors. Adopted from (Chaker-Margot 2018).

Besides the recruitment of new factors, others are released. This might be triggered through the unwinding activity of RNA helicases, of which several are present within the SSU-processome (Granneman et al. 2006; Chaker-Margot et al. 2015). For instance Dbp4p, which is required for the release of U14 snoRNA (Kos and Tollervey 2005; Soltanieh et al. 2015) or Rok1p, which releases snR30 from the pre-ribosome (Bohnsack et al. 2008; Hoareau-Aveilla et al. 2012; Wells et al. 2017). The activity of the latter one may as well involve Rrp5p, as ATP hydrolysis to ADP by Rok1p has been shown to trigger Rrp5p release from pre-40S subunits, allowing its binding to pre-60S subunits where it can fulfill its function for large subunit biogenesis (Khoshnevis et al. 2016).

3.5.1.2 Final assembly of the small subunit

Biogenesis to mature 40S subunits is accompanied by several significant structural and compositional changes of the SSU processome. The most dramatic events involve the endonucleolytic cleavage at processing sites A_1 and A_2 (see also 3.3), formation of the central pseudoknot as well as the complete removal and degradation of the 5´-ETS particle. The latter one is of special importance in order to recycle associated biogenesis factors, which again become available for the SSU-processome assembly machinery. The removal of the 5´-ETS is suggested to be performed by the exosome (Allmang et al. 2000b). However, the mechanism by which this process is regulated and mediated is not fully understood. One possibility is indicated by Utp18, a component of the UTP-B complex which harbors an arch interaction motif (AIM-domain) at its N-terminus. It was shown to interact with Mtr4p, an adaptor of the exosome, thereby possibly recruiting the exosome to the 5´-ETS (Thoms et al. 2015). This could be facilitated via the concerted action of Lcp5p and Sas10p, located at the 18S 5´-domain and both containing a protein domain that resembles the exosome cofactor Rrp47 (Costello et al. 2011; Barandun et al. 2017). In order to process the pre-rRNA at its intrinsic cleavage sites, the helicase Dhr1p releases the U3 snoRNA from the SSU processome, which promotes once the formation of the central pseudoknot structure and twice the cleavage at sites A_1 and A_2 by Utp24 or Rcl1p (Bleichert et al. 2006; Horn et al. 2011; Sardana et al. 2015; Wells et al. 2016).

To ensure export competence of the pre-ribosomes into the cytoplasm, most of the assembly factors with exception of Enp1, Pno1p and Rrp12p are removed, whereas Rio2p, Ltv1p, Dim1p and Trs1p are recruited, as well as a further set of r-proteins (Schäfer et al. 2003; Ferreira-Cerca et al. 2005; Ferreira-Cerca et al. 2007; McCaughan et al. 2016; Heuer et al. 2017; Scaiola et al. 2018).

Once in the cytoplasm, a series of concerted events takes place to form the mature small subunit. Although the temporal succession of these events cannot be defined, the interdependence of certain biogenesis factors is well understood (Figure 12).

Rps3, which is involved in the late SSU maturation steps, assembles with the pre-40S subunit through incorporation of its C-terminus. Its associated chaperoning factor Yar1p is replaced by Ltv1p, thereby fixating the N-terminal domain of Rps3 (Mitterer et al. 2016). Essential contacts between Rps20 and

Rps3 are formed, which weakens the interaction of Ltv1p with the pre-40S subunit. Subsequently, Hrr25p phosphorylates Ltv1p which possibly disrupts its interaction to Enp1 (Mitterer et al. 2019). Notably, Enp1p and Ltv1p which chaperone the immature structure of the beak. This results in release of Enp1p/Ltv1p. In turn, Ltv1p release results in orientation of Rps3 at its final position within the subunit (Mitterer et al. 2016). Upon Enp1p/Ltv1p release, Rps10 and Asc1p to bind to the pre-40S subunit to form the mature beak (Schäfer et al. 2006; Ghalei et al. 2015; Collins et al. 2018; Scaiola et al. 2018).

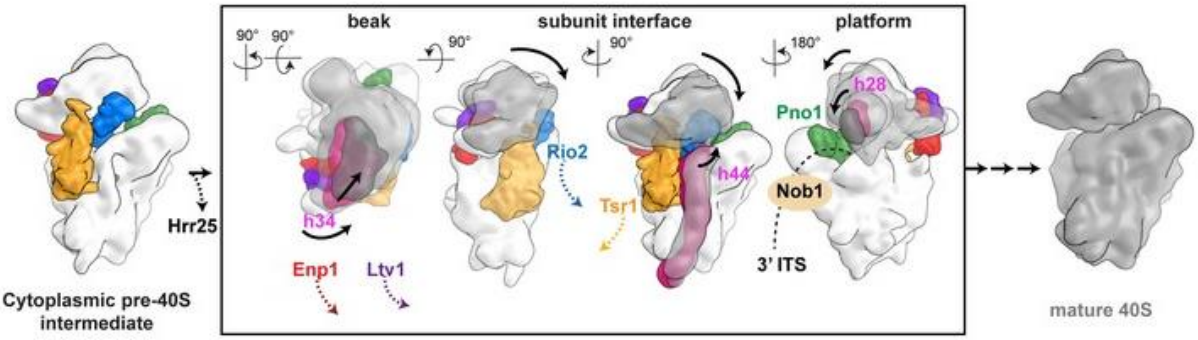

Figure 12: Model for the final cytoplasmic maturation of the small subunit in *Saccharomyces cerevisiae*.
The boxed region of this scheme represents a single species and indicates the main release of assembly factors and structural rearrangement events of rRNA (white/pink for the pre-40S- and gray/dark gray for the mature 40S subunit) to form the mature 40S subunit. Notably, the temporal succession of the events is not defined. Adopted from (Scaiola et al. 2018)

Crosslinking studies and cryo-EM have revealed that assembly factors are positioned on the pre-40S particle in a way to prevent premature translation initiation (Granneman et al. 2010; Strunk et al. 2011). Tsr1p and Rio2p are located at the subunit interface, blocking the final formation of the decoding center (Strunk et al. 2011; Heuer et al. 2017). It is suggested that the release of Enp1p/Ltv1p induces a conformational rearrangement which enables Rio2p to success its intrinsic ATPase activity. Doing so, Rio2p is released from the pre-40S particle by autophosphorylation, and subsequently Tsr1 (Ferreira-Cerca et al. 2012; Scaiola et al. 2018). Notably, the correct position of Rps20 has been shown to be essential for the release of both Enp1p/Ltv1p and Rio2p (Mitterer et al. 2019).

Pno1p (partner of Nob1p) is associated with the D-site endonuclease Nob1p (Fatica et al. 2003a; Lamanna and Karbstein 2009) (see 3.3). Rio1p associates with pre-40S subunits after Rio2p release, whereas its catalytic activity regulates its pre-40S association (Ferreira-Cerca et al. 2014). Hydrolysis of ATP by Rio1p then triggers Pno1p release, promoting Nob1p to perform its endonucleolytic activity on the pre-rRNA (Turowski et al. 2014). The final SSU maturation steps involves a translation-like cycle, initiated subsequently to the release of Rio2p/Tsr1p through binding of the translation initiation GTPase eIFB5 and association of the 60S subunit (Strunk et al. 2012; Lebaron et al. 2012). Moreover, the Rio1p-Nob1p-Pno1p network has been found to establish a checkpoint, preventing pre-mature SSUs to join the translating pool of mature ribosomes (Parker et al. 2019)Together, these mechanisms serve as quality control mechanism for the newly synthesized subunits.

3.5.2 Assembly of the LSU

3.5.2.1 Nucleolar stages of large subunit assembly

This chapter focuses on several aspects of early to intermediate steps of LSU assembly: i) co-transcriptional binding of biogenesis factors and initial compaction of earliest LSU-precursors, ii) early maturation steps with focus on $27SA_2$ pre-rRNA processing, iii) intermediate maturation steps with focus on 27SB pre-rRNA processing and iv) the preparation for the transition of the pre-LSUs into the nucleoplasm. Notably, the particles, which reflect the certain maturation states will be addressed in more detail according to the association of LSU r-proteins and the association/release of biogenesis factors. Some quality control- and checkpoint-mechanisms will be outlined.

Due to the more elaborate structure and composition of the large subunit, its assembly follows a more complex pathway. LSU maturation proceeds via several distinct pre-60S particles that are characterized by the incorporated pre-rRNA species (Figure 6) and the set of assembly factors they are associated with. Most knowledge of LSU assembly is derived from particles that have undergone A_2 processing and are thus separated from the pre-40S subunits. Nevertheless, the presence of several LSU biogenesis factors in particles prior to A_2 cleavage have already been demonstrated – for instance the Rrp5p/Noc1p/Noc2p protein module (Milkereit et al. 2001; Hierlmeier et al. 2012), Npa1p (Dez et al. 2004), the heterotrimer Nop7p/Erb1p/Ytmp1, Rpf2p and Rrs1p (Zhang et al. 2007).
Notably, the latter two are required for incorporation of the 5S RNP consisting of rpL5, rpL11 and the 5S rRNA into pre-ribosomes which apparently occurs at an very early step during biogenesis, as Rpf2p and Rrs1p co-purify 35S pre-rRNA (Zhang et al. 2007). Rpf2p, Rrs1p, rpL5 and rpL11 directly interact with each other and can be isolated as a complex together with 5S rRNA. However, it remained unclear for a long time if this RNP is formed stepwise on the maturing pre-ribosomal particles or recruited *en bloc*. Recent experiments suggest that the nuclear import adaptor protein Syo1p chaperones a pre-5S RNP containing rpL5 and rpL11 as sole protein constituents which gets imported into the nucleus and incorporated in the maturing pre-ribosome (Kressler et al. 2012; Calviño et al. 2015). It is however unclear, whether additional factors, for instance Rpfp2 and Rrs1p, or rearrangements are therefore required. The crystal structure of a Syo1p-rpL5-rpL11 complex suggests, that Syo1p shields the binding site of rpL11 to 25S rRNA which was recently resolved to be located at helix (H) 84 (Leidig et al. 2014; Calviño et al. 2015). Competition of H84 with Syo1p for the rpL11 binding site in its pre-ribosomal context might trigger Syo1p release from the pre-5S RNP.
Nucleolar LSU assembly occurs in a hierarchical fashion (Ohmayer et al. 2013; Gamalinda et al. 2014). Since interactions of biogenesis factors with the earliest pre-ribosomes have been characterized, determining the association of LSU r-proteins at that state is, however, very challenging due to weak interactions, that only strengthen during ongoing biogenesis. The successive formation of early pre-

ribosomal intermediates occurs stepwise as indicated for the small ribosomal subunit (Chaker-Margot et al. 2015; Chaker-Margot et al. 2017), however in a much less dramatic manner for the large subunit (Chen et al. 2017; Chaker-Margot and Klinge 2019).

Formation of the earliest pre-60S particle occurs upon processing at site A_2 (see 3.3), from which point both the large and the small ribosomal subunit follow independent assembly routes. As described in section 3.3.1, A_2 cleavage can occur co- or post-transcriptionally, whereas the selection between these pathways is not fully understood. The further processing of $27SA_2$ pre-rRNA at site A_3 by MRP requires the correct formation of the 3´-ETS and cleavage at B_0 by Rnt1p (Lindahl et al. 1992; Chu et al. 1994b; Elela et al. 1996; Kufel et al. 1999; Allmang and Tollervey 1998; Hitchen et al. 1997). RpL3, the largest LSU r-protein associates very early during LSU biogenesis and spans over various domains, connecting the 3´-end of the 25S rRNA and the 5´-end of the 5.8S rRNA (Ben-Shem et al. 2011). Therefore, and due to the fact that its depletion causes a global pre-ribosomal instability and a drastic reduction of almost all 27S pre-rRNA species, rpL3 is supposed to mediate between the proper 3´-ETS formation and ITS1 processing (Rosado et al. 2007b; Gamalinda et al. 2014). This might provide a checkpoint for subsequent maturation. Furthermore, the long-range interactions formed by rpL3 might contribute to the organization and compaction of pre-ribosomal structure. In general, arising LSU precursors of very early maturation states are compacted from loose to tight assembly, which has also been observed for the SSU-processome (Osheim et al. 2004).

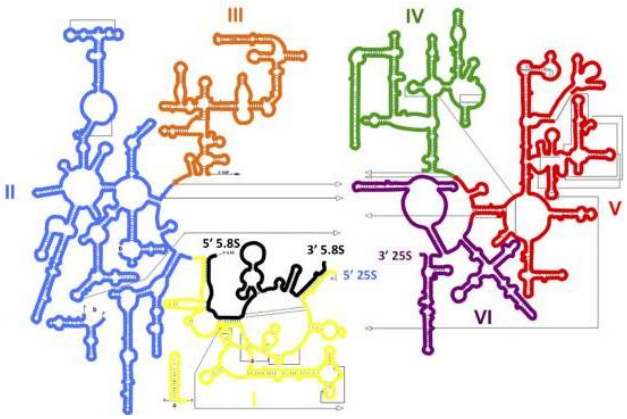

Figure 13: Secondary structure domains of the 25S and 5.8S rRNA from *Saccharomyces cerevisiae*.
The 25S rRNA comprises six secondary structure domains (I-VI) which are highlighted in different colors and annotated. These are phylogenetically conserved throughout all kingdoms of life, although eukaryotic rRNA contains expansion segments which are not found in prokaryotic or archaeal organisms. The sites of base pairing of the 5.8S rRNA (black) with domain I of 25S rRNA (yellow) are shown. Adopted from (Konikkat and Woolford 2017).

A further, well studied assembly factor that is amongst others supposed to contribute to the compaction of pre-ribosomes is Rrp5p. Rrp5p contains 12 RNA-binding motifs, 7 tetratricopeptide repeats (TPR), which are binding domains, and binds at multiple sites on the nascent 35S pre-rRNA transcript. As described in section 3.5.1.1, Rrp5p is involved in the maturation of the small subunit (Lebaron et al. 2013). Its N- and C-terminal domains are important for LSU- and SSU- maturation as

well as for A_3 and A_2 processing, respectively. Therefore, Rrp5p is described to be important for the coordination and maturation of both the small and the large ribosomal subunit (Venema and Tollervey 1996; Eppens et al. 1999; Torchet et al. 1998; Young and Karbstein 2011; Lebaron et al. 2013; Khoshnevis et al. 2019). Due to its multiple roles and interactions with both rRNA and proteins, Rrp5p is suggested to be jointly responsible for packaging and compaction of pre-ribosomes. Evidence for this hypothesis is provided by electron microscopy analyses of chromatin spreads, where depletion of Rrp5p was found to influence the integrity of the terminal knobs resulting in loose and less dense arrangements (Lebaron et al. 2013). Furthermore, Rrp5p is thought to exhibit its role for the coordination of processing events and compaction of pre-ribosomal particles together with rpL3 (Gamalinda et al. 2014).

Moreover, at least eight different RNA helicases are associated with early pre-ribosomal particles containing $27SA_2$ pre-rRNA (Dez et al. 2004). This leads to the conclusion, that several significant structural rearrangements might occur within these early particles, that in turn influences the packaging of pre-ribosomes. One subcomplex, which has been well characterized is depicted by Npa1p, Npa2p, Nop8p, Rsa3p and the helicase Dbp6 (La Cruz et al. 2004; Rosado et al. 2007a). The remaining six helicases present in those particles are Dbp2, Dbp3, Dbp7, Dbp9, Mak5 and Rrp43p (for reviews see (Rodríguez-Galán et al. 2013; Sloan and Bohnsack 2018). In total, the concerted action of the above mentioned and of further proteins contributes to the formation of the earliest detectable pre-60S particle. Thereby, domains I, II and VI are assembled at first (Figure 13), which constitute the major part of the solvent exposed shell (Kater et al. 2017; Sanghai et al. 2018b; Zhou et al. 2019a). The entire inner layer of the pre-60S particles are formed later. These include for instance the PET and the PTC.

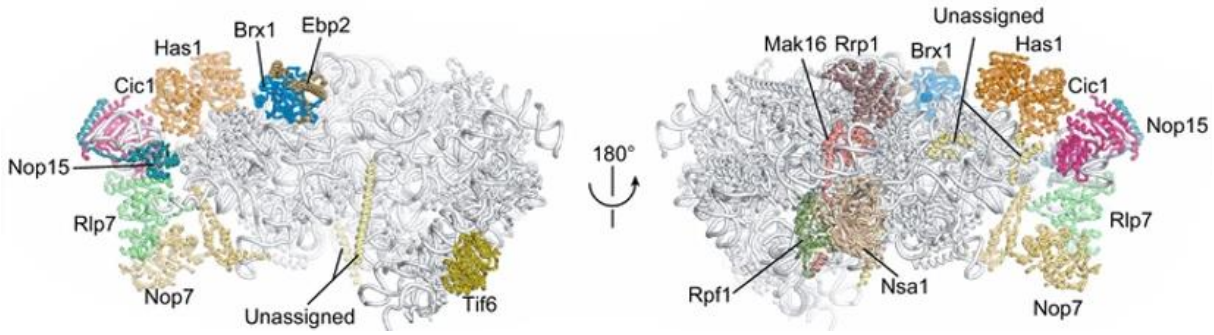

Figure 14: Cryo-EM structures of nucleolar pre-60S particles in state 2.
Structural model of a pre-60S particle from an interface side view (left) and from a solvent side view (right). Ribosomal proteins and rRNA are indicated in grey, the assembly factors are colored differently. Adopted from (Zhou et al. 2019a).

In early nucleolar 60S precursors, that have been resolved in cryo-EM analyses, solely domains I, II and VI are resolved (Figure 14). Domains III, IV and V are present as well, but are disordered and therefore not visible, due to high structural flexibilities.

The structure depicted in Figure 14 represents a Rpf1p-associated pre-ribosomal particle (Zhou et al. 2019a) and includes biogenesis factors belonging to the Nsa1-module (Nsa1p, Rpf1p, Mak16p, Rrp1p) and the A_3 cluster (Rlp7, Nop7, Nop15, Cic1p, Has1p). The folding of the ITS2 with associated biogenesis factors Nop15, Cic1p, Nop7 and Rlp7 and r-proteins rpL8 and rpL15 initiate the formation of the "foot" structure, a hallmark of the pre-60S particle. Furthermore, the 5.8S rRNA, domain I and parts of domains I and VI form the outer solvent exposed shell of the particle (Figure 14). The Nsa1-complex consisting of Nsa1p, Rpf1p, Mak16p and Rrp1p (McCann et al. 2015; Baßler et al. 2017) stabilizes the solvent exposed site by clamping domains I and II, which closely resembles the mature configuration.

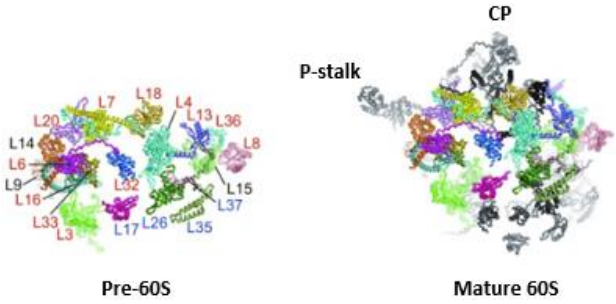

Figure 15: LSU r-protein coverage of a pre-60S and mature 60S particle from a solvent side view.
Views from the solvent exposed site on r-proteins of the Rpf1p-TAP pre-60S particle (left) and mature 60S subunit (right). "Early" r-proteins are colored in red, "middle" r-proteins in blue, unclassified r-proteins in black. R-proteins present in the 60S mature subunit are color coded and those missing in pre-60S particles are black. Adopted from (Zhou et al. 2019a).

Additionally, 19 LSU r-proteins, which are not annotated, belong to the classes of "early" acting r-proteins (rpL3, rpL4, rpL6, rpL7, rpL8, rpL13, rpL16, rpL18, rpL20, rpL33, rpL36) and "middle" acting r-proteins (rpL17, rpL26, rpL35, rpL37) (Figure 14). RpL9, rpL14 and rpL15 are absent compared to the mature subunit (Figure 15).

Importantly, as described for the maturation of the small subunit (see 3.5.1), the absence of r-proteins from cryo-EM structures does not necessarily exclude their presence in those particles. Assembly of r-proteins is stabilized when particles mature (Ohmayer et al. 2013). The terminology "early" and "middle" acting r-proteins reflects their role at specific stages of pre-rRNA processing. The same classification can be applied to categorize assembly factors (for reviews see Woolford and Baserga 2013; La Cruz et al. 2015). Concrete examples of r-proteins and assembly factors being important for a certain pre-rRNA processing step will be discussed in this and in the following chapters.

To further drive pre-ribosomal maturation, incorporating $27SA_2$ pre-rRNA has to be processed to $27SA_3$- and finally to 27SB pre-rRNA. These events necessitate the removal of ITS1 sequences starting at processing site A_3, as shorty described in section 3.3. Endonucleolytic cleavage at A_3 by MRP (Lindahl et al. 1992; Chu et al. 1994a) is followed by 5´-3´-trimming of ITS1 sequences involving the exonucleases Rat1p, Xrn1p and Rrp17 (Henry et al. 1994; Oeffinger et al. 2009) which, in the main pathway, halt at the B_{1S} site of $5.8S_S$ rRNA, yielding $27SB_S$ pre-rRNA.

Besides endo- and exonucleases, A_3 processing and ITS1 trimming requires a set of assembly factors termed "A_3 factors". Initially, seven were found to be necessary for proper ITS1 processing. However, further analysis has expanded the set of proteins required for this processing step to at least fourteen biogenesis factors, as all of them were shown to be important for $27SA_3$ turnover: Ytm1p, Erb1p, Nop7, Rlp7, Nsa3p/Cic1p, Nop15, Has1p, Drs1p, Rpf1p, Pwp1, Nop12, Rrp1p, Brx1p and Ebp2 (Miles et al. 2005; Pestov et al. 2001; Adams et al. 2002; Oeffinger et al. 2002; Dunbar et al. 2000; Fatica et al. 2003a; Fatica et al. 2003b; Oeffinger and Tollervey 2003; Dembowski et al. 2013a; Wehner and Baserga 2002; Talkish et al. 2014a; Wu et al. 2001; Horsey et al. 2004; Shimoji et al. 2012; Granneman et al. 2011; Sahasranaman et al. 2011).

The recruitment of six A_3 factors, Nop7, Erb1p, Ytm1p, Cic1p, Nop15 and Rlp7, is mutually interdependent. Rlp7 was initially suggested to act as placeholder for rpL7 due to high sequence homology (Dunbar et al. 2000). This seemed plausible, as several placeholders act during ribosome biogenesis to prevent premature recruitment of proteins and formation of structures (for review see Espinar-Marchena et al. 2017). However, crosslinking experiments revealed the binding sites of rlp7 and rpL7 in the mature ribosome are that distant from each other, that steric binding interference could be excluded (Ben-Shem et al. 2011; Babiano et al. 2013; Dembowski et al. 2013b). Nop7 and Erb1p form a heterotrimer together with Ytm1p, associating with 90S pre-ribosomes (Miles et al. 2005; Tang et al. 2008). Their association however depends on preceding assembly of rpL8 (Jakovljevic et al. 2012). Interestingly, crosslinking experiments revealed the binding site of Erb1p to be located immediately adjacent to rpL8 (Granneman et al. 2011). The same is true for the binding site of Nop7. This leads to the conclusion that the stable association of the Erb1p/Ytm1p/Nop7p heterotrimer depends on rpL8. The converse is not true, as assembly of rpL8 was found to be independent of the presence of Erb1p (Sahasranaman et al. 2011). Nop7, Cic1p and Nop15 were not crosslinked in proximity to Erb1p, however, recent cryo-EM studies indicate a direct interaction with rpL8 (Figure 16, A) (Wu et al. 2016). Remarkably, they have been unexpectedly crosslinked apart from the ITS1 in the ITS2 (Granneman et al. 2011; Dembowski et al. 2013b). Assembly of these six A_3 factors is required for recruiting the exonuclease Rrp17 (Sahasranaman et al. 2011). Subsequent association of Brx1p and Ebp2 (for binding sites see Figure 14) drives the binding of the DEAD-box helicases Drs1p and Has1p which are suggested to constitute the only two proteins among the A_3 factors that exhibit enzymatic activity (Sahasranaman et al. 2011; Shimoji et al. 2012; Dembowski et al. 2013a). As indicated, efficient recruitment of several A_3 factors requires stable assembly of rpL8, which is bound to domain I. Interestingly, the absence of rpL7, which is bound to domain II and as well important for early pre-ribosomal biogenesis does not impair the recruitment of the same set of A_3 factors to this extent Therefore, it can be clearly distinguished from the rpL8 induced phenotype (Jakovljevic et al. 2012; Ohmayer et al. 2015). The biogenesis factors Brx1p, Ebp2, Has1p, Cic1p/Nsa3p, Nop7, Rlp7, Ytm1p,

Nop15 and Nop16 are severely diminished from pre-ribosomes upon depletion of rpL8 but not upon depletion of rpL7 (Ohmayer et al. 2015). However, depletion of either rpL7 or rpL8 leads to the same pre-rRNA processing defect as the absence of A_3 factors (Pöll et al. 2009) and furthermore to diminishment of domain I r-proteins (rpL13, rpL15, rpL36) and domain II r-proteins (rpL6, rpL14, rpL20, rpL33) (Jakovljevic et al. 2012), whereas depletion of rpL7 affects the latter and depletion of rpL8 the former r-protein cluster (Ohmayer et al. 2015). These findings indicate two similar but for some aspects diverse phenotypes that can be observed for depletion of either rpL7 or rpL8. Moreover, both depletion of Rlp7, and probably also the other interdependent A_3 factors, as well as of rpL7/rpL8 severely impedes the assembly of rpL17, rpL26, rpL35 and rpL37 to pre-ribosomes (Sahasranaman et al. 2011; Jakovljevic et al. 2012). Hence rpL7, rpL8, and the A_3 factors provide an example, how r-protein assembly and the function of biogenesis factors can be interconnected.

In addition, formation of 27SB pre-rRNA apparently requires rearrangements within the ITS1/5.8S rRNA region. Structural models suggest, that in a pre-ribosomal context, base-pairing of the 5.8S rRNA is formed with ITS1 sequences (Yeh et al. 1990; van Nues et al. 1994). In mature ribosomes however, sequences of the 25S rRNA domain II are involved in an extensive secondary structure network through the formation of base pairs with 5´-sequences of the 5.8S rRNA (Pöll et al. 2009; Ben-Shem et al. 2011). Therefore, the ITS1 has to be trimmed, in order to enable mature interactions (Figure 16, B). The trimming depends on the exonuclease Rat1p, as described above. Rat1p is as well involved in the degradation of aberrant pre-rRNA species, as described in section 3.3.2. This provides a potential link between r-protein assembly, pre-rRNA processing and surveillance pathways.

The formation of a distinct 5´-end of 5.8S rRNA requires a mechanism to stop exonucleolytic digestion of Rat1p at a certain point and to prevent the pre-rRNA from over-digestion. Otherwise, this would result in a loss of mature rRNA sequences (Figure 16,C) (Pöll et al. 2009; Sahasranaman et al. 2011). Besides depletion of rpL7 or rpL8, the absence of several other r-proteins of the large ribosomal subunit (rpLs) also affects $27SA_3$ processing (Pöll et al. 2009; Gamalinda et al. 2014). Remarkably, all r-proteins required for this step, with exception of rpL3, are localized in 25S rRNA domains I and II. Therefore, absence of these r-proteins might impair the correct formation of the structural network, which is formed through base pairing between 5.8S and 25S rRNA (Figure 16, B). This network in turn is suggested to constitute a physical road block to Rat1p (Pöll et al. 2009). Alternatively, a cluster of r-proteins (rpL17, rpL26, rpL35 and rpL37) might define a further road-block, as the interaction between 25S and 5.8S rRNA provides a binding site for rpL17 in the mature ribosome (Ben-Shem et al. 2011; Sahasranaman et al. 2011). In addition, this r-protein cluster is absent upon depletion of A_3 factors (Figure 16 ,A, D) which might therefore define a further road-block,

In conclusion, the majority of biogenesis factors and r-proteins necessary for correct ITS1 trimming spans a complex interaction network among the proteins (Figure 16, E). It has been suggested to

chaperone the pre-LSU particle, helping to coordinate processing events, and further, to ensure that 5´-end maturation of 5.8S rRNA precedes ITS2 processing.

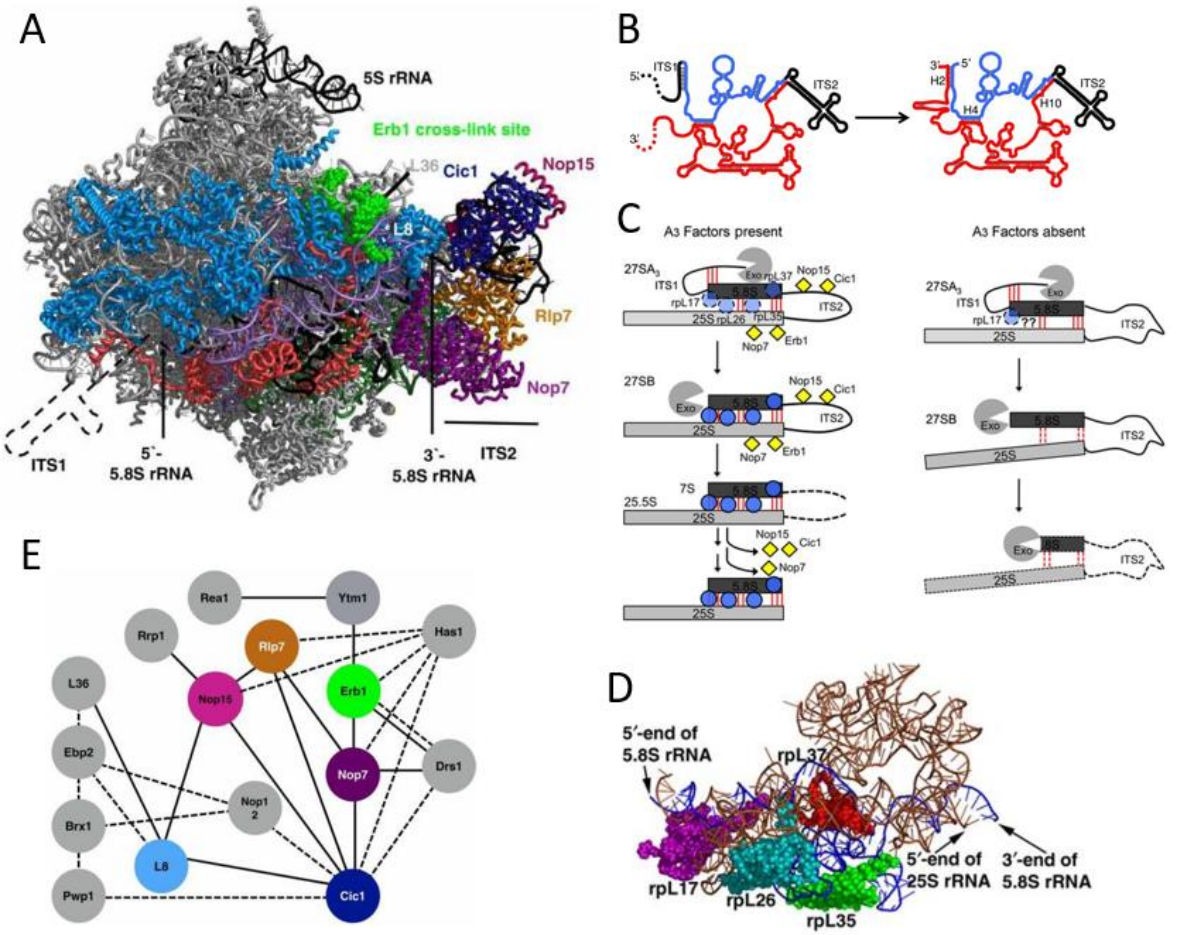

Figure 16: The role of A_3 factors in the main pre-rRNA processing pathway of $27SA_2$ pre-rRNA yielding 27SB pre-rRNA.
(A) Cartoon representation of a Nog2p-associated pre-ribosomal particle. Early r-proteins are colored in light blue, 25S rRNA domain I in light violet, 25S rRNA domain III in dark green, 5S and 5.8S rRNA in black. Selected "A_3 factors" are diversely colored which bind on or close to the ITS2. Depletion of A_3 factors severely impedes the association of rpL17, rpL26, rpL35 and rpL37, colored in red. Adapted from (Konikkat and Woolford 2017). (B) Proposed base-pairing site of the ITS1 region (black) with 5.8S rRNA sequence (blue, left) prevents binding of 5.8S rRNA sequences with 25S rRNA sequences (red) as found in the mature ribosome (right). Adapted from (Jakovljevic et al. 2012). (C) Proposed degradation of pre-rRNA by Rat1p. While the binding of r-proteins (blue circles) and A_3 factors (yellow rectangles) blocks pre-rRNA processing at site B_{1S} (left), their absence (right) induces a turnover from proper processing to degradation of the pre-rRNA. Red lines indicate base pairing between 5.8S and ITS1 or 25S rRNA sequences. Adopted from (Sahasranaman et al. 2011). (D) LSU r-proteins whose assembly is dependent on the A_3 factors cluster around 5.8S rRNA. 25S rRNA domain I is highlighted in brown, sequences corresponding to the 5.8S rRNA are blue. R-proteins are color coded in purple (rpL17), teal (rpL26), green (rpL35) and red (rpL37). Adopted from (Sahasranaman et al. 2011). (E) Protein-protein interaction network of A_3 factors as inferred in (Konikkat and Woolford 2017). Direct interactions are indicated by solid lines, interactions derived from yeast-two-hybrid assays are indicated with dashed lines.

After assembly of all A_3 factors (see also Figure 14 and Figure 15), the removal of the ITS2, which separates 5.8S and 25S rRNA sequences from each, other occurs in several steps, starting with endonucleolytic cleavage at site C_2 in the ITS2 (see 3.3.2). To do so, the function of at least 13 assembly factors, termed "B-factors", is required for this step including Nip7p, Nop2, Rpf2p, Rrs1p, Spb4p,

Mak11, Dbp10, Rlp24, Tof6p, Nog1p, Nsa2p, and the dual A_3/B-factors Has1p and Drs1p (Woolford and Baserga 2013). Importantly, the putative GTPase Nog2p has been initially implicated as B-factor as well. However, Nog2p is not strictly required for 27SB pre-rRNA processing, as a substantial amount of 7S pre-rRNA, arising from C_2 processing, could be observed upon depletion of Nog2p (Saveanu et al. 2001). Further studies have revealed that the binding site of Nog2p, which is located at the subunit interface, overlaps with the binding site of Nmd3p. Nmd3p ,however, is an essential export adaptor protein, which interacts with the nuclear export machinery (further details see 3.5.2.2). It is therefore involved in the export of the pre-LSUs into the cytoplasm. Therefore, it has been suggested, that Nog2p might rather serve as "monitoring" GTPase for pre-60S maturation, which links pre-ribosomes after its release from a Nmd3p placeholder site to the recruitment of the nuclear export machinery (Matsuo et al. 2014).

Most of the B-factors associate with the pre-ribosome in the form of subcomplexes, probably serving as building blocks to minimize the complexity of pre-ribosomal assembly (Saveanu et al. 2003; Lebreton et al. 2008a; Talkish et al. 2012; Biedka et al. 2018).

Their recruitment occurs in a semi-hierarchical order, starting with the Nip7p-Nop2p heterodimer and branches in two parallel pathways that converge to the ultimate association of the GTPase Nog2p (Talkish et al. 2012; Biedka et al. 2018). Notably, most B-factors associate even before A_3 processing, several among them are already present at an early stage of biogenesis – for instance Npa1 (Dez et al. 2004), others likely in the 90S pre-ribosomes as indicated for Rpf2p and Rrs1p (Zhang et al. 2007). Importantly, Nip7p and Nop2 are recruited to the nascent pre-ribosome co-transcriptionally (Chen et al. 2017) and are bound to 25S rRNA domain V, both being important for ribosome biogenesis and pre-rRNA processing (Hong et al. 1997; Zanchin et al. 1997). However, due to high structural flexibilities, Nip7p cannot be resolved in cryo-EM analyses at this state. Therefore, cryo-EM information on Nip7 can only be obtained upon transition to later pre-LSU assembly intermediates (Figure 18), which coincides with the appearance of domains III and parts of domains IV and V (Kater et al. 2017).

As mentioned, the successive assembly of B-factors occurs in two largely independent branches. In one branch, the preceding assembly of Nip7p/Nop2 is required for association of Rpf2p/Rrs1p together with the r-proteins rpL5 and rpL11 which form the 5S RNP, and further downstream assembly of Spb4p (Talkish et al. 2012). Notably, the 5S RNP incorporated atop of the pre-60S subunit forms the central protuberance (see also 3.1.4), cannot be resolved at this, but only at later nucleoplasmic maturation states (Wu et al. 2016; Kater et al. 2017). In the second branch, for instance Rlp24p, Tif6 and Nog1p are recruited whose assembly is interdependent and required for binding of Nsa2p (Saveanu et al. 2003; Lebreton et al. 2008a).

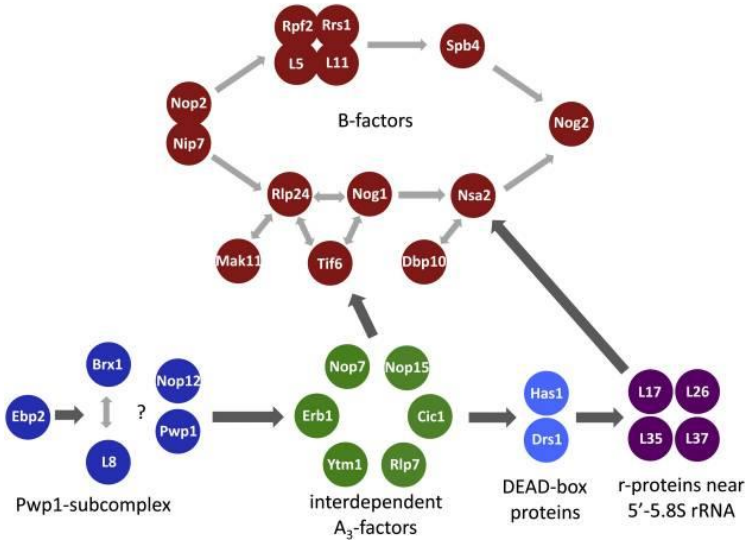

Figure 17: Model of a hierarchical recruitment of LSU assembly factors and some LSU r-proteins involved in early and intermediate pre-rRNA processing steps.
(A) A hierarchical pathway for the stable association of factors required for $27SA_2$ and 27SB pre-rRNA processing to LSU precursors is illustrated. The assembly of B-factors depends on the preceding association of other biogenesis factors including the A_3 factors and some r-proteins. Two branches beginning with the stable incorporation of Nop2/Nip7p converge in the final assembly of the GTPase Nog2p. Adopted from (Woolford and Baserga 2013).

The correct completion of both assembly branches yielding Nsa2p and Spb4p associated with the pre-ribosomes is essential for Nog2p assembly. Notably, their individual presence was not found to be sufficient therefore (Talkish et al. 2012). Two parallel pathways may ensure, that Nog2p is not prematurely loaded onto pre-ribosomes, thus avoiding premature cleavage at C_2. Therefore, the hierarchical B-factor recruitment ultimately leading to Nog2p assembly may depict a quality control checkpoint for pre-LSU assembly and maturation.

However, the list of assembly factors, being important for 27SB processing, has to be extended beyond the B-factors. The B-type DNA polymerase Pol5p has been recently described to be important for 27SB turnover (Braun et al. 2020). The same accounts for Noc3p, an assembly factor that joins the pre-LSU in the nucleolus and whose depletion leads to an accumulation of 27SB pre-rRNA (Master Thesis Fabian Teubl, 2016). In addition to the assembly factor set, a certain assembly state of LSU r-proteins has to be established, to enable efficient processing of 27SB pre-rRNA. This involves the r-proteins rpL17, rpL26, rpL35 and rpL37, whose association was severely affected upon depletion of A_3 factors (see above) and further rpL9, rpL19, rpL23, rpL25, rpL27, rpL31 and rpL34 (Pöll et al. 2009). Depletion of rpL9 or rpL23, which are located more distantly of the C_2 processing site and of domain III diminishes the presence of assembly factors, that are required for this processing step. This involves for instance Noc3p and Nsa2, and as well assembly factors that act on a later maturation state, associating after 27SB processing, for instance Nop53p or Rsa4p. The latter ones are equally diminished from the pre-ribsomes upon depletion of DIII r-proteins as rpL25, rpL27, rpL34 or rpL35 (Doctoral Thesis Uli Ohmayer, 2014). This enforces the need of collaboration between the association of assembly factors

and establishing a certain r-protein assembly state. Hence, for the facts described in this chapter, the successive recruitment of B-factors is accompanied and often functionally linked to the stable assembly of r-proteins and the formation of mechanistic important sites, for instance the PET or the PTC.

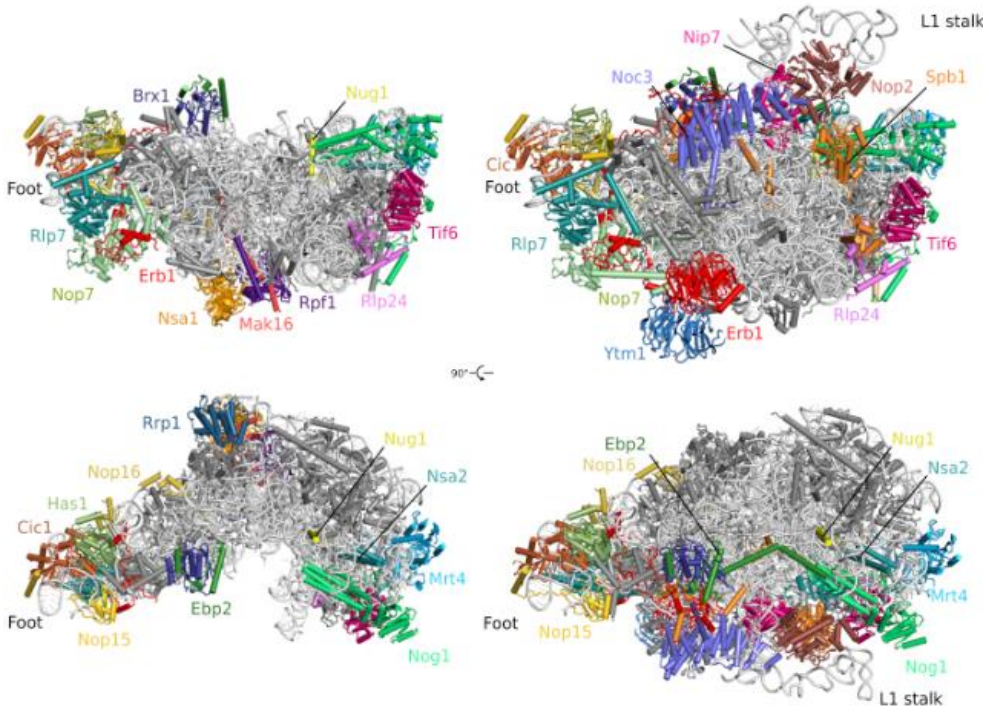

Figure 18: Cryo-EM structure of two nucleolar pre-60S assembly intermediates.
Front (above) and top views (below) of two differently LSU precursors at state C (left) or state E (right). rRNAs and r-proteins are colored in light and dark grey, respectively. Biogenesis factors are highlighted in different colors. The architectural hallmarks "foot" and L1-stalk are indicated and annotated. Adopted from (Kater et al. 2017).

Recent cryo-EM studies have deciphered the structure of large subunit precursors, preceding C_2-processing, thereby revealing the binding sites and -interfaces of the B-factors on pre-ribosomes (Kater et al. 2017; Sanghai et al. 2018b). Besides, comparison of pre-ribosomal particles of earlier states B and C with later ones of state D and E (Kater et al. 2017) or with the intermediate state described by the Klinge-group (Sanghai et al. 2018b) indicates significant structural rearrangements. The shape of the maturing pre-60S particles changes from an arch-like morphology to a more globular shape, which resembles the mature subunit (Figure 18).

As assembly proceeds, Nsa1p and probably the whole cluster, comprising Nsa1p, Rpf1p, Rrp1 and Mak16p, is removed by the AAA ATPase Rix7p (Kressler et al. 2008). According to recent cryo-EM structures, Rpf1p protrudes into the nascent tunnel, suggesting that this cluster may play a role in the initial formation of the PET (Kater et al. 2017). The stable association of rpL19, rpL31 and rpL25, which form the rim of the PET, was, with exception of the latter one, severely affected in B-factor mutants (Biedka et al. 2018). It is likely, that their association is coupled with the release of Ssf1p-Rrp15p and Rrp14p, as binding sites between rpL31 and Ssf1p overlap (Sanghai et al. 2018b). This indicates that

the recruitment of assembly factors to pre-ribosomes is as important as their release. The association of both rpL19, rpL31 and additionally of rpL25 can be visualized upon transition from state C to D, concomitantly with the stable assembly of 25S rRNA domain III (Ben-Shem et al. 2011; Kater et al. 2017). Notably, LSU domain III is extensively contacted by these r-proteins (Ben-Shem et al. 2011). RpL17, rpL35 and rpL37, which surround the PET, can be visualized earlier, however, their stable assembly depicts an important prerequisite for the association of Nop2 and Nog2p and hence for 27SB pre-rRNA processing (Gamalinda et al. 2012).

Interestingly, several r-proteins, which are required for 27SB processing at site C_2 (Pöll et al. 2009), do bind to 25S rRNA domain III, which is located near the ITS2. Among them are rpL19, rpL27 and rpL34 as well as rpL25, rpL35 or rpL37, which connect domain III with domain I and 5.8S rRNA (Ben-Shem et al. 2011). Two further r-proteins, being as well necessary for proper 27SB processing, are depicted by rpL9 and rpL23 (Pöll et al. 2009). However, they are located more distant from the ITS2, than are the others. RpL23 is located adjacent to the binding site of rlp24, whereas rpL9 binds adjacent to the binding site of Nsa2, both located in domain V (Wu et al. 2016; Kater et al. 2017). In fact, several B-factors (Nip7p, Nop2, Nog1p, Nsa2p, Mak11p and Nog2p) bind to 25S rRNA domain V, located distantly from the actual site of pre-rRNA processing in the ITS2. Moreover, maturation of domain V, which largely builds the later PTC, failures in almost every B-factor mutant, suggests, that defects at this step likely prevents proper formation of the PTC (Biedka et al. 2018).

Just before cleavage at C_2, the AAA-ATPase Rea1p/Mdn1 releases the Ytm1p-Erb1p subcomplex from the pre-ribosome through mechano-chemical action (Ulbrich et al. 2009; Bassler et al. 2010). Erb1p consists of a globular C-terminal domain which interacts with Ytm1p and a large N-terminal domain which functions as multivalent interaction hub throughout large parts of the pre-60S particle. In total, Erb1p connects eight assembly factors Ytm1p, Nop7, Rlp7, Sbp1p, Noc3p, Ebp2, Brx1p, Nop16 and Has1p, three r-proteins rpL27, rpL36 and rpL38, and 25S rRNA domains I, III and IV (Kater et al. 2017). Hence Erb1p removal is linked with a fundamental remodeling of the subunit interface that allows transition of the pre-ribosomes to the nucleoplasm.

First, removal of Erb1p disrupts a small structural element to Rlp7, that in turn initiates its rotation towards the foot. This movement allows remodeling of the foot and subsequent nucleoplasmic association of Nop53, whose binding site was occupied by Erb1p. Second, the remodeling of the foot allows the L1 stalk, which is chaperoned and kept in an unusual conformation by Rbp2, Noc3p, Nop2, Nip7p and Nsa2p (see Figure 18), to adopt its mature position (Kater et al. 2017; Sanghai et al. 2018b). The release of these factors and of Has1p, Brx1p, Ebp2p and Nop16 contributes to the rearrangement of the subunit interface, the reorganization of 25S rRNA domains IV and V and further to the progression to state F (Kater et al. 2017).

Finally, C_2 is processed by the long sought endonuclease Las1p (Gasse et al. 2015), yielding 7S- and 25.5S pre-rRNA. The mechanism, by which Las1p recognizes its substrate, is unknown. However, the before mentioned remodeling events triggered, by the release of Erb1p, might alter Las1p accessibility to the ITS2, thereby allowing its association. Strikingly, depletion or mutational inactivation of Las1p resulted in the formation of polyribosomes that contain a foot structure, suggesting that they are able to perform translation (Biedka et al. 2018). Intriguingly, a similar phenomenon has been observed in mutants that cannot process 7S pre-rRNA and therefore form mature ribosomes containing 5.8S +30 or 5.8S +5 (see 3.3.2) pre-rRNA (Rodríguez-Galán et al. 2015). The assumption, that ITS2 processing constitutes a checkpoint in pre-60S assembly raises the question why failures in this step are not recognized nor impair later stages of 60S subunit maturation which requires further investigation for a better understanding.

3.5.2.2 Nuclear stages of large subunit assembly

This chapter focuses on nucleoplasmic maturation and assembly steps of the pre-LSUs. This includes further processing of 25.5S- and 7S- pre-rRNA, which is generated by processing of 27SB pre-rRNA (see section 3.5.2.1). Further, key aspects of nuclear maturation steps of the PTC and the PET will be summarized. Finally, an overview about rendering nuclear export competence and nuclear export of the pre-LSUs will be given.

Upon arrival in the nucleoplasm, further significant structural and compositional changes of the maturing pre-60S particle continue (Konikkat and Woolford 2017). Trimming of 7S pre-rRNA requires the late acting r-proteins rpL2, rpL43 and rpL39, which are stably assembled at this maturation state. Notably, the assembly of rpL2 and rpL43 is interdependent (Ohmayer et al. 2013).

Besides, most biogenesis factors, that have been associated with early pre-60S particles containing 27SB pre-rRNA, are released and a new set of factors is recruited. One among them is depicted by Nop53, that joins pre-ribosomes at an late, nucleoplasmic state and is required for proper processing of 7S pre-rRNA (Thomson and Tollervey 2005; Granato et al. 2005; Granato et al. 2008). Nop53 docks onto the ribosome near the ITS2 foot structure with its C-terminus around the 3´- end of the 7S pre-rRNA in close localization to Nop15, Cic1p, Rlp7 and Nop7 (Wu et al. 2016) (Figure 19, A). Besides, Nop53 was described as adaptor protein, that interacts through its N-terminal AIM domain with Mtr4p, thereby recruiting the exosome to the pre-60S particle (Thoms et al. 2015; Falk et al. 2017; Cepeda et al. 2019), which results in trimming of 7S pre-rRNA. Concomitantly, processing of the 25.5S pre-rRNA occurs via The Las1p-complex that includes Rat1p (see also 3.3.2). Recent studies suggest that Nop53 enters pre-ribosomes after release of Nsa1p (Biedka et al. 2018). This might indicate that Nop53 gets assembled in the nucleolus. However, its timely association with pre-60S particles occurs at a later

state, in the nucleoplasm. More precisely, both the association of Nop53 and Mtr4p, as well as of Nog2p, depend on the preceding stable assembly of rpL25 (Ohmayer et al. 2013). In turn, rpL25 is on the one hand essential for Nog2p association, on the other hand essential for proper C_2 processing (Pöll et al. 2009), which occurs after preceding removal of Erb1p (see above). C_2 processing however depends on the presence of Rea1p (Bassler et al. 2010), which fails to associate with pre-ribosomes when Nog2p is absent (Biedka et al. 2018). In addition, the removal of Erb1p is indispensable to allow binding of Nop53 as its binding site is occupied by Erb1p (Wu et al. 2016; Kater et al. 2017; Sanghai et al. 2018b). For this it can be concluded that Nop53p, and Mtr4p, associate with the pre-60S particle in the nucleoplasm, after C_2 processing and release of Erb1p, whereas Nog2p gets assembled in the nucleolus.

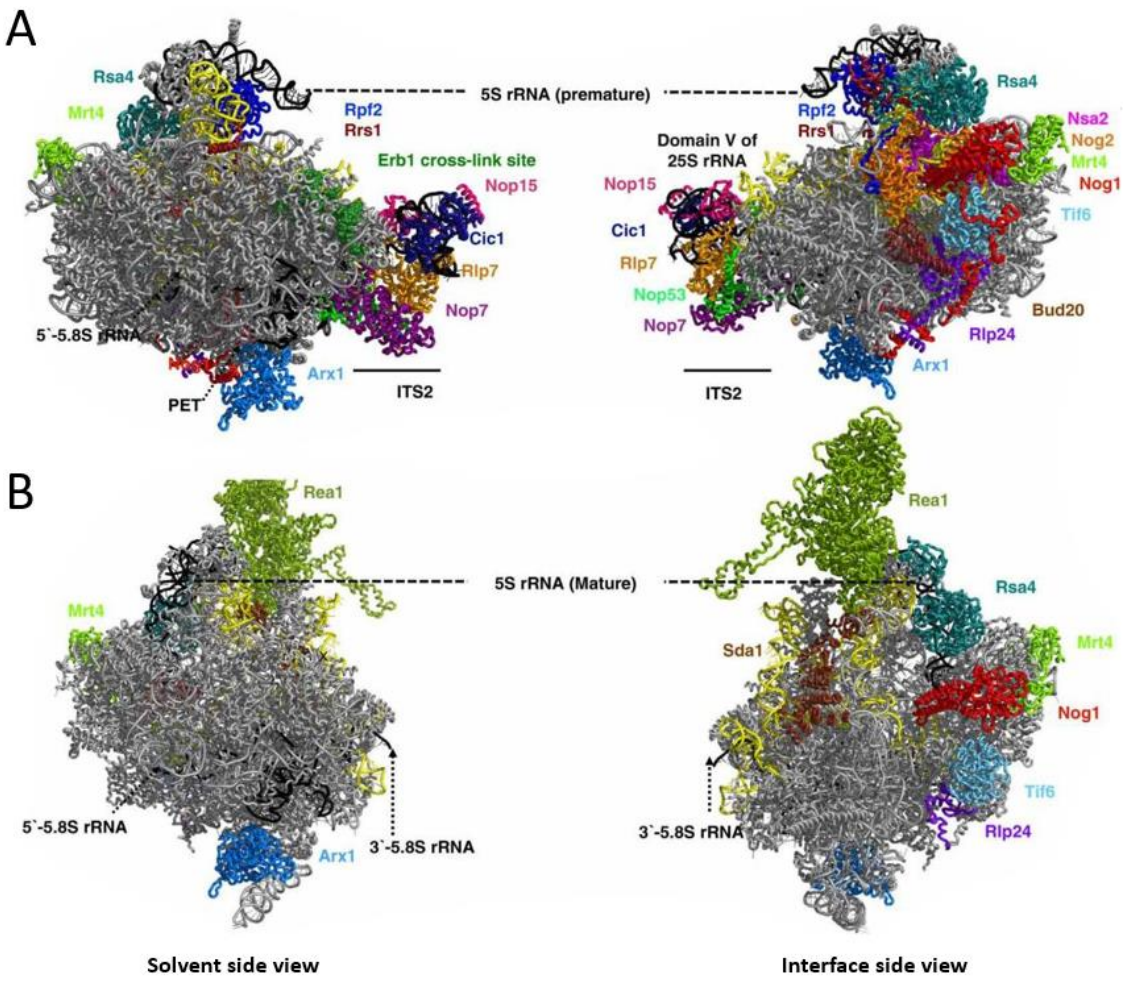

Figure 19: Cryo-EM structures of two nucleoplasmic LSU precursor particles.
Cryo EM structures of a Nog2p (A) and a Rix1p (B) associated pre-LSU particle from a solvent side (left) or an interface side view (right). (A) Is of an earlier assembly intermediate in which the ITS2 has not yet been removed and the 5S RNP is in a premature conformation. In contrast, in (B) the ITS2 has been removed and the 5S rRNP has rotated to its mature conformation. In both (A) and (B) the 25S rRNA domain V is highlighted in yellow and the associated biogenesis factors are differently colored. The remaining 25S and the 5.8S rRNA as well as r-proteins are colored in grey. Adapted from (Konikkat and Woolford 2017).

Figure 19, A, illustrates a nucleoplasmic Nog2p-particle (Wu et al. 2016). Notably, the 5S RNP gets stably associated and can therefore be resolved at this maturation state, which was not possible for earlier pre-60S intermediates (Kater et al. 2017). As described above and at the beginning of this chapter, the biogenesis factors Rpf2p and Rrs1p get assembled with pre-ribosomes after co-transcriptional association of Nip7p/Nop2 (Talkish et al. 2012). Furthermore, they and can be isolated in a complex with 5S rRNA, rpL5 and rpL11 (Zhang et al. 2007). Because the binding sites of Nip7p and Nop2 partially overlap with Rpf2p and Rrs1p in nucleoplasmic particles, the transition of the 5S RNP to a more stable conformation could depend in part on the release of these factors (see above). However, the 5S RNP is distorted to nearly 180 degrees, when comparted to the mature situation. This necessitates a substantial rearrangement within this region. The assembly factor Nog2p binds at the center of the pre-60S subunit, making extensive contacts to helices adjacent to the twisted CP (Wu et al. 2016). The arrangement seems to be stabilized by the bound assembly factors, particularly Rpf2p and Rrs1p, and therefore displays an energetically favored intermediate state (Leidig et al. 2014).

Regarding the PTC, the biogenesis factor Nog1p protrudes with its C-terminal domain all the way through the PET, which has been unoccupied after release of the “Nsa1-cluster”, and reaches to the PTC (Wu et al. 2016). Moreover, Nog1p, Nog2p and Nsa2p partially occupy the PTC. These extensive interactions might explain a potential role for late nuclear stages of construction of the PTC, protecting it from premature binding of translation factors and sensing a certain level of maturation (Wu et al. 2016; Biedka et al. 2017).

Regarding the PET, Arx1p, which is involved in pre-60S nuclear export (Hung et al. 2008), is bound in front of the PET, contacts rpL25 and rpL35, binds close to rpL19, and crosslinks to rRNA of ES27 and ES24 (Bradatsch et al. 2012). Therefore, Arx1p might act as proofreader for proper accommodation of these r-proteins in and around the tunnel.

Regarding the foot, its removal is induced through trimming of ITS2 sequences of the 7S pre-rRNA by the exosome (see above and 3.3.2). However, the mechanism or the order by which the associated biogenesis factors are released is unknown (Figure 19, B).

For the final maturation of the CP/5S RNP, the ribosome-assembly factor Sda1p (Dez et al. 2006) joins the pre-60S particle. This is supposed to induce the release of the Rpf2p/Rrs1p complex, which forms extensive interactions with both the 5S RNP, with rRNA around the CP and as well with Rsa4p (Madru et al. 2015; Kharde et al. 2015; Asano et al. 2015). Breakage of these interactions and release of Rpf2p/Rrs1p initiates H84 and the 5S RNP to perform a semi-circular movement to achieve its mature conformation (Leidig et al. 2014). By this, H38, which is adjacent to the CP, is pushed towards the subunit interface closer to its mature-like position (Leidig et al. 2014). Additionally, rpL21, which is located at the base of the 5S RNP is at least indirectly required for 5S RNP reorientation. RpL21 enables

the release of Rpf2p, Rrs1p, Rsa4p and Nog2p which accumulate under rpL21 depleted conditions (Ohmayer et al. 2013).

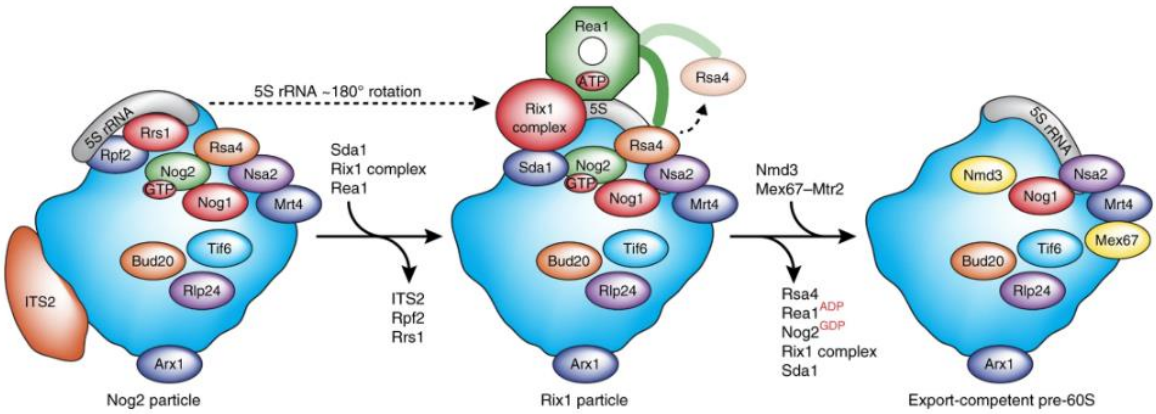

Figure 20: Scheme for selected pre-60S maturation steps for acquisition of export competence.
The Nog2-particle (left) is decorated with a set indicated biogenesis factors, the ITS2 and the re-oriented 5S RNP (grey). Upon transition to the Rix1-particle (middle), Rpf2p and Rrs1p leave the pre-ribsome, the ITS2 is removed, the 5S RNP has achieved its mature position, and the Rix1-remodelling complex removes Rsa4p. Transition to an export competent pre-60S particle (right) requires association of export adaptors and -receptors (as indicated for Nmd3p and Mex67p/Mtr2p) and the release of Rea1, Nog2p, Sda1p and the Rix1-complex. The large subunit including 25S rRNA and 5.8S rRNA as well as r-proteins and biogenesis factors (except the ones which are highlighted) is shown as blue silhouette. Only assembly factors with known binding sites are indicated and highlighted in variegated colors. Adopted from (Peña et al. 2017).

Following rotation, the Rix1p subcomplex, consisting of Rix1p/Ipi1p/Ipi3p, assembles together with Rea1p to the pre-LSU (for overview of these steps see Figure 20). These establish multiple contacts with the pre-ribosome, amongst others with the initial Rpf2p/Rrs1 interaction area, and Rea1. By this, they stabilize the pre-ribosomal particle with the 5S RNP in its rotated state (Barrio-Garcia et al. 2016). Notably, foot incorporating ITS2 sequences of the 7S pre-rRNA as well as associated biogenesis factors have been removed (see above) and the Rix1p subcomplex is positioned vertically on the subunit interface on top of the 5S RNP, interacting with Rea1p (Figure 19, B). ATP hydrolysis through activation of Rea1p powers the release of Rsa4p from pre-ribosomes (Ulbrich et al. 2009). Recent cryo-EM studies on pre-LSUs have structurally uncovered several aspects of these large-scale transitions (Kater et al. 2020). Importantly, the interacting partner Nsa2p stays associated. As a consequence, Nog2p is stimulated to hydrolyze GTP, which triggers its own, and subsequently release of Sda1p as well as of the Rix1p-complex (Ulbrich et al. 2009) (Figure 20). At this state, the PTC has already acquired a mature-like conformation, which enables binding of Nmd3p to the previously Nog2p-occupied site (see above). Nmd3p serves as nuclear export adaptor and recruits its own export receptor Crm1p to the pre-60S particles via its nucelar export signal- (NES) sequence (Ho et al. 2000; Gadal et al. 2001). Besides Crm1p, Nmd3p interacts with the L1-stalk protein rpL1. However, correct assembly of the L1-stalk has not been demonstrated to be essential for pre-60S export (Musalgaonkar et al. 2019).
Nevertheless, current cryo-EM analyses provide a detailed structural view on L1-stalk maturation. Assembly factors, which stabilize the L1-stalk in its pre-mature position are released, thus rendering

flexibility to the stalk. At the same time, the biogenesis factor Spb1p prevents the stalk to adopt its mature conformation. Only upon release of Spb1p, the L1-stalk can fully mature as found in the mature LSU (Kater et al. 2020). Furthermore, Nmd3p recognizes the nearly mature-like 25S rRNA helices around the PTC (Matsuo et al. 2014; Sengupta et al. 2010; Ma et al. 2017), suggesting, that Nmd3p binding to the PTC serves as quality control step of the pre-60S particle before nuclear export.

Besides Arx1p, Nmd3p and Crm1p, nuclear export of LSU precursors requires Alb1p, Rrp12p, Bud20, Mtr2p, Mex67p, Npl3p, Ecm1p and Gle2p (for review see Nerurkar et al. 2015). The subunit interface is relatively deprived of LSU r-proteins, however, assembly factors like Nog1p, Nsa2p, Rlp24p, Tif6p and Mtr4p remain associated during nuclear export (Liang et al. 2020). They help to shield the negative charges of the rRNA, facilitate efficient export through the nuclear pore complex (NPC) and are released in the cytoplasm (see 3.5.1.2 and 3.5.2.3).

3.5.2.3 Final cytoplasmic maturation of the large subunit

After arrival in the cytoplasm, the pre-60S particles undergo final maturation to become mature large subunits. This includes the removal of all biogenesis factors, that mostly decorate the functional centers, assembly of the remaining r-proteins, the final trimming of the 3´-end of 5.8S rRNA and the proofreading of functional centers (for overview see Figure 21).

The assembly factor Rlp24 recruits the cytoplasmic AAA-ATPase Drg1p and stimulates its intrinsic ATPase-activity. Hydrolysis of ATP triggers the release of the placeholder Rlp24 and the r-protein rpL24 can assemble. As rpL24 lacks the motif that is recognized by Drg1p, the removal is unidirectional (Pertschy et al. 2007; Lo et al. 2010; Kappel et al. 2012). The shuttling/export factor Bud20p, which has been assembled to the pre-60S subunit in the nucleus is thereby removed as well (Altvater et al. 2012). Besides Rlp24 and Bud20p, the GTPase Nog1p is simultaneously released from the pre-ribosome (Pertschy et al. 2007). Notably, the C-terminus of Nog1p reaches deep into the PET which gets now extracted.

The assembly factors Rei1p, Jjj1p and Ssa1p bind to the LSU precursor which is required for the release of the Arx1p/Alb1p dimer (Hung and Johnson 2006; Meyer et al. 2007; Meyer et al. 2010; Demoinet et al. 2007). Rei1p binds adjacent to Arx1p and Alb1p, whereas the former is localized on top of the PET. Alb1p mediates its contact to the pre-60S subunit. After release of Arx1p, Rei1p inserts its C-terminal sensor domain into the PET to check its correct assembly and folding (Greber et al. 2016). Upon release of Rei1p, Reh1p joins the pre-60S particle and inserts its C-terminal domain into the tunnel (Ma et al. 2017). Notably, the C-termini of Rei1p and Reh1p share high homology and are therefore supposed to play a partially redundant role (Parnell and Bass 2009). In combination, Nog1p, Rei1p and Reh1p are sequential tunnel inspectors that ensure the correct conformation of the PET which is essential for the nascent polypeptide chain to protrude during translation.

The assembly of the P-stalk requires the protein phosphatase Yvh1p to release the P0-homolog Mrt4p from the premature stalk region (Lo et al. 2009; Kemmler et al. 2009). Interestingly, an alternative pathway of P-stalk assembly exists, in which rpL12 and P0 assemble in the nucleus to the pre-60S subunit followed by export into the cytoplasm promoted by the P-stalk proteins P1and P2 (Rodríguez-Mateos et al. 2009a; Rodríguez-Mateos et al. 2009b; Francisco-Velilla et al. 2013).

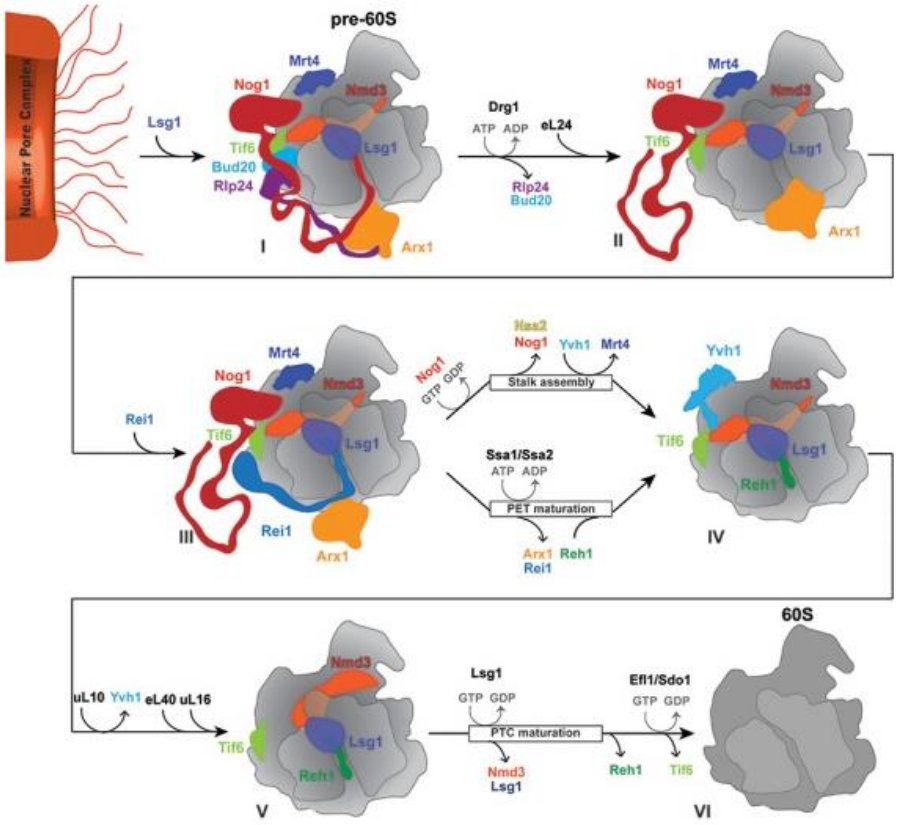

Figure 21: Model for cytoplasmic maturation of pre-60S particles.
After transport through the nuclear pore complexes and arrival in the cytoplasm, further maturation is initiated by the action of Drg1p and follows a complex succession of maturation steps that involve GTPases, ATPases as well as finals building of the functional centers and proofreading mechanisms. For further details see the running text. Adapted from (Klingauf-Nerurkar et al. 2020).

Concomitantly, Nog1p release allows H89 to rearrange in its nearly mature conformation, which is engaged by Nmd3p. This movement opens the binding site of rpL10 adjacent to the P-stalk, whose assembly completes the formation of the P-stalk and as well of the PTC (Zhou et al. 2019b). For these findings, it is suggested, that Nog1p couples quality control and assembly of spatially distant functional centers (Nerurkar et al. 2018; Klingauf-Nerurkar et al. 2020). P-stalk maturation allows the binding of the GTPase Efl1p via its co-factor Sdo1p which is associated at the P-site after final PTC assembly (Ma et al. 2017; Luviano et al. 2019; Zhou et al. 2019b). Importantly, the proper maturation and integrity of the P-stalk including rpL10 is required for efficient recruitment of Efl1p (Bussiere et al. 2012).

Therefore, binding of Efl1p is supposed to serve as marker for correct stalk assembly. Both Efl1p and Sdo1p are required for the release of Tif6p (Weis et al. 2015).
Nmd3p stimulates the GTPase-activity of Lsg1p, thereby triggering its own release (Hedges et al. 2005; Malyutin et al. 2017). Final removal of the remaining biogenesis factors and assembly of the missing r-proteins completes the maturation of the large ribosomal subunit.

3.6 Structural dynamics accompanying large subunit biogenesis

The solved crystal structure of a mature yeast 80S ribosome at 3.0 Å resolution in 2011 was an outstanding milestone in the field of structural biology that gave researchers a first detailed insight into rRNA folding and where r-proteins are bound on the mature subunits (Ben-Shem et al. 2011). However, the structural information about ribosomal precursors remained at first less complete.
During the last years, tremendous effort has been made to complement these gaps on the conformation of pre-60S subunits with detailed maps of LSU-precursor particles at sub-nanometer and sub-atomic resolution (Greber et al. 2012; Leidig et al. 2014; Barrio-Garcia et al. 2016; Ma et al. 2017; Kater et al. 2017; Sanghai et al. 2018b; Zhou et al. 2019a). Thereby, structural mechanisms underlying conformational rearrangements could be directly observed.
In fact, the pre-60S particle is subjected to a plethora of structural changes and conformational dynamics during its maturation from 90S pre-ribosomes to mature large subunits. Some of them have been discussed in section 3.5.2. Among them are the initial compaction of terminal knobs at the end of chromatin spreads which form the nascent pre-ribosomes, the ITS2 trimming accompanied by the complete removal of the foot structure and associated biogenesis factors, the sequential formation of the PET and the PTC, the 5S RNP rotation and the maturation of the L1 stalk, to mention few of them.
In 2017, Kater and colleagues purified nucleolar pre-60S particles via split-tag affinity purification which employs two differently tagged biogenesis factors and sequential purification steps. A further subset was obtained by single bait purification of arrested particles at a distinct maturation state during early pre-60S biogenesis. The purified material was subjected to single molecule cryo-EM, where six different populations could be deduced and resolved to atomic or near atomic resolution (Kater et al. 2017). Remarkably, the structural information increased with prolonged maturation of the particles (see Figure 22). Increasing parts of 25S rRNA are stably assembled and can be unambiguously resolved due to decreased flexibility in these regions. Notably, it has been already shown for the assembly of r-proteins, that their interactions with the pre-ribosomal particles strengthen as maturation progresses (Zhang et al. 2007; Ohmayer et al. 2013; Gamalinda et al. 2014). The same is suggested for ribosomal RNA. Stable rRNA domain assembly observed by Kater et al. follows a sequential rRNA folding pathway (similar results obtained by (Chen et al. 2017; Sanghai et al. 2018a). Interestingly, stable integration of rRNA domains into the pre-60S core proceeds via a non-

transcriptional but yet linear series beginning with domains I, II and VI and subsequently followed by domains or parts of domains III, IV and V (Kater et al. 2017). More and more regions of the pre-60S particle decorated with LSU r-proteins and biogenesis factors prominent for a respective maturation state are resolved concomitantly with ongoing biogenesis. Recent cryo-EM analyses of the same group indicate further stable integration of domains IV and V at later stages of pre-LSU biogenesis (Kater et al. 2020). These findings can be retrieved to the loss of conformational flexibility and structural rearrangements leading to stable integrity of these rRNA regions. A reminiscent modular assembly has been as well observed for prokaryotic LSU biogenesis, albeit parallel pathways have been suggested (Davis et al. 2016).

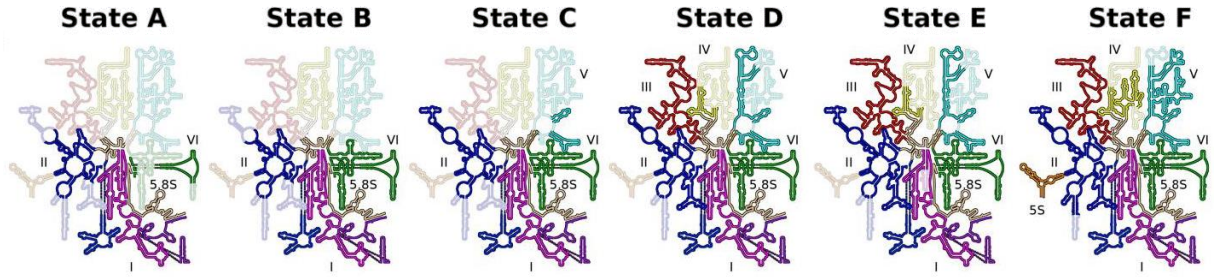

Figure 22: Sequential incorporation of 25S rRNA domains into the maturing pre-60S subunit.
The six 25S rRNA secondary structure domains of the yeast *Saccharomyces cerevisiae* are illustrated in different colors. States A-F correspond to cryo-EM models of distinct pre-60S maturation states that have been resolved by cryo-EM. The densities that could be structurally assigned are indicated in bold, the unresolved parts are pale. Adopted from (Kater et al. 2017).

Besides the stable incorporation of rRNA domains, r-proteins, biogenesis factors and large-scale transitions, for instance the re-orientation of the 5S RNP, pre-rRNA dynamics and folding events of more distinct regions that occur at a plethora. Each of them contribute to the entirety of structural remodeling events that are necessary to mold the mature subunits. These can be changes in the folding of single rRNA helices or forming and breaking up secondary rRNA interactions. For instance, the 5.8S rRNA base-pairs with the 25S rRNA and undergoes major structural rearrangements during the processing of $27SA_2$ to 27SB pre-rRNA (Burlacu et al. 2017). Moreover, evidence for a global structural reorganization including several hotspots along the pre-rRNA during maturation of pre-60S particles that incorporate $27SA_2$- to those than contain 27SB- pre-rRNA has been obtained by chemical and tethered enzymatic structure probing (Pöll et al. 2017; Burlacu et al. 2017). The same is true for the maturation to particles incorporating 25S rRNA (Pöll et al. 2017). Changes in accessibility to chemical or enzymatic probes accounts for structural changes and altered conformational dynamics in these regions.

Further subtle, locally restricted restructuring events are often triggered by the release of biogenesis factors, the binding of r-proteins or the activity of energy-dependent enzymes (Burlacu et al. 2017).

In general, the establishment of ribosomal specific features and conformational arrangements that are recognized and bound by r-proteins, assembly factors or other structural components are often supposed to constitute checkpoints for quality control. Among them are for instance the Rix1p-Rea1p checkpoint machinery that senses correct position of the 5S RNP rotated to a mature-like conformation, or the subsequent probing of the PET through sequential occupation of biogenesis factors (see Barrio-Garcia et al. 2016; Greber et al. 2016).

3.7 RNA structure probing

Imaging techniques like x-ray crystallography, NMR and single molecule cryo-EM have provided detailed insight into structures of mature ribosomes and their precursor particles (for instance Kater et al. 2017; Chen et al. 2017; Barandun et al. 2017; Chaker-Margot 2018; Sanghai et al. 2018a; Kater et al. 2020). Owing these methods, structural arrangements and interactions between proteins and rRNA can be directly visualized and retraced over several maturation states. However, comparison of different pre-ribosomal high-resolution structures to figure out subtle changes of structural rearrangements and folding states of individual rRNA regions during biogenesis are quite challenging and laborious. Moreover, parts of rRNA or proteins are often impossible to be properly resolved by using these techniques due to high conformational flexibilities in these regions. To overcome these obstacles, chemical and enzymatic structure probing is an efficient way to analyze and determine higher-order structures of RNPs and their conformational changes over the time (see for instance Pöll et al. 2017; Burlacu et al. 2017).

In the 80s, first approaches to address RNA structures have come up by using reagents that modified only those nucleobases or riboses of the RNA molecule that were somehow accessible to the reagents (Peattie and Gilbert 1980; Ehresmann et al. 1987; Stern et al. 1988). This can be a metal ion, a small molecule or even a RNAse enzyme – depending on the respective agent or enzyme, the accessibility, flexibility, the secondary or tertiary fold of the respective RNA molecule can be analyzed *in vivo* or *in vitro*. Over the past decades, structure probing approaches have been intensively used to study the secondary and tertiary structure of rRNA or other RNA molecules. Combined with a high-throughput sequencing readout, these analyses can be applied in a genome- or transcriptome-wide manner (see for instance Kwok et al. 2015).

One chemical, dimethyl sulfate (DMS) has been extensively used for RNA structure probing. DMS leads to methylation of all accessible adenines at position N-1 and cytosines at position N-3, respectively, in single stranded regions that can be detected by stops in primer extension reactions (Tijerina et al. 2007). Using this reagent, the secondary structure of all four ribosomal RNAs *in vivo* lacking the non-essential r-protein rpL26, plus 32 additional noncoding RNAs have been analyzed. In combination with primer extensions and high-throughput sequencing of the resulting cDNAs, this technique provides a

valuable tool for studying long RNAs and complex RNA mixtures (Talkish et al. 2014b). A further example is depicted by the analysis of mRNA structures *in vivo* which were found to be far less structured in rapidly growing cells than observed *in vitro* (Rouskin et al. 2014).

Another method, SHAPE (selective 2´-hydroxyl acylation analyzed by primer extension), has been widely used to study nucleotide flexibility of RNA molecules (Smola et al. 2015). Therewith, secondary and tertiary interactions of the 35S pre-rRNA in 90S pre-ribosomes have been probed with focus on the 5´-ETS, the ITS1, the formation of the central pseudoknot of the small subunit (see 3.1.3) and the influence of the essential biogenesis factor Mrd1p on these very early nucleolar maturation steps (Lackmann et al. 2018).

The pool of chemicals with different properties, e.g. reaction kinetics, membrane pervasiveness or tagging with a fluorophore, for structure probing has been constantly increased over the years which opens up further possibilities to analyze the structure of RNA molecules *in vitro* and *in vivo* (for reviews see e.g. Kubota et al. 2015; Xia et al. 2017; Mitchell et al. 2019).

Besides structure probing with chemicals, a plenty of enzymatic approaches have been established during the past decades. Different substrate specificities of the single enzymes (outlined for instance in (Ziehler and Engelke 2001) allowed their application in various biochemical approaches (for instance Zheng et al. 2010; Underwood et al. 2010; Kertesz et al. 2010).

One enzyme used for structure probing is represented by micrococcal nuclease (MNase), which is secreted by the bacterium *Staphylococcus aureus*. MNase exhibits strictly calcium dependent exo- and endoribonucleolytic activities, that cleaves both DNA and RNA, with preference for single stranded and A/T or A/U rich regions (Anfinsen et al. 1971; Dingwall et al. 1981). MNase has been widely used for analyzing DNA and chromatin structure. In a typical nucleosome mapping experiment, MNase is added *ex vivo* to chromatin in order to perform a limited digest. Positions of DNA cleavage sites and regions that are less accessible for MNase digestion can be subsequently mapped and altered chromatin structures and DNA compaction of transcribed or silenced genes can be addressed (Reeves 1984).

In 2004, a variation of this method has been developed which enabled the mapping of the genomic interaction sites of chromatin associated proteins (Schmid et al. 2004). Thereby, a DNA binding protein of interest is expressed in *Saccharomyces cerevisiae* as fusion to MNase *in vivo*, which remains inactive due to low intracellular calcium concentrations. After cell lysis, MNase activity is induced by addition of excess of calcium, introducing cleavage events into the DNA in close vicinity of the respective MNase fusion protein. Therefore, this method has been termined “ChEC” (chromatin endogenous cleavage). The resulting fragments obtained by MNase introduced cuts at distinct positions can subsequently be analyzed by Southern blotting or by high-throughput sequencing to obtain a genome-wide data set (Zentner et al. 2015; Babl et al. 2015; Grünberg and Zentner 2017).

MNase can be as well used to study RNA structure. In 2012, an approach has been established that makes use of MNase tethered to r-proteins of the large ribosomal subunit to probe their local tertiary rRNA structure in a ribosomal context (Ohmayer et al. 2012). Later, this approach was successfully applied in combination with high-throughput sequencing to study conformational changes of pre-ribosomes during the biogenesis process (Pöll et al. 2017).

In general, strains used for MNase structure probing of RNPs are usually designed to express a desired protein component of an RNP as fusion to MNase. The fusion protein gets incorporated at its dedicated position within the RNP, which can be, for instance, the large ribosomal subunit. Local conformational flexibilities of both the MNase connected via a protein linker to its anchor protein as well as of the RNP brings the nuclease in close proximity to local accessible RNA bases (see Figure 23). Subsequently, cutting events in the local three-dimensional environment occur which can be detected through appropriate readouts like primer extension.

The purification of distinct pre-ribosomal populations via associated biogenesis factors combined with MNase structure probing allows more specific insights into the conformation and the spatial orientation of pre-rRNA regions as well as their flexibilities in a pre-ribosomal context. The radius of nuclease action can be adapted by changing the size of the linker that separates MNase from its desired anchor protein (Ohmayer et al. 2012). Depending on the linker size, the distance from the anchor protein can be obtained with longer linker variants, whereas for shorter ones more proximal cuts are observed. Thus, this approach can further reveal the region to which the anchor protein is bound to. This is particularly helpful in cases with sparse or lacking structural data.

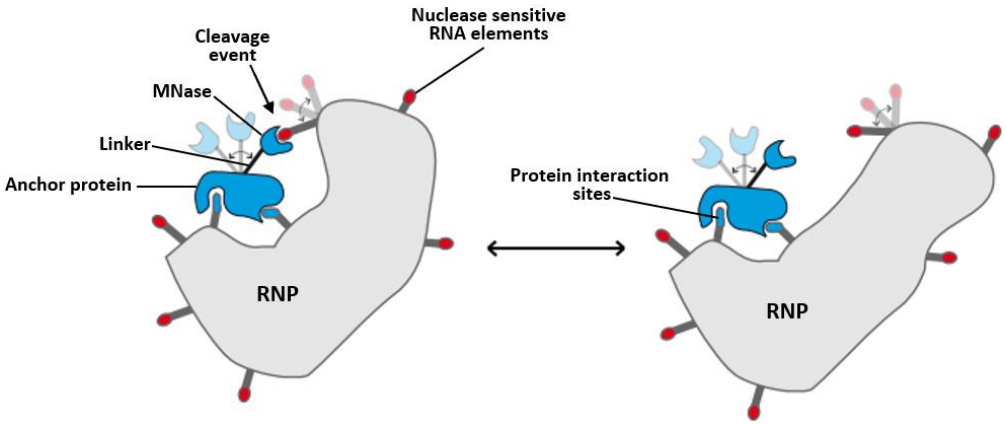

Figure 23: Possible mode of action of MNase fused to an anchor protein incorporated into an RNP.
Two different conformations of a RNP are shown (left and right) which might be the consequence of changes in the RNP´s interacting partners. The transparent shapes of the linker, the MNase and small arrows indicate varying local conformations. The MNase/Linker is fused to an anchor protein (blue) which is associated with the RNP via protein interaction sites (blue matches). Nuclease sensitive RNA elements of the RNP are indicated by red matches. Conformational flexibilities of both the RNP as well as of the MNase/Linker lead to cutting events in the local 3D-environment of the anchor protein. Adapted from (Ohmayer et al. 2012).

It should however be kept in mind that the calcium concentration in the model organism *Saccharomyces cerevisiae* is too low to enable *in vivo* structure probing. Therefore, disruption of the cells and addition of exogenous calcium is inevitable to activate MNase.

Anyway, published structural data of mature ribosomes or their precursors have been obtained through affinity purification of the respective particles under native conditions, similar to how enrichment of (pre-) ribosomes for MNase structure probing are gained which allows comparison of respective data sets with the present structural models.

3.8 Classification of Noc3p in the context of large subunit biogenesis

Noc3p belongs to the NOC- (nucleolar complex-associated) proteins, a subgroup of ribosomal biogenesis factors, which includes additionally Noc1p, Noc2p, Noc4p and Noc5p/Nop14. The Noc-proteins are evolutionarily conserved among eukaryotes regarding their structure and their function. Noc4p and Noc5p/Nop14, which form a dimer, are involved in the maturation of the small ribosomal subunit (Milkereit et al. 2003), whereas Noc1-3p are essential for the large subunit (Milkereit et al. 2001). The latter ones form two distinct complexes, Noc1p/Noc2p and Noc2p/Noc3p, which can be isolated from yeast cells independent of pre-ribosomes, whereas Rrp5p associates together with the Noc1p/Noc2p complex (Milkereit et al. 2001; Hierlmeier et al. 2012).

Noc1-5p are largely comprised of α-helical repeats, similar to HEAT-repeats. Noc3p and Noc4p could be resolved in cryo-EM analyses of the large subunit and the SSU-processome, respectively (Kater et al. 2017; Barandun et al. 2017).

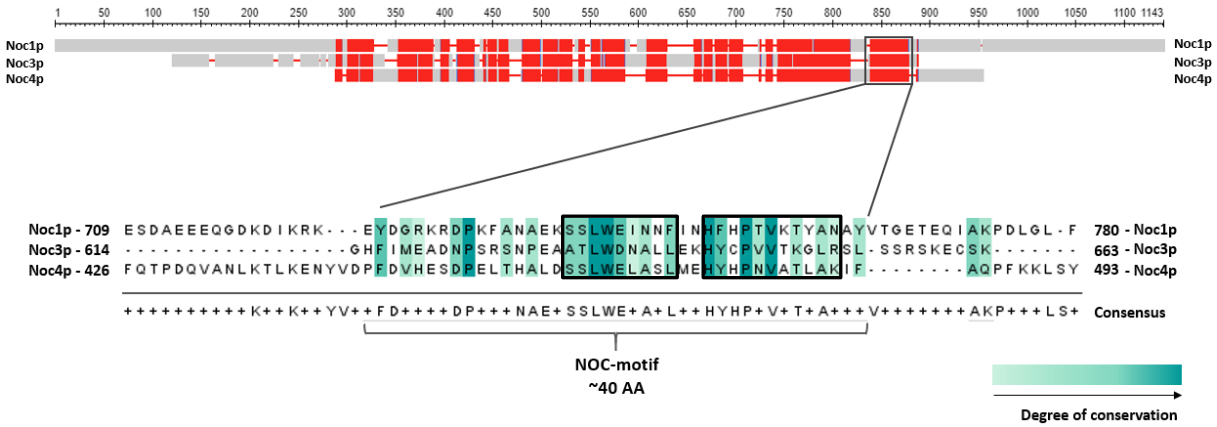

Figure 24: Protein sequence alignment between Noc1p, Noc3p and Noc4p, characterization of the NOC-motif.
The sequences of Noc1p, Noc3p and Noc4p obtained from the yeast genome database (https://yeastgenome.org/) have been aligned using COBALT (https://www.ncbi.nlm.nih.gov/tools/cobalt/re_cobalt.cgi) and further processed in Jalview (6.1.11) (upper part). Conserved regions according to the standard COBALT-settings are highlighted in red. The NOC-motif according to (Kühn et al. 2009) has been highlighted in the primary structure (lower part). The degree of conservation among the single AA residues is color coded as followed: dark turquoise for identical residues, turquoise for AA of the same group (e.g. polar), light turquoise for similar AA in size.

Significant sequence similarity has been observed for the C-terminal ~45 amino acids, which are conserved between Noc1p, Noc3p and Noc4p. It has been referred to as NOC-domain or NOC-motif (Figure 24) (Milkereit et al. 2001; Milkereit et al. 2003; Dlakić and Tollervey 2004).

Alignment of the Noc1p, Noc3p and Noc4p primary structure generally reveals a high conservation among the three proteins (Figure 24, upper part). A continuous pattern of red bars is indicated in the schematic representation of the protein sequences, which reflects conserved parts that mostly form the HEAT-repeat core of the Noc-proteins (Figure 24, upper part). These structural motifs are retraced by available high-resolution recordings of Noc1p, Noc4p and Noc5p/Nop14 (see Figure 26 for Noc3p and Noc4p, Figure 27 for Noc5p/Nop14). Importantly, conservation in this case does not necessitate identical residues but similar amino acids that are able to form the helical repeats, which therefore constitutes a structural conservation among the proteins. The NOC-motif that encompasses approximately 40-45 amino acids and is localized in the C-terminal region of Noc1p and at the very C-terminus of Noc3p and Noc4p shares a high degree of conservation among the proteins (Figure 24, lower part) (Dlakić and Tollervey 2004). Structurally, the NOC-motif has solely been resolved for Noc4p (Barandun et al. 2017). It constitutes two small, oppositely arranged helices, separated and flanked by unstructured amino acid sequences (Figure 26, D, highlighted in orange). Notably, two small “blocks” of highly conserved residues within the NOC-motif (Figure 24, lower part, black frames) belong for the most part to these small helical structures.

As repeatedly mentioned during the introduction, a series of nucleolar pre-ribosomal particles has been recently purified and deciphered to atomic and near-atomic resolution by cryo-EM (Kater et al. 2017). Thereby, large parts of Noc3p could be resolved as well. Noc3p is located at the central part of the subunit interface with its N-terminus facing towards the lower part of the structure and the foot, whereas the C-terminus reaches towards the Nip7p/Nop2 dimer in LSU domain V (Figure 25, A).

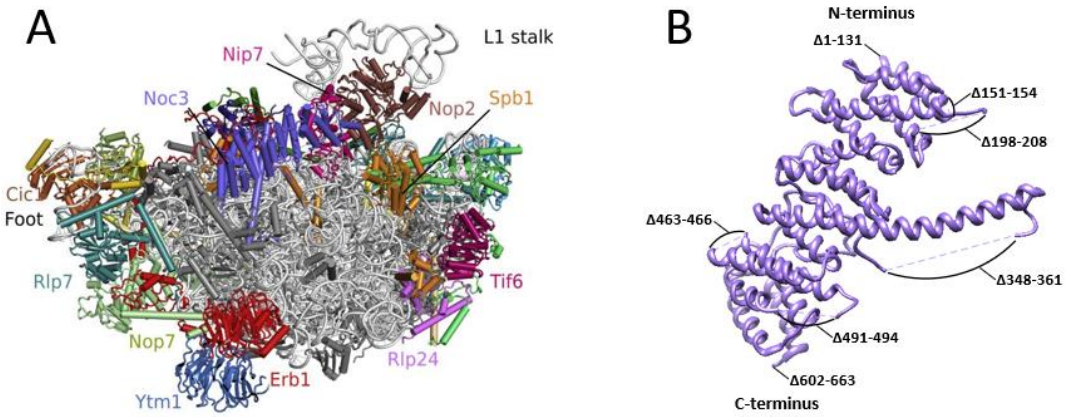

Figure 25: Structure of a nucleolar pre-60S particle with the associated biogenesis factor Noc3p.
(A) Front view of an LSU precursor particle. rRNAs and r-proteins are colored in light and dark grey, respectively. Biogenesis factors are highlighted in different colors. Noc3p is localized at the central part of the subunit interface and highlighted in purple. The architectural hallmarks “foot” and L1-stalk are indicated and annotated. Adopted from (Kater et al. 2017). (B) Noc3p isolated from its pre-ribosomal context. Unresolved parts of the C- and N-terminus as well within the protein are indicated and annotated according to the positions of the respective amino acids counting from the N-terminus, respectively. Adapted from PDB 6EM5.

In agreement with previous structure probing analyses using MNase fused to the C-terminus of Noc3p, an approximate localization of Noc3p at the subunit interface has already been indicated (Master Thesis Fabian Teubl, 2016).

Regarding the solved structure of Noc3p, outlined in Figure 25 (B), the N-terminal amino acids 1-131 as well as the C-terminal amino acids 602-663 were not resolved. This indicates, that these regions are most likely structurally flexible (Figure 25, B). Interestingly, sequence alignment between Noc3p and Noc4p reveals no corresponding amino acid sequence of Noc4p that belongs to the unresolved N-terminus of Noc3p. In fact, The N-terminal part of Noc4p constitutes a conserved sequence that starts at amino acids 133 of Noc3p (Figure 24, upper part). Solely Noc1p, the largest Noc-protein, possesses a large N-terminal region preceding the first conserved block, which is in turn not conserved with the N-terminal region of Noc3p (Figure 24, upper part). In addition to the N- and C-terminus, flexible regions within Noc3p are not resolved as well. These include mostly those parts, that connect the single helices, which form up the HEAT-repeats, among each other. This accounts for amino acids 151-154, 198-208, 348-361, 463-466 and 491-494 (Figure 25, B) (for detailed structures see (Kater et al. 2017). The N-terminal region is in proximity to the foot-structure, whereas the C-terminus reaches close to the L1-stalk. Therefore, these regions could possibly interact with other protein segments or rRNA domains that have not been resolved as well.

Due to the partial structural conservation between Noc3p and Noc4p (Figure 24, upper part), and the availability of high-resolution structures for both proteins, a direct comparison between them will be described in the following.

The structures of Noc3p and Noc4p, obtained by cryo-EM analyses, are depicted in Figure 26. In order to better navigate throughout the proteins, a nomenclature according to the single helices is proposed. Therefore, the first helix starting at the N-terminus of both proteins is termed H1 (helix 1). As the N-terminus of Noc3p is not fully resolved, it cannot be excluded, that further helices are localized in this part of the structure. Therefore, helix 1 of Noc3p is termed Hn+1 (“n” for N-terminus). Subsequent helices are sequentially named with ascending numbers as indicated in Figure 26 (A-D). The unstructured protein chains between the helices that link these among each other are not further characterized or designated. To better keep the overview, five helices are highlighted in colors in A, B and C, respectively, as outlined in Figure 26.

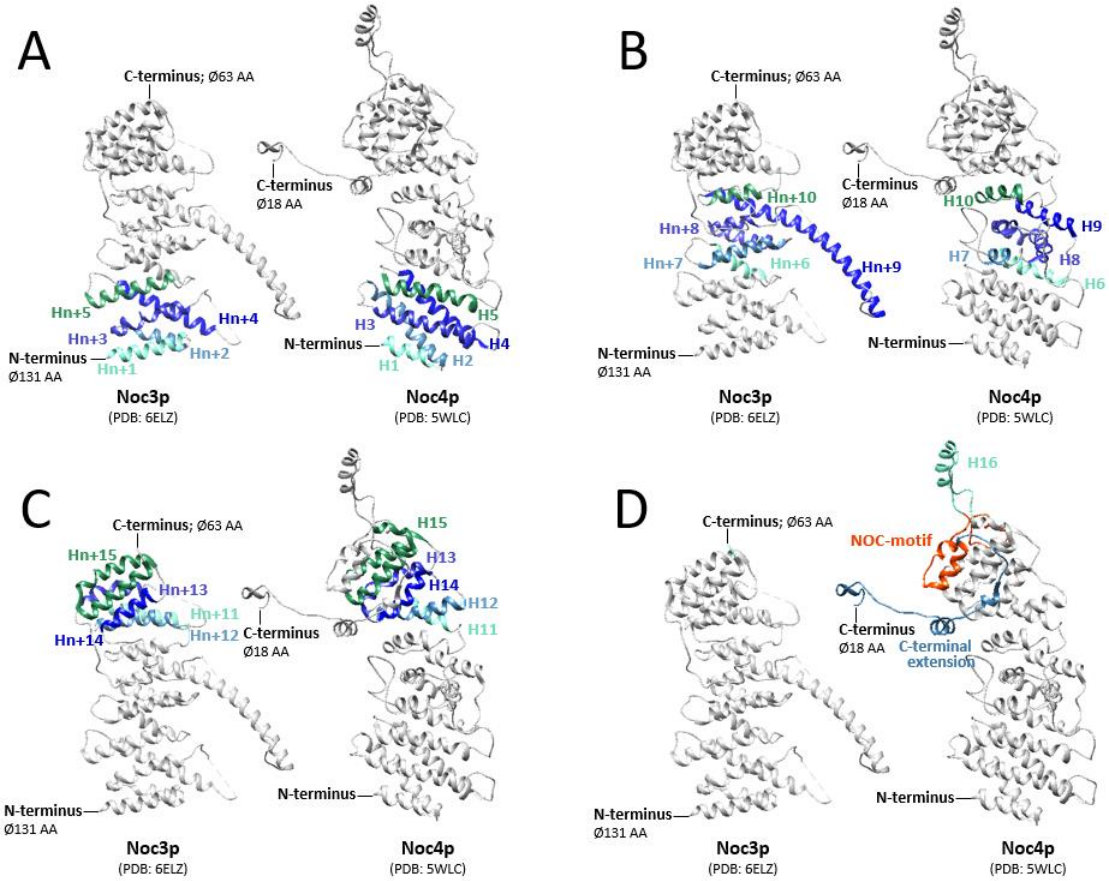

Figure 26: Structural comparison between Noc3p and Noc4p and suggestion of a nomenclature.
(A-C) Noc3p and Noc4p are shown isolated from their pre-ribosomal context. Five helices are highlighted in different colors and termed Hn+x for Noc3p and Hx for Noc4p, whereas "x" stands for the number of the helix, starting at the N-terminus, respectively. (D) H16 (turquoise), the NOC-motif (orange-red) and the C-terminal extension (blue) of Noc4p are highlighted. The subsequent 2 resolved AA at the C-terminus of Noc3p after Hn+15 (in turquoise) are highlighted as well. Adapted from PDB 6ELZ (Noc3p) and 5WLC (Noc4p) using the software UCSF ChimeraX (6.1.11).

Regarding the N-terminus, Hn+1, Hn+3 and Hn+5 of Noc3p are mirror-inverted compared to the corresponding helices of Noc4p, whereas H2 and H4 share the same conformational arrangement. Additionally, H3 of Noc3p and H2 of Noc4p are not continuous but interrupted by a small unstructured part consisting of 3 or 1 amino acid, respectively. The last five helices from the C-terminus of Noc3p, Hn+11-Hn+15, share as well roughly the same properties compared to H11-H15 of Noc4p concerning length, conformation and orientation (Figure 26, C). Hn15 and H15 are separated by 4, as the case may be by 3 amino acids that follow no strict helical shape. Notably, the N- and C-terminal parts of Noc3p and Noc4p are structurally quite similar to each other (Figure 26, A and C).

The central parts of the proteins however, differ substantially from each other (Figure 26, B). Whereas Hn+6 and H6 as well as Hn+10 and H10 of Noc3p and Noc4p, respectively, are quite similar to each other, H7 of Noc4p is shorter compared to Hn7 of Noc3p but flanked by longer unstructured amino acid sequences. The helical shape of Hn+8 of Noc3p is disrupted by 4 amino acids, whereas H8 of Noc4p is continuous and shifted to 90° in a clockwise direction. The most striking difference is depicted by Hn+9 of Noc3p which constitutes a 52 AA long helical stretch that reaches to the 25S rRNA domain III

(see also Figure 38 and PDB: 6ELZ, Kater et al. 2017). In contrast, the corresponding helix H9 of Noc4p is approximately one third in length but possesses a long unstructured part (Figure 26, C). Hn+15 is the last resolved helix at the C-terminus of Noc3p. The subsequent 63 AA including the NOC-motif has not been resolved in the current structure. Regarding Noc4p, H15 is separated from the NOC-motif by a further helix, H16 (Figure 26, D), which seems to be unique for Noc4p, as no sequence data for amino acids between Hn+15 and the NOC-motif are available for Noc3p (Figure 24, upper part). Furthermore, the protein chain of Noc4p continues beyond the NOC-motif with a 50 AA long extension to form its C-terminus, whereas the last 18 AA are not resolved (Figure 26, D).

In contrast to Noc3p, its binding partner Noc2p has not been resolved in current cryo-EM analyses, nor are any evidences indicated therefore (Kater et al. 2017). However, the Noc4p/Noc5p heterodimer and thus the contact/binding sites between the two proteins could be resolved in structural analyses of the SSU-processome (Figure 27 and Barandun et al. 2017). Notably, similar to Noc1/3/4p, Noc2p and Noc5p share as well conservation amongst each other. Most prominently, Noc5p has a long N-terminal part which is absent for Noc2p, whereas Noc2p shows additional sequences midst the protein (Figure 27, A).

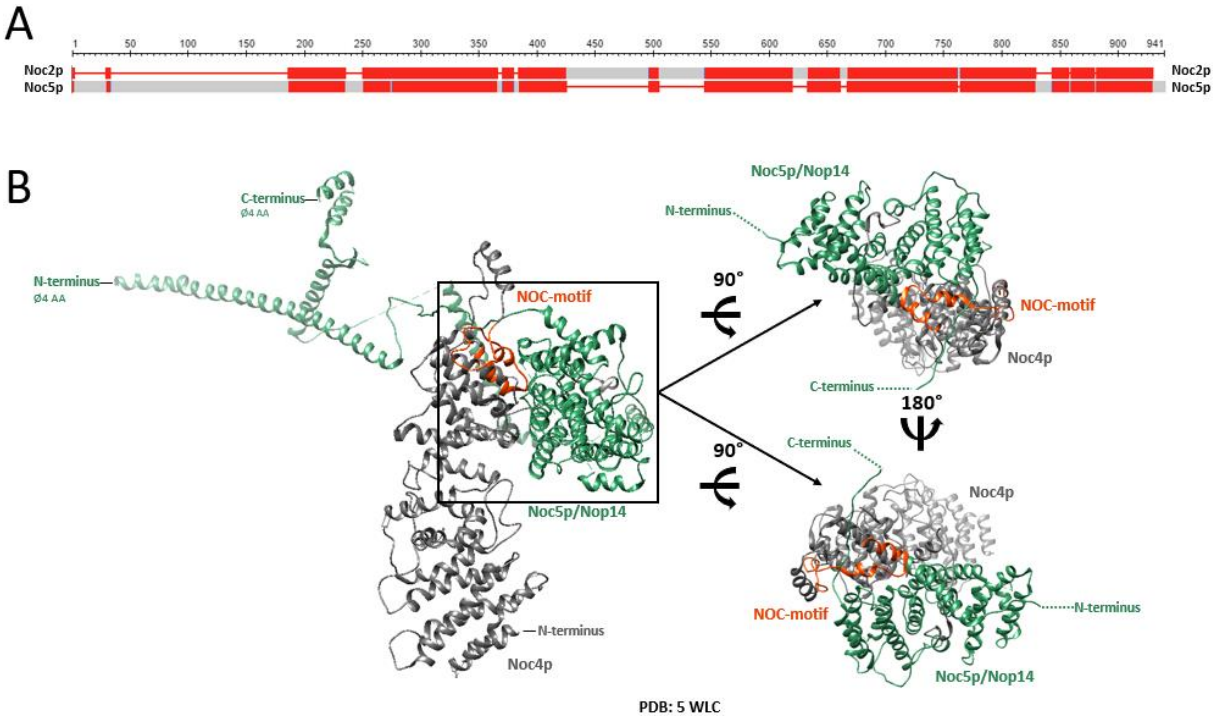

Figure 27: Sequence alignment between Noc2p and Noc5p/Nop14 and structure of the Noc4p/Noc5p heterodimer.
(A) The sequences of Noc2p and Noc5p/Nop14 obtained from the yeast genome database (https://yeastgenome.org/) have been aligned using COBALT (https://www.ncbi.nlm.nih.gov/tools/cobalt/re_cobalt.cgi) (upper part). Conserved regions according to the standard COBALT-settings are highlighted in red. (B) The structures of Noc4p (dark grey) and Noc5p/Nop14 (sea-green) isolated from their pre-ribosomal context are shown. The NOC-motif of Noc4p is highlighted in orange-red. Views from different perspectives are shown to better illustrate the parts of Noc4p and Noc5p/Nop14 that participate in the formation of the heterodimer between them. Adapted from PDB 5WLC using the software UCSF ChimeraX (6.1.11).

As indicated in B (Figure 27), the N- and the C-terminus of Noc5p/Nop14 seem not to participate in the binding to Noc4p. However, the helical HEAT-repeats of Noc5p/Nop14, mostly those closer to its C-terminus seem to be in the immediate proximity of the NOC-motif of Noc4p (Figure 27, B, best viewed on the bottom right). Probably, the interaction between the proteins is formed by the NOC-motif of Noc4p and the helical repeats of Noc5p/Nop14p. Interestingly, previous studied revealed the NOC-motif as indispensable for the formation of the heterodimer (Kühn et al. 2009). Due to (i) the structural conservation among Noc2p and Noc5p as well as among Noc3p and Noc4p and (ii) the conserved NOC-motif at the C-terminus of Noc3p and Noc4p, the localization of the binding site(s) between Noc4p and Noc5p/Nop14 can be, at least partially, transferred to Noc2p and Noc3p.

Regarding the formation of the heterodimer, it was found, that the C-terminus of Noc2p is important for its interaction with Noc3p (Thomas Hierlmeier, Diploma Thesis, 2008). In that study, Noc2p has been divided in 7 domains by comparison of sequence homologies between *S. pombe*, *S. cerevisiae*, *C. elegans*, *D. melanogaster*, *M. musculus*, and *H. sapiens* and sequentially truncated. Truncation of domain 6 severely impaired the association with Noc3p (for further details see 4.2.1).

How the contact of the Noc2p/Noc3p dimer to its pre-ribosomal population is formed remains however unknown. Previous functional studies on the binding interdependence indicated that Noc2p potentially needs Noc3p to bind particles that incorporate 27SB pre-rRNA (Bachelor Thesis Fabian Teubl, 2013). When looking at the SSU processome structure including Noc4p and Noc5p/Nop14, it seems if the contact to the particle may only partially be formed by the HEAT-repeat core of Noc4p. It is however obvious, that the long N- and C-terminal stretches of Noc5p (Figure 27, B) are highly interwinded with protein and rRNA components of the SSU processome (see PDB 5WLC and Barandun et al. 2017). The N-terminal stretch of Noc5p/Nop14 is potentially absent for Noc2p, at least when regarding the sequence alignment (Figure 27, A). Therefore, it remains to be explored how and if the C-terminus of Noc2p contacts the pre-ribosome or if the association is solely performed by Noc3p.

Additionally to the conserved structural features, it could be shown, that Noc1p is mainly localized in the nucleolus, Noc3p mainly in the nucleoplasm, and that Noc2p is intermediately distributed both in the nucleolus as well as in the nucleoplasm (Milkereit et al. 2001). Besides, the association of Noc1/2/3p with pre-ribosomal particles has been analyzed by sucrose gradient centrifugation. It was found, that Noc3p co-sedimented predominantly with 27SB and 7S pre-rRNAs. In contrast, Noc1p and Noc2p co-sedimented with 35S, 27S and 7S pre-rRNA. Notably, 27S includes $27SA_2$- as well as 27SB-pre-rRNA. However, these could be further separated using this technique. Accordingly, it was suggested that the Noc1p/Noc2p complex is associated with nucleolar 90S pre-ribosomes, whereas the Noc2p/Noc3p complex is bound to later, nucleoplasmic pre-ribosomal particles. Experiments in strains, in which Noc3p was depleted, indicated a processing defect and thus an accumulation of 27SB pre-rRNA (Bachelor Thesis Fabian Teubl, 2013), whereas depletion of Noc1p leads to a general

destabilization of all pre-rRNA populations and hence to an accumulation of 35S pre-rRNA (Hierlmeier et al. 2012). Furthermore, experiments in temperature sensitive (ts) noc1-1, noc2-1 and noc3-1 mutant strains indicated accumulation of LSU precursor particles either in the nucleolus, the entire nucleus or in the nucleoplasm, respectively (Milkereit et al. 2001), which is in correlation with the localization of the particular Noc-proteins. As many other ribosome biogenesis factors, the Noc-proteins are required for the translocation of pre-ribosomal particles from the nucleolus into the nucleoplasm (Milkereit et al. 2001).

3.9 Objectives of this work

The goal of this work was to further characterize the role of Noc3p for large ribosomal subunit maturation in the model organism *Saccharomyces cerevisiae*, trying to better understand intermediate steps of ribosome synthesis.

It was thus aimed to address the following questions:

- Can the structure of Noc3p and possibly the one of Noc2p be further deciphered?
- Is Noc3p associated with different pre-ribosomal populations?
- Does the pre-ribosomal assembly state influence the recruitment and the release of Noc3p to and off pre-LSUs?
- Do structural rearrangements or single r-proteins influence the association behavior of Noc3p with pre-ribosomes?
- Which regions of Noc3p are important for the association with Noc2p and with pre-LSUs?

Therefore, a multidisciplinary concept based on yeast genetics, molecular biology, and biochemical approaches has been applied. To answer the first two questions, Noc3p associated pre-ribosomal particles have been subjected to single-molecule cryo-EM. To address the third question, pre-ribosomal particles have been affinity purified by Noc3p under depletion of selected r-proteins and analyzed with regard to co-purified pre-rRNAs. To tackle the fourth question, a tethered tertiary structure probing approach utilizing MNase fusion proteins of Noc3p has been applied. Regarding the influence of single r-proteins, the structure probing approach has been applied on strains, that express truncation variants of a selected r-protein. Finally, structure-based mutagenesis according to the published structure of Noc3p helped to delete certain regions within Noc3p. Association with Noc2p and with pre-LSUs has been further analyzed to answer the fifth question.

4 Results

4.1 Single molecule cryo-electron microscopy reveals different populations of large ribosomal subunit precursors associated with Noc3p and delivers first structural hints on Noc2p

The shape of particles including Noc3p was previously described via cryogenic electron microscopy (cryo-EM) as sub-population out of a broad range of pre-ribosomal intermediates. Pre-ribosomes for this purpose were obtained by two consecutive affinity purifications using differently tagged versions of the biogenesis factors Nsa1/Ytm1 or Rix1/Rpf2, respectively (Kater et al. 2017).

To further investigate pre-LSUs containing Noc3p, Noc3p-associated particles are specifically enriched and analyzed in order to tackle several issues: (i) Obtaining structural information on unresolved parts of Noc3p (Figure 25), especially concerning the C-terminus at which the NOC-motif is located (compare Figure 24 and Figure 26), (ii) improving the characterization of the Noc2p/Noc3p interaction and (iii) characterizing the localization of Noc2p and interaction sites with Noc3p, as no structural data is available on Noc2p, and (iv) obtaining a more complete overview of the assembly events and structural rearrangements within the pre-ribosomal populations during association with Noc3p.

To do so, a strain expressing Noc3p as a genomically encoded TAP-fusion protein was used. Therewith, the respective Noc3p-associated pre-ribosomal population(s) was affinity purified and the obtained particles were subjected to single molecule cryo-EM. The entire procedure which includes cell culture, affinity purification, cryo-EM fixation on appropriate cryo-grids, pre-screening of the grids as well as all associated quality controls were performed on-site by the group of Dr. Philipp Milkereit, primarily by the technician Gisela Pöll. The so prepared, pre-screened grids were sent to the Rudolf-Virchow Zentrum at the Julius-Maximilians university in Würzburg, Germany. There, the data acquisition was accomplished by the group of Prof. Dr. Bettina Böttcher on a Titan-Krios G3 cryo-EM equipped with a Falcon III direct detector camera. The received data were processed with the software RELION-3.0 for cryo-EM structure determination.

The following flow-chart summarizes the main steps that were conducted in order to obtain meaningful structural information for the present data set consisting of 5,658 movies (Figure 28). First, beam induced motions were corrected using the algorithm MotionCor2 (Zheng et al. 2017) in order to align the micrographs. Subsequently, particles were picked with Relion´s integrated auto-picking function. To improve the yield of particles, the micrographs were manually checked for undetected ones. In total, 310,175 particles were extracted from the micrographs for subsequent analysis. Notably, the resolution for these picked particles has been lowered to save computing time for this large data set.

Reference-free 2D-classification of the picked particles was performed to group them into different 2D-classes based on their structural shape and orientation as recorded by the microscope. Repetitive rounds of 2D-classification and manual inspection of the classes helped to further eliminate bad recordings of particles, junk, artefacts, not assignable particles and contamination with mature ribosomes (Figure 28, left side), which made up 78,9 % of the initially extracted particles. Thereby, the initial data set was gradually sorted out to yield a selection of 65,550 particles. These were subjected to reference-based 3D-classification in order to distinguish different populations from each other.

The 3D-classification sorted the data set into 10 different 3D-classes (Figure 28, middle part). At next, the respective particles have been re-extracted from the original micrographs – re-centered and at the highest possible resolution. Using Chimera (6.1.11), a program for interactive visualization and analysis of molecular structures, these 3D-classes have been regarded more precisely. According to their structural shape, they were clustered in different groups.

Besides, class 3 has been directly further processed by 3D auto-refinement, which yielded the volume map Noc3-TAP-4 at 8,18 Å resolution (Figure 28, bottom, left side).

The remaining classes reflect different populations of pre-LSUs. Therefore, groups 4, 6 and 7 were pooled as they could be mapped with high congruence to the recently published cryo-EM structure of pre-LSUs at state C (Nsa1p-TAP / Ytm1p-FLAG) (Kater et al. 2017). Besides, groups 2, 8 and 9, were mapped to state E (TAP-FLAG- Ytm1p E80A) (Kater et al. 2017) and pooled as well. Subsequently, a new round of 3D-classification for each of the two groups has been conducted (Figure 28, lower part). Further processing and 3D auto-refining of certain sub-selections of the resulting 3D-classes ultimately yielded three volume maps: Noc3-TAP1 at 4,57 Å-, Noc3-TAP2 at 5,99 Å- and Noc3-TAP-3 at 6,86 Å-resolution, respectively (Figure 28, bottom). These classes will be described in more detail in the following.

The 3D-classification of state C-like particles produced the two volume density maps, Noc3-TAP-2 and Noc3-TAP-3, which share a high consistency within their shape. In agreement with state C, these precursor intermediates revealed volumes for 25 S rRNA domains I, II and VI. A hallmark of the large subunit precursor, the “foot” which is formed by the ITS2 and associated biogenesis factors could also be resolved. In contrast to Noc3-TAP-2, the Noc3-TAP-3 volume map shows defined volume densities for additional rRNA, detectable on the subunit interface side. Vice versa, the Noc3-TAP-2 volume map exhibits densities for the Nsa1-Rrp1-Rpf1-Mak16-cluster on the solvent side of the particle, bound to 25 S rRNA domains I and II, which cannot be observed in the Noc3-TAP-3 map. For these reasons and due to the fact that Nsa1p gets released during ongoing maturation (Kressler et al. 2008) it can be concluded, that even though the Noc3-TAP-3 particle is very similar to Noc3-TAP-2, it is of a further matured state.

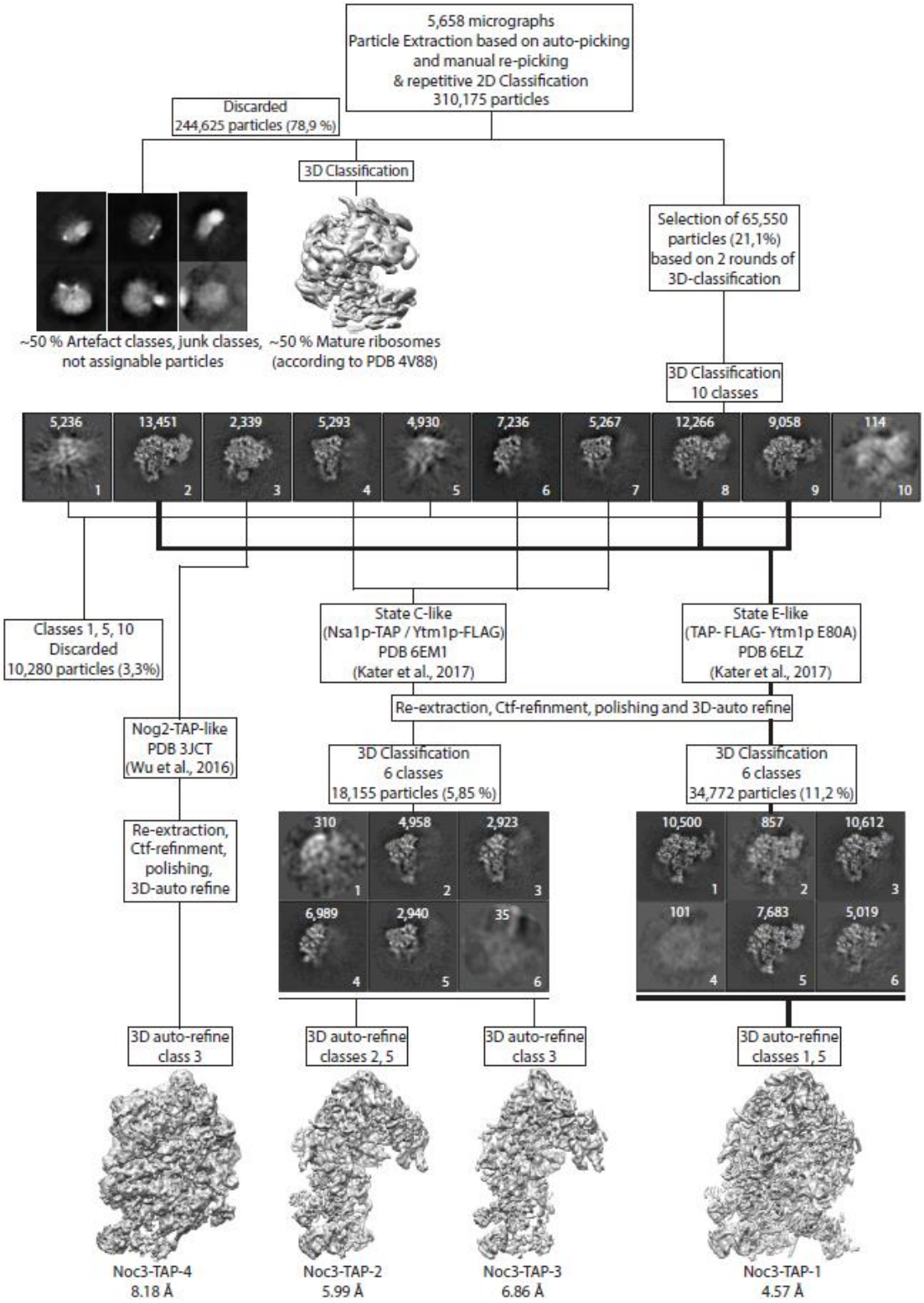

Figure 28: Cryo-EM data processing workflow of Noc3p associated particles.
The data collection yielded 5,658 micrographs. These micrographs were aligned using MotionCor2 (Zheng et al. 2017) with dose weighting and subsequently further processed in Relion-3.0. Manual and automated picking resulted in 310,175 particles. Those were "cleaned" by repetitive 2D-classification and manually, yielding a total of 65,550 "good" particles. A 3D classification resulted in 10 classes, as indicated, of which 3 were discarded. All particles were re-extracted from the original images at highest possible resolution and re-centered. Class 3 has been 3D-auto refined to yield the Noc3-TAP-4 volume map as indicated. The remaining 3D classes were pooled according to structural similarity (analyzed with UCSF chimera 6.1.11) and anew 3D-classified. Thereof, sub-selections of structurally highly identic volume maps were 3D auto-refined, which ultimately yielded three volume maps, Noc1-TAP-1, Noc3-TAP2 and Noc3-TAP-3. All steps were performed using Relion 3.0 (6.1.11).

The Noc3-TAP-4 volume density map, derived from refinement of class 3, represents the latest pre-60S population, which was co-purified by Noc3p. Its shape is similar to the nucleoplasmic Nog2-particle (Wu et al. 2016). Due to low abundance with only 2,239 particles in this class, the final resolution was solely 8.18 Å. Therefore, further progressing from the core particle towards the periphery impedes the exact assignability of volume densities to rRNA or protein chains. Hence, specific differences between the volume map and the PDB structure are not clearly predictable. Nevertheless, structural characteristics of the Nog2-associated pre-ribosome like the “foot”, the 5 S RNP in its pre-mature state and all 25 S rRNA domains are visible. In contrast to the published structure, volume density for Arx1p, which is important for nuclear pre-ribosomal export (see 3.5.2.2) was clearly not found.

Notably, densities for Noc3p were neither found in Noc3-TAP-2, nor in Noc3-TAP-3 or in Noc3-TAP-4. However, due to the fact, that Noc3p was used as bait protein for affinity purification, it is inevitably present in these particles. A comparatively high flexibility within these sub-populations combined with poor particle abundance among the classes might be a cause for its poor retrievability.

In contrast, the volume map Noc3-TAP-1 at 4,57 Å resolution (Figure 28, bottom, right side), reveals volume density for Noc3p. The shape of this volume map fits nearly perfectly to the published structure of pre-60 S particles at state E (Figure 29, PDB 6ELZ) (Kater et al. 2017). Local alignment of rRNA or proteins to the obtained volume density of Noc3-TAP-1 renders no significant structural changes of the published PDB structure. However, density for the protein chain Ybl028cp, has not been observed in Noc3-TAP-1 (Figure 29, left side, brown protein).

For the Noc3-TAP-1 volume, secondary structure elements of all expected r-proteins and biogenesis factors that are unambiguously placed within the structure can be observed, including Noc3p. The resolution is sufficient to localize rRNA and protein structures. However, the identification of rRNA bases or amino acids of proteins via their side chains through assignment of volume density is not possible. In some cases, unstructured parts of proteins that form heterogenous secondary structure elements are not resolved in the current volume density map of Noc3-TAP-1 (Figure 29, right side, yellow protein chain). In general, the coverage of volume density to the solvent exposed side which is largely formed by rRNA domains I, II and VI at an very early stage (Kater et al. 2017) is better and more defined that it is the case on the subunit interface side (Figure 29).

As mentioned above, the Noc3-TAP-1 volume map as well as the previously published structure of state E are characterized by structural stably incorporated 25S rRNA domains I, II, III and VI (Kater et al. 2017). In contrast, domains IV and V showed a partial stable conformation, whereas large parts of them are lacking in the structure. As indicated in Figure 30 (left side, rRNA depicted in gray), only subtle parts of domain IV are resolved in state E, splitting the domain in an “upper” and “lower” resolvable section. Structural information on rRNA within and in between these sections are lacking (25S rRNA bases 1954-2094, 2105-2121, 2131-2319).

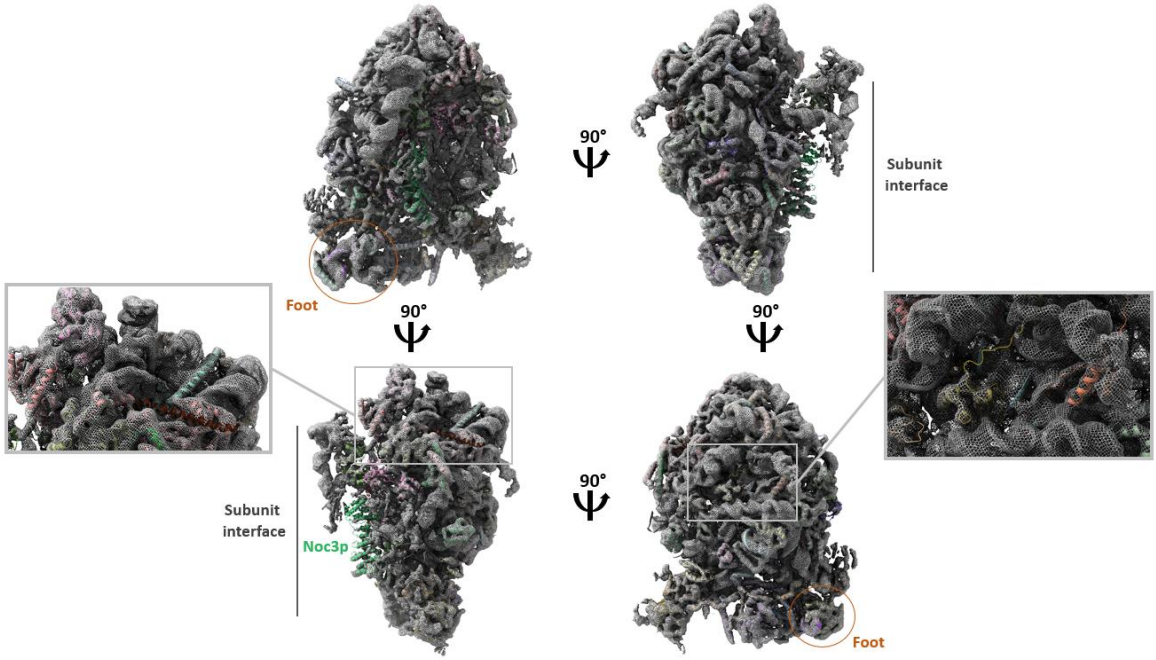

Figure 29: Fitting the volume density map of Noc3-TAP-1 to PDB 6ELZ.
The volume density map which was obtained for Noc3-TAP-1 (Figure 28) is fitted to the PDB structure 6ELZ (Kater et al. 2017). The matching was performed with ChimeraX (6.1.11). The volume density is colored dark grey, the PDB structure various colors, whereas Noc3p is highlighted in turquoise. Noc3p, the foot as well as the subunit interface are indicated for better orientation. The same overlay is shown in four different views, shifted by 90 °C across the y-axis, respectively.

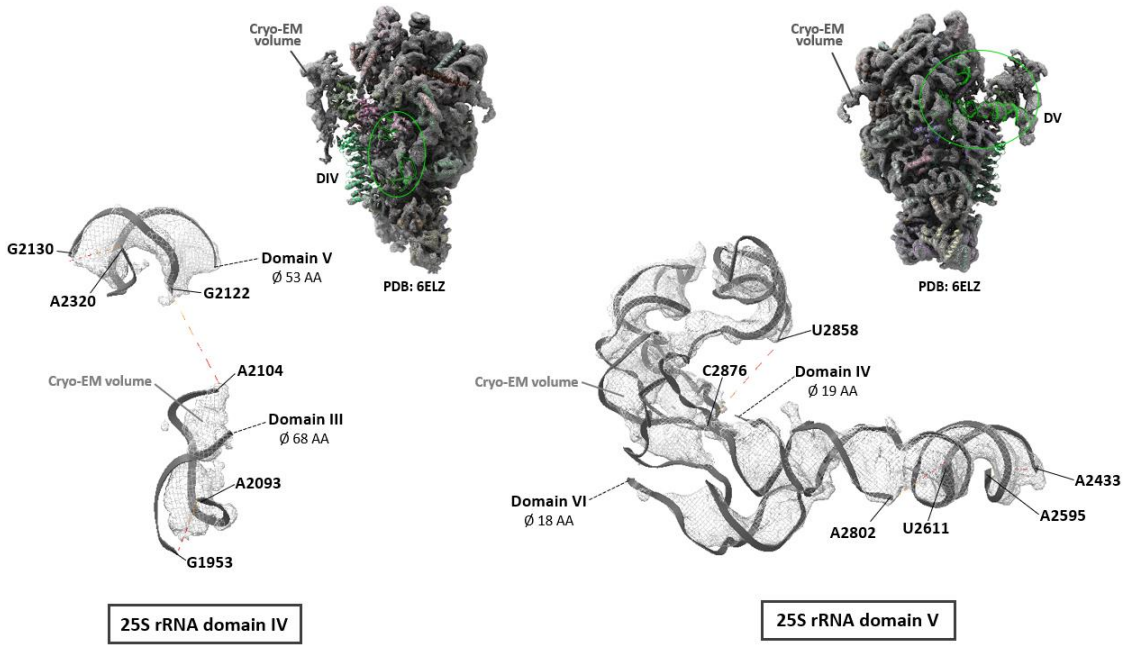

Figure 30: 25S rRNA domains IV and V are hardly stable assembled in Noc3-TAP-1 and PDB 6ELZ.
The volume density map which was obtained for Noc3-TAP-1 (Figure 28) is fitted to the PDB structure 6ELZ (Kater et al. 2017). The matching was performed with UCSF ChimeraX (6.1.11). The 25S rRNA domains IV (left side, "DIV") and V (right side, "DV") are highlighted in light green within the pre-60S particle fitted to Noc3-TAP-1 (compare Figure 29). Both domains are shown extracted from the particle (grey) and fitted to the volume density at these positions of Noc3-TAP-1 (light grey). Positions of particular rRNA bases are indicated.

The volume map of Noc3-TAP-1 (Figure 30, light grey mesh) fits to the placed nucleotides of DIV (domain IV). However, no additional volume density for unassigned rRNA of DIV can be deduced. The same accounts for domain V (Figure 30, right side). Certainly, larger parts of DV could be resolved, but, nevertheless, several are still lacking in the structure (25S rRNA bases 2434-2594, 2612-2801, 2859-2875). For these observations it can be concluded that in agreement with previous findings (Kater et al. 2017), pre-ribosomal particles that contain Noc3p are characterized by nearly completely stably folded rRNA domains I, II, III and VI, whereas domains IV and V have still high conformational flexibility. On the other hand, several extra densities were resolved to secondary structure resolution, both for rRNA and proteins. These extra densities are located at different positions within the particle. To better identify them, a volume map derived from state E (PDB 6ELZ) was generated, aligned with Noc3-TAP-1 and subsequently subtracted. This allowed the generating of a subtraction map, which is indicated in Figure 31 as orange mesh. Volume densities thus designated are exclusively found in Noc3-TAP-1 but not in state E.

As shown in A (Figure 31), the RNA helicase Has1p is only resolved to its C-terminal domain in state E. However, the current cryo-EM map Noc3-TAP-1 revealed a barrel-shaped volume nearby. It fits to the N-terminal domain of Has1p which is lacking in state E, when overlaid with the full length Has1p structure, obtained from a previously resolved pre-LSU (Sanghai et al. 2018b); PDB 6CB1). Thus, our data confirm the presence of full length Has1p in these Noc3p-associated pre-LSUs.

In B (Figure 31), additional volume density for Noc3-TAP-1 was observed in a hook-like shape at the solvent side of the pre-ribosome in the 25 S rRNA domain I. The shape and size of this volume suggests a rRNA structure rather than a protein one. The nucleotides 441-493 present in the expansion segment (ES) 7 were not resolved in the present structure. It seems meaningful that they localize within this extra density of Noc3-TAP-1. A possible trajectory of the rRNA extension throughout this volume is drawn in a black dashed line.

Further defined volume densities were observed at the subunit interface side of the pre-60 S particle close to the methyl transferase Nop2 (C, Figure 31). These extra volumes of Noc3-TAP-1 provide hints, of how the unresolved extensions of 25 S rRNA nucleotides 2435-2594 and 2612-2801 might progress throughout the subunit interface surrounding. In detail, the nucleotides 2434 and 2495 of the 25 S rRNA point away from the pre-ribosomal particle towards the subunit interface area. There, a corkscrew-like shaped volume density of Noc3-TAP-1 elongates with an offset of approximately 90 degrees to the rRNA extension, parallelly aligned to the core particle. The unresolved nucleotides may be somehow localized within this volume. A possible trajectory of how these nucleotides might be oriented is drawn in a black dashed line. However, extra density is not only observed above the horizontal plane of the rRNA extension but also beneath. For this, the exact rRNA course cannot be predicted.

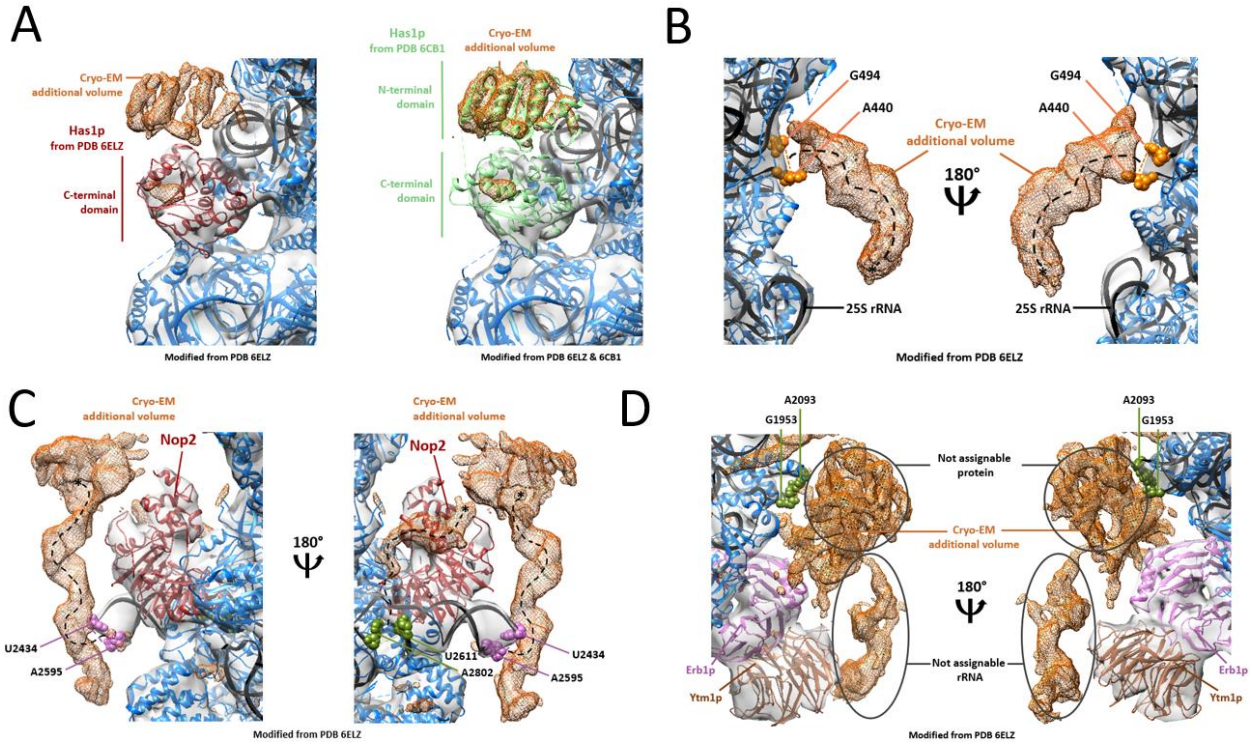

Figure 31: Characterization of extra densities in Noc3-TAP-1.
The volume density map of Noc3-TAP-1 was fitted to PDB 6ELZ as described for Figure 29 in UCSF chimera (6.1.11). A volume map based on 6ELZ was created with UCSF chimera (6.1.11) in slightly greyish and overlaid. This volume was subtracted from Noc3-TAP1 for direct identification of additional volumes (orange mesh). 6ELZ is colored in blue, whereof the 25 S rRNA is colored in black, respectively. (A) The C-terminal domain of Has1 is colored in brownish (left). Full length Has1 from PDB 6CB1 (Sanghai et al. 2018b) was fitted to Noc3-TAP-1 and colored in light green (right). (B) Atoms for the nucleotides G494 and A440 of the 25 S rRNA are shown and colored in orange. A possible trajectory of the missing nucleotides 441-493 of 25 S rRNA through the additional volume of Noc3-TAP-1 is indicated as black dashed line. (C) The atoms for U2434/A2595 and U2611/A2802 of 25 S rRNA are shown and colored in purple or green. Nop2 is highlighted in brown. Possible trajectories of the missing nucleotides 2435-2594 and 2612-2801 through the additional volume of Noc3-TAP-1 are indicated as black dashed line. (D) Atoms for the nucleotides G1953 and A2093 of 25 S rRNA are shown and colored in green. Erb1 is highlighted in purple, Ytm1 in brown. Extra volume of Noc3-TAP1 is classified in not assignable protein(s) and rRNA and indicated by black circles.

The nucleotides 2611 and 2802 of the 25 S rRNA are located in the immediate neighborhood of the ones mentioned above. A clear assignment of the missing bases to extra volume densities of Noc3-TAP-1 is yet difficult to achieve. The first nucleotides of this unresolved rRNA extension might suit into a volume tube which points towards Nop2 (Figure 31, C, right image). A possible trajectory for this option is drawn in a black dashed line. However, with 192 nucleotides in length, this rRNA section represents a relatively long unresolved portion. It seems possible, that this rRNA extends to the enlarged head of the corkscrew-shaped volume. However, its course throughout the volume densities of Noc3-TAP-1 cannot be defined more precisely.

Besides these rather defined findings for extra volume densities within Noc3-TAP-1, volumes were observed for which it was not possible to assign them to a certain protein or to draw a possible continuation of unresolved rRNA. These findings are shown in D (Figure 31). Here, two subsections of additional volume could be detected. One section constitutes a stretched volume, winded within itself,

similar to C (Figure 31). It is located close to the biogenesis factors Ytm1p and the C-terminal domain of Erb1p. The other section constitutes a rather undefined aggregate that implies volume structures that may rather fit to a protein structure than to rRNA one. Concomitantly, it seems possible, that volumes for rRNA are present as well. For instance, the 25S rRNA nucleotides 1954-2092 are not resolved in state E which form the ES 27 of 25S rRNA domain IV. The flanking 25S rRNA nucleotides 1953 and 2093 are, as indicated in D (Figure 31), adjacently localized to this volume aggregate. Possibly, ES 27 might pass through this volume and progress towards Ytm1p and Erb1p. However, these suggestions remain highly speculative and need further investigation.

As already mentioned, volume density for Noc3p could be observed in Noc3-TAP-1. This volume fits as a whole perfectly to the described structure of Noc3p from state E (Figure 32). The Noc3-TAP-1 map reveals no extra volume for the N-terminus of Noc3p. Hence, the shape and orientation of 131 unresolved AA at its N-terminus remains further elusive. However, additional volume density could be detected at the C-terminus. Here, Noc3-TAP-1 reveals a triangle-shaped volume adjacent to the last resolved amino acid at the C-terminus of Noc3p. Therefore, additional information of its C-terminus including the NOC-motif can be deduced to secondary structure resolution (for structure of the NOC-motif see Figure 26).

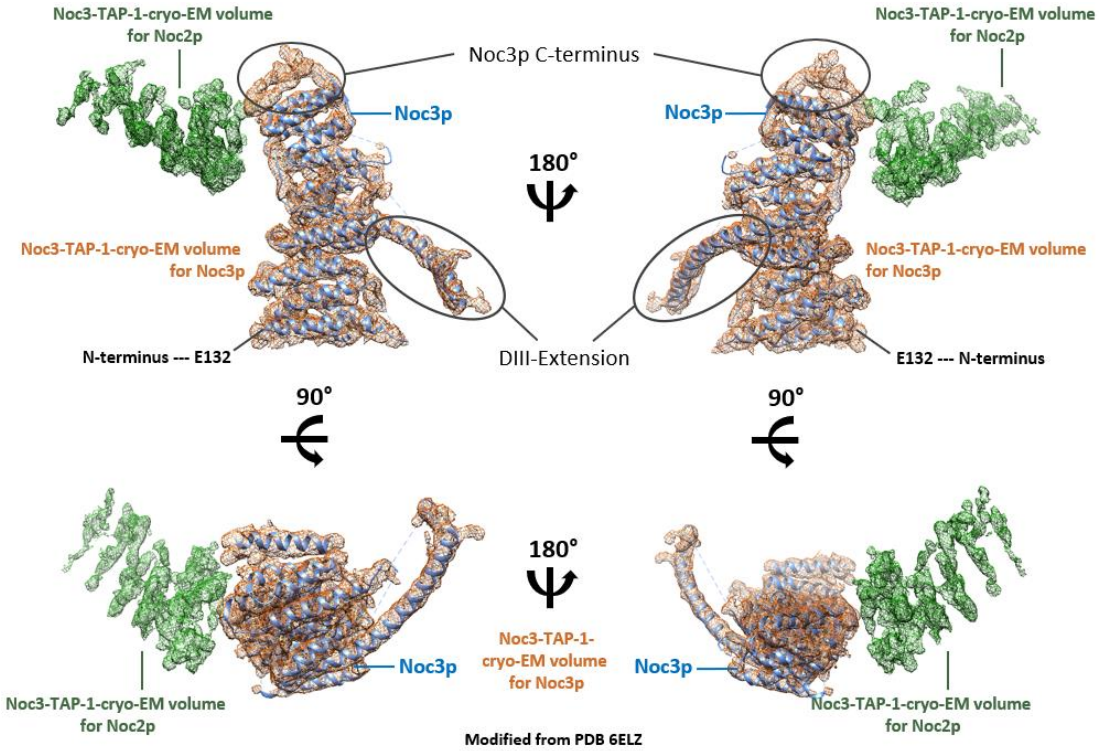

Figure 32: Detected volume densities for the Noc2p-Noc3p heterodimer in Noc3-TAP-1.
The volume density map of Noc3-TAP-1 was fitted to PDB 6ELZ as described for Figure 29 in UCSF chimera (6.1.11). A subtracted volume map for Noc3-TAP-1 and 6ELZ was generated. Parts of Noc5p derived from PDB 5WLC (Barandun et al. 2017) were fitted to unassigned volume densities in the subtraction map close to Noc3p. The respective volume densities for Noc3p obtained from Noc3-TAP-1, volume derived from Noc5 and additional volume observed at the C-terminus of Noc3p from the subtraction map were split and fitted to the structure of Noc3p (6ELZ). Noc3p is colored in blue, its associated volume in orange and the predicted volume for Noc2p in green.

Moreover, we were looking for volumes that indicates the localization and orientation of the binding partner of Noc3p, Noc2p. To reveal them, the Noc4p/Nop14/Noc5p dimer from PDB 5WLC (Barandun et al. 2017) has been placed in the map of Noc3-TAP-1. This was possible to the fact that Noc3p and Noc4p share high structural homology with each other (Figure 24). Hence, the volume map pf Noc3-TAP-1 can be fitted with the Noc4p/Nop14/Noc5 heterodimer, at least for the main parts of the proteins. The findings indicate a possible volume density for Noc2p, close to the C-terminus of Noc3p (Figure 32, green volume). The volume forms tubular structures similar to HEAT-repeats, which are characteristic for the Noc-proteins.

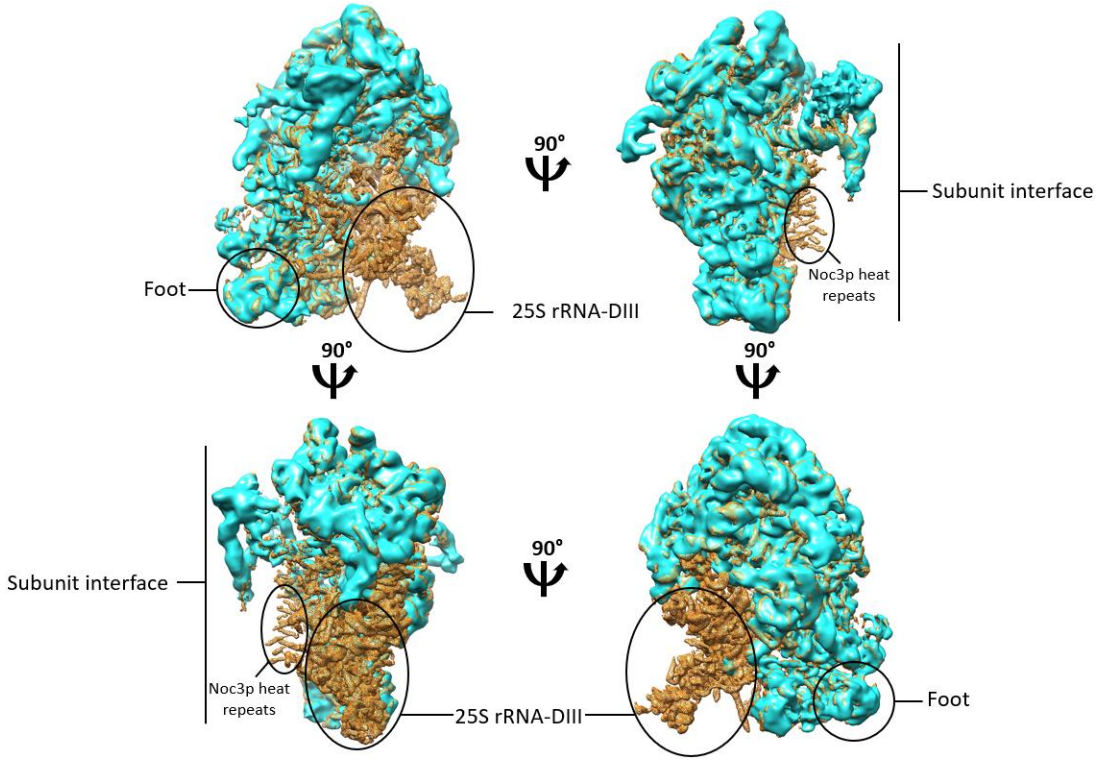

Figure 33: Difference map between Noc3-TAP-2 and Noc3-TAP-1.
The volume density maps of Noc3-TAP-2 (turquoise) and Noc3-TAP-1 (orange mesh) were fitted to 6ELZ (not shown) in UCSF chimera (6.1.11). The resulting difference map reveals similarities and differences between the two sub-populations associated with Noc3p. For better orientation, the subunit interface, the foot and the 25 S rRNA domain III are labelled. The same overlay is shown in four different views, shifted by 90 °C across the y-axis, respectively.

Altogether, the cryo-EM analysis provides insights into the structural conformation and resolvability of Noc3p associated pre-ribosomal main- and subpopulations. The difference map shown in Figure 33 points out similarities but especially differences between the earliest detectable population Noc3-TAP-2 and the “main” population Noc3-TAP-1.

The findings indicate, that Noc3p associates already with pre-ribosomes upon their stable assembly of domains I, II and VI. Notably, resolvability of the domains means visibility of the rRNA and not of all associated proteins. Moreover, the rRNA conformation within the particular precursor does not reflect the rRNA conformation as it will be in the mature large subunit. At this state, domain III is yet not

resolved as it is not yet stably oriented. The shape of this Noc3-TAP-2 particle is largely in agreement with state C (Kater et al. 2017). The main population of pre-LSU particles associated with Noc3p is represented by Noc3-TAP-1. Its conformational shape is highly similar to state E (Kater et al. 2017). In addition, extra densities, especially on the subunit interface side, could be resolved and roughly assigned to the particle as well. Importantly, Noc3p is resolved in the volume map of Noc3-TAP-1, contrarily to the remaining maps Noc3-TAP-2, Noc3-TAP-3 and Noc3-TAP-4. The latest Noc3p associated pre-ribosomal population is represented by Noc3-TAP-4. Notably, these Nog2-like particles to which Noc3p associates contain a stably positions 5S rRNA atop of the pre-LSU. In these particles, larger parts of LSU domains IV and V are well resolved, which is not the case in Noc3-TAP-1 (compare Figure 30). This indicates, that Noc3p stays associated with pre-60 S particles until the 25 S rRNA domain III has been stably oriented and furthermore, gets released upon a maturation state similar to the Nog2-particle (Wu et al. 2016).

4.2 Functional characterization of the Noc2p/Noc3p interaction and their association with pre-ribosomes

4.2.1 Noc2p interacts with Noc3p via domain 6 close to its C-terminus

Noc2p/Noc3p build a protein heterodimer that associated with large ribosomal subunit precursors (Milkereit et al. 2001). Previous experiments on the association of Noc-proteins with ribosomal precursors by sucrose gradient centrifugation revealed a co-sedimentation of Noc3p together with particles containing 27SB and 7S pre-rRNA (Milkereit et al. 2001). In contrast, Noc1p co-sediments with pre-ribosomes that contain 35S and $27SA_2$, pre-rRNA. For this it was concluded, that Noc1p and Noc3p are associated pre-ribosomes of different maturation states. Notably, as Noc2p binds to both Noc1p and Noc3p, it has been found to co-sediment with the respective pre-rRNAs (35S-, $27SA_2$-, 27SB- and 7S- pre-rRNA). Therefore, Noc1p/Noc2p already associates with early 90 S-, whereas Noc2p/Noc3p mostly associates with 66 S pre-ribosomes, depicting an intermediate maturation state (Milkereit et al. 2001; Hierlmeier et al. 2012) (see also 3.8).

However, it is not clearly known, how the interaction between Noc2p and Noc3p is formed. Based on homology-modelling shown in Figure 27, Noc2p and Noc5p share a high degree of homology for structurally similar domains. According to available structural data on Noc4p and Nop14/Noc5p from cryo-EM analyses (Barandun et al. 2017), it can be deduced, where the two proteins are in close physical proximity to each other.

Hence, Noc2p is subjected to more detailed analysis to figure out possible interaction sites with Noc3p. Therefore, the Noc2p-truncation-constructs created by Thomas Hierlmeier during his diploma thesis (see 3.8) have been utilized. These truncation variants are schematically illustrated in Figure 34. In

order to check, whether the respective ProtA-Noc2-ΔXp alleles can at all complement the intrinsic function of *NOC2*, complementation tests have been performed.

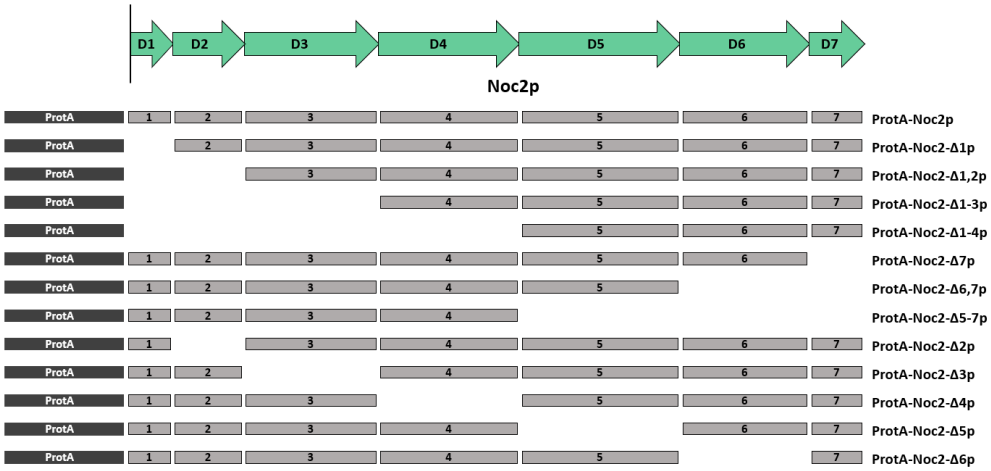

Figure 34: Schematic overview of Noc2p truncations.
The domains of Noc2p according to homology modelling are schematically shown (green arrows). The different ProtA-Noc2p/ProtA-Noc2p-ΔXp fusion proteins that were analyzed are shown and indicated by black and grey rectangles, respectively. The length of the rectangles correlates to the size of the domains.

The genetic system for this approach is illustrated in Figure 35 (A). In the strain Y1656 (6.1.1), the gene *NOC2* has been genomically deleted. The resulting lethal phenotype is rescued by a plasmid containing the sequence encoding a functional Noc2p, which in addition contains the gene *URA3* to complement the uracil auxotrophy marker of the yeast strain used. Plasmids containing the different pNOP-PA-*NOC2*/*noc*-ΔX alleles fused to the TAP tag were introduced in the described yeast strain and transformants were selected by the LEU2 gene. For the entire experimental procedure, a temperature of 24 °C has been chosen. For this, the different ProtA-Noc2-ΔXp variants will not be interpreted as unfunctional due to possible temperature sensitivity.

Using this system, the functionality of the different Noc2p-ΔXp variants has been analyzed. For this, the transformants have been counter-selected in medium containing FOA. Notably, FOA (5´-Fluoroorotic acid) is converted into a toxic metabolite in the presence of the gene *URA3*, encoded on the plasmid containing the wild type *NOC2* sequence. Hence, strains which are able to lose the "wild type plasmid" produce a functional Noc2-ΔXp. To test this, eight arising colonies of each strain have been subjected to a complementation test on $SDC_{\text{-Leu +FOA}}$ plates (Figure 35, B).

Only the strains that express the Noc2p variants PA-noc2-Δ1, PA-noc2-Δ2, PA-noc2-Δ1,2, and PA-noc-Δ7 (K1019, K1020, K1021, K2027 and K1139, respectively) were able to form colonies on the FOA-containing plates at 24 °C (Figure 35, B). These strains are therefore able to lose the YCplac33-*NOC2* plasmid indicating that the N-terminal domains 1 and 2 as well as the C-terminal domain 7 do not significantly contribute to the function of Noc2p.

A

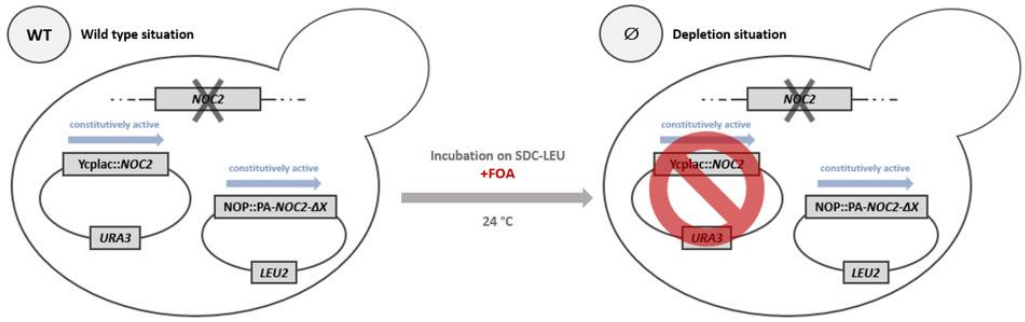

B

DB	Plasmid	Growth
V17	pNOP-PA	-
K1019	pNOP-PA-*NOC2*	+
K1020	pNOP-PA-*noc2-Δ1*	+
K1021	pNOP-PA-*noc2-Δ1,2*	+
K1027	pNOP-PA-*noc2-Δ2*	+
K1022	pNOP-PA-*noc2-Δ1-3*	-
K1135	pNOP-PA-*noc2-Δ3*	-

DB	Plasmid	Growth
K1023	pNOP-PA-*noc2-Δ1-4*	-
K1136	pNOP-PA-*noc2-Δ4*	-
K1025	pNOP-PA-*noc2-Δ5-7*	-
K1137	pNOP-PA-*noc2-Δ5*	-
K1024	pNOP-PA-*noc2-Δ6,7*	-
K1138	pNOP-PA-*noc2-Δ6*	-
K1139	pNOP-PA-*noc2-Δ7*	+

Figure 35: Complementation test of different PA-noc2-ΔX alleles.
The strain Y1656 (6.1.1) has been transformed with plasmids that contain the different PA-*NOC2*/*noc2-ΔX* alleles indicated in Figure 34 (and 6.1.2) and incubated for 3 days at 24 °C on SDC_{-Leu} plates. Arising colonies have been streaked out for complementation analysis on $SDC_{-Leu\ +FOA}$ and incubated for another 3 days at 24 °C. (A) Schematic illustration of the genetic system and experimental procedure that has been applied for the complementation test. (B) The complementing Noc2-alleles on the respective pNOP-PA derivate are indicated by a "+/-" in the column "growth". They have been identified by selection on FOA-containing agar plates. These strains have lost the YCplac33-*NOC2* plasmid. V17 is the empty vector control.

Knowing, which Noc2-ΔXp variants were able to replace wild type Noc2p, focus was at next laid on the molecular characterization of the different variants. Therefore, their ability to associate with Noc3p and to get incorporated into pre-ribosomal particles has been analyzed in more detail. This required an intact *NOC2* allele than can, when necessary, be shut down or inactivated. Characterization of the Noc2-ΔXp variants against the background of a functional Noc2p is possible but could lead to competitive effects and complicate the interpretation. As cell culture with medium containing FOA is not possible and a depletion strain was not available, a temperature sensitive mutant strain bearing a *noc2-1* allele has been used for this purpose (Figure 36, A). At temperatures of 30 °C the respective Noc2p gene product loses its function which was observed by changes in pre-rRNA processing (Milkereit et al. 2001). This strain was transformed with the plasmids carrying the sequence information for the *noc2-ΔXp* alleles (Figure 34). Additionally, Noc3p is expressed as genomically encoded Myc-tag fusion protein in order to detect its presence within the complex together with the Noc2-ΔXp variants.

Regarding the Western blot analysis, the expression pattern varies among the Noc2p-ΔXp variants. The individual Noc2-ΔXp variants are, even though at different levels, detected both in the inputs and enriched in the affinity purified factions (Figure 36, B). However, signals for PA-noc2-Δ5-7 and PA-noc2-Δ5 are hardly detectable, which might indicate a very low expression of these proteins (Figure 36, B,

lanes 23-26). It seems, that N-terminal truncated variants of Noc2p are still detected in higher amounts in contrast to large C-terminal deletions. Obviously, the latter one has a destabilizing effect on the protein itself.

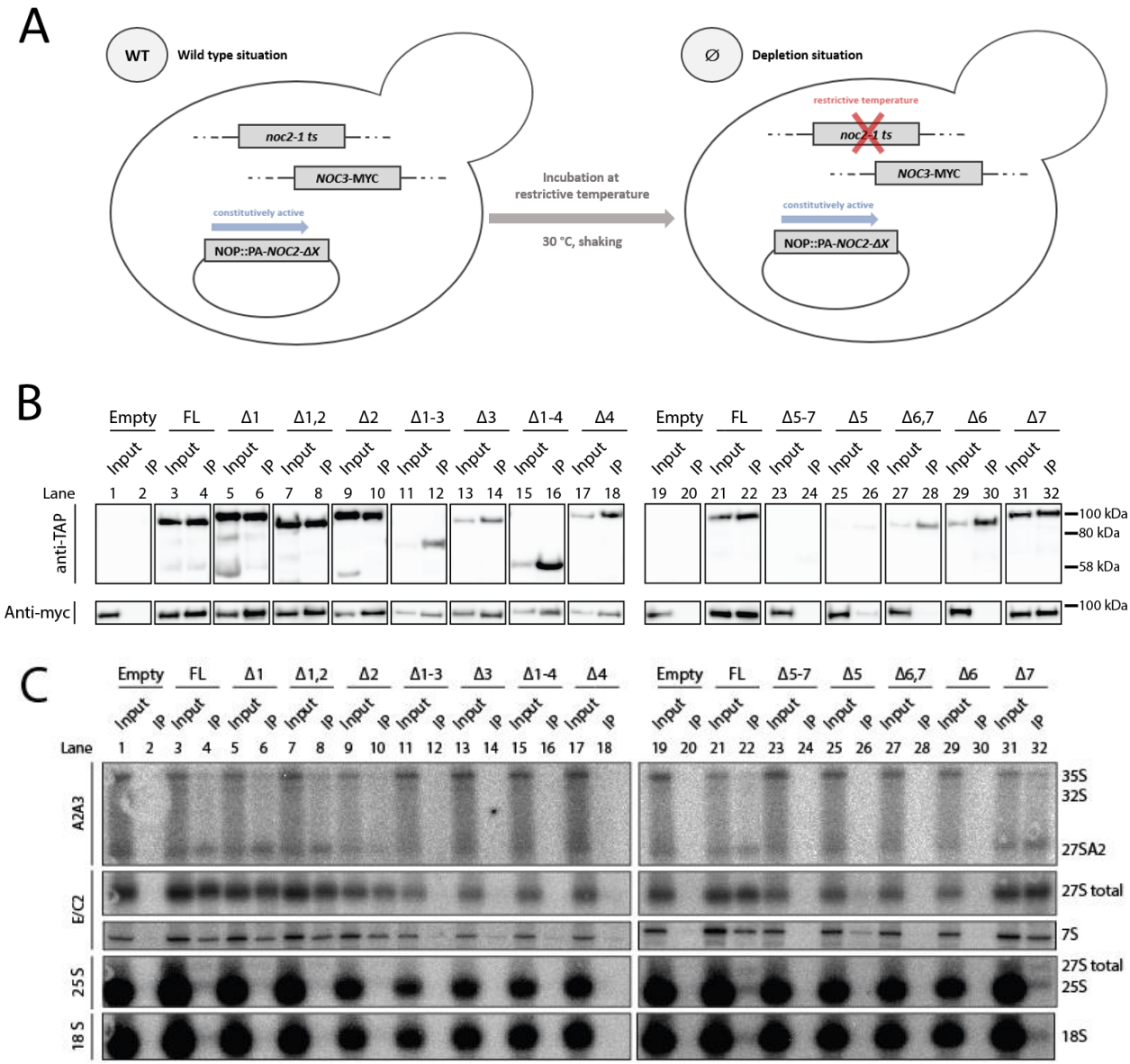

Figure 36: Analysis of pre-rRNA and Noc3p co-purified with tagged PA-Noc2-ΔXp truncation versions.
(A) The strain Y1640 (6.1.1) has been transformed with the plasmids that contain the different PA-*NOC2*/*noc2-ΔX* alleles indicated in Figure 34. The genetic system used for this approach as well as the experimental procedure is schematically described. (B) Exponentially growing yeast cells of Y1640 transformed with the noc2-ΔX alleles (6.1.2) which were grown at 24 °C were used to inoculate fresh medium. The cultures were incubated at the restrictive temperature of 30 °C for 4 h and subsequently harvested. PA-Noc2-ΔXp associated pre-ribosomal particles were affinity purified from the respective total cell extracts (6.2.6.3) using IgG sepharose beads (6.1.9). Aliquots of cells corresponding to 0,63 % of the input and 11 % of the purified material were separated by SDS-PAGE (6.2.5.3) and analyzed by western blotting (6.2.5.4). The bait proteins were visualized using the PAP detection reagent (6.2.5.6). (C) Total RNA was isolated by phenol/chloroform extraction (6.2.4.1). Total RNA was size separated on agarose and acryl amide gels. 0,32 % of total input and 11 % of the purified material (IP) were loaded, respectively, and analyzed by sequential northern hybridization using the indicated probes. For hybridization sites of the oligos see 6.1.3.3.

Noc3p was largely detected in the affinity purified fractions. Regarding its association with the Noc2p-ΔXp variants, N-terminal truncations of Noc2p did not affect its association with Noc3p. Even if the first four domains from the N-terminus were truncated, Noc3p was nevertheless co-purified (Figure 36, C, lane 16). Regarding the C-terminal truncations, only truncation of domain 7 allowed an efficient co-purification of Noc3p (C, lane32). If more domains were lacking, the formation of the Noc2p/Noc3p heterodimer is prevented. However, if single domains within Noc2p excluding domain 6 are truncated, the co-purification of Noc3p and hence the formation of the heterodimer is in turn possible. Noc3p is still co-purified by these mutants with truncated domains 2 (lane 10), 3 (lane 14), 4 (lane 18) or 5 (lane 26). For the truncation of domain 6 however, no Noc3p has been co-purified. These findings indicate that solely domain 6 of Noc2p is indispensable for the formation of the heterodimer with Noc3p.

Regarding the association of these Noc2-ΔXp variants with pre-ribosomes shows a similar trend as their ability to functionally replace wild type Noc2p. Signals for co-purified pre-rRNAs were, beside for full length Noc2p, solely observed for the truncated versions Noc2-Δ1p, Noc2-Δ2p, Noc2-Δ1,2p and Noc2-Δ7p (Figure 36, C, lanes 4, 6, 8, 22, 32). In these mutants, 35S-, $27SA_2$-, 27SB- and 7S-pre-rRNA has been co-purified, respectively. This reflects the co-purification of different ribosomal precursor populations associated with Noc1p and Noc3p. As introduced (see section 3.8), Noc2p binds to pre-ribosomes together with Noc1p at an early, in complex with Noc3p at an intermediate maturation state (Milkereit et al. 2001). The signal intensities for the respective pre-rRNA species in the affinity purified fractions are comparatively similar to the wild type situation observed for full length Noc2p (Figure 36, C, Lanes 4, 22). Obviously, these truncated versions of Noc2p do neither impair the maturation of pre-ribosomes nor the association with each other. This coincides with their ability to complement the function of full length Noc2p (Figure 35, B).

The remaining Noc2-ΔXp variants hardly co-purify any pre-rRNA, indicating that the association with pre-ribosomes in these mutants is strongly disturbed. Regarding the input fractions of these mutants, the 35S pre-rRNA seems to slightly increase over the $27SA_2$ pre-rRNA which indicates a possible processing defect already at an early state. The cause for low co-purification of pre-rRNA species by certain Noc2p-ΔXp variants is however unclear. It might be, that the respective variants are unable to associate with pre-ribosomes, or, if they get assembled, they fail to fulfill their function which blocks pre-rRNA processing at an early state (also discussed in section 5.3).

4.2.2 Structure based mutagenesis of Noc3p

Having analyzed the formation of the Noc2p/Noc3p heterodimer in dependence of Noc2p, the next step is to further reveal the structural prerequisites of Noc3p which are necessary for their interaction. To do so, a series of Noc3p mutants has been generated. According to the deciphered structure of Noc3p in state E (Kater et al. 2017), its N- and C-termini have been successively truncated.

Therefore, a vector that implies the full-length sequence of wild type Noc3p has been used as PCR template. Appropriate primers have been designed (6.1.3.1) to generate PCR products (6.2.3.3) that lack a desired 5´- or 3´- sequence which reflects the corresponding amino acids of Noc3p to be truncated. Using standard cloning methods (6.2.3) the PCR-amplified *NOC3* sequences have been inserted into an appropriate vector (see 6.1.2). Flanking to restriction sites for insertion of the PCR product, the vector backbone contains a RPS28-promotor and a FLAG-tag for affinity purification, followed by a LEU2-marker gene used for selection of positive transformants. Hence, the newly generated vectors constitutively produce a mutated Noc3p fused to a C-terminal FLAG tag *in vivo*.
Additional to N- and C-terminal truncations, the loop of Noc3p, which originates between the heat-repeats of Noc3p and reaches to the 25 S rRNA domain III of the pre-ribosome has also been modified (for further details see Figure 38). To generate the respective vectors for this purpose, the sequences of the modified Noc3p-extensions have been ordered as gene synthesis products and directly integrated in the vector described above.

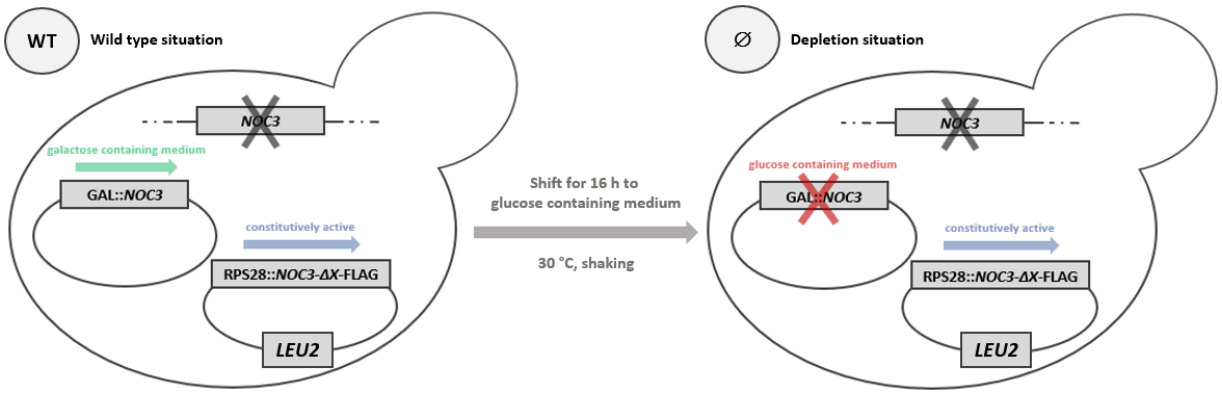

Figure 37: Genetic system for analyzing Noc3p mutants.
The strain Y777 (6.1.1) serves as basis for this purpose in which the genomic information of *NOC3* has been deleted. The strain additionally includes a plasmid which implies the sequence information of wild type Noc3p, however, under the control of a galactose inducible, glucose repressible GAL1/10 promoter. The Noc3p variants to be analyzed are under the control of a constitutively active RPS28-promotor. Upon shift to glucose containing medium, wild type *NOC3* is repressed and solely the Noc3p variants are transcribed.

The genetic system for the analysis of Noc3p mutants is schematically illustrated in Figure 37. In the parent strain for this purpose, the genomic sequence of *NOC3* has been deleted. The deletion has been replaced by a plasmid that encodes for wild type *NOC3* under the control of a galactose inducible, glucose repressible galactose promoter (strain Y777, see 6.1.1). The plasmids containing the mutated versions of Noc3p are transformed in this strain. After induction of an expressional shut down for full length *NOC3* on glucose containing medium for 16 h, the mutated versions of Noc3p can be subjected to detailed analysis.

4.2.3 The loop of Noc3p contacting the 25S rRNA-DIII is essential for cell growth and impairs the association of Noc3p with pre-ribosomes

Previous cryo-EM analyses have deciphered the structure of a series of large subunit precursors and associated proteins including Noc3p to near atomic resolution (Kater et al. 2017). These studies provide detailed information to specifically mutate desired strtuctural elements or residues within proteins and to further analyze their function.

Regarding Noc3p, it is apparent, that a long helical extension, helix Hn+9 (Figure 26) emerges approximately from the middle of the protein between two α-helical repeats and reaches close to the 25 S rRNA domain III, probably directly contacting it or associated protein(s). From the "tip" of the extension a peptide chain of an undefined structure reaches back to the core protein. Importantly, both the extension, designated as helix Hn+9 (see Figure 26) and the protein chain reaching back are together referred to and hereafter called as "loop".

To analyze a possible function of the loop on the association of Noc3p with pre-ribosomes, several mutant alleles of *NOC3* within the respective coding region have been created. The following experiments have been performed with the genetic system and the vectors described in 4.2.2 if not stated otherwise. This issue has been adressed by two approaches.

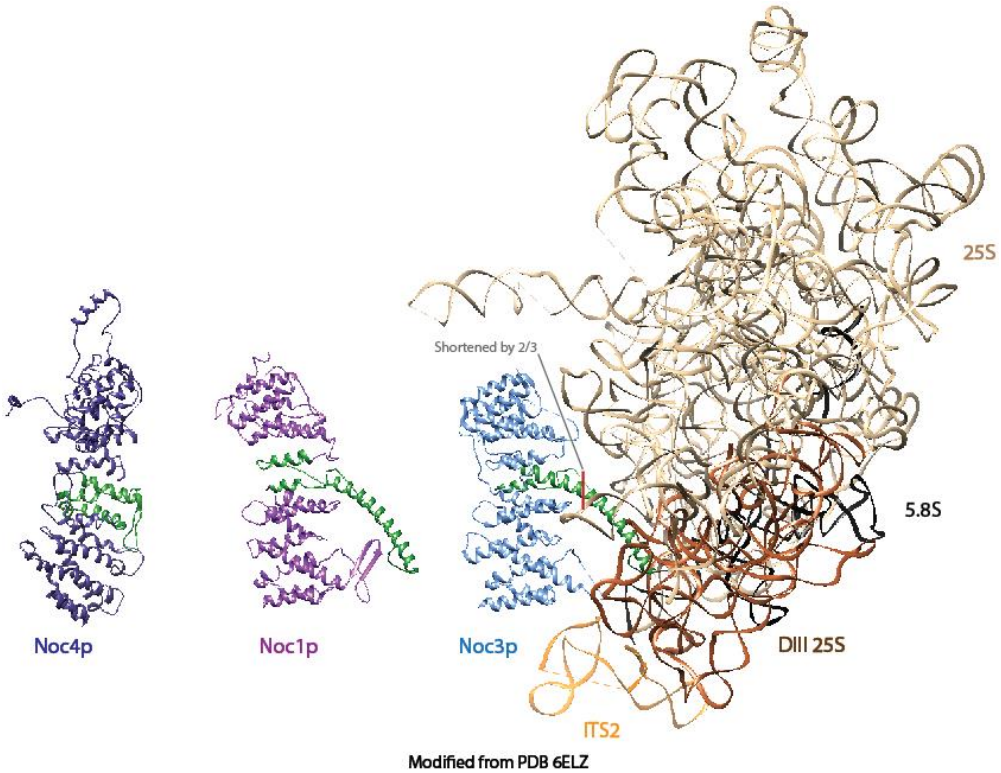

Figure 38: Altering the 25 S rRNA domain III extension of Noc3p.

The following illustrations were created using UCSF chimera (6.1.11). Noc3p associated with pre-ribosomes of state E (PDB 6ELZ) is shown on the right. The 25 S rRNA is colored in tan, whereof its intrinsic domain III is highlighted in brown. The ITS2 (orange) and 5.8 S rRNA (black) are indicated as well. The domain III extension of Noc3p is colored in green. It has been replaced by structure emerging at the same position of Noc1p (violet) and Noc4p (purple), colored in green- respectively. The structure of Noc4p has been obtained from PDB 5WLC, the structure of Noc1p by prediction according to homology modeling to known protein sequences (Pyhre 2, http://www.sbg.bio.ic.ac.uk/~phyre2/).

On the one side, the extension of Noc3p was shortened by two third of its original length and as well fully truncated. On the other side, it has been replaced by homologous structures from Noc1p or Noc4p. The corresponding polypeptide chains are indicated in green in Figure 38. The structure of Noc4p has been recently resolved by cryo-EM analysis of the SSU processome (see also Figure 26, section 3.8) (Barandun et al. 2017). The structure of Noc1p has been predicted via homology modeling to known protein sequences using an online tool for structure fold recognition (Phyre 2; http://www.sbg.bio.ic.ac.uk/~phyre2/).

At first, the domain III extension variants were tested for complementation. Therefore, spot tests as described in 6.2.1.7 of Y777 (Figure 37) transformed with the different *noc3*-alleles have been performed (Figure 39, A). The strains were grown in selective medium lacking leucin to select for cell containing the plasmids encoding the Noc3p-variants. Colony formation was compared between galactose and glucose containing medium.

As expected, the strain transformed with the plasmid encoding functional Noc3p was able to form colonies both providing either glucose or galactose as fermentable carbon source (Figure 39, A, “Full”). In contrast, the strain containing the empty plasmid did not grow on glucose containing medium due to the expression shut down of Noc3p (Figure 39, A, “Empty”).

The full deletion as well as shortening of the loop by two third of its original length is lethal. The transformants were not able to grow on glucose (Figure 39, A, “No Loop” and “Short”). This indicates that these *noc3*-alleles do not produce a functional Noc3p. The loop or parts of it seem to be essential for Noc3p to fulfill its correct function. Furthermore, replacement of this feature by homologous sequences from Noc4p or Noc1p (Figure 39, A, “Loop Noc1p” and “Loop Noc4p”) did not improve growth on glucose when compared to the short-loop or the complete loop-deletion. Notably, the “extension” of Noc4p is short and with undefined structure (Figure 38; see also Figure 26). The extension of Noc1p seems to be similar in size and shape compared to Noc3p´s, however, a structure prediction does not necessarily reflect the real situation. Therefore, the extension of Noc3p seems to be unique and specifically adapted for its intrinsic function.

To check, whether the pre-ribosomes underlie a processing defect as consequence of the Noc3p extension mutants, the rRNA processing phenotype has been characterized (Figure 39, B). Therefore, the strains have been cultivated in glucose containing medium to shut down the expression of wild type Noc3p. After 0, 6, 9, 16 and 22 h growth, equal cell amounts have been harvested and subjected to detailed RNA analysis. Given by the fact, that Noc3p associates predominantly with LSU precursors of an intermediate maturation state (Milkereit et al. 2001), the 27SB pre-rRNA has been quantified over the 7S pre-rRNA (Figure 38, B, northern blots not shown).

Regarding the 0 h time point, the ratios of 27 SB- over 7 S- pre-rRNA are very high and heterogenous. This may be due to growth in selective medium over night before they were shifted to full medium.

After 6 h, at least, the ratios in all strains were noticeably reduced to a uniform value. With exception of cells expressing the full-length Noc3p, which showed a constant ratio of 27SB/7S over the time course, the longer the cells were cultivated in glucose containing medium, the higher the accumulation of 27SB over 7S pre-rRNA can be observed. The “empty” control as well as the complete truncation of the loop reach their maximum accumulation of 27SB over 7S pre-rRNA after 16 h. The replacements of the loop by structures of Noc1p and Noc4p also generate a continuous increase of the 27SB/7S ratio.

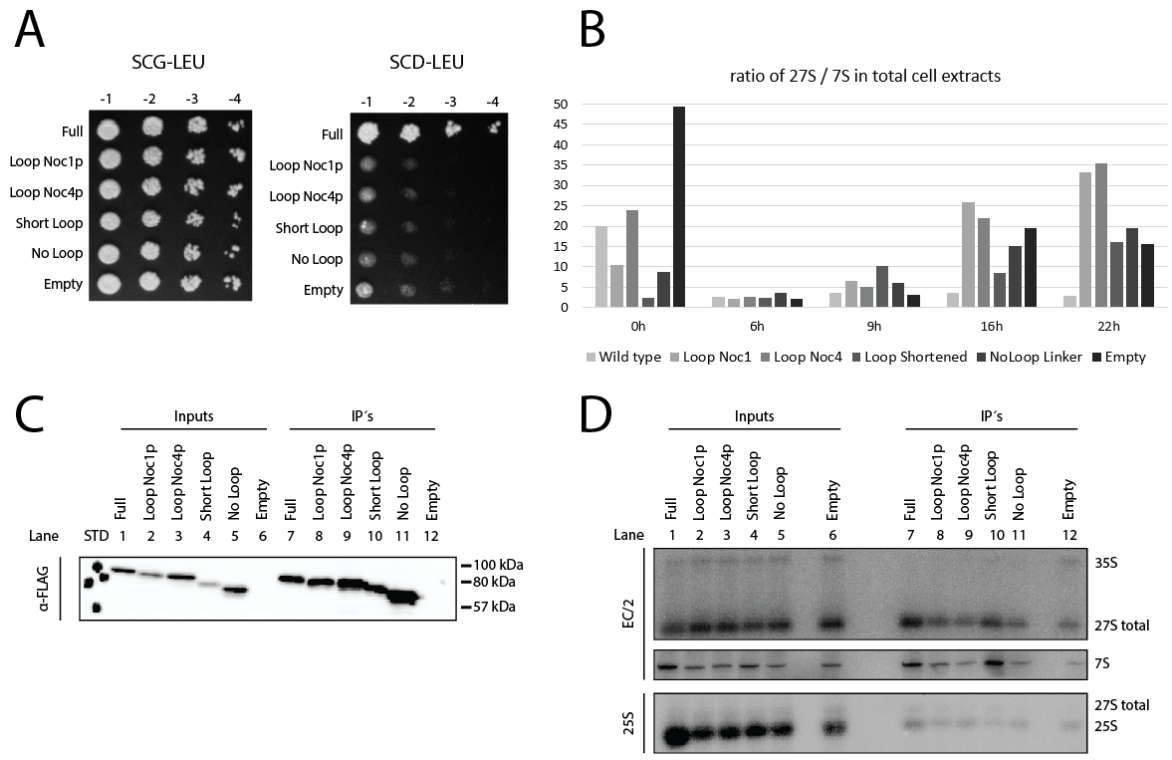

Figure 39: Analysis Noc3p-associated pre-ribosomes with an altered domain III extension concerning pre-rRNA incorporation, complementation and pre-rRNA processing.

The strain Y777 (6.1.1) has been transformed with the plasmids that contain the different *NOC3* alleles (6.1.2) indicated in Figure 38. The genetic system used for this approach is described in Figure 37. Exponentially growing yeast cells of Y777 transformed with the different *NOC3*-alleles were used to inoculate glucose containing medium. The depletion time was set to 16 h. (A) Exponentially growing cells on glucose containing medium corresponding to 2 OD_{600} have been harvested at the indicated time points. The cells were directly subjected for isolation of total RNA by phenol/chloroform extraction (6.2.4.1). Total RNA was size separated on agarose and acryl amide gels (6.2.4.2 and 6.2.4.3). (B) Signal ratios of 27 SB and 7 S pre-rRNA were quantified using MultiGauge software (Fujifilm) (6.1.11) from the agarose membrane (not shown). Calculated ratios are shown for each time point and each mutant, respectively. (C) Affinity purification was performed from total cell extracts (6.2.6.4) using M2-Anti FLAG affinity gel (6.1.9). Aliquots of cells corresponding to 0,8 % of the input and 11 % of the purified material were separated by SDS-PAGE (6.2.5.3) and analyzed by western blotting (6.2.5.4). The bait proteins were visualized using the PAP detection reagent (6.2.5.6). (D) Total RNA was isolated by phenol/chloroform extraction (6.2.4.1). Total RNA was size separated on agarose and acryl amide gels (6.2.4.2 and 6.2.4.3). 0,4 % of total input and 11,1 % of the purified material (IP) were loaded, respectively and analyzed by sequential northern hybridization using the indicated probes. For hybridization sites of the oligos see 6.1.3.3.

The shortened extension induces a continuously increasing accumulation as well, remains however below the latter ones. A longer period of growth in glucose containing medium has not been considered as reasonable due to side effects that may arise as consequence of ribosomal depletion

over time. The data indicate a disturbed processing of 27SB pre-rRNA to 7S and 25.5S pre-rRNA for all loop variants.

To further characterize the domain III extension of Noc3p and its variants, their capability to associate with pre-ribosomes has been analyzed. Therefore, pre-ribosomal particles have been affinity purified via the FLAG tag, which is C-terminally fused to the respective Noc3p variant (see section 4.2.2). The depletion time was set to 16 h, as accumulation of 27SB pre-rRNA was observed to reach its maximum at this time point for the empty control (Figure 39, B).

The western blot for this analysis indicates an efficient expression and a successful affinity purification of the Noc3p variants. Their size is in agreement with the amount of deleted or replaced residues of the domain III extension (Figure 39, C).

Regarding the input fractions of the northern analysis, the ratio of 27SB to 7S pre-rRNA inverts when comparing the strain which expresses the full-length version of Noc3p to the strain containing the empty plasmid (Figure 39, D, lanes 1 and 6). 7S pre-rRNA can be detected for full-length Noc3p, however, a substantial higher amount of 27SB pre-rRNA arises for the empty control. This indicates an affected processing of 27SB pre-rRNA in the absence of Noc3p and hence an accumulation of this pre-rRNA species. Congruently, the same observation has already been made when analyzing the processing phenotype as described above (Figure 39, B). Moreover, the decreased levels of 25S rRNA are lower, thus indicating the impaired maturation of pre-LSUs (Figure 39, D, lanes 1-6). The levels of 7S pre-rRNA versus 27SB pre-rRNA are lower in the “Loop Noc1p”, “Loop Noc4p” and the “Short Loop” variants compared to full-length Noc3p (Figure 39, D, lanes 1-6). This indicates an affected conversion of 27SB pre-rRNA to 25.5S- and 7S- pre-rRNA in these strains.

The validity of the affinity purified fractions is however not clear, due to high background signals of the empty control for all pre-rRNA species (Figure 39, D, lane 12). At least for the Noc3p variant equipped with a truncated domain III extension it appears, that higher amounts of 7S pre-rRNA are co-purified compared to 27SB pre-rRNA. This in turn indicates a release defect of Noc3p from pre-ribosomes in this situation (Figure 39, D, lane 10).

4.2.4 Different domains of Noc3p have different roles on the assembly with Noc2p and with pre-LSUs

In a next attempt, the dependence of the N- and C-terminus, as well as of the loop (Figure 38) of Noc3p for the interaction with Noc2p and with pre-LSUs, has been addressed. To do so, successive truncation mutants from both termini of Noc3p, indicated in Figure 40, have been generated (described in section 4.2.2). The loop-variants used for this purpose are shown in Figure 38 (section 4.2.3).

Due to incomplete structural information on the N-terminus of Noc3p, the missing 131 amino acids (AA), as indicated in Figure 25, have been entirely truncated. Within this area, 50 as well as 100 AA have been truncated from the N-terminus as well, by random selection and not according to structural features. Besides, further N-terminal truncations of 180, 240 and 305 AA have been generated according to the HEAT-repeats (Figure 40).

Regarding the C-terminus, structure has been assigned according to volume densities observed in cryo-EM analyses to Noc3p (section 4.1), which closely resembles the NOC-motif of Noc4p (Figure 26). The structural information obtained in this way has been used as basis for the introduction of C-terminal truncations of Noc3p (illustrated in Figure 40). These comprise four different variants.

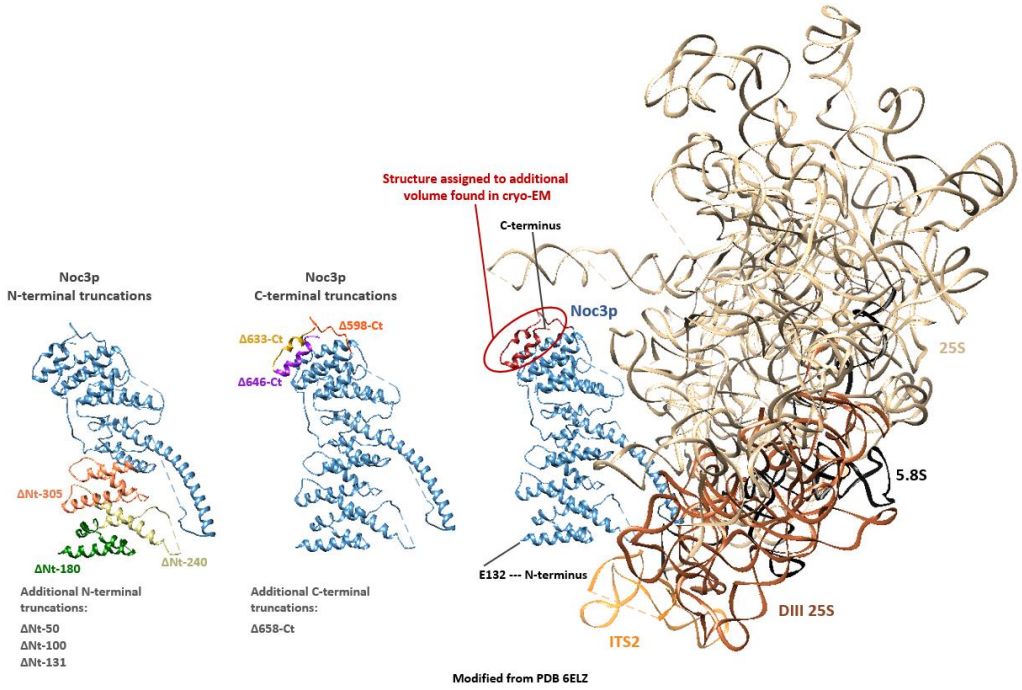

Figure 40: N- and C-terminal truncations of Noc3p.
The following illustrations were created using UCSF chimera (6.1.11). Noc3p associated with pre-ribosomes of state E (PDB 6ELZ) is shown on the right. The 25 S rRNA is colored in tan, whereof its intrinsic domain III is highlighted in brown. The ITS2 (orange) and 5.8 S rRNA (black) are shown as well. Structure has been assigned to the C-terminus of Noc3p according to resolved volume density for Noc3-TAP-1 by cryo-EM analysis (see 4.1). Noc3p is shown two more times in order to visualize the N- and C-terminal truncations (left and middle). The respective amino acid deletions are highlighted in color. Note that the N-terminal truncations ΔNt-50, ΔNt-100, ΔNt-131 as well as the C-terminal truncation Δ658-Ct are not highlighted due to missing structural information of these parts.

Δ658-Ct ("Ct" for C-terminus) reflects truncation of all remaining 5 AA from the C-terminus of Noc3p, which have not been resolved in the cryo-EM analyses outlined in section 4.1 (compare also Figure 32). For variant Δ646-Ct, the first helical element of the NOC-motif, close to the C-terminus has been additionally truncated (Figure 40). Further truncation of the second helix within the NOC-motif is represented by Δ646-Ct. In Δ598-Ct, the remaining parts of the C-terminus, the whole NOC-motif and an adjoining unstructured part of the protein, reaching up until helix Hn+15 of Noc3p, are completely truncated.

The genetic system for this approach is illustrated in Figure 37 (described in section 4.2.2). Notably, these strains additionally express a TAP-tagged fusion variant of Noc2p, which is used for subsequent affinity purification.

The western blot analysis reveals signals for Noc2p-TAP for both inputs and affinity purified fractions of all strains (Figure 41, A). Signals for the different Noc3p variants can be observed in the input fractions, respectively. However, as affinity purification has been performed on Noc2p, IP-signals are not observed for each Noc3p variant (Figure 41, A). This depends on whether the respective Noc3p variant can associate with Noc2p or not. In the following, the N- and the C-terminal truncation variants of Noc3p as well as the loop variants will be analyzed en bloc, respectively.

First, regarding the situation for full length Noc3p (Figure 41, A, lanes 1, 2), the protein has been identified in the input as well as in the affinity purified fraction. According to the northern analysis, a significant amount of 7S pre-rRNA and 27S pre-rRNA species comprising both $27SA_2$ and 27SB pre-rRNA has been detected in the input fraction (Figure 41, B, lane 1). Affinity purification enriches the signals for 27S pre-rRNA but hardly for 7S pre-rRNA (Figure 41, B, lane 2). As introduced in section 3.8, Noc2p forms a complex both with Noc1p as well as with Noc3p. Therefore, its association with pre-LSUs accompanies such that incorporate $27SA_2$, 27SB and little amounts of 7S pre-rRNA, i.e. several populations of nucleolar and nuclear pre-ribosomal intermediates.

In contrast, when Noc3p is absent, signals for $27SA_2$ pre-rRNA in the input fraction are severely diminished. (Figure 41, B, lane 3). However, a strong signal for 27S total pre-rRNA reveals the presence of large amount of 27SB pre-rRNA in this situation. This indicates that processing of $27SA_2$ pre-rRNA is not affected, but processing of 27SB pre-rRNA (Figure 41, B, lane 4). Moreover, regarding the ratio of co-purified 35S to 27S total (Figure 41, B, lanes 2, 4), it clearly shifts towards 35S pre-rRNA for the “empty”-control compared to full-length Noc3p. This might be the cause of less co-purified 27SB pre-rRNA but similar amounts of $27SA_2$ pre-rRNA by Noc2p. Congruently, the co-purification efficiency of total 27S pre-rRNA diminishes (Figure 41, C). These results possibly indicate that the association of Noc2p to 27SB incorporating pre-LSUs is predominantly mediated through Noc3p. The consequences of this circumstance will be discussed in section 5.3.

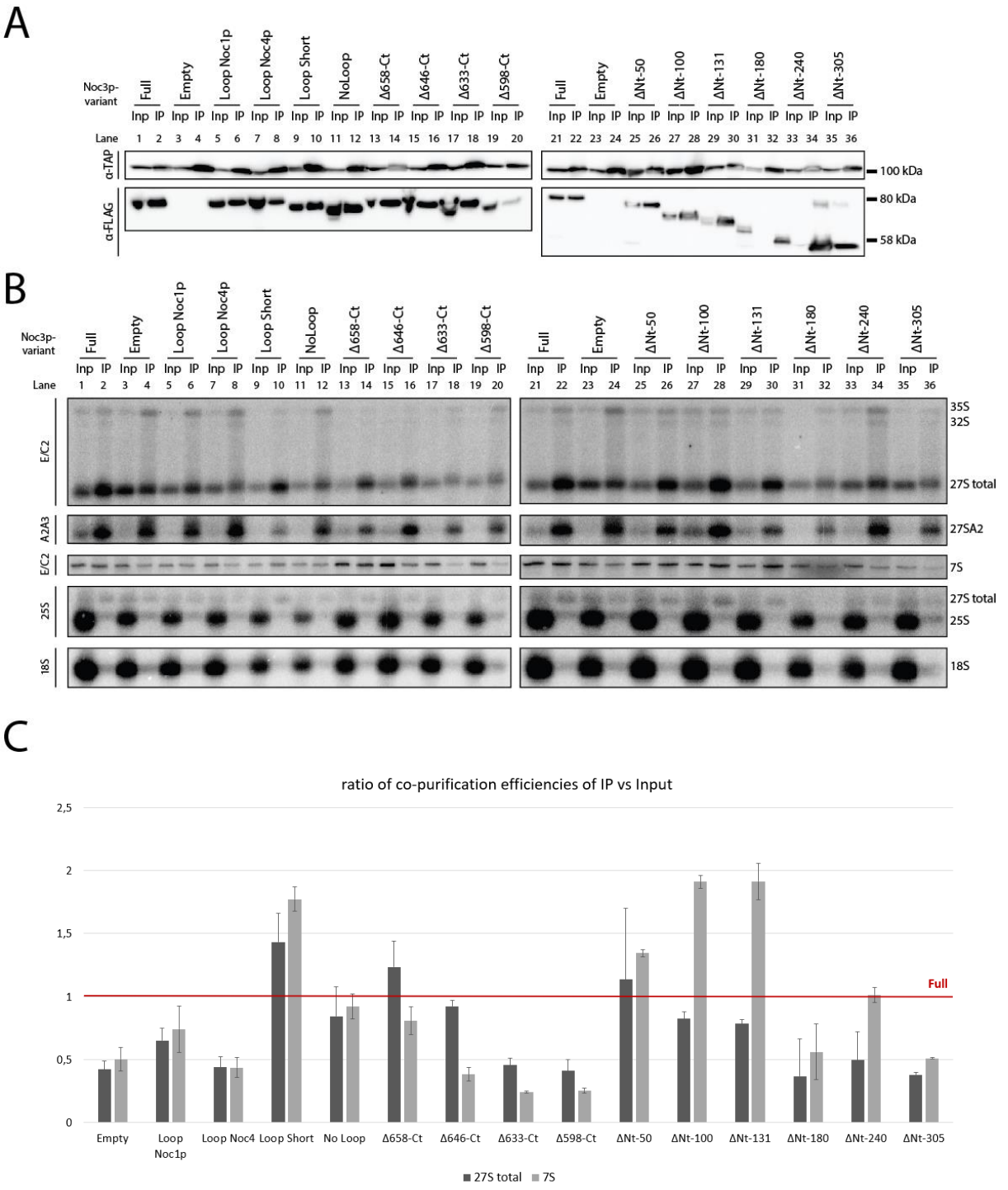

Figure 41: Analyzing the incorporation of pre-rRNA and the formation of the heterodimer of Noc2p with Noc3p variants. (A) Exponentially growing yeast cells of Y2940 containing a genomically encoded Noc2p-TAP fusion (6.1.1) transformed with the constructs encoding the FLAG-tagged Noc3p variants (6.1.2) on galactose containing medium were shifted to glucose containing medium for 16 h to shut down expression of wild type Noc3p. Affinity purification was performed from total cell extracts (6.2.6.4) using IgG Sepharose matrix (6.1.9). Total RNA was isolated by phenol/chloroform extraction (6.2.4.1). Total RNA was size separated on agarose and acryl amide gels (6.2.4.2 and 6.2.4.3). 0,19 % of total input and 11 % of the purified material were loaded, respectively and analyzed by sequential northern blotting using the indicated probes. For hybridization sites of the oligos see 6.1.3.3. (B) Aliquots of cells corresponding to 0,39 % of the input and 11,1 % of the purified material were separated by SDS-PAGE (6.2.5.3) and analyzed by western blotting (6.2.5.4). The proteins were visualized using the PAP detection reagent (6.2.5.6). (C) Signals for both the input and the affinity purified fractions in the northern blot of (A) were quantified using MultiGauge software (Fujifilm) (6.1.11). Indicated signal ratios for pre-rRNA species were calculated for each strain to visualize the amount of the incorporated pre-rRNA species. Signal ratios were normalized to full length Noc3p ("Full") for each strain and each pre-rRNA species, respectively.

Regarding the Noc3p loop-variants, protein signals for all variants can be detected both in the inputs as well as in the affinity purified fractions (Figure 41, A, lanes5-12). This indicates that the loop displays no essential element for the binding to Noc2p. Regarding the rRNAs, hardly $27SA_2$ pre-rRNA for the loop-variants "Loop-Noc1p", "Loop-Noc4p" and "No Loop" can be detected in the input fractions (Figure 41, B, lanes 5-12). However, significant amounts of 27SB pre-rRNA can be observed. Moreover, the 35S- seems to accumulate over the 27S- pre-rRNA, which is comparable to the "empty-control" (Figure 41, B, quantification in C). Therefore, the formation of the Noc2p/Noc3p heterodimer still occurs, however, the assembly to pre-LSUs incorporating 27SB pre-rRNA seems to be disturbed.

In contrast, another situation can be observed for the Noc3p variant "Loop short". Even though, hardly $27SA_2$ pre-rRNA is detected in the input (Figure 41, B, lane 9), 27SB pre-rRNA is enriched in the affinity purified fraction (lane 10). Additionally, higher amounts of 7S pre-rRNA are co-purified, compared to full-length Noc3p (Figure 41, C). This indicates, that the Noc2p/Noc3p heterodimer stays more associated with particles in which 27SB- conversion to 25.5S- and 7S- pre-rRNA has occurred to a reduced efficiency. Possibly, the release of the dimer from pre-LSUs is affected in this situation. The same observations have been made in section 4.2.3, when directly affinity purifying the Noc3p variants and associated pre-ribosomes (Figure 39).

Regarding the N-terminal truncation variants, their association with Noc2p seems not to be impaired as well. Signals for all these variants are detectable in the input- and IP-fractions, respectively (Figure 41, A, lanes 25-36). Exceptionally, truncation of 180 or 240 AA from the N-terminus of Noc3p yields no IP protein signals (lanes 31 and 33). As the formation of the Noc2p/Noc3p heterodimer is again possible upon truncating 305 AA, it might be the case that truncation of 180 or 240 AA induces a folding misconduct of these Noc3p variants.

The northern analysis for the N-terminal truncations ΔNt-50, ΔNt-100 and ΔNt-131 reveals signals for both $27SA_2$-, 27SB- and 7S pre-rRNA in the inputs, respectively, comparable to full-length Noc3p (Figure 41, B, lanes 25, 27, 29). When comparing the IP lanes (26, 28 and 30), the co-purification efficiency is higher for 7S pre-rRNA than for 27SB pre-rRNA. This indicates, as observed for the "Loop Short" (see above) a possible slight release defect for these variants in association with Noc2p (Figure 41, C). However, larger truncations, ΔNt-180, ΔNt-240 and ΔNt-305 show a similar pre-rRNA pattern as the "empty-control" Figure 41, B, lanes 31-36). This observation is reflected by hardly signals of $27SA_2$ but strong signals for 27SB pre-rRNA in the inputs and an accumulation of 35S pre-rRNA over 27S total pre-rRNA in the IP fraction (see also quantification in C, Figure 41). This finding indicates, as already observed for several loop variants (see above), an unaffected binding between Noc2p and Noc3p independently of pre-ribosomes but a possibly impaired association with intermediate pre-LSUs.

Regarding the C-terminal truncation variants, the association with Noc2p seems to be severely reduced for Δ598-Ct. Importantly, the remaining C-terminal variants, Δ658-Ct, Δ646-Ct and Δ633-Ct, of Noc3p

can be co-purified by Noc2p. This finding is indicated by strong signals in the respective IP-fractions of the western analysis (Figure 41, B, lanes13-18). Apparently, the binding between Noc2p and Noc3p is mediated in large parts by the area between AA 598 and 633 of Noc3p.

The northern analysis of these variants reveals different patterns of co-purified pre-rRNAs. For truncation Δ658-Ct, rather weak signals for $27SA_2$ pre-rRNA and slightly enhanced signals for total 27SB pre-rRNA can be observed in the input fractions (Figure 41, B, lane 13). Affinity purification enriches the signals for these pre-rRNA species, which is comparable to the full-length control (Figure 41, A, lane 14; quantification in C). The same observations can be made for Δ646-Ct, whereas the enrichment of $27SA_2$ pre-rRNA-signals are more elevated (lanes 15, 16). Concomitantly, the co-purification of 27SB pre-rRNA is lower (Figure 41, C), thus possibly indicating an altered association with pre-LSUs incorporating this pre-rRNA species.

In contrast, truncations Δ633-Ct and Δ598-Ct reveal no signals for $27SA_2$- and hardly total 27S- pre-rRNA signals in the inputs (Figure 41, B, lanes 17, 19). Affinity purification leads to an enrichment of $27SA_2$ pre-rRNA but not of 27SB pre-rRNA in these cases (lanes 18, 20). Moreover, the signals in the IP-fractions for these two variants are slightly elevated compared to the input. This indicates the presence of mostly $27SA_2$ pre-rRNA, co-purified by Noc2p and thus an impeded assembly of the dimer with pre-LSUs.

Altogether, the findings indicate different functions for the different domains of Noc3p. The formation of the heterodimer with Noc2p on the part of Noc3p depends in large parts on the C-terminus of Noc3p, more precisely to N-terminal parts of the NOC-motif. Furthermore, all domains of Noc3p analyzed in this chapter are somehow important for the proper assembly of the resulting Noc2p/Noc3p dimer with pre-LSUs incorporating 27SB pre-rRNA. Either these dimers are not efficiently recruited to the pre-ribosomes or their release seems to be affected (see also section 4.3 for recruitment and release of Noc3p to pre-ribosomes).

4.3 Noc3p associates with pre-ribosomes of an intermediate maturate state and its recruitment and release is dependent on the pre-ribosomal assembly state

The different domains of Noc3p, which are important for the formation of the heterodimer with Noc2p and the association to pre-LSUs have been analyzed in more detail in the previous chapter (section 4.2). Hence, in this chapter, the recruitment and the release of Noc3p to LSU precursor populations will be addressed according to the pre-ribosomal assembly or maturation state.

In order to analyze how association and release of Noc3p are coordinated with the assembly of the large subunit, yeast strains were utilized where the expression of certain LSU-proteins can be shut

down. The genetic system for this approach is outlined in Figure 42. In these strains, genes encoding for a certain r-protein of the large ribosomal subunit (rpL) are genomically deleted but expressed from a plasmid encoding the respective protein under the control of a galactose inducible and glucose repressed promotor (pGal). For this reason, the rpL of interest is only expressed when yeast cells are cultivated in galactose containing medium but repressed in the presence of glucose containing medium. These yeast strains were further genetically modified to express the essential biogenesis factor Noc3p C-terminally fused to a TAP-tag (Rigaut et al. 1999). Thereby, depletion of the respective rpL will cause assembly defects in ribosome biogenesis and large amounts of these pre-ribosomal subunits can be affinity purified by their association with Noc3p. Since depletion of different rpL block ribosome synthesis at different maturations steps (see 3.5.2 and Pöll et al. 2009), the quantity and identity of (pre-) rRNAs co-purified with Noc3p might allow to establish a link between the assembly state and recruitment/ release of Noc3p.

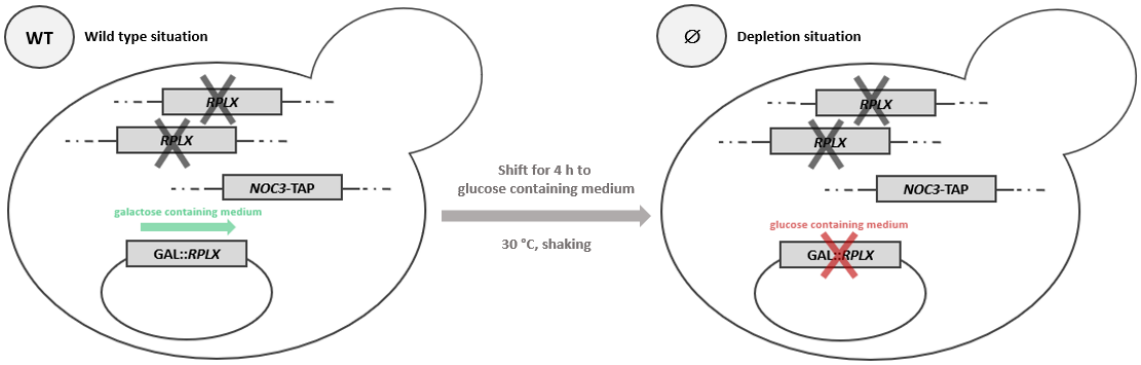

Figure 42: Genetic system for studying the recruitment and release of Noc3p to misassembled pre-ribosomes.
Strains in which the genomic copy(-ies) of a certain r-protein of the large ribosomal (rpLX) subunit are genomically deleted were used. In these strains, the deletion of the respective alleles is complemented by a plasmid that encodes for the r-protein under a galactose inducible, glucose repressible promotor. Therefore, cultivation of these strains in glucose containing medium induces an expressional shut down of the particular r-protein. Additionally, Noc3p is expressed as genomically encoded TAP-fusion protein for affinity purification.

The association and the release of Noc3p to pre-LSUs has been analyzed under depletion of rpLs, which stop ribosome biogenesis at an early, intermediate or late step. The binding sites of the particular LSU r-proteins are based on the crystal structure of the yeast 80 S ribosome that has been published in 2011 (Ben-Shem et al. 2011) using the standard protein nomenclature according to the *Saccharomyces cerevisiae* database (https://www.yeastgenome.org/).

The first, "early" class is characterized by a significant delay in generating the 5´-end of 5.8 S rRNA which occurs by successive trimming of ITS1 sequences of $27SA_2$ and $27SA_3$ pre-rRNAs. LSU r-proteins which exhibit this phenotype are rpL3, rpL7 and rpL8 (Rosado et al. 2007b; Jakovljevic et al. 2012; Pöll et al. 2009) (for processing scheme see Figure 6). For the second, "middle" class of r-proteins, a delay in processing of the ITS2 which generates 7S and 25.5S pre-rRNAs can be observed and hence an

accumulation of 27SB pre-rRNA after *in vivo* depletion. Among them are rpL9, rpL19, rpL23, rpL25, rpL27, rpL34 and rpL35 (Pöll et al. 2009). For shut down of members of the last, "late" class of LSU r-proteins, 27SB pre-rRNA can be still processed, however, further processing of the resulting 7S pre-rRNA is disturbed. Proteins belonging to this class are rpL2, rpL5, rpL10, rpL21 and rpL43 (Pöll et al. 2009). One LSU r-protein however, rpL1, cannot be categorized in one of these classes. Though rpL1 is essential, it has shown to be not strictly required for pre-rRNA processing (Pöll et al. 2009). Depletion of the respective r-proteins has been performed for 4 h. In a previous study, this time period has been determined for a sufficient establishment of the pre-rRNA processing phenotypes among the mutant strains, respectively (Pöll et al. 2009).

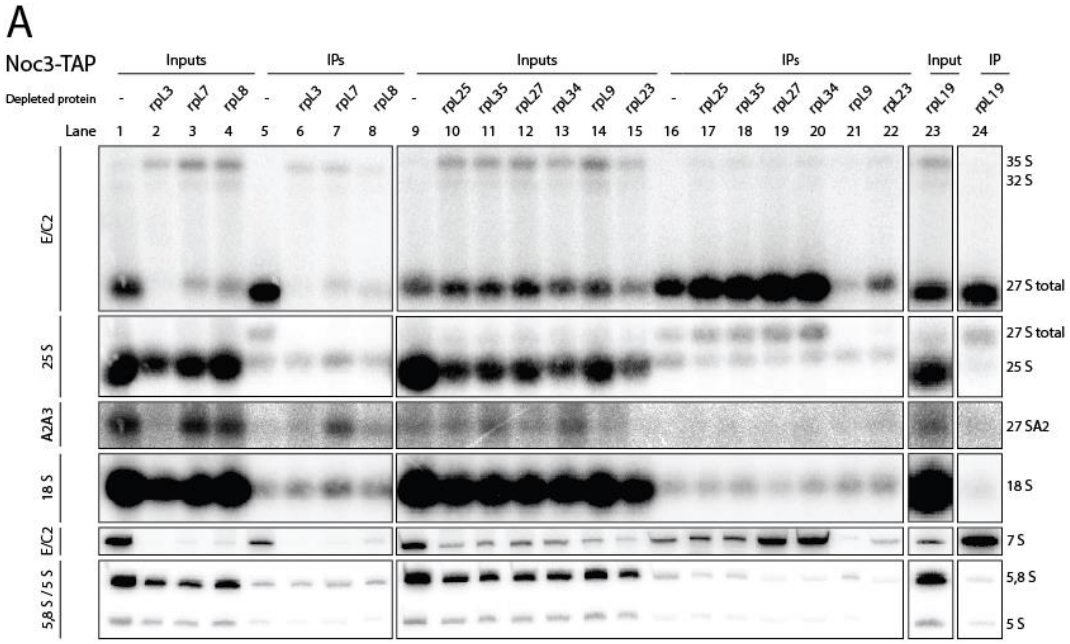

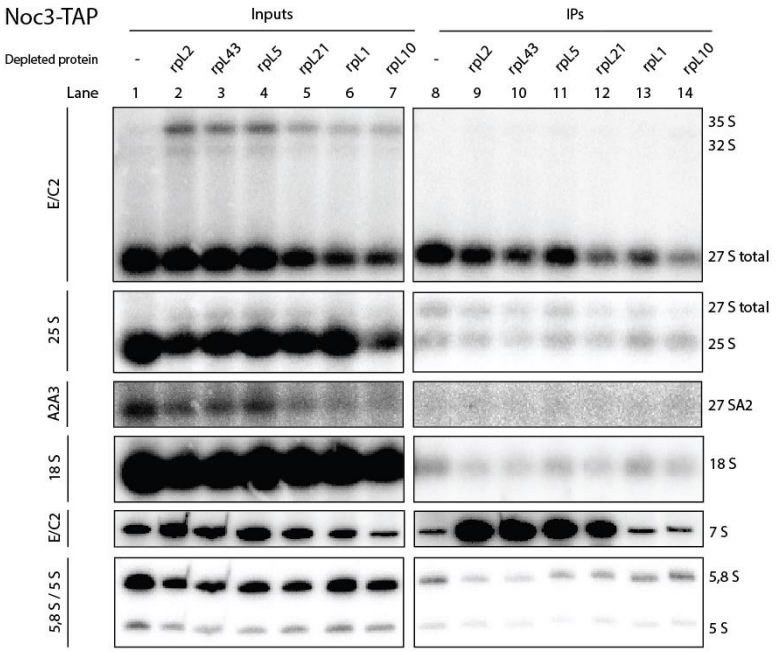

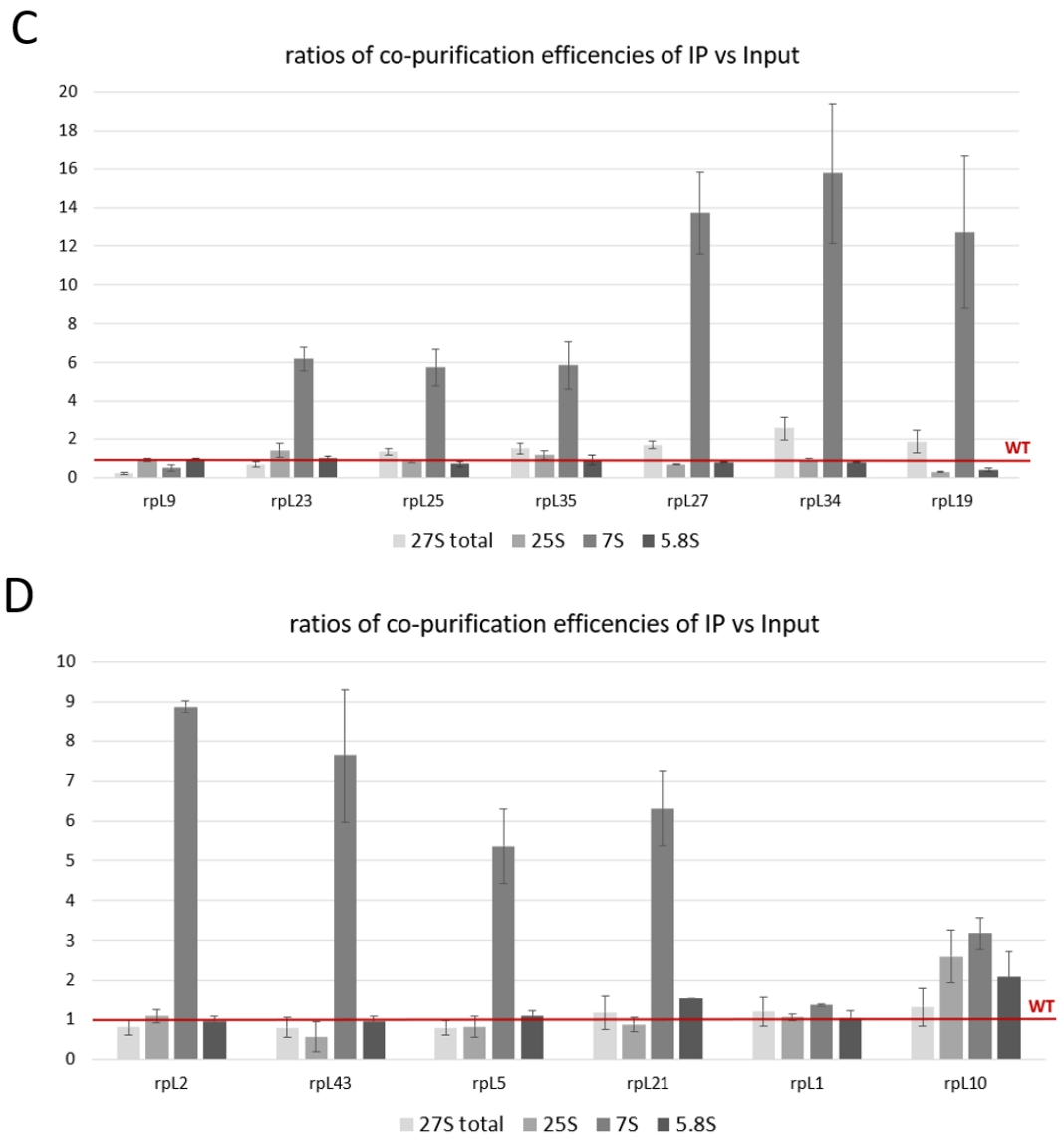

Figure 43: Impact of *in vivo* depletion of LSU r-proteins on the recruitment and release of Noc3p.
Exponentially growing yeast cells (Y2601, Y3104, Y3333, Y3335, Y3337, Y3343, Y3420, Y3421, Y3781, Y3783, Y3785, Y3982, Y3984, Y4021, Y4023, Y4025, Y4027, Y4029) (6.1.1) on galactose containing medium were shifted to glucose containing medium for 4 h to shut down expression of the respective r-protein. Affinity purification was performed from total cell extracts (6.2.6.3) using IgG-Sepharose (6.1.9) to selectively enrich for Noc3p-TAP associated pre-ribosomes. Total RNA was isolated by phenol/chloroform extraction (6.2.4.1). Total RNA was size separated on agarose and acryl amide gels (6.2.4.2 and 6.2.4.3). 0,26 % of total input and 13,3 % of the purified material were loaded, respectively and analyzed by sequential northern blotting using the indicated probes (A+B) For hybridization sites of the oligos see 6.1.3.3. (C+D) Signals for both the input and the affinity purified fractions in northern blots A and B were quantified using MultiGauge software (Fujifilm) (6.1.11). Indicated signal ratios for pre-rRNA species were calculated for the indicated strains to visualize the amount of the incorporated pre-rRNA species. Signal ratios were normalized to the wild type ("WT") for each strain and each pre-rRNA species, respectively.

As Noc3p associates predominantly with particles of an intermediate maturation state, 27 SA_2 pre-rRNA was hardly detectable in purified samples with Noc3p (Figure 43, A, lane 5, "A2A3"). Furthermore, low levels of 7S pre-rRNA were enriched with Noc3p, indicating the release of Noc3p shortly after C_2 cleavage. As expected, almost no 25S rRNA was enriched in the Noc3p purification.

In vivo depletion of r-proteins belonging to the "early" class (rpL3, rpL7, rpL8) leads to a strong delay in the formation of the 5´-end of 5.8S rRNA, thus accumulating $27SA_2$ pre-rRNA and impairs the production of 27SB pre-rRNA. Accordingly, 27SB pre-rRNA was neither detected in the input, nor hardly co-purified by Noc3p in any of these cases (Figure 43, A, lanes 2-4 and 6-8, "EC2"). Therefore, assembly defects of ribosomal proteins associated with LSU domains I and II leads to early maturation defects, which interfere with the recruitment of Noc3p. However, depletion of rpL7 still allows to some extent the incorporation of Noc3p with 27 SA_2 pre-rRNA, as signals in the affinity purified fraction of depleted rpL7 are higher compared to those obtained for depletion of rpL3 and rpL8 (Figure 43, A, lanes 6-8).

As introduced, depletion of rpL9, rpL23, rpL19, rpL25, rpL27, rpL34 and rpL35 results in the accumulation of 27SB pre-rRNA because of a delayed conversion of 27SB pre-rRNA to 7S- and 25.5S (Pöll et al. 2009) (see also section 4.2.3).

For rpL9 and rpL23, lower levels of 27 SB pre-rRNA were detected in the affinity purified fractions when compared to the input (Figure 43, A, compare lanes 14/15 with 21/22; quantification in C). This effect was most evident for rpL9 where the co-purification of 27 SB pre-rRNA was lowered to approximately one eight when compared to the wild type situation. For rpL23, 27 SB pre-rRNA was co-purified in the range of one third compared to the wild type. For depletion of rpL23 higher levels of 7 S pre-rRNA were as well detected to be elevated. However, the latter may presumably be due to quantification mistakes derived from low signals in the range of background contamination for 7 S pre-rRNA both in the input as well as in the affinity purified fraction (Figure 43, A, compare lanes 23 with 15; quantification in C). According to the outcome of these analyses, it cannot be distinguished, whether Noc3p is not recruited upon assembly defects of rpL9 and rpL23, or whether Noc3p has already been released. However, current cryo-EM analyses on successive pre-LSUs indicate, that domain VI forms before domain III. For these reasons it can be suggested that the LSU domain VI has to be properly assembled to ensure an efficient recruitment of Noc3p to pre-ribosomes (also discussed in section 5.1.1).

In contrast, depletion of the "middle" class r-proteins rpL19, rpL25, rpL27, rpL34 and rpL35 all clearly show a higher ratios of 27SB pre-rRNA in the affinity purified to the input fractions, similar to that what was found for the wild type (Figure 43, A, compare lanes 17-20 with 10-13 and 24 with 23; quantification in C). More precisely, the levels are slightly elevated over the wild type which indicates a mild release defect of Noc3p from these pre-ribosomal assembly mutants. This effect was observed to be comparably higher for depletion of rpL19, rpL27 and rpL34. Strikingly, levels of co-purified 7S pre-rRNA were tremendously increased for depletion of rpL19, rpL25, rpL27, rpL34 and rpL35, likely indicating an impaired release of Noc3p from residual pre-ribosomal populations in which processing of 27SB pre-rRNA still occurred with a reduced efficiency. This release defect according to 7S pre-rRNA incorporation of Noc3p-associated misassembled LSU precursors was found to be threefold higher for

rpL19, rpL27 and rpL34 compared to rpL25 and rpL35. Hence, the LSU assembly defects upon depletion of middle acting r-proteins of LSU domain III interferes with the release of Noc3p.

Depletion of "late" class of LSU r-proteins is characterized by an intact processing of 27SB pre-rRNA but to a disturbed further processing of resultant 7S pre-rRNA. As described above, Noc3p hardly associates with pre-ribosomes that incorporate 7S pre-rRNA in the wild type situation. However, shut down of rpL2, rpL5, rpL21 and rpL43 lead, similar to the depletion of particular "middle" class r-proteins, to an obvious release defect of Noc3p (Figure 43, B, compare lanes 9-12 with 2-5; quantification in C). Apparently, progression of LSU maturation drives the release of Noc3p from pre-ribosomes through stable assembly of these r-proteins, either direct or indirect, which is impeded in the respective r-protein depleted situation. Notably, rpL5 and rpL21 are located more distant from Noc3p at the central protuberance (Ben-Shem et al. 2011) but nevertheless affect its release, though to a lesser extent than rpL2 and rpL43.

In vivo depletion of rpL10 was previously found to not completely block the production of pre-LSUs that incorporate mature RNAs (Pöll et al. 2009). Gently higher levels of co-purified 7S pre-rRNA and of mature 25 S and 5.8 S rRNA compared to the wild type and therefore a mild release defect of Noc3p were observed for shut down of the LSU r-protein (Figure 43, A, compare lane 14 with 7; quantification in C). For depletion of rpL1 however, no significant change of co-purification of any of the (pre)-rRNA species was observed. As described above, rpL1 was found to not be strictly required for pre-rRNA processing. Therefore, depletion of rpL1 neither affects the recruitment nor the release of Noc3p to LSU precursors.

Altogether, the findings indicate, that a certain assembly state of the pre-LSUs has to be reached, in order to recruit Noc3p. This involves a correct assembly of LSU domains I, II and probably domain VI. On the other side, an impaired release of Noc3p may occur upon assembly defects resulting from the absence of middle-acting r-proteins. Hence, domain III seems to be involved in Noc3p release. Moreover, late acting LSU r-proteins are as well needed for its efficient release as indicated by the northern analyses.

4.4 The 25S rRNA domain III undergoes significant conformational rearrangements upon depletion of certain LSU r-proteins

As analyzed in the previous section (4.3), assembly defects of certain r-proteins affects the proper LSU assembly, which in turn interferes with the recruitment or the release of Noc3p. At next, it shall be analyzed, whether the association/release of Noc3p is related with structural changes in the pre-ribosomal particles. To shed further light on this, the consequences of an *in vivo* depletion of the corresponding LSU r-proteins on the conformation and integrity of pre-rRNA regions shall be addressed

in a structural manner. To do so, a tethered tertiary structure probing approach was applied, that makes use of micrococcal nuclease (MNase) fusion proteins, as described in the introduction (section 3.7). Based on the exo- and endoribonucleolytic activity of MNase, preferentially in single stranded RNA regions, MNase cleaves local accessible rRNA, which leads to a specific cutting pattern in the local rRNA environment.

Here, MNase dependent cuts are analyzed for different r-protein depleted situations. Therefore, rpL19, rpL25, rpL27, rpL34 and rpL35, which belong to the "middle" class of LSU r-proteins were depleted. Likewise, members of the "late" class rpL2, rpL5 and rpL43, which also induce a Noc3p release defect following their expressional shut down, are used for analysis. To define bands in the northern blot, that arise as consequence of assembly defects, the MNase-Noc3p cutting pattern has also been analyzed under non-depleted conditions. Finally, Noc3p associated pre-ribosomes have been purified under wild type conditions without fusion to MNase as well.

The genetic system for this purpose is highly similar to that, used for analyzing the recruitment and release of Noc3p (Figure 42). The expression of a certain LSU r-protein was be shut down by growth of the yeast cells in glucose containing medium. Here, Noc3p expressed as a fusion protein linked at the N-terminus to MNase (Figure 44). To allow the affinity purification of pre-ribosomal particles and detection of Noc3p in western blot analyses, three repetitive FLAG tags (3x-FLAG) were also introduced.

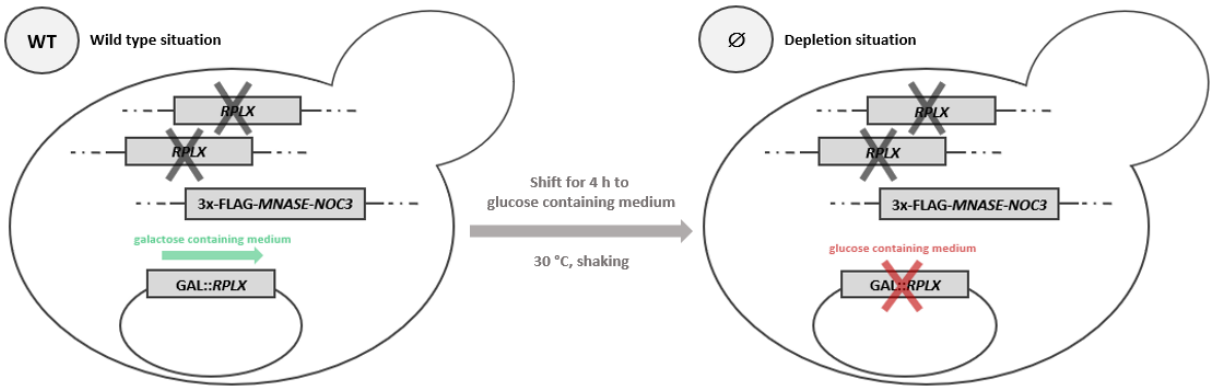

Figure 44: Genetic system for studying the three-dimensional rRNA environment of Noc3p in assembly mutants.
Strains in which the genomic copy(-ies) of a certain r-protein of the large ribosomal (rpLX) subunit are genomically deleted were used for this purpose. In these strains, the deletion of the respective alleles is complemented by a plasmid that encodes for the particular r-protein under a galactose inducible, glucose repressible promotor. Therefore, cultivation of these strains in glucose containing medium induces an expressional shut down of the r-protein. Additionally, Noc3p is expressed as genomically encoded MNase fusion for structure probing assays, implying a 3x-FLAG tag for affinity purification.

In order to keep these analyses comparable with the recruitment and the release of Noc3p (see section 4.3), the time period for depletion of a certain rpL was as well set to 4 h. Thereafter, cell extracts of exponentially growing yeast cells of the respective strains were prepared (6.2.6.1). Buffers used for extract preparation and later affinity purification contain EGTA to quench free Ca^{2+}-ions, possibly

released from breakage of subcellular compartments during cell lysis. Otherwise, uncontrolled increase of Ca^{2+}-levels could unintentionally activate MNase. Noc3p associated pre-ribosomal particles were then affinity purified on anti-FLAG affinity matrix. Finally, MNase was induced by addition of exogenous calcium to the purified fractions for a defined period of time. RNA fragments were subsequently analyzed by northern blotting to find out MNase induced cleavage-patterns under depletion of different r-proteins (Figure 45).

Regarding the wild type situation without fusion to MNase, purification of pre-LSUs by Noc3p specifically enriches 27SB pre-rRNA over the input (Figure 45, A, compare lines 19 with 9). Neither a band for 7S pre-rRNA nor bands of 27SB-fragments were detected. This indicates that a specific co-purification of Noc3p associated pre-ribosomes was possible.

For the MNase-Noc3p fusion however, the signal obtained for 27SB pre-rRNA was comparably weaker. Additionally, three major fragments of lower size could be detected indicating a calcium induced fragmentation of rRNA by MNase in this sample (Figure 45, A, lane 20). The respective bands are indicated by a red frame and signed I-III. As signals for 25S rRNA increase compared to 27SB pre-rRNA for the MNase fusion, the results indicate the specific degradation of 27SB pre-rRNAs (Figure 45, A, compare lanes 20 with 19, “25S probe”). Therefore, the nuclease activity of the MNase-Noc3p fusion acted specifically on the pre-ribosomal population it is associated with. Importantly, a band with a similar size than 7S pre-rRNA was detected with the same probe used for detection of 7S pre-rRNA, both in the wild type, as well as in all mutant strains, respectively (Figure 45, A, lanes 11-18 and 20). However, affinity purification of Noc3p without fusion of MNase reveals no band at that size (Figure 45, A, lane 19). Moreover, the band appears fuzzy, which suggests the presence of multiple cleavage sites. Therefore, the band might be due to MNase-Noc3p dependent cuts around the C2-site, but not the result of a proper 27SB pre-rRNA processing by the Las1p endonuclease according to the literature (Gasse et al. 2015). For further details on this, see the results in section 4.5.

In any case, the defined cutting pattern observed for MNase-Noc3p undergoes no significant changes for most mutant strains analyzed here. Neither additional bands appear, nor disappear others. Moreover, the signal intensities of the corresponding bands do not alter among each other (Figure 45, A, lanes 11-18). Apparently, structural rearrangements of mis-assembled LSU precursors for middle acting r-proteins rpL19, rpL25 and rpL35 as well as for late acting proteins rpL2, rpL5 and rpL43 depletion do not occur, at least not in the local three-dimensional rRNA environment of Noc3p.

However, expressional shut down of rpL27 or rpL34 leads to a significantly altered cutting pattern (Figure 45, A, lane 12 and 13). In the analyses of these strains, a prominent band appears (red frame “IV”), whereas bands I and III seem to almost completely disappear when compared to the wild type (Figure 45, A, lane 20).

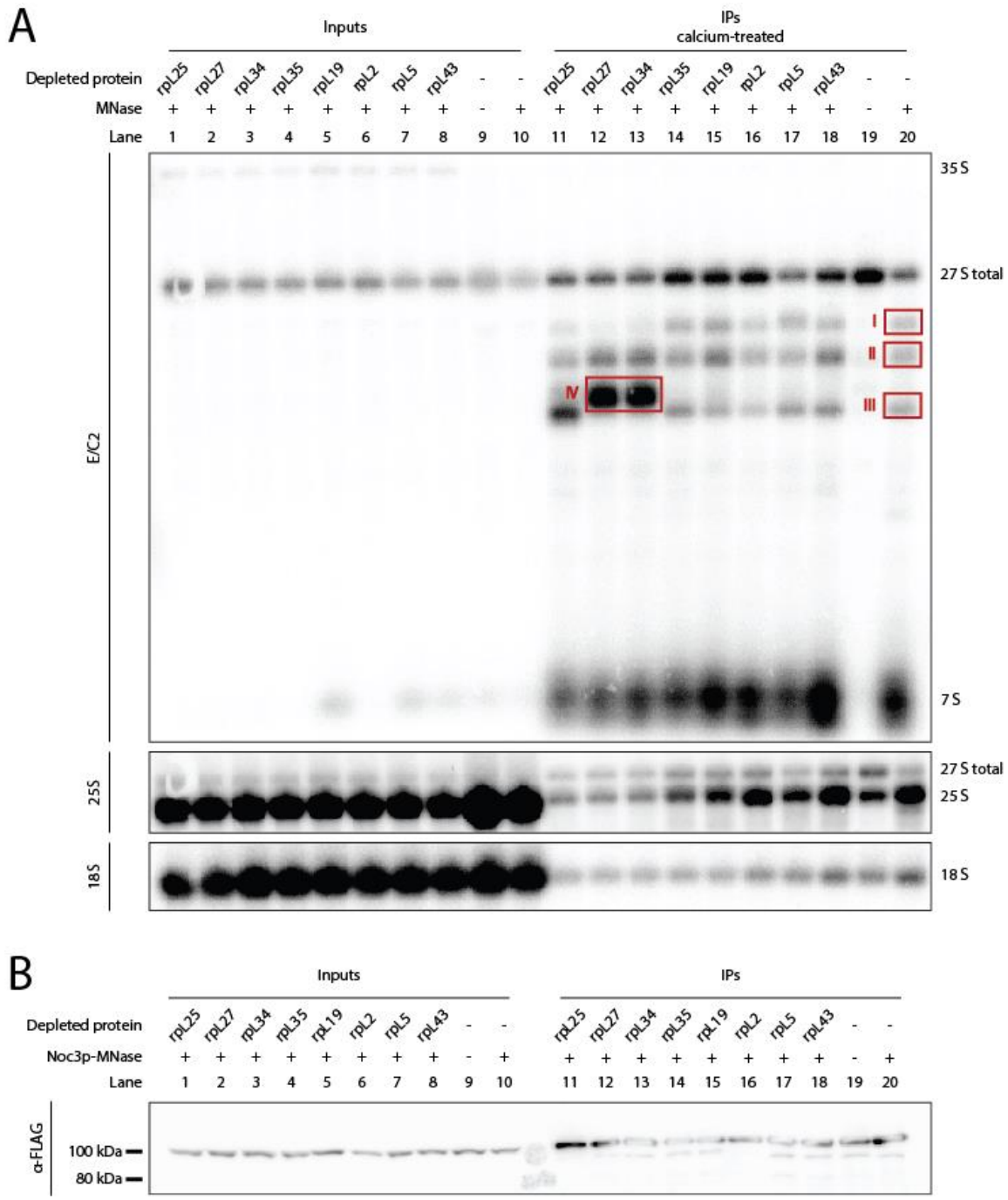

Figure 45: Analysis of calcium induced fragmentation of pre-rRNA in mis-assembled LSU precursors which were purified from strains expressing MNase as fusion proteins of Noc3p.

Exponentially growing yeast cells (Y3449, Y3956, Y4167, Y4169, Y4171, Y4173, Y4175, Y4177, Y4179, Y4181) (6.1.1) on galactose containing medium were shifted to glucose containing medium for 4 h to shut down expression of the respective r-protein. Affinity purification was performed from total cell extracts (6.2.7.2) with buffers containing EGTA (6.1.6) using M2-anti FLAG affinity matrix (6.1.9). The purified fraction was treated with 8 mM calcium chloride for activation of MNase N-terminally fused to Noc3p and incubated for 15 min at 16 °C. (A) Total RNA was isolated by phenol/chloroform extraction (6.2.4.1), Total RNA was size separated on agarose and acryl amide gels (6.2.4.2 and 6.2.4.3). 0,053% of total input an 13,33% of the purified material were loaded, respectively and analyzed by sequential northern hybridization using the indicated probes (A) For hybridization sites of the oligos see 6.1.3.3. The main fragments arising through MNase induced cuts in the wild type situation are indicated with red frames (I-III). A specific fragment that only shows appears upon depletion of rpL27 and rpL34 is indicated by a red frame as well (IV) (B) Aliquots of cells corresponding to 0,053 % of the input and 3,33 % of the purified material were separated by SDS-PAGE (6.2.5.3) and analyzed by western blotting (6.2.5.4). The bait proteins were visualized using the PAP detection reagent (6.2.5.6).

Remarkably, this observation was identical for both rpL27 and rpL34 but not found for depletion of rpL19 (Figure 45, A, lane 15), although the Noc3p release defect appeared to be similar as observed for depletion of rpL27 and rpL34 (section 4.3). These findings suggest drastic structural changes of rRNA for the local 3D-environment of Noc3p in this mis-assembled pre-ribosomal context (discussed in section 5.1.2.2).

western blotting analysis showed in general strong signals for the MNase-Noc3p fusion both in the input as well as in the affinity purified fractions (Figure 45, B). For this reason, the observed changes in cutting patterns for *in vivo* depletion of rpL27 and rpL34 are not due to expressional changes or co-purification efficiencies.

In order to precisely map the positions of MNase-dependent cuts within the (pre-) rRNA, primer extension analyses were performed (6.2.7.3). In total, fifteen primers were used to cover the complete 27 SB pre-rRNA (for binding sites of the primers see 6.1.3.2). The 5´-end of the resulting cDNAs are referred to stops in primer extension. To assign these stops to a certain rRNA position, sequencing reactions (6.2.7.4) were performed as well. Both approaches were size separated on denaturing sequencing gels (6.2.7.5). Importantly the primers used for both reactions are radioactively labelled, thus allowing the detection of bands via autoradiography.

The bands obtained in this way can be assigned to the 5´-end of the respective co-purified (pre-) rRNAs, the formation of secondary structure elements in the RNA molecule, which the reverse transcriptase cannot overcome, or base modifications as methylations, which as well impede the progression of the reverse transcriptase. In turn, stops occurring in any of the samples but not detected in the control without MNase would give clear evidence for the localization of MNase induced cuts.

At first, the MNase-Noc3p induced cutting pattern, defined by three distinct bands, observed in the wild type situation was to be further analyzed (Figure 45, A, lane 20, red frames). Additionally, sequential northern hybridization using oligos that bind at different positions within the 27SB pre-rRNA allowed to roughly estimate the size of the bands, which supported the results obtained from the primer extension analyses (blots not shown). As the wild type cutting pattern also arises among the assembly mutants (Figure 45, A), both rpL25, rpL27, rpL34, rpL35 and rpL5 depleted situations were additionally analyzed, representing the “middle” and “late” class of LSU r-proteins, respectively. Additional to N-terminal MNase-Noc3p fusions, MNase was also fused to the C-terminus of Noc3p. The different variants are indicated as “N” or “C” in Figure 46. Cuts that are detected for both fusion variants might allow to appreciate flexibilities of certain rRNA segments within the particles.

For determining the exact rRNA position of the cut that produces fragment “I” in the northern analysis (Figure 45, A, lane 20, red frame “I”) a prominent stop was detected at 25S rRNA position 2558 in the ES 31 (Figure 46, left side, lane 7). However, a cut at this position was not found for the C-terminal MNase fusion (lane 8). Therefore, it can be concluded that ES31 is rather oriented towards the N-terminus of Noc3p. Interestingly, the respective rRNA position has not been resolved in any structure obtained for the LSU precursor, probably due to high conformational flexibility.

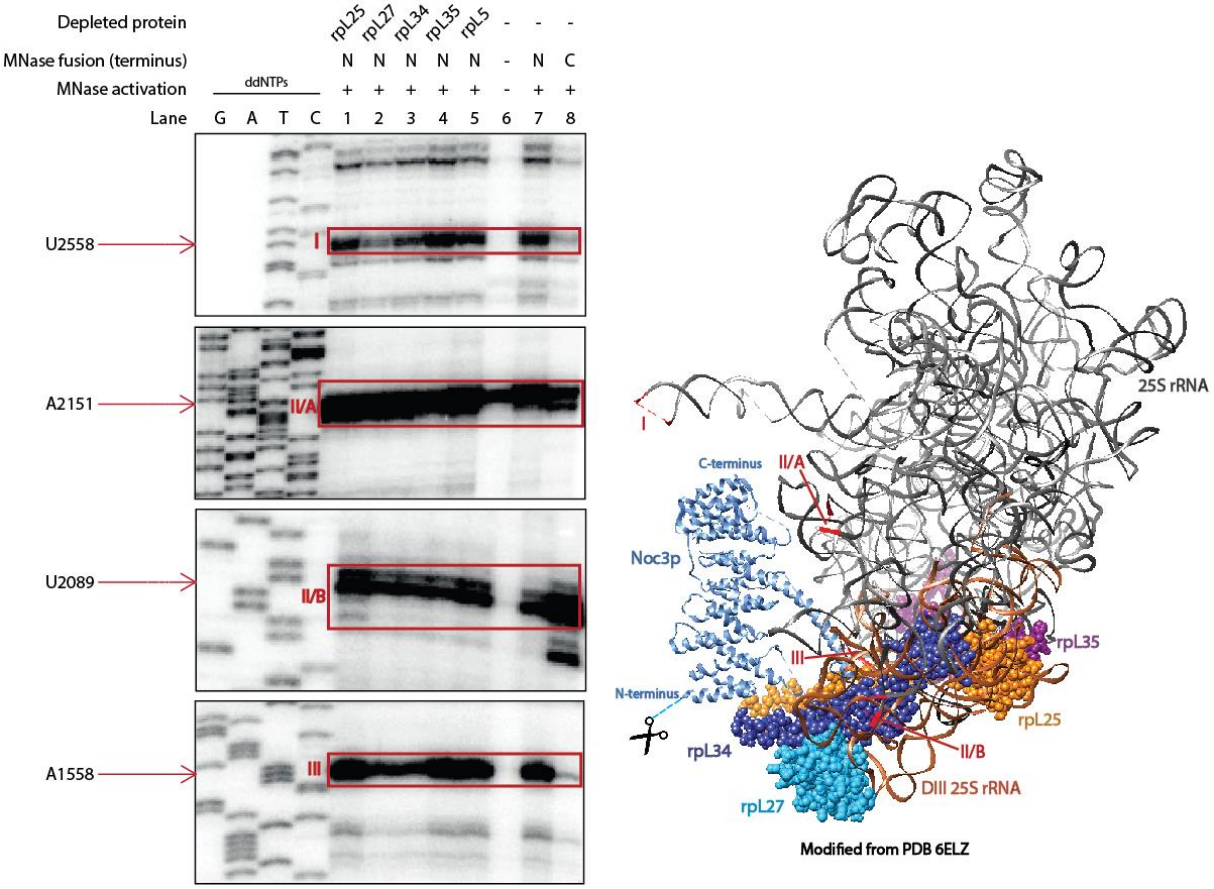

Figure 46: Primer extension analyses to precisely map the position of MNase-Noc3p induced cuts in the 25 S rRNA sequence of 27 SB pre-rRNA.

Exponentially growing yeast cells (Y3433, Y3449, Y3956, Y4167, Y4169, Y4171, Y4173, Y4179) (6.1.1) on galactose containing medium were shifted to glucose containing medium for 4 h to shut down the expression of the respective r-protein. Affinity purification was performed from total cell extracts (6.2.7.2) with buffers containing EGTA (6.1.6) using M2-anti FLAG affinity matrix (6.1.9). The purified fraction was treated with 8 mM calcium chloride for activation of MNase N-terminally fused to Noc3p and incubated for 15 min at 16 °C. Total RNA was isolated by phenol/chloroform extraction (6.2.4.1). Primer extension reactions (6.2.7.3) using radioactively labelled primers (6.2.4.6) that bind downstream of the indicated positions were performed with 250 ng of RNA derived from affinity purified fractions, respectively. Sequencing reactions were performed with the same set of radioactively labelled primers (6.2.7.4). The resulting cDNA of sequencing and primer extension reactions was size separated on sequencing gels (6.2.7.5) (left side). On the right side, Noc3p associated with pre-ribosomes of state E (PDB 6ELZ, modified with UCSF chimera (6.1.11) is shown. The 25 S rRNA is colored in grey, whereof its intrinsic domain III is highlighted in brown. LSU r-proteins rpL25 (orange), rpL27 (turquoise), rpL34 (purple) and rpL35 (violet) are shown together with Noc3p (cornflower blue). MNase fused to its N-terminus is indicated by scissors. Note, that 131 AA from the N-terminus of Noc3p are missing in the structure. The position of MNase induced cuts in the 25 S rRNA corresponding to the primer extension analyses (indicated by red frames on the left) are highlighted in red. Note that the residues for cut I and IIA/IIB are not resolved in the present structure. Therefore, flanking 5´- and 3´-nucleotides are colored in red.

The band of fragment “II” (Figure 45, A, lane 20) is the consequence of two cuts at sites situated close to each other when regarding their positions within the 25S rRNA sequence. The corresponding cuts are denoted as “II/A” and “II/B” in the primer extension analysis (Figure 46, left side). Cut “II/A” is located at 25 S rRNA position 2151. Remarkably, a primer extension stop was also found in the sample without MNase, indicated by a considerably weaker and slightly upwards shifted band (Figure 46, left side, lane 6). Notably, Bmt2p has been previously described to introduce a m^1-methylation to an adenine nearby, at 25 S rRNA position 2142 (Sharma et al. 2013), which might result in this primer extension stop. Cut “II/B” was found to occur at 25 S rRNA position 2089. Both cuts were detected for the N- and the C-terminal MNase-Noc3p fusion, respectively (Figure 46, left side, lanes 7,8). It seems, that these unresolved rRNA segments, to which the respective primer extension stops “II/A” and “II/B” could be referred, are thus flexible in their conformation to closely reach both termini of Noc3p. Additionally, unresolved parts for both the N- and C-terminus of Noc3p might enlarge the range of MNase, therefore explaining these findings (see also Figure 25).

The third fragment “III” (Figure 45, A, lane 20) was referred to a cut at 25 S rRNA position 1558 as indicated by the primer extension analysis (Figure 46, left side). As the respective cut was not found to occur for the C-terminal Noc3p-MNase fusion (Figure 46, left side, lane 8), it can be concluded, that this position lies within the range of the N-terminal MNase-Noc3p fusion. As mentioned above, the wild type cleavage pattern could be retrieved in nearly all assembly mutants. Therefore, it is not surprising, that each primer extension stop described here was found in the wild type situation and in all assembly mutants. However, the signals for primer extension stops corresponding to the fragments “I” and “III” were found to be comparably weaker after depletion of rpL27 and rpL34 (Figure 46, left side, lanes 2, 3). This result might explain the weaker detection of the respective fragments were by northern blotting (Figure 45, A, lanes 12, 13).

At next, fragment “IV”, which arises exclusively after depletion of rpL27 or rpL34 (Figure 45, A, lane 12, 13) was further addressed. Primer extension analysis reveals the position of the corresponding cut to be located in the 25 S rRNA domain III around nucleotide 1694, close to the N-terminus of rpL34 (Figure 47, left side, lane 2,3, red frame “IV”). Notably, this position is, in the wild type ribosome, buried within the pre-ribosome and therefore not easily accessible. This indicates, that the LSU domain III in the Noc3p-associated pre-ribosomal particle possibly undergoes significant structural rearrangements in upon depletion of rpL27 or rpL34 that (also discussed in section 5.1.2.2).

A series of further cuts was observed in close proximity to 25 S rRNA nucleotide 1694. The signal intensities for these cuts at 25 S rRNA positions 1714, 1724, 1729, 1741 and 1858 are significantly weaker than the main cut at position 1694. Even though these positions, seem to be rather superficially located, according to the structure, and hence easier accessible for MNase (Figure 47, right side), they are not cleaved by the latter one in the wild type situation.

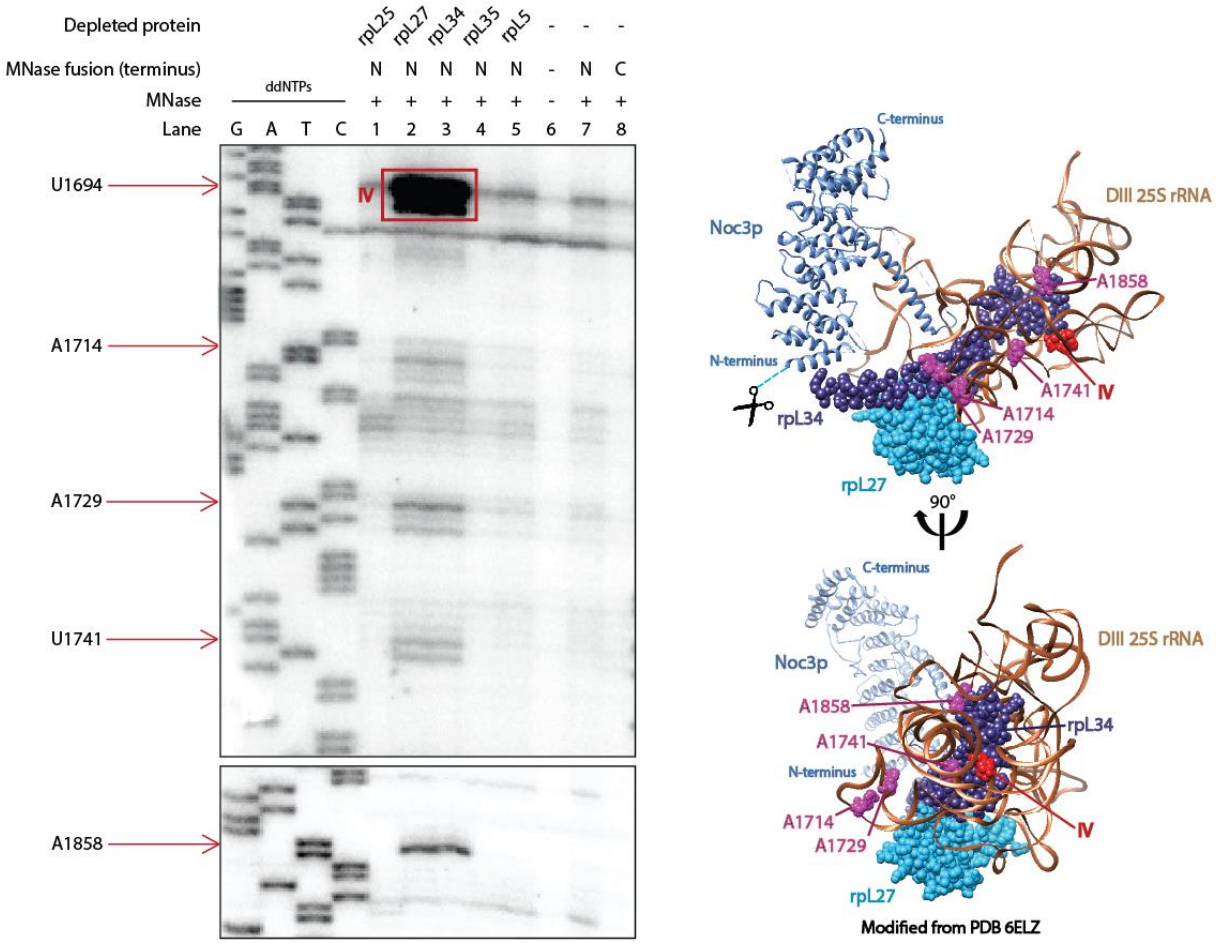

Figure 47: Characterization of the MNase-Noc3p induced cuts in 25 S rRNA domain III for depletion of rpL27 and rpL34 by primer extension analysis.

Exponentially growing yeast cells (Y3433, Y3449, Y3956, Y4167, Y4169, Y4171, Y4173, Y4179) (6.1.1) on galactose containing medium were shifted to glucose containing medium for 4 h to shut down the expression of the respective r-protein. Affinity purification was performed from total cell extracts (6.2.7.2) with buffers containing EGTA (6.1.6) using M2-anti FLAG affinity matrix (6.1.9). The purified fraction was treated with 8 mM calcium chloride for activation of MNase N-terminally fused to Noc3p and incubated for 15 min at 16 °C. Total RNA was isolated by phenol/chloroform extraction (6.2.4.1). Primer extension reactions (6.2.7.3) using radioactively labelled primers (6.2.4.6) that bind downstream of the indicated positions were performed with 250 ng of RNA derived from affinity purified fractions, respectively. Sequencing reactions were performed with the same set of radioactively labelled primers (6.2.7.4). The resulting cDNA of sequencing and primer extension reactions was size separated on sequencing gels (6.2.7.5) (left side). On the right side, Noc3p associated with pre-ribosomes of state E (PDB 6ELZ, modified with UCSF chimera (6.1.11) is shown. Only domain III is shown, colored in orange. LSU r-proteins rpL27 (turquoise) and rpL34 (purple) are shown together with Noc3p (cornflower blue). MNase fused to its N-terminus is indicated by scissors. The position of MNase induced cuts in the 25 S rRNA domain III corresponding to the primer extension analyses (indicated on the left) are highlighted in red.

This indicates that the action radius of the MNase-Noc3p fusion is yet to low to reach these nucleotides in the wild type situation and for depletions of rpL25, rpL35 and rpL5 (Figure 47, lanes 1, 4, 5 and 7). However, the structural rearrangement induced by depletion of either rpL27 or rpL34 obviously brings the thus misfolded domain III and Noc3p closer to each other, more precisely, to the N-terminus of Noc3p. Besides primer extension analyses, sequential northern hybridization allowed to undoubtedly identify and to assign the primer extension stops to the respective positions within the 25 S rRNA (Figure 48).

A

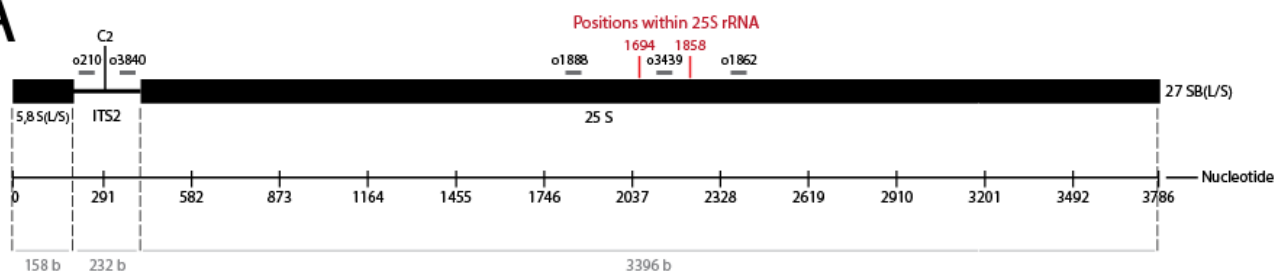

B

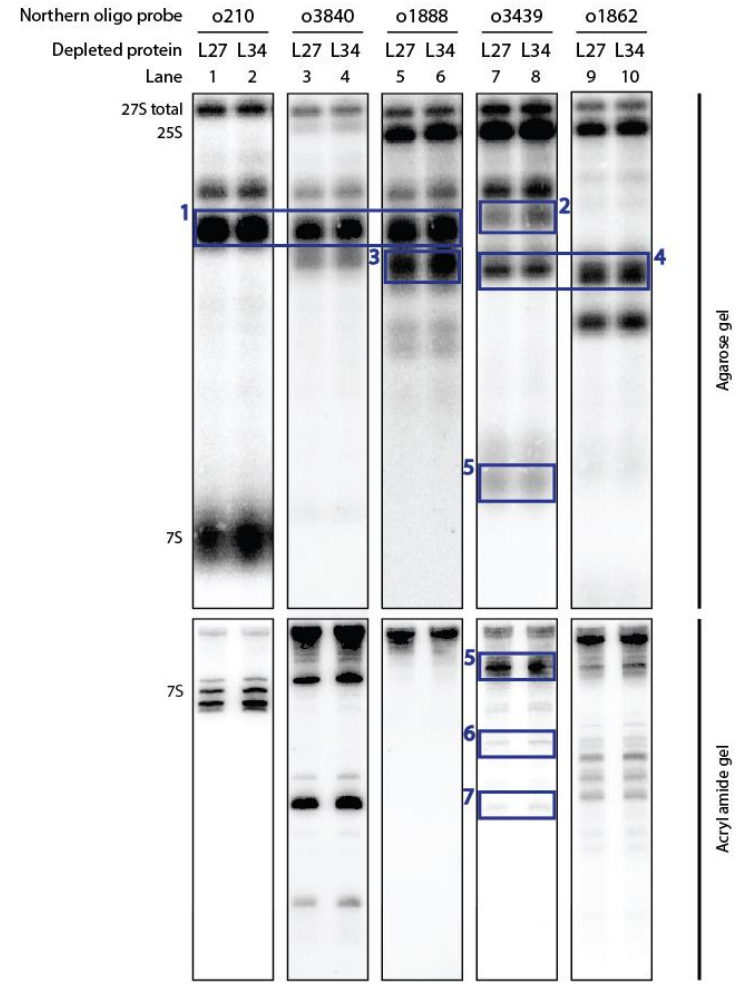

C

Fragment	5´-End	3´-End	Length [b]
1	5´-27SB	U1694 in 25S rRNA	2,039
2	5´-27SB	A1858 in 25S rRNA	2,203
3	A139 ITS2 (C_2)	U1694 in 25S rRNA	1,787
4	U1694 in 25S rRNA	3´-25S rRNA	1,702
5	U1694 in 25S rRNA	U2089 in 25S rRNA	395
6	U1694 in 25S rRNA	A1858 in 25S rRNA	164
7	A1729 in 25S rRNA	A1858 in 25S rRNA	129

Figure 48: Sequential northern analysis of the MNase-Noc3p induced main cut under rpL27 or rpL34 depleted situation. Exponentially growing yeast cells (Y3449, Y3956, Y4167, Y4169, Y4171, Y4173, Y4175, Y4177, Y4179, Y4181) (6.1.1) on galactose containing medium were shifted to glucose containing medium for 4 h to shut down expression of the respective r-protein. Affinity purification was performed from total cell extracts (6.2.7.2) with buffers containing EGTA (6.1.6) using M2-anti FLAG affinity matrix (6.1.9). The purified fraction was treated with 8 mM calcium chloride for activation of MNase N-terminally fused to Noc3p and incubated for 15 min at 16 °C. Total RNA was isolated by phenol/chloroform extraction (6.2.4.1). Total RNA was size separated on agarose and acryl amide gels (6.2.4.2 and 6.2.4.3). 0,053% of total input an 13,33% of the purified material were loaded, respectively. (A) Schematic representation of the 27 SB rRNA precursor. Nucleotide positions and sizes of 5.8S rRNA, ITS2 and 25S rRNA sequences are shown. The binding sites of oligonucleotides which were used for northern hybridization and the cutting events for the MNase-Noc3p fusion at 25 S rRNA position 1694 and 1858 are indicated. (B) Sequential northern hybridization of the blot shown in Figure 45, A, using the indicated probes was performed. Additionally, the acryl amide blot (6.2.4.5) is shown as well. For hybridization sites of the oligos see 6.1.3.3. Please note, that only lanes of rpL27 and rpL34 are shown in order to maintain the overview. Bands that are in context with the MNase-Noc3p induced main cut (Figure 45, A, lanes 12, 13, red frame "IV") are indicated by purple frames and asterisks, respectively. (C) The 5´- and 3´- ends of the fragments highlighted in (B) as well as the respective sizes of the fragments are given.

Figure 48, B, shows the northern blot for this analysis, probed with the indicated oligos. To maintain the overview, solely the lanes for rpL27 and rpL34 depletion are shown. All fragments that arise in the context of the MNase-Noc3p induced cuts revealed in primer extension analyses (Figure 47, left side), are marked by a purple frame. The remaining, not annotated bands, represent either the particular (pre-) rRNA species or appear in all the other samples and are therefore not specific in connection with depletion of rpL27 or rpL34.

With the probes o210, o3840 and o1888 that bind in the ITS2 or in the 25 S rRNA (Figure 48, A), a major fragment with a size of approximately 2 kb (Figure 48, B, 1) was detected, which is the result of a MNase cutting event at 25 S rRNA nucleotide 1694. Therefore, fragment (1) represents the main cutting event for the MNase-Noc3p fusion detected for depletion of rpL27 or rpL34 (see also Figure 45, A, lanes 12, 13 and Figure 47, left side, lanes 2, 3). With oligos o3439 and o1862, all binding 3´ of this cutting position, the associated fragment (4) with a calculated size of ~ 1,7 kb could be detected.

Fragment (2) is exclusively detected with o3439. It is slightly larger in size than the main fragment (1). This indicates that its 3´-end has to be located downstream of 25 S rRNA nucleotide 1694. Indeed, a further cutting event at position 1858 has been observed in the primer extension analysis (Figure 47, left side). The calculated size of this fragment with ~2,2 kb fits well to the observed pattern.

Fragment (3), detected with o1888 is slightly larger in size than fragment (4) and as well the result of a MNase induced cut at 25 S rRNA position 1694. However, in contrast to (1), its 5´-end is not the 5´-end of the 5.8 S rRNA but the consequence of a cut at position C2 in the ITS2. This results in a size of nearly 1,8 kb for this fragment which is consistent with the positions of the observed fragments in the northern. However, as described above, the latter cutting event is either due to C2-processing by the endonuclease Las1p or to a cut by the MNase-Noc3p fusion.

Fragment (5) is, in contrast to the beforementioned fragments, much smaller in size. Its 5´- end is produced by the main cut at 25 S rRNA position 1694. Therefore, it can be detected with o3439. However, its 3´- end cannot be deduced from MNase-Noc3p dependent cutting events which are

specific for depletion of rpL27 or rpL34. In fact, the 3´-end corresponds to a cut at 25 S rRNA nucleotide 2089 or 2151 which represent the cuts "II/A" and "II/B" (Figure 46, left side) that as well occur under non-depleted conditions.

Finally, two fragments of a smaller size were detected in the acryl amide blot with o3439 (Figure 48, B, lower blot). Fragment (6) represents the intermediate fragment that arises through cutting events at 25 S rRNA position 1694 and 1858. The smallest fragment (7) is the result of cuts at 25 S rRNA positions 1729 and 1858.

Summarizing these findings, it can be concluded that depletion of either rpL27 or rpL34 induces a significant conformational rearrangement of certain rRNA elements of 25 S rRNA domain III, which probably results directly or indirectly in a release defect of Noc3p as already indicated in section 4.3.

4.5 Depletion of certain LSU domain III r-proteins does not affect the structure and orientation of the ITS2

The observed release defect of Noc3p from pre-ribosomes upon depletion of certain r-proteins (section 4.3) has been structurally addressed using a versatile structure probing approach, which revealed a conformational rearrangement of LSU domain III for depletion of rpL27 and rpL34 (section 4.4). To check, whether r-protein depletions, which impair the release of Noc3p, affect the structure or orientation of the ITS2, tethered MNase structure probing has been utilized to address this issue. It might be the case, that the structural reorganization and an altered conformation of the ITS2 influences the release of Noc3p as 27SB pre-rRNA processing occurs in this region.

So far, the structure of the ITS2 rRNA region has not been completely resolved in structure studies (Wu et al. 2016; Kater et al. 2017), and the conformation of the central part of the ITS2 remains unresolved (further details discussed in section 5.1.2.3). Previously, MNase fusions of rpL27 have been successfully used to probe the ITS2 in wild type strains (Pöll et al. 2017). It has been observed, that the structure prediction illustrated in Figure 49 (B) is rather favorable in intermediate LSU precursor particles associated with Noc3p (Pöll et al. 2017).

As indicated in section 4.4, the action radius of MNase fused to the N-terminus of Noc3p ranges to LSU domain III. Therefore, this fusion has been considered as suitable to analyze the ITS2 in the r-protein assembly mutant strains. By this, misassembled Noc3p-associated pre-ribosomal particles can be probed for differences in their orientation and structure of the ITS2 region, respectively (Figure 49, A). The positions of the cuts were equally determined to nucleotide resolution in primer extension reactions and mapped to the respective ITS2 structure predictions shown in Figure 49 (B, C).

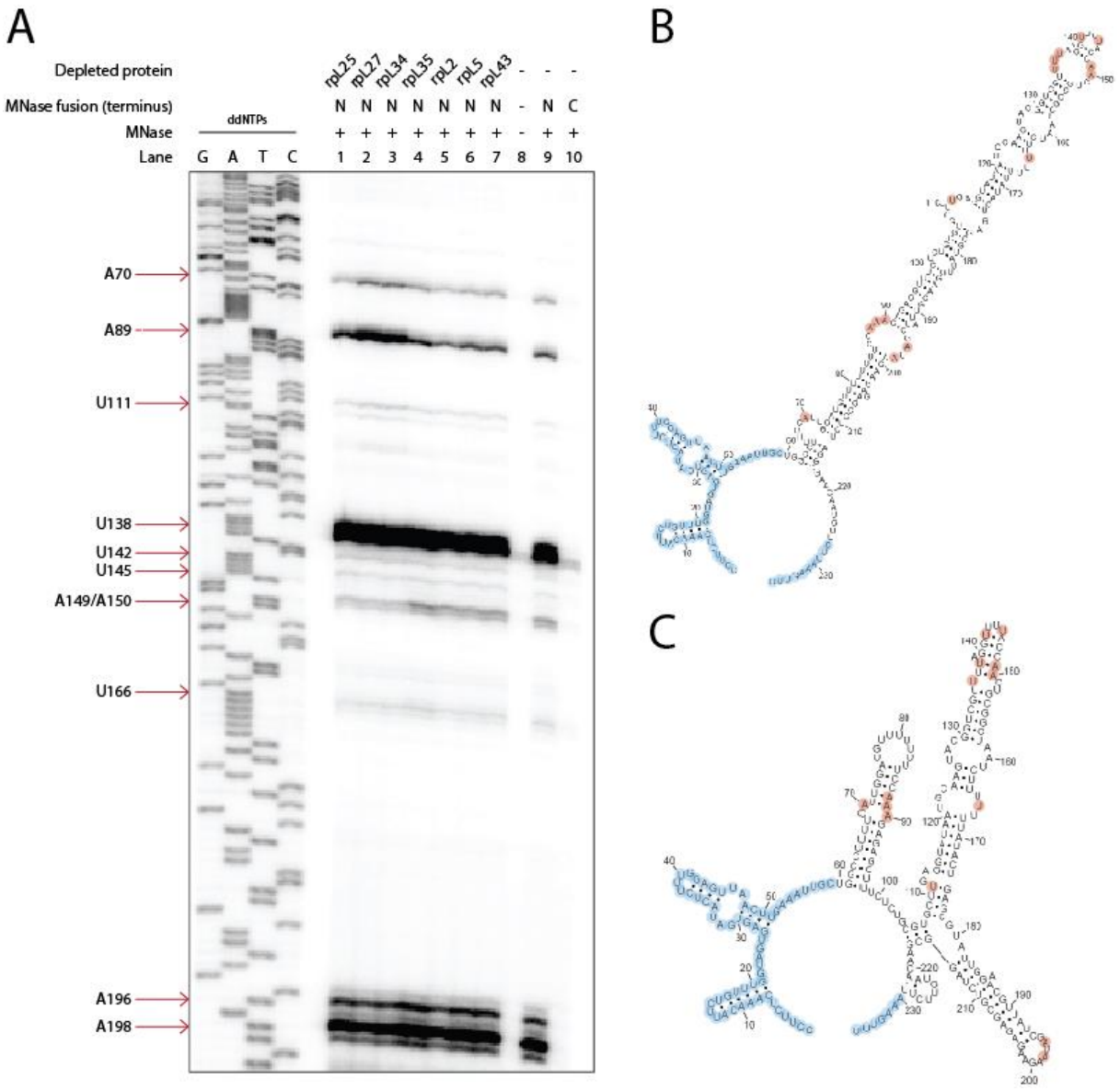

Figure 49: Location of Noc3p tethered MNase induced cleavages in the ITS2 rRNA region.
(A) Exponentially growing yeast cells (Y3433, Y3449, Y3956, Y4167, Y4169, Y4171, Y4173, Y4179) (6.1.1) on galactose containing medium were shifted to glucose containing medium for 4 h to shut down the expression of the respective r-protein. Affinity purification was performed from total cell extracts (6.2.7.2) with buffers containing EGTA (6.1.6) using M2-anti FLAG affinity matrix (6.1.9). The purified fraction was treated with 8 mM calcium chloride for activation of MNase N-terminally fused to Noc3p and incubated for 15 min at 16 °C. Total RNA was isolated by phenol/chloroform extraction (6.2.4.1). Primer extension reactions (6.2.7.3) using radioactively labelled primers (6.2.4.6) that bind downstream of the indicated positions were performed with 250 ng of RNA derived from affinity purified fractions, respectively. Sequencing reactions were performed with the same set of radioactively labelled primers (6.2.7.4). The resulting cDNA of sequencing and primer extension reactions was size separated on sequencing gels (6.2.7.5). (B), (C) ITS2 structure predictions modified from (Pöll et al. 2017) are shown. Cutting events of the MNase-Noc3p fusion under wild type conditions found in (A) are indicated by red circles. Regions with a secondary structure that match to cryo-EM analyses are colored in blue – for further details see (Pöll et al. 2017).

Regarding the wild type situation (Figure 49, A, lane 9), the N-terminal MNase-Noc3p fusion introduces defined cuts at specific positions within the ITS2 rRNA region. The most sensitive region for nuclease action is located around ITS2 position 138 which reflects the C2 processing site. Less efficient cleavage events were observed in close proximity to C2 at nucleotides 142, 145, 149 and 150. All of these

identified cleavages fall into single stranded regions, which is the preferred substrate of MNase, for the proposed ITS2 secondary structure model shown in B (Figure 49, bases highlighted in red). Two further significant cutting events were observed at ITS2 positions 196, 198 and 89. According to the structure prediction in C (Figure 49), the latter nucleotide is however base paired and therefore not preferentially cut by MNase.

For these findings it can be suggested that the proposed model for the ITS2 rRNA region shown in B rather reflects the real *in vivo* situation at least in intermediate Noc3p-associated pre-ribosomes prior to C2 processing. Notably, the observed cutting events were solely found for the N-terminal MNase fusion to Noc3p but not for the C-terminal one (Figure 49, A, lane 10). These findings indicate, that both the ITS2 rRNA region and the N-terminus of Noc3p are thus flexible to reach a sufficient spatial proximity to each other that enables MNase structure probing.

Having analyzed the ITS2 in the wild type situation, the consequence of LSU assembly defects had to be taken into consideration. Therefore, a set of assembly mutant strains in which the expression of rpL25, rpL27, rpL34, rpL35, rpL2, rpL5 and rpL43 has been shut down was used for ITS2 structure probing with the MNase-Noc3p fusion. As indicated, cutting patterns among the mutant strains were identical compared to the wild type situation (Figure 49, A, lanes 1-7). Possibly, pre-LSU assembly defects resulting from depletion of the indicated LSU r-proteins neither affect the structure nor the orientation of the ITS2 rRNA region in Noc3p-associated LSU precursors. However, signals observed for MNase introduced cuts at nucleotide positions 70 and 89 were comparably stronger for depletion of rpL27 or rpL34 (Figure 49, A, lanes 2, 3). This might indicate that structural rearrangements of LSU domain III which were observed in these mutants (see section 4.4) possibly contribute to further decrease the distance between the MNase-Noc3p fusion and the proximal parts of the ITS2.

4.6 N-terminal truncations of rpL34 are mostly lethal and only conditionally assembled in ribosomes

As described in section 4.4, the findings suggest that an expressional shut down of LSU r-proteins -27 or -34 induces a substantial structural rearrangement of LSU domain III. As consequence, rRNA regions which are usually buried within the pre-ribosome become accessible for MNase cleavage. This effect is particularly strong for the 25 S rRNA nucleotide 1694 (Figure 47, left side, lanes 2, 3). Interestingly, this position is located in close proximity to the N-terminus of rpL34 (Figure 47, right side).

This leads to the question, whether the rpL34 N-terminus has a stabilizing effect on the positional and conformational orientation of this rRNA region. To address this issue, truncation variants of the N-terminal domain of rpL34 have been generated, according to secondary structure motifs (Figure 51). An additional mutant was generated by truncation of, the long α-helix at the C-terminus of rpL34. To

generate the DNA fragments encoding for these variants, a PCR-based approach as described for the generation of the Noc3p-truncations (section 4.2.2) has been applied. For a later affinity purification and detection in western blot analysis, the rpL34 variants employ a N-terminal FLAG-tag.

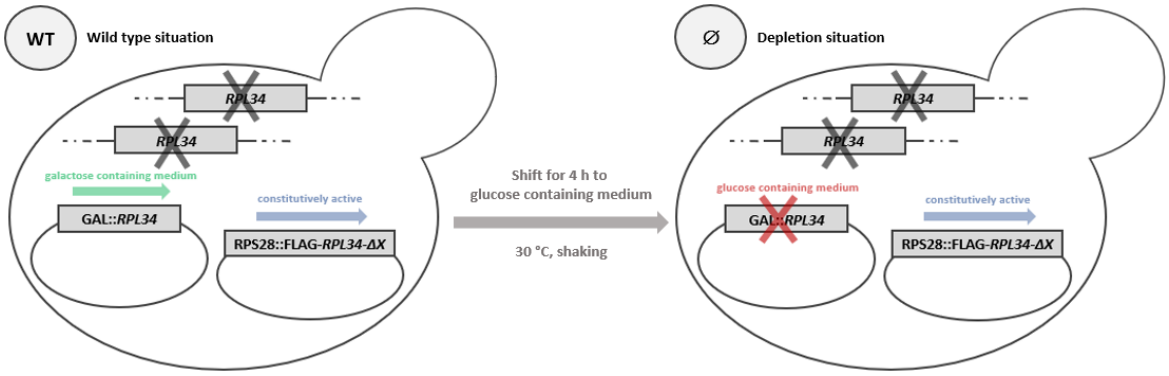

Figure 50: Genetic system for studying the incorporation of truncation variants of rpL34 in ribosomes.
The strain Y930, in which the genomic copies of *RPL34* are genomically deleted was used for this purpose. In this strain, the deletion of the respective rpL34-alleles is complemented by a plasmid that encodes for the r-protein under a galactose inducible, glucose repressible promotor. Additionally, plasmids encoding a N-terminal FLAG-tagged version of full length *RPL34* and truncations thereof under a constitutively active RPS28-promotor are transformed in this strain. Therefore, cultivation of these strains in glucose containing medium induces an expressional shut down of rpL34 and the effects of the truncation variants can be analyzed.

The plasmids encoding the *RPL34*-variants have been transformed in the strain in which both alleles encoding for *RPL34* were genomically deleted and cell growth was supported by expression of *RPL34* from a plasmid under the control of a galactose inducible, glucose repressed promoter (Y930, see 6.1.1). Therefore, expression of wild type *RPL34* is shut down by growth of the yeast cells in glucose containing medium. The genetic system therefore is schematically illustrated in Figure 50. Cells, which constitutively expressed truncation variants of rpL34 were analyzed for possible LSU assembly defects and their ability to be incorporated in ribosomes.

To check, whether the respective rpL34 N- or C-terminal truncations can complement the intrinsic function of wild type rpL34, complementation tests have been performed. Therefore, the strain Y930 has been transformed with the different rpL34-plasmids (Figure 50). The resulting transformants were spotted on SGC_{-Leu} plates to select for cells containing the plasmids encoding the truncation variants of rpL34. To analyze cell growth when only the rpL34 truncation mutants are expressed, cells were spotted on SDC_{-Leu} plates to shut down expression of wild type rpL34.

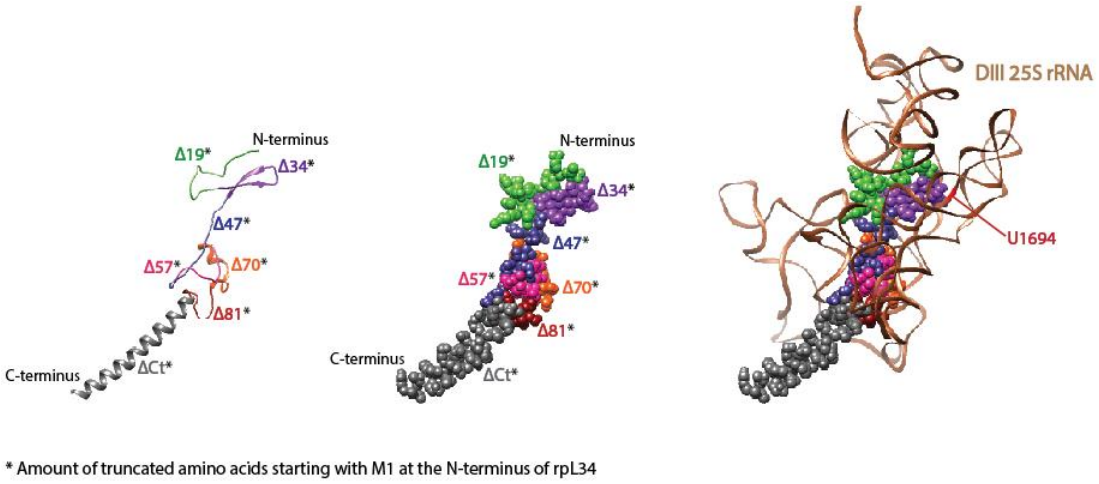

Figure 51: N- and C-terminal truncations of rpL34.
The following illustrations were created using UCSF chimera (6.1.11). The structure of rpL34 has been derived from pre-ribosomal particles state E (Kater et al. 2017). Left: Introduced truncations according to secondary structural motifs are indicated by different colors. The number of truncated amino acids, starting at the N-terminus of rpL34 are annotated. Middle: The visualization of secondary structure motifs has been replaced by displaying the atoms of rpL34 as spheres. Right: rpL34 incorporated in LSU domain III (brown). The 25 S rRNA nucleotide position 1694 is highlighted in red.

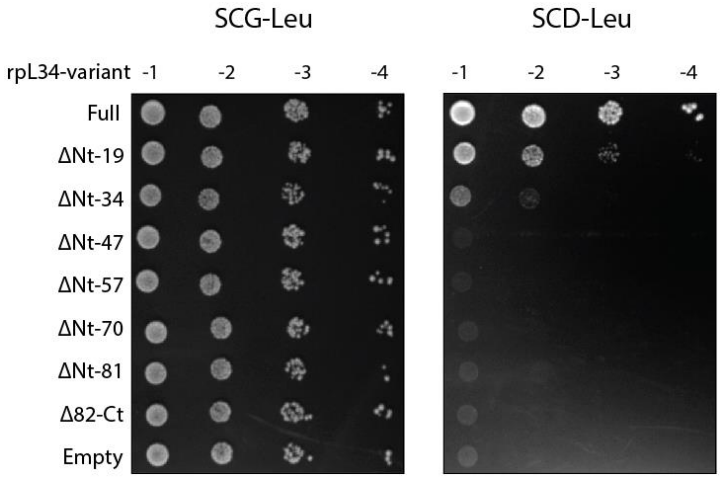

Figure 52: Complementation tests of the different FLAG-tagged rpL34-truncations.
Exponentially growing yeast cells of the strain Y930 (6.1.1) transformed with the constructs encoding the FLAG-tagged *RPL34*-truncation variants were used to perform spot tests on glucose containing plates (6.2.1.7). The plates were incubated for 3 days at 30 °C. Resultant colonies were analyzed fir growth.

After three days of growth at 30 °C, all strains grew identically on galactose containing plates, regardless of the rpl34-truncations expressed, (Figure 52, left side) since full length rpL34 was expressed in all of them. These results discard any dominant negative effect caused by truncation of rpL34. In contrast, only the strain which expressed the full length *RPL34* was able to grow properly (Figure 52, right side).

Upon truncation of 19 AA from the N-terminus which represents a small unstructured part of the whole protein (Figure 51, green part), a significant growth defect could already be observed. Arising

colonies on the glucose containing plates were less and smaller in size (Figure 52, right side). This indicates that the N-terminus of rpL34 is important for proper growth of the cells. Truncation of 34 AA, which makes up already one third of the whole protein and lacks the adjacent beta-sheet to the ΔNt-19 (Figure 51, purple), enhances the growth defect but does not completely prevent growth (Figure 52, right side). If larger parts were truncated from the N-terminus, the strains, which were transformed with the respective plasmids, were not able to grow. Therefore, these rpL34 variants do not complement the function of full length rpL34. Finally, truncation of the α-helix at the C-terminus, which reflects 32 AA, induced the same severe growth phenotype.

At next, the rpL34 truncations were analyzed for their ability to assemble with (pre-)ribosomes. It cannot be excluded, that the truncation variants can bind to pre-ribosomes, however, they might influence or block pre-rRNA processing, maturation, or ribosomal function of the pre-ribosomes. To address this aspect, the strains were cultivated for 4 h in glucose containing medium to shut down the expression of functional rpL34. RpL34 truncation variants were then affinity purified by the FLAG-tag, which was fused to the N-terminal part of the rpL34 variants (6.2.6.4). Purified samples were subsequently analyzed by northern blotting for the characterization of putatively enriched rRNA species and precursors (Figure 53).

Regarding the western analysis, signals for full-length rpL34 and the truncated versions ΔNt-19, ΔNt-34, ΔNt-47, ΔNt-57 and ΔNt-70 were detected in the affinity purifications (Figure 53, A, lanes 10-15), although to a decreasing intensity with increasing length of the truncation. However, signals ΔNt-81 and the C-terminal truncation Δ82-Ct were not detected in the western (B, lanes 16, 17), probably reflecting folding misconduct.

Regarding the input fraction of the northern analysis, the signals for 25 S rRNA decrease for the truncation variants ΔNt-19 and ΔNt-34, compared to the wild type situation (B, compare lanes 2, 3 with 1). Concomitant with the complementation tests, these truncated proteins were only partly able to complement the absence of full length rpL34 (Figure 52 and Figure 54). Since depletion of rpL34 blocks processing of 27SB pre-rRNA (Pöll et al. 2009) processing of 27SB to 7S pre-rRNA seems, however, not to be affected for ΔNt-19 and ΔNt-34, as the ratios are similar to the wild type situation (Figure 53, C). This suggests that both these two rpL34 truncations are probably incorporated in LSU precursor particles but establish an assembly defect that impedes the production of fully functional and processive ribosomes.

Truncation of larger N-terminal regions of rpL34 causes an accumulation of 27SB and hence a processing delay to 7S pre-rRNA with increasing size of the truncation. As indicated in Figure 53 (B, lanes 4, 5; quantification in C), the ratio of 27SB over 7S pre-rRNA rises to twofold for ΔNt-47 and to ~2,5-fold for ΔNt-5, compared to the wild type, although they seem to be expressed and could be purified (A, lanes 13, 14).

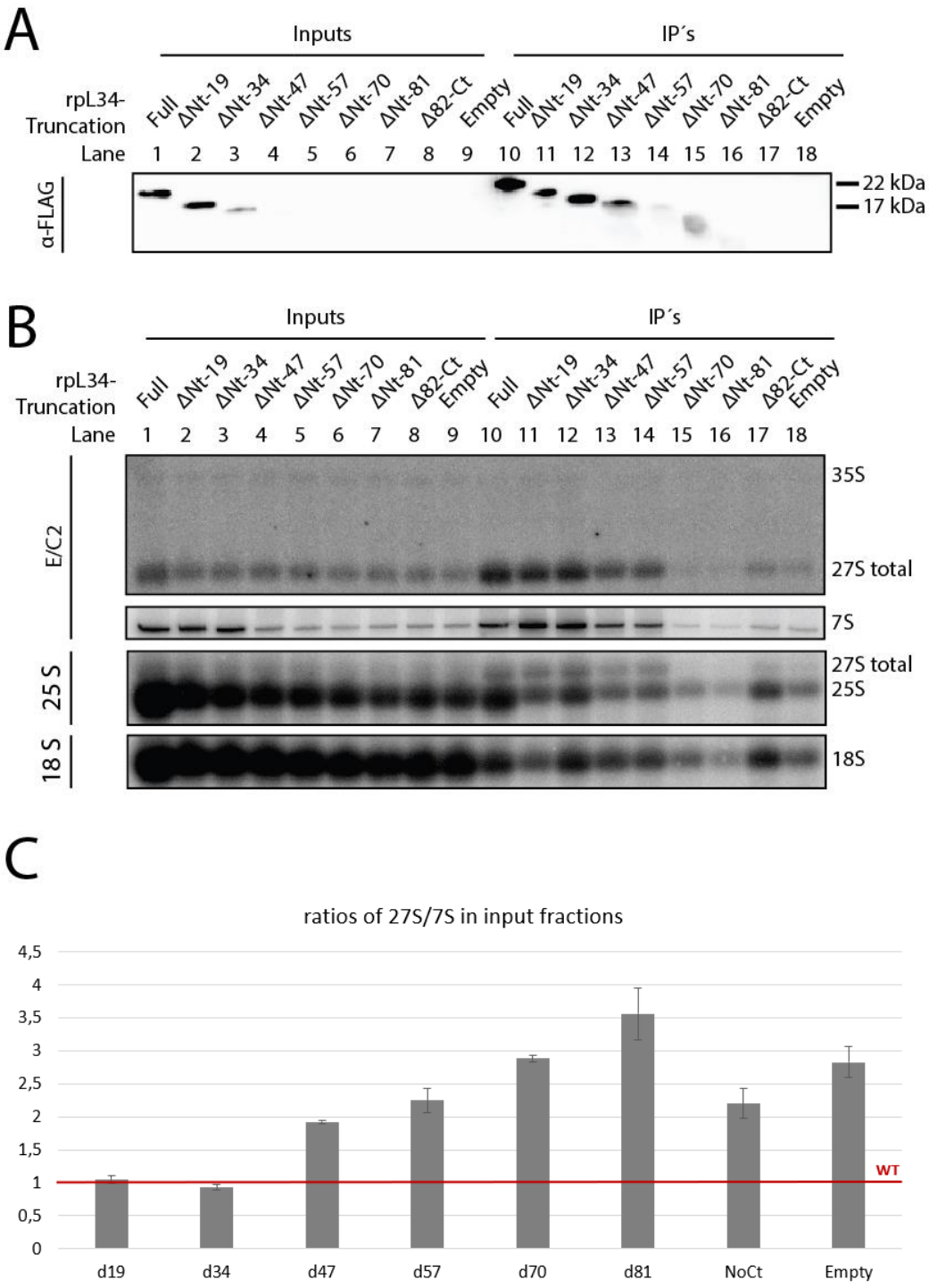

Figure 53: Analyzing the incorporation of rpL34 truncation variants in ribosomes.
(A) Exponentially growing yeast cells of Y930 (6.1.1) transformed with the constructs encoding the FLAG-tagged *RPL34*-truncation variants (6.1.2) on galactose containing medium were shifted to glucose containing medium for 4 h to shut down expression of the respective r-protein. Affinity purification was performed from total cell extracts (6.2.6.4) using M2-Anti Flag affinity matrix (6.1.9). Aliquots of cells corresponding to 0,22 % of the input and 11 % of the purified material were separated by SDS-PAGE (6.2.5.3) and analyzed by western blotting (6.2.5.4). The bait proteins were visualized using the PAP detection reagent (6.2.5.6). (B) Total RNA was isolated by phenol/chloroform extraction (6.2.4.1). Total RNA was size separated on agarose and acryl amide gels (6.2.4.2 and 6.2.4.3). 0,22 % of total input and 11 % of the purified material were loaded, respectively and analyzed by sequential northern blotting using the indicated probes. For hybridization sites of the oligos see 6.1.3.3. (B). (C) Signals for both the input and the affinity purified fractions in the northern blot of A were quantified using MultiGauge software (Fujifilm) (6.1.11). Indicated signal ratios for pre-rRNA species were calculated for each strain to visualize the amount of the incorporated pre-rRNA species. Signal ratios were normalized to the wild type ("WT") for each strain and each pre-rRNA species, respectively.

Due to the fact, that the signal intensities for 27SB and 7S pre-rRNA in the respective affinity purified fractions were clearly higher than in the “empty-control” (Figure 53, B, compare lanes 13 and 14 with 18), it can be concluded, that these truncation variants still assemble with pre-ribosomes. However, for ΔNt-70 a 3-fold higher ratio of 27SB over 7S pre-rRNA was measured, which is similar to the “empty-control” (Figure 53, C). As no signal for the particular pre-rRNA species can be detected in the co-purified fraction (B, lane 15; quantification in C), this truncated version of rpL34 seems not to be incorporated in pre-ribosomes, albeit a signal in the western analysis could be detected (Figure 53, A, lane 15). Strikingly, the ratio of 27SB over 7S pre-rRNA for the rpL34 variant Δ82-Ct is only approximately twofold higher compared to the wild type situation and therefore similar to ΔNt-47. It seems, that truncation of the C-terminal helix of rpL34 allows the protein to assemble with pre-ribosomes, but causes an assembly defect, accompanying a delayed conversion of 27SB to 7S pre-rRNA (Figure 53, A, lane 17; quantification in C). However, reliable statements concerning co-purification efficiencies of pre-rRNA species cannot be made neither for Δ82-Ct nor for any other N-terminal truncation variant of rpL34 due to high background signals detected in the affinity purified fraction for the “empty-control” (Figure 53, B, lane 18).

4.7 Structure probing of Noc3p associated pre-ribosomes reveals a misfolded 25S rRNA DIII independent of the rpL34 truncation variant

As described in section 4.4, the assembly defect that occurs as consequence of rpL34 depletion is characterized by structural rearrangements of rRNA regions in LSU domain III. Furthermore, the length of rpL34 truncations from the N-terminus correlates with increased accumulation of 27SB pre-rRNA over 7S pre-rRNA (Figure 53, C). Hence, a possible causal relationship between the size of the truncated region from the N-terminus of rpL34 and folding of LSU domain III shall be investigated (see also section 4.4).

To do so, the tethered tertiary structure probing approach which involves N-terminal MNase fusions of Noc3p as described in section 4.4 was applied. Importantly, the truncation variants of rpL34 were expressed as untagged proteins to do not interefere with the affinity purification of the FLAG-tagged MNase-Noc3p fusion. Therefore, structure probing can be specifically performed on Noc3p-associated LSU precursors that incorporate the rpL34 protein variants. The genetic system used for this analysis is similar to the one described in Figure 50, except that Noc3p is expressed as fusion to MNase from its endogenous locus (corresponds to strain Y4171, see section 6.1.1). Prior to structure probing, yeast cells were transformed with the plasmids encoding the rpL34-truncation variants and analyzed for complementation of rpL34 with the trunctaion mutants as described in section 4.6 to exclude influences due to the different strain background.

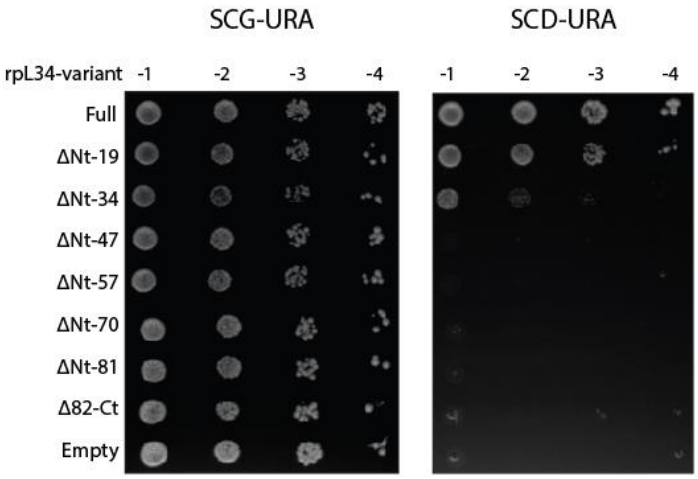

Figure 54: Complementation tests of the different untagged rpL34-truncations.
Exponentially growing yeast cells of the strain Y4171 (6.1.1) transformed with the constructs encoding the untagged *RPL34*-truncation variants (6.1.2) were used to perform spot tests on glucose containing plates. The plates were incubated for 3 days at 30 °C. Resultant colonies were analyzed fir growth.

As expected, all strains grew identically with galactose as carbon source (Figure 54, left side). However, on glucose containing plates, which repressed the expression of the wild type rpL34, solely the strain transformed with the full-length version of *RPL34* was able to grow properly (Figure 54, right side). The growth phenotypes observed under expression of ΔNt-19 and ΔNt-34 were similar to the ones observed in Figure 52. The remaining truncations were not able to support cell growth on glucose containing plates. In agreement with the previous observations (Figure 52, section 4.6), these results indicate that the absence of the first 19 and 34 AA allow a partial complementation of rpL34 function, while the other truncations produced non-functional variant of rpL34.

For the structure probing assays, the strains were cultivated for 4h in glucose containing medium to *in vivo* deplete rpL34. Subsequently, Noc3p-associated pre-ribosomes incorporating the rpL34 truncations were affinity purified from total cell extracts (6.2.7.2). These fractions were split in two equal volumes, whereof one sample was treated with calcium to activate MNase. The second sample was treated with H_2O and used as control.

As shown in the northern blot analysis of Figure 55, in the input fractions, a processing delay of 27SB pre-rRNA, already detected for the FLAG-tagged truncation versions ΔNt-47 and ΔNt-57 of rpL34 (section 4.6) was observed.

In contrast, full length rpL34 and the N-terminal truncations ΔNt-19 and ΔNt-34 showed similar signals of 27SB and 7S pre-rRNA (Figure 55, A, lanes 1-3). This indicates a yet largely unaffected conversion of 27SB to 7S pre-rRNA in these situations, when compared to full-length rpL34. This indicates that these mutants do not play a role on C_2 cleavage. Under expression of ΔNt-47, the ratio was clearly shifted to 27SB pre-rRNA, indicating the accumulation of this pre-rRNA species and hence an established processing delay (Figure 55, A, lane 4).

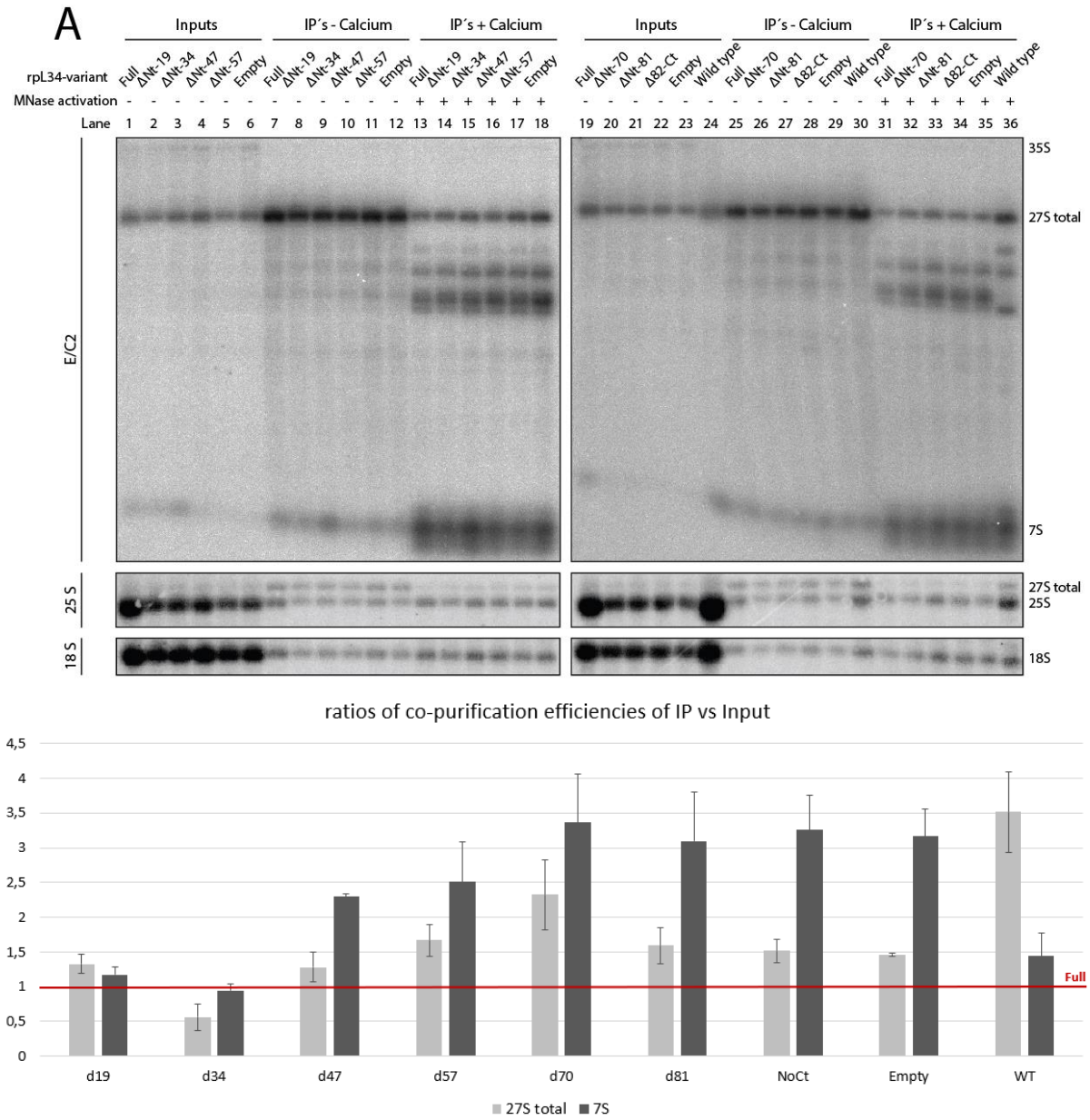

Figure 55: Effects of rpL34 truncations on the assembly of LSU precursors analyzed by structure probing of strains which express MNase as fusion proteins of Noc3p.

(A) Exponentially growing yeast cells of Y4171 (6.1.1) transformed with the constructs encoding the *RPL34*-truncation variants (6.1.2) on galactose containing medium were shifted to glucose containing medium for 4 h to shut down expression of the respective r-protein. Affinity purification was performed from total cell extracts (6.2.7.2) using M2-Anti Flag affinity matrix (6.1.9). The purified fraction was split to two samples with equal volumes. Sample 1 was treated with 8 mM calcium chloride for activation of MNase N-terminally fused to Noc3p and incubated for 15 min at 16 °C. Sample 2 was treated with H_2O and incubated as well. Total RNA was isolated by phenol/chloroform extraction (6.2.4.1). Total RNA was size separated on agarose and acryl amide gels (6.2.4.2 and 6.2.4.3). 0,19 % of total input and 8,33 % of the purified material were loaded, respectively and analyzed by sequential northern blotting using the indicated probes. For hybridization sites of the oligos see 6.1.3.3. (B) Aliquots of cells corresponding to 0,19 % of the input and 5,55 % of the purified material were separated by SDS-PAGE (6.2.5.3) and analyzed by western blotting (6.2.5.4). The bait proteins were visualized using the PAP detection reagent (6.2.5.6). (C) Signals for the input and the affinity purified fractions not treated with calcium in the northern blot of A were quantified using MultiGauge software (Fujifilm) (6.1.11). Indicated signal ratios for pre-rRNA species were calculated for each strain to visualize the amount of the incorporated pre-rRNA species. Signal ratios were normalized to the wild type ("WT") for each strain and each pre-rRNA species, respectively.

In agreement, 7 S pre-rRNA was detectable neither for this rpL34 truncation variant nor for ΔNt-57, ΔNt-70, ΔNt-81, and the C-terminal truncation Δ82-Ct (Figure 55, A, lanes 5, 20-22). Hence, these results confirmed the observed processing phenotype upon truncating more than 34 AA from the N-terminus of rpL34 (see section 4.6).

Regarding the co-purification efficiencies, equal amounts of 27SB and 7S pre-rRNA have been co-purified from strains that express either full length rpL34 or the truncation variants ΔNt-19 or ΔNt-34 (Figure 55, A, lanes 7-9 quantification in C), in agreement the unaffected processing of 27SB pre-rRNA. However, under expression of ΔNt-47, 7S pre-rRNA is preferentially enriched with Noc3p when compared to 27SB pre-rRNA (Figure 55, C). This tendency was also observed for larger N-terminal truncations of rpL34 (ΔNt-57, ΔNt-70 and ΔNt81) (Figure 55, C). The ratios for co-purification of 27SB- and 7S pre-rRNA for ΔNt-70, ΔNt-81, and for the C-terminal truncation Δ82-Ct were is similar to the situation observed for the “empty-control” (Figure 55, C).

The western blotting analysis showed in general strong signals for the MNase-Noc3p fusion in both the input as well as in the affinity purified fractions (Figure 55, B). For this, the observed altered 27SB and 7S co-purifications are not the result of differences in Noc3p-purification efficiencies.

These results would indicate a release defect of Noc3p from the pre-ribosomal population containing N-terminal truncations of rpL34, as has been observed after depletion of rpL34 (see section 4.3). Notably, rpL34-variants including the full-length version are expressed via a plasmid-based system under the control of a constitutive active RPS28-promoter.To discard a possible effect due to a possible different expression pattern between the rpL34 alleles, the parental strain expressing rpL34 from its endogenous promoter and chromosomal locus has been analyzed as well. Interestingly, the co-purification of 27SB pre-rRNA in the wild type strain was 3-fold higher when compared with the full-length version of rpL34 expressed from a plasmid. In addition, the amount of 7S- co-purification was similar (Figure 55, C). This result indicates a similar release of Noc3p upon processing of 27SB pre-rRNA in both cases. However, expression of rpL34 from its endogenous locus seems to increase the pool of pre-ribosomes that incorporate 27SB pre-rRNA, as indicated by increased co-purification levels.

Calcium triggered activation of MNase on the affinity purified fractions induced a defined cutting pattern among the samples (Figure 55, A, lanes 13-18 and 31-36). Three distinct bands appeared as consequence of MNase activity. Two among them had a larger size, whereas the third band had a similar size than 7 S pre-rRNA. The described cutting pattern resembled the one observed for MNase structure probing upon depletion of rpL27 or rpL34 (section 4.4, Figure 45, A, lanes 12, 13). Notably, the lower band among the two of larger size was initially found to solely appear in rpL27 and rpL34 depleted conditions (Figure 45, lanes 12 and 13; red frame “IV”). It could therefore be assigned to the cutting event at 25 S rRNA nucleotide 1694 (Figure 47, left side, lanes 2 and 3). Cutting events at this

positions have been interpreted due to a possibly misfolded LSU domain III (also discussed in section 5.1.2.2). This pattern observed for the "empty-control", as well as for the truncations ΔNt-70, ΔNt-81 and Δ82-Ct, which were found to probably not associate with pre-ribosomes (section 4.6), confirms this assumption. However, no differences were found among the rpL34 truncations compared to the full-length (Figure 55, A). Exceptionally, the parental wild type strain showed a distinct altered MNase induced cutting pattern (Figure 55, A, lane36), which was similar to what was observed without depletion of any rpL (section 4.4, Figure 45, lane 20). These results did not allow to support the influence of a certain rpL34 truncation variant on the structural rearrangement of LSU domain III. A possibly different expression pattern of the rpL34 variants, which are expressed under the control of a RPS28 promotor, compared to endogenous expression might be a reason for these findings.

Finally, primer extension reaction were performed (6.2.7.3) to confirm the identity of the bands observed in the northern analysis (Figure 55, A, lanes 17-24). Therefore, focus was laid on the region around 25 S rRNA nucleotide 1694 as these segments were observed to suffer increased accessibility to MNase cleavage upon depletion of rpL34 (compare Figure 47, left side, lane 3).

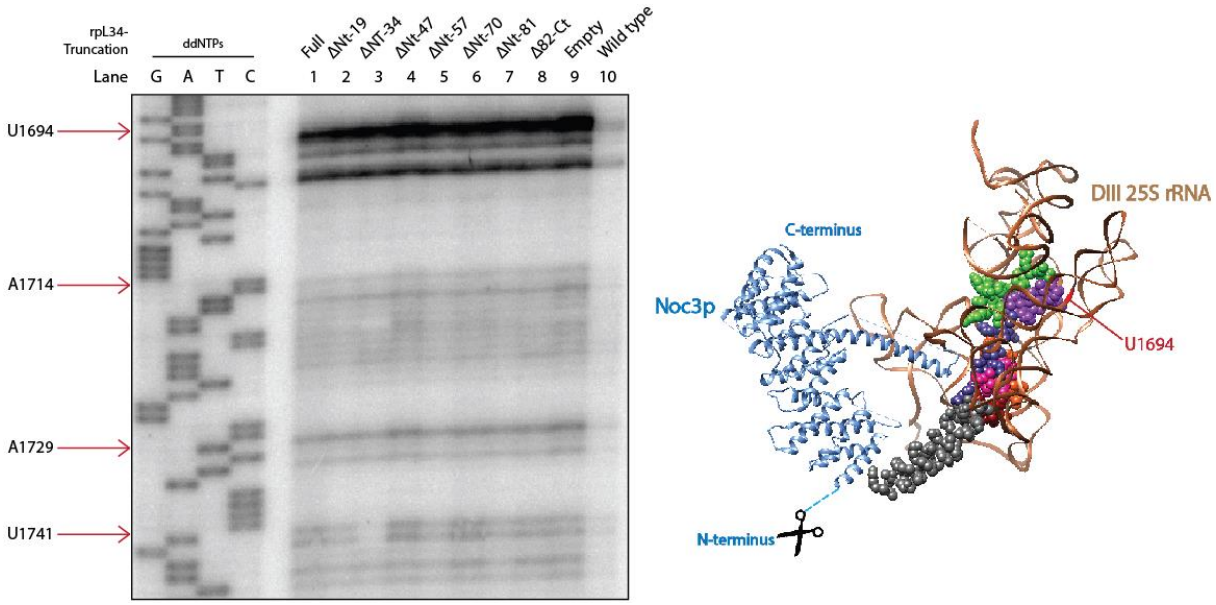

Figure 56: Characterization of the MNase-Noc3p induced cuts in 25 S rRNA domain III for rpL34 truncation variants analyzed by primer extension.

Exponentially growing yeast cells of Y4171 (6.1.1) transformed with the constructs encoding the *RPL34*-truncation variants (6.1.2) on galactose containing medium were shifted to glucose containing medium for 4 h to shut down expression of the respective r-protein. Affinity purification was performed from total cell extracts (6.2.7.2) using M2-Anti Flag affinity matrix (6.1.9). The purified fraction was treated with 8 mM calcium chloride for activation of MNase N-terminally fused to Noc3p and incubated for 15 min at 16 °C. Total RNA was isolated by phenol/chloroform extraction (6.2.4.1). Primer extension reactions (6.2.7.3) using radioactively labelled primers (6.2.4.6) that bind downstream of the indicated positions were performed with 250 ng of RNA derived from affinity purified fractions, respectively. Sequencing reactions were performed with the same set of radioactively labelled primers (6.2.7.4). The resulting cDNA of sequencing and primer extension reactions was size separated on sequencing gels (6.2.7.5) (left side). On the right side, rpL34 and Noc3p (blue) associated with the 25 S rRNA domain III (brown) of pre-ribosomes state E (PDB 6ELZ, modified with UCSF chimera (6.1.11) are shown. MNase fused to the N-terminus of Noc3p is indicated by scissors. The color code of rpL34 reflects the different truncations (compare Figure 51). The position of 25 S rRNA nucleotide 1694 is highlighted in red.

According to the observed cutting pattern in the northern analysis (Figure 55, A, lanes 17-24), a prominent primer extension stop at 25 S rRNA position 1694 was expectedly found (Figure 56, left side, lanes 1-9). Additional weaker signal intensities for bands corresponding to further MNase introduced cuts were detected through primer extension stops at 25 S rRNA nucleotides 1714, 1729 and 1741. These results indicated a significant structural rearrangement of LSU domain III for the rpL34 truncations, similar to the situation observed under depletion of rpL34 in previous experiments (see section 4.4). As indicated in the northern analysis (Figure 55, lane 36), no band corresponding to the cut at 25S rRNA nucleotide position 1694 could be observed by primer extension for the wild type strain (Figure 56, lane 10). Therefore, the putative misfolding of rRNA domain III might be due to an altered availability of rpL34 for this step, compared to the endogenously expressed rpL34 in the parental strain.

5 Discussion

5.1 The correct pre-ribosomal assembly state accounts for the timely controlled recruitment and release of Noc3p

Previous studies indicated that Noc3p is mainly associated with pre-ribosomes at intermediate maturation states containing 27SB- or 7S- pre-rRNA (Milkereit et al. 2001). Depletion of Noc3p impairs processing at the C_2 site, which blocks production of 25.5S and 7S pre-rRNA and, hence leads to accumulation of 27SB pre-rRNA (Figure 39, B). In this work, the requirements for the efficient recruitment and the release of Noc3p were further investigated.

5.1.1 Prerequisites for the recruitment of Noc3p to pre-LSU particles

Based on the results from section 4.3, an efficient recruitment of Noc3p to LSU-precursors seems to depend on the pre-ribosomal assembly state. As shown in Figure 43, depletion of several early acting rpLs (rpL3, rpL7, rpL8, rpL9 and rpL23) severely reduces the co-purification efficiency of 27S pre-rRNA species with Noc3p indicating its absence from these mis-assembled pre-ribosomal particles.

RpL3, the largest r-protein, is essential for very early steps of LSU biogenesis (Rosado et al. 2007b) and is mainly bound to 25S rRNA domain VI in mature ribosomes (Ben-Shem et al. 2011). The depletion of rpL3 causes a global instability of pre-ribosomes and decreases the abundancy of most rpLs as found in mass spectrometry analyses (Gamalinda et al. 2014). Notably, levels of r-proteins that affect the recruitment of Noc3p, as described above, are lowered as well when rpL3 is depleted.

In this work, hardly 27SB pre-rRNA has been co-purified with Noc3p upon depletion of rpL3. Notably, rpL3 depletion leads to a drastic decrease of $27SA_3$-, resulting from processing of $27SA_2$- pre-rRNA (Rosado et al. 2007b). This indicates that particles containing $27SA_2$ pre-rRNA are not accessible for the stable association of Noc3p (Figure 43, A lane 6).

Similar effects were observed for the depletion of rpL7 or rpL8, which are bound to domain II and I, respectively. As outlined in section 4.3, their depletion affects both processing of early 27S- pre-rRNA species and the correct assembly of the domains they are bound to. Consequently, Noc3p and other late acting biogenesis factors are diminished in these situations as well (Jakovljevic et al. 2012). In contrast, depletion of either rpL7 or rpL8 leads to increased levels of Noc1p in these mis-assembled pre-ribosomes (Jakovljevic et al. 2012; Ohmayer et al. 2015).

Interestingly, Noc1p forms a complex with Noc2p and Rrp5p (Hierlmeier et al. 2012) and its release is tightly linked to the removal of ITS1 sequences downstream of A_2 cleavage (Hierlmeier et al. 2012). In addition, the presence of Noc1p and Noc3p in pre-ribosomal particles is mutually exclusive (Milkereit

et al. 2001). Therefore, the proper establishment of domains I and II as well as the release of Noc1p might contribute to the recruitment of Noc3p.

In addition, rpL9 and rpL23 might further affect the recruitment of Noc3p (Figure 43, A). Both r-proteins are important for processing of 27SB pre-rRNA (Pöll et al. 2009) and their depletion produces similar phenotypes as observed for the depletion of middle acting r-proteins (Ohmayer et al. 2013). This is interesting insofar, as depletion of middle acting r-proteins causes not a recruitment- but a release defect of Noc3p (discussed below). Notably, most middle acting r-proteins are bound to LSU domain III, however, rpL9 and rpL23 are contacting domains IV, V and VI (Ben-Shem et al. 2011). Since Noc3p levels were observed to be strongly decreased in mis-assembled particles initiated upon depletion of the domain VI binders rpL9 or rpL23 (Doctoral Thesis Uli Ohmayer, 2014) it is likely that, besides the proper assembly of LSU domains I and II, a certain correct assembly state of domain VI needs to be established to enable association of Noc3p with these particles. Interestingly, recent cryo-EM analyses indicate that LSU domain VI and subsequently domain III get stably oriented with respect to the earlier stably incorporated domains I and II (Kater et al. 2017).

5.1.2 Prerequisites for the release of Noc3p from pre-LSUs

5.1.2.1 Assembly defects upon depletion of LSU r-proteins affect the release of Noc3p

As for recruitment, a certain assembly state seems necessary for the subsequent release of Noc3p from pre-ribosomal particles. As shown in Figure 43 depletion of r-proteins associated with domain III are required for intermediate LSU pre-rRNA processing events. In these strains, higher amounts of 27SB pre-rRNA, and particularly increased levels of 7S pre-rRNA, could be co-purified by Noc3p when compared to the wild type.

Since Noc3p is mainly associated with pre-LSUs that incorporate 27SB pre-rRNA, but not with particles containing 7S pre-rRNA, depletion of rpL27, rpL34 and rpL19 might exert a pronounced impact on the release of Noc3p as indicated by the increased levels of co-purified 7S pre-rRNA.

A similar release defect of Noc3p from mis-assembled pre-ribosomes at an intermediate maturation state has been previously observed in mass spectrometry analyses. In agreement with the findings in section 4.3, depletion of rpL19, rpL27 and rpL34 affected the release of Noc3p to a higher extent than depletion of rpL25 or rpL35 (Ohmayer et al. 2013, Doctoral Thesis Uli Ohmayer, 2014). The tight control of Noc3p recruitment by domain VI binders (rpL9 and rpL23) and of Noc3p release by domain III binders (rpL19, rpL25, rpL27, rpL34 and rpL35) might define the “time window” for the association of Noc3p with pre-ribosomal particles.

Depletion of late acting r-proteins, for instance rpL2 or rpL43, also caused a release defect of Noc3p (see 4.3/ discussed in 5.1.2.4). A similar effect has been indicated for depletion of even later acting r-

proteins as rpL21, rpL10, and rpL1 (Figure 43), even though the extent of Noc3p release was not as strong as indicated for earlier acting r-proteins.

Depletion of rpL5, a component of the 5S RNP at the CP might impair the release of Noc3p from its pre-ribosomal population as well (Figure 43). However, the CP is located atop of the LSU, far away of domain III. As discussed above for rpL9 and rpL23, r-proteins located far from Noc3p also affected the release of Noc3p from pre-ribosomes. It might be the case, that maturation of the CP "communicates" with parts of the pre-LSU, distributed over the whole particle by far-reaching interactions mediated through (r-) proteins and/or rRNA folding. Previous studies proposed a role for the CP as signal transducer between the functional centers of the large subunit through various physical connections (section 3.1.5). It is however unclear, whether the CP exerts a similar role as signal transducer during the LSU biogenesis process that coordinates assembly and folding events.

5.1.2.2 Conformational rearrangements produced during folding of domain III impede the release of Noc3p

As discussed above, the release of Noc3p from the large subunit interface is hypothesized to be at least partly controlled by local r-protein assembly events in LSU domain III. Therefore, influences of LSU domain III binding r-proteins on the pre-ribosomal assembly state has been further analyzed. Due to the facts, that (i) Noc3p co-assembles with the stable integration of these r-proteins in pre-LSUs, that (ii) the depletion of these r-proteins induces a release defect of Noc3p and that (iii) Noc3p co-purifies these mis-assembled pre-ribosomal intermediates at a high efficiency (Figure 43), provided a sound basis for tethered enzymatic structure probing assays using MNase (see section 3.7) fused to Noc3p. This allows the generation of a pre-rRNA accessibility map within the local three-dimensional environment of Noc3p in its pre-ribosomal context. Thereby, causes of the release defect could be structurally addressed.

Tethered MNase structure probing has been previously performed in mature LSU or SSU particles (Ohmayer et al. 2012) as well as in LSU precursors, which were obtained by affinity purifications of tagged biogenesis factors, for instance Noc3p (Pöll et al. 2017). In these studies, MNase was fused to r-proteins, which yielded a defined cutting pattern along the (pre-) rRNAs. In other studies, Noc3p has already been used as probe in the wildtype strain by fusion of the MNase to its C-terminus (Master Thesis Fabian Teubl, 2016). However, these analyses mostly yielded cuts in LSU domain IV. Recently published structures of pre-LSUs (Kater et al. 2017) revealed that Noc3p is located lengthwise on the subunit interface with its C-terminus oriented in opposite direction of LSU domain III (Figure 25). Based on these findings, MNase has been fused to the N-terminus of Noc3p in this study to probe the local 3D-pre-rRNA environment of Noc3p after *in vivo* depletion of certain LSU r-proteins

As indicated in Figure 45, tethered tertiary structure probing revealed very strong and highly specific cuts in LSU rRNA domain III of rpL27 and rpL34 depleted intermediate LSU precursors. Consistent with previous experiments, the presence of both proteins in pre-ribosomes is interdependent (Doctoral Thesis Uli Ohmayer, 2014). Notably, rpL27 and rpL34 interact with each other and form, together with rpL30, a protein cluster in LSU rRNA domain III (Ben-Shem et al. 2011). Additionally, the same severe release defect of Noc3p could be observed for both rpL27 and rpL34 (Figure 43). After *in vivo* depletion of the mentioned two r-proteins, the MNase sensitive sites were localized between helix 57 and helix 58 of 25S rRNA, whereof 25S rRNA nucleotide 1694 showed highest nuclease sensitivity.

Interestingly, this region is directly contracted by the N-terminal protrusion of rpL34 (Figure 47). To this reason, as will be discussed later, rpL34 truncations have been also analyzed to further shed light on these findings (see section 5.2).

Previous high resolution cryo-EM structures of pre-ribosomal large subunits that include Noc3p (Kater et al. 2017) revealed, that this position is usually buried by several LSU rRNA domain III elements, for instance helix 53 and 59.

This finding suggests that the conformational arrangement of LSU domain III has been substantially impaired upon depletion of both rpL27 or rpL34 to enable Noc3p-MNase induced cuts at the indicated positions. However, misfolding of LSU domain III could not be observed under depletion of rpL19 (Figure 47), even though its depletion induces a comparatively severe release defect of Noc3p when compared with rpL27 or rpL34 (Figure 43). In contrast to the latter two LSU r-proteins, rpL19 is located aside from them in domain III (Ben-Shem et al. 2011). Accordingly, a LSU domain III conformational rearrangement was neither observed for depletion of rpL25 nor for depletion of rpL35, whereas their impact on Noc3p release was weaker (Figure 43). As indicated by cryo-EM analyses, rpL25 seems to be stably assembled with pre-LSUs preceding to rpL27 (Kater et al. 2017; Sanghai et al. 2018b). Therefore, particles lacking rpL25 might have a different folding state than those lacking rpL27, which in turn does not allow cleavage at the indicated positions (Figure 47). These results suggest that the N-terminus of Noc3p, which has not been completely resolved in cryo-EM analyses (see 3.8) can orient towards the LSU rRNA domain III and the local folding state of this domain significantly depends on the assembly of rpL27 and rpL34.

It should however be kept in mind, that these structure probing assays have been performed *ex vivo*, as MNase is inactive *in vivo* in the model organism *Saccharomyces cerevisiae* (see 3.7). For reliable *in vivo* structure probing, a different experimental setup has to be developed that uses nucleases with an *in vivo* inducible activity. Alternatively, base modifying enzymes, for instance ADAR as previously used by the group of Dr. Rosbash could be considered (McMahon et al. 2016). The use of different agents for *in vivo* structure probing is as well generally suitable. However, structural local pre-rRNA re-arrangements might not be easily traceable if they do not involve changes in the base pairing or

accessibility to the solvent. Finally, applying imaging techniques as cryo-EM are challenging. On the one hand, high heterogeneity of the sample complicates the evaluation of a data set and impairs the generation of structures at high resolution. On the other hand, flexible parts within the structure are not resolved. Notably, even in the wild type situation, several MNase induced cuts could not be retraced in current structures (Figure 46).

5.1.2.3 The ITS2 remains unaffected in Noc3p release mutants and shapes with the proposed ring-pin model

Usually, Noc3p gets released from pre-ribosomes after processing at site C_2, which separates 25.5S pre-rRNA from 7S pre-rRNA (see section 4.3). As the indicated release defect of Noc3p is characterized by higher amounts of co-purified 27SB- and 7S- pre-rRNAs (Figure 43), an altered or disturbed 27SB processing within the ITS2 could not be excluded under depletion of middle- or late-acting r-proteins. Therefore, the orientation and structure of the ITS2 has been analyzed as well by Noc3p tethered MNase structure probing as discussed in section 5.1.2.2.

Moreover, as a side benefit of these analyses, the secondary structure of the ITS2 could be assigned to a distinct proposed model. The presence of different ITS2 secondary structures has been often controversially discussed throughout the literature. Several structure models have been proposed since now for the ITS2. The “ring” model (Figure 49, B) has been proposed according to phylogenetic analyses (Joseph et al. 1999). The “hairpin” model is largely based on enzymatic and chemical RNA structure probing. The “ring-pin” model is mostly based on phylogenetic data (Coleman 2015) and constitutes a hybrid of the ring and the hairpin model (Figure 49, C).

As indicated in Figure 49, the cutting pattern among the strains under depletion of different r-proteins rendered no differences when compare to the wild type. The observed conformational reorganization upon depletion of rpL27 or rpL34 seems to remain restricted to LSU domain III (discussed in 5.1.2.2), as no altered MNase activity in the ITS2 has been observed after their depletion compared to the wild type. The same accounts for rpL19, which has been described to impair the release of Noc3p to a similar extent compared to rpL27 and rpL34. Notably, recently published results have already demonstrated, that the absence of rpL19 does not affect the structure of the ITS2 (Biedka et al. 2018).

Regarding the structure predictions for the ITS2, a conformational switch has been proposed that might occur for the ITS2, based on combined results of enzymatic and chemical structure probing as well as of phylogenetic analysis. Indeed, an altered sensitivity to structure probing chemicals at the stem of the ITS2 has been previously deduced, which might be due to the association of the A_3-factors (Granneman et al. 2011; Dembowski et al. 2013b). However, a more recent study has not observed such a dramatic change in the ITS2 from 35S- to 27SB- pre-rRNA and a conformation that reflects the ring-pin structure (Burlacu et al. 2017). Regarding the results described for the wild type in Noc3p-

associated pre-LSUs in section 4.5 (Figure 49, lane 9), the position of the indicated cutting events match to the proposed ring-ping model of the ITS2. Indeed, several Noc3p-MNase induced cuts were found when mapped on the ring- or pin-model of the ITS2 to be located at positions which are in base pairing (Figure 49). As MNase has a strong preference of single stranded RNA (see 3.7), the Noc3p-MNase fusion would cleave most possible in the ring structure. Further defined cutting events at distinct positions within the ITS2 observed in Figure 49 are in agreement with previous studies which argue as well for the ring-pin model (Pöll et al. 2017). Moreover, cryo-EM on 7S pre-rRNA containing pre-60S particles has revealed the conformation of the terminal parts of the ITS2 to be as well oriented as indicated in the ring-pin model (Wu et al. 2016). Interestingly, MNase fusions to the C-terminus of Noc3p yielded no significant cutting events, which is probably due to the orientation of Noc3p within pre-LSUs (Figure 49, lane 10).

It should however be noted, that, in this study, the ITS2 secondary structure has been analyzed in intermediate, Noc3p-associated pre-ribosomes and can therefore not be applicated to all pre-LSU populations. Additionally, an ITS2 conformational switch at early stages within ribosome biogenesis as discussed above, cannot be confirmed nor excluded by these analyses.

5.1.2.4 Absence of late acting LSU r-proteins L2/L43 impede Noc3p release and are diminished from pre-LSUs upon depletion of Noc3p

As mentioned above (5.1.2.1), pre-ribosomal assembly defects upon depletion of rpL2 or rpL43 cause a release defect of Noc3p (see also section 4.3). The same has been observed in previous studies, where depletion of rpL2 or rpL43 lead to increased levels of Noc3p associated with pre-ribosomes (Ohmayer et al. 2013). RpL2 and rpL43 form a connecting hub between the LSU domain III and domains II, IV and V (Ben-Shem et al. 2011). Usually, stable assembly of rpL2 and rpL43 is tightly linked to the release of Noc3p (Doctoral Thesis Uli Ohmayer, 2014). Hence, rpL2/rpL43 and Noc3p are possibly not associated in the same pre-LSU population.

Previous cryo-EM analyses show that the binding site of Noc3p partially overlaps with those of rpL2 and rpL43 (Kater et al. 2017) which is shown in Figure 57 .

When comparing the structure of mature ribosomes (Ben-Shem et al. 2011) with the structure of pre-LSUs at state E (Kater et al. 2017), a clear overlap of the binding sites for rpL2/rpL43 and Noc3p can be observed (Figure 57). In fact, the long helical extension of Noc3p (Hn+9; for nomenclature on the helices see Figure 26) penetrates the rpL2/rpL43 dimer. Furthermore, large parts of rpL2 (green) collide with structure elements of Noc3p in its lower part (helices Hn+1-8), whereas a helical extension of rpL43 (rosy brown) penetrates helix Hn+3 of Noc3p. Therefore, it seems unlikely, that both Noc3p and rpL2/43 are present in the same pre-LSU particle.

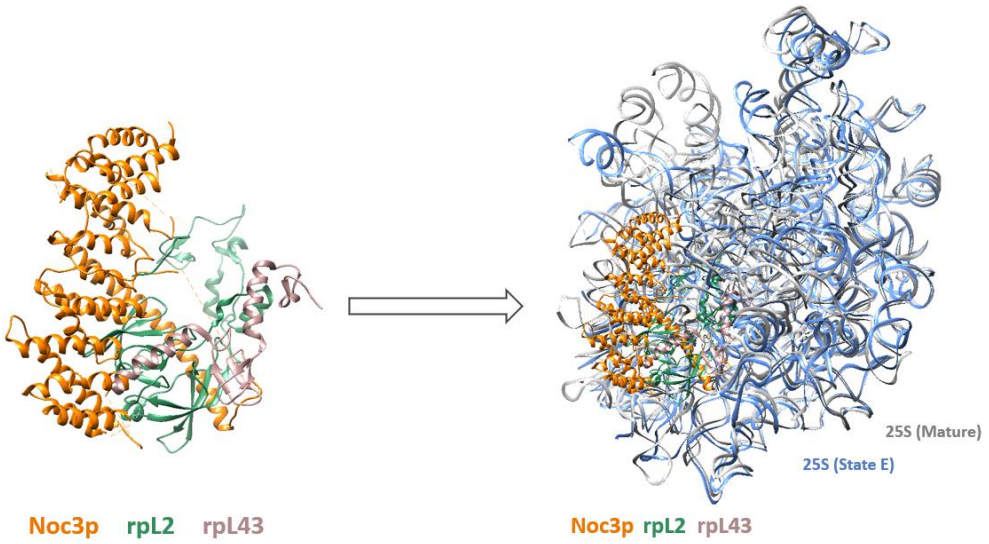

Figure 57: Overlay of the binding sites of Noc3p in pre-LSUs and rpL2/43 in mature LSUs.
The following illustrations were created using UCSF chimera (see 6.1.11). The 25S rRNA of pre-LSU state E (6ELZ) and mature LSU (4V88) were aligned. Note, that the 25S rRNA from state E (blue, right side) and mature large subunits (grey, right side) match largely well to each other. Left: Noc3p, highlighted in orange is shown isolated from its pre-ribosomal context of state E (PDB 6ELZ). RpL2 (sea green) and rpL43 (rosy brown) are shown isolated from its mature ribosomal context (PDB 4V88). The binding sites of Noc3p and the two r-proteins overlap with each other. Right: The same overlay of Noc3p, rpL2 and rpL43 (left side) is shown integrated into the 25S rRNA obtained from state E (blue, incorporating Noc3p) or mature subunits (grey, incorporating rpL2/43).

Depletion of Noc3p might, however, have an impact on the stable assembly of rpL2 and rpL43. To analyze this issue, mass spectrometry analyses of pre-LSU particles using Nog1p and Nop7 as bait proteins for affinity purification under Noc3p depleted conditions showed a strong decrease of rpL2 (unpublished, performed by Dr. Thomas Hierlmeier, see Figure 58). Although rpL43 was not detected by a significant amount of peptides in this study, published work suggests a similar effect for rpL43, since both proteins have a co-dependent assembly in the pre-ribosomes (Ohmayer et al. 2013). Altogether, it can be proposed, that the assembly of rpL2 and rpL43 required the presence of Noc3p in the pre-LSUs, which is concomitantly released.

Furthermore, the outcome of these analyses indicates highly reproducibly that Noc3p itself might be involved in the stable assembly of certain LSU domain III binding r-proteins. As shown in Figure 58, rpL25, rpL27, rpL34, rpL35 are slightly diminished from pre-ribosomes upon depletion of Noc3p, whereas rpL19 seems to be severely affected.

Interestingly, the B-type DNA polymerase Pol5p has been recently described to be also important for recruitment of these LSU domain III r-proteins (Braun et al. 2020). Furthermore, particles lacking Pol5p contain Noc3p and accumulate 27SB pre-rRNA (Braun et al. 2020). Possibly, Noc3p is involved in the recruitment of Pol5p.

Conversely, r-proteins which are already assembled in pre-ribosomes at this stage, for instance the domain I binders rpL8, rpL13 or rpL4 as well as the domain II binders rpL7, rpL32, rpL33 or rpL18 are not affected, as the correct assembly of these domains displays a prerequisite for the recruitment of

Noc3p. In addition, effects were seen on late assembling r-proteins, for instance on r-proteins rpL21, rpL10 and rpL1 (Figure 43). Coincidently with their impact on Noc3p release, rather mild downregulation of their presence in pre-ribosomes has been observed. It should however be kept in mind, that Noc3p depletion blocks the biogenesis of pre-ribosomes at a certain intermediate maturation state and that the indicated r-proteins are stably assembled at later stages.

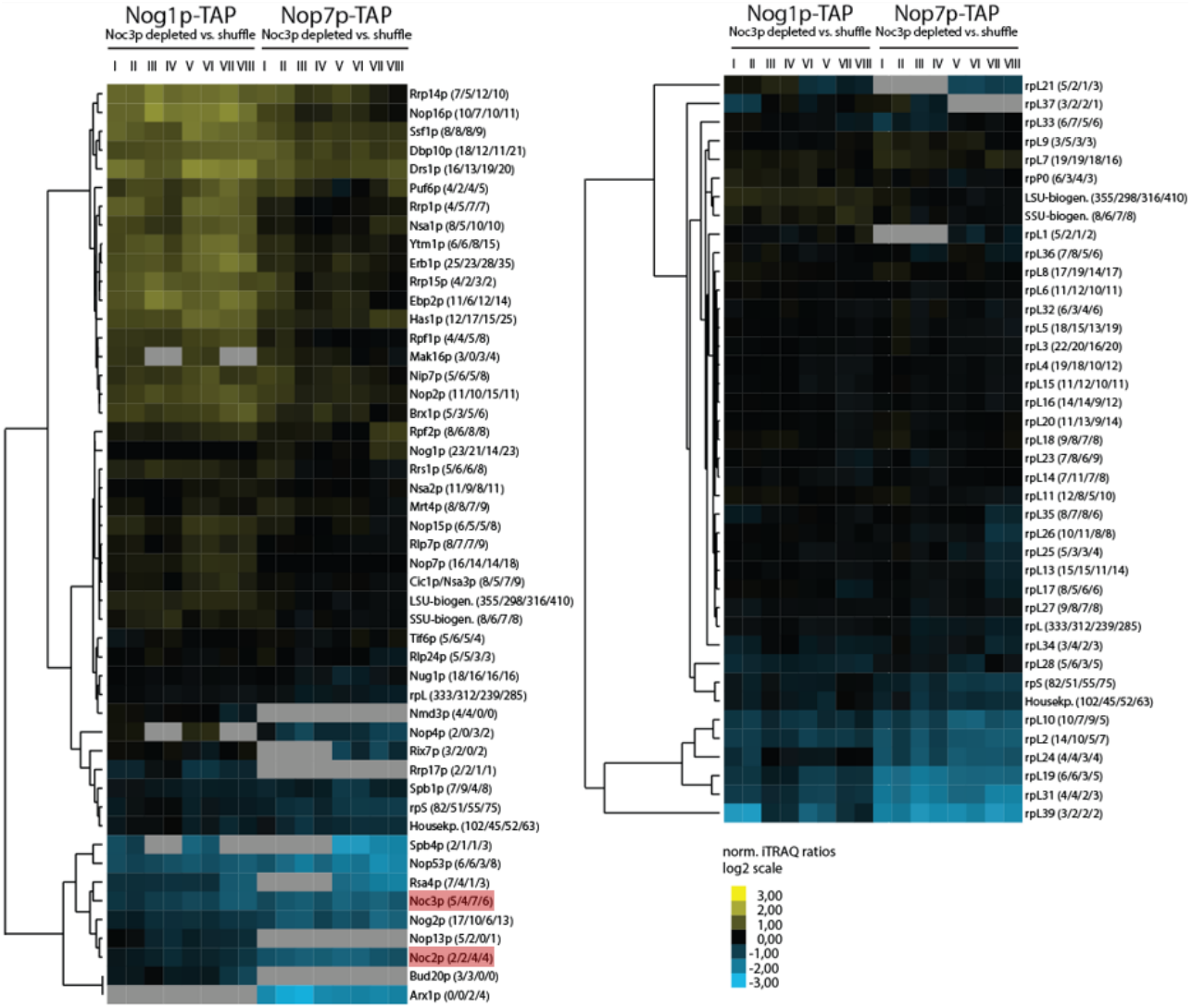

Figure 58: Mass spectrometry analyses of Nog1p- and Nop7p-associated pre-ribosomes under Noc3p depletion.
The experiments were performed, data sets were generated and generously provided by Dr. Thomas Hierlmeier (chair of biochemistry III, University of Regensburg, unpublished). Yeast strains depleted or not depleted of Noc3p which express chromosomally encoded protein A fusion proteins of Nog1p or Nop7p were grown for 16 h in rich medium to an OD_{600} ~0.5-0.8. Nog1p or Nop7p associated pre-ribosomal particles were affinity purified using IgG-Sepharose and subjected to comparative mass spectrometry analysis using iTRAQ reagents by LC-MS/MS. For proteins identified with at least one peptide with an ion score confidence interval of more than 95%, the iTRAQ-ratio was calculated to determine the relative abundance of the respective protein in the Noc3p-depleted fraction compared to the non-depleted fraction (shuffle strain). The results of eight experiments for each bait protein (Nog1p and Nop7p) were subjected to statistical analysis using clustering algorithms to determine groups of proteins specifically associated with Nog1p- or Nop7p-purified pre-ribosomes. Noc3p and its binding partner are highlighted via red boxes. Biogenesis factors are shown on the left, r-proteins on the right. For further details on the experimental procedures see for instance (Ohmayer et al. 2013).

The mass spectrometry analyses (Figure 58) furthermore show that downstream acting biogenesis factors, which are required for ITS2 processing subsequently after the C_2 cut and further maturation steps, such as Nop53, Arx1p or Rsa4p (section 3.5.2.2) are absent (also shown by Braun et al. 2020). This indicates an important role for the proper turnover of 27SB pre-rRNA incorporating, Noc3p-associated pre-ribosomes.

Altogether, the analyses on the pre-LSU assembly requirements for both recruitment and release of Noc3p (section 4.3) as well as structure probing studies (4.4) and the mass spectrometry of Noc3p depleted strains as shown above (Figure 58) allow to further classify the role of Noc3p in LSU biogenesis. Considering furthermore the results obtained by cryo-EM in section 4.1, the difference map of two volumes obtained through processing of distinct Noc3p-associated pre-ribosomal particle populations (Figure 33) clearly indicates, that Noc3p associates with pre-ribosomes that lack a stably assembled LSU domain III and leaves the particles upon correct DIII incorporation into the LSU.

For these findings, a kind of monitoring function could be attributed to Noc3p, and possibly to its interaction partner Noc2p and/or other factors close-by. The release of factors monitors the correct assembly and failed release causes accumulation of kinetically trapped particles, which will be degraded by the exosome (Allmang et al. 2000a). In this case, Noc3p is proposed to play such a role in the progression from 27SB- to 25.5S- and 7S- pre-rRNA containing pre-LSUs. Possibly, Noc3p senses the correct fold and assembly of certain regions within the pre-LSU at intermediate nuclear steps of LSU maturation, in this case probably local r-protein clusters. The model of sensing correct assembly checkpoints by specific biogenesis factors has been previously proposed for r-protein clusters of the small subunit (Linnemann et al. 2019).

5.2 N-terminal truncations of rpL34 have an impact on pre-rRNA processing, Noc3p release and the structural integrity of LSU domain III

The results shown in section 4.4 clearly demonstrate, that upon depletion of rpL34 and rpL27 a rRNA position in LSU domain III within the Noc3p-associated LSU pre-ribosome becomes accessible to MNase which is usually buried within the particle (also discussed in section 5.1.2.2). As this rRNA region is contacted by the N-terminal protrusion of rpL34, it was thus aimed to bring some light in the assembly of rpL34.

As indicated in Figure 53, even small N-terminal truncations affect the growth of the resulting mutant strains. The same phenomenon has been observed for the N- as the case may be for the C-terminal extension(s) of rpL7, rpL8 and rpL35 which were found to be essential for optimal growth (Tutuncuoglu et al. 2016). In contrast, the association with pre-ribosomes remains unaffected by these truncations Larger depletions are lethal (Figure 52) and impede the correct transition of 27SB- to 7S- and 25.5S-

pre-rRNA (Figure 53). However, 7S levels in the co-purified fraction of the variants with small N-terminal truncations seem to be slightly higher than observed for the wild type (Figure 53). This might be a cautious hint, that the N-terminal protrusion of rpL34 is not essential for proper 27SB- but for further pre-rRNA processing and maturation of the pre-LSU. A similar phenomenon has been observed for rpL8. Previous studies have revealed the N-terminal extension of rpL8 is important for intermediate to late pre-rRNA maturation steps, whereas the globular part of rpL8 acts much earlier in LSU biogenesis (Tutuncuoglu et al. 2016). The remaining truncations of rpL34 are characterized by a high accumulation of 27SB pre-rRNA, compared to the negative control, thus indicating, that the remaining parts of rpL34 cannot fulfil the correct function for C_2 processing. This finding is in agreement with previous studies on r-protein depleted strains (Pöll et al. 2009).

Regarding the release of Noc3p from pre-ribosomes that incorporate rpL34 truncation variants, large N-terminal truncations impede the release of Noc3p, whereas the severity of the release defect correlates with the increasing size of the truncation (Figure 55). Therefore, it might be that case, that in combination with the findings discussed above, the N-terminal part of rpL34 is neither essential for 27SB pre-rRNA processing nor for Noc3p release, nor are the respective truncations lethal. However, due to growth defects observed for ΔNt-19 and ΔNt-34 (see Figure 52 and Figure 54), these rpL34 variants might be assembled into pre-LSUs, but produce deficient ribosomes of less processivity compared to wild type ones.

Remarkably, in the wild type strain, in which rpL34 including its adjoining endogenous promoter have not been genomically deleted, higher amounts of 27SB pre-rRNA are co-purified by Noc3p (Figure 55, lane 30, quantification in C). Obviously, the altered expression pattern of rpL34 due to the RPS28-promoter reduces the pool of intermediate pre-LSUs containing 27SB pre-rRNA. Possibly due to this reason, the impact of each rpL34 truncation variant, including full length rpL34, on the conformation of LSU domain III is identical to the empty control (Figure 55). The MNase cutting patterns reflect the situation, what was observed in section 4.4, upon depletion of rpL34 (Figure 45, lane 13). Hence, a gradual effect on the integrity of LSU domain III in the presence of rpL34 truncations cannot be further elucidated.

Notably, previous studies on the effect of r-protein truncation uses as well plasmid-based expression systems, however bearing the endogenous promoter for each r-protein, respectively (Gamalinda and Woolford 2014; Tutuncuoglu et al. 2016).

5.3 Structural and functional characterization of Noc2p/Noc3p

5.3.1 Single molecule cryo-EM provides structural information on the C-terminus of Noc3p and suggests volume density for Noc2p

Based on the results described in section 4.1, additional volume density and hence structural information on the C-terminus of Noc3p could been obtained (Figure 32). The volume density fits to the NOC-motif, which is conserved among Noc1p, Noc3p and Noc4p, that has been structurally deciphered via cryo-EM analysis for Noc4p (Figure 26 and Figure 59). However, according to the structural comparison between Noc3p and Noc4p (Figure 26 and Figure 59), no insertion of protein sequences after helix Hn+15 and before the NOC-motif could be observed for Noc3p. In contrast, Noc4p presents a small helical element after helix H15 proceeding the NOC-motif. According to homology modelling, this insertion can as well be observed for Noc1p (see Figure 24).

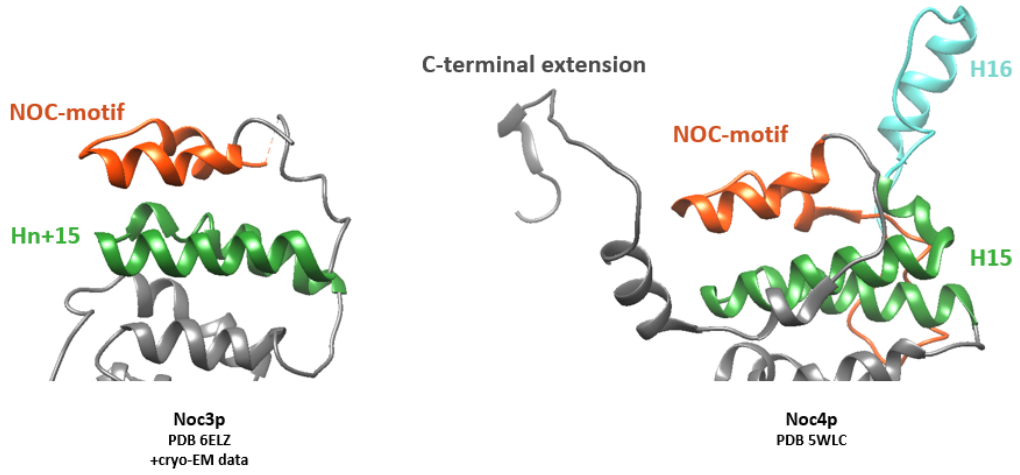

Figure 59: Structural comparison between the C-terminal parts of Noc3p and Noc4.
The following illustrations were created using UCSF chimera (see Software6.1.11). Solely the C-terminal part of Noc3p and Noc4p are shown (for whole protein representation see Figure 26). The amino acid chain of Noc3p´s C-terminus is fitted into the volume density obtained through single-molecule cryo-EM (4.1). The NOC-motif of both Noc3p and Noc4p according to Figure 24 are highlighted in orange. The helix Hn+15 of Noc3p and the corresponding helix H15 of Noc4p (see also Figure 24) are colored in green, the helix H16 of Noc4p in turquoise, the remaining parts of both proteins are dim gray.

The remaining 5 amino acid from the C-terminal part of Noc3p´s NOC-motif are missing, probably due to high conformational flexibility (Figure 59, left side, orange). Further structural information about the N-terminus of Noc3p was not possible to decipher. As indicated by published high-resolution structures (see Figure 25), 131 amino acids are missing, possibly due to high flexibilities within this region. The same accounts for structures within Noc3p, in particular small unstructured protein chains that are sitting in between the HEAT-repeats, thus connecting one among another (Figure 25).

In general, the obtained resolution (4.57Å, see section 4.1) does not allow to provide atomic resolution for identification of side chains of Noc3p. Moreover, this nominal resolution solely applies for the core of the particle and continuously decreases towards the periphery. Therefore, the resolution is worse than 4.57Å for Noc3p, which is located at the subunit interface than for proteins or rRNA elements that are centric within the pre-LSU.

Regarding Noc2p, whose position and orientation within the large subunit precursor has not been resolved yet, volume, which can be observed at the C-terminal part of Noc3p suggests a HEAT-repeat-like shape (Figure 32, green volume). This finding would be consistent with the cryo-EM reconstruction of Noc4p/Noc5p within the SSU-processome (PDB 5WLC), which indicates an interaction mediated via their C-termini (see also Figure 27). Moreover, the Noc4p/Noc5p dimer cannot be formed upon truncation of the NOC-motif of Noc4p (Kühn et al. 2009).

5.3.2 Structural important sites for the formation of the Noc2p/Noc3p heterodimer and the association with pre-ribosomes

According to studies on Noc4p (Kühn et al. 2009), the NOC-motif has been indicated as important for both the binding to its interaction partner Nop14/Noc5p as well as for the association with pre-ribosomes. However, rather large parts encompassing the NOC-motif as well as N- and C-terminal sequences have been deleted within Noc4p in the respective analyses (Kühn et al. 2009). Therefore, smaller truncations within the NOC-motif of Noc3p and the flanking N- and C-terminal areas have been generated in this work and analyzed under the same aspects.

As indicated in section 4.2.4, the NOC-motif has not been observed to be essential for association with Noc2p (Figure 41, B). However, it is important for the proper association with pre-ribosomes (Figure 41, A). The binding to Noc2p seems to rely in large parts on a disordered part within Noc3p, located between helix Hn+15 and the NOC-motif. Regarding Noc2p, domain 6 which is located close to its C-terminus has as well been observed to be essential for formation of the heterodimer (section 4.2.1, Figure 36).

These findings indicate that regions close to the C-terminus of both Noc2p and Noc3p are important for their association with each other, respectively. Regarding Noc4p and Nop14/Noc5p, a physical proximity between regions close-by to their C-termini could be revealed in cryo-EM studies (Barandun et al. 2017).

Sequence alignments between Noc1p/3p/4p (Figure 24) and Noc2p/5p (Figure 27), which show high similarities among the proteins, respectively, allow to transfer the situation of Noc4p/Noc5p to that of Noc2p/Noc3p. Moreover, the cryo-EM analyses in this work show a similar finding (section 4.1; discussed in section 5.3.1). Apart from that, attempts on generating strains that express Noc3p as C-terminal fusion to the TAP tag and additionally Noc2p as C-terminal fusion to MNase, failed (data not

shown). In contrast, fusion of MNase to the N-terminus of Noc2p was possible and the strains grew normal.

Having analyzed structural important sites for the binding between Noc2p and Noc3p, further focus was laid on Noc3p, and which parts of it might be essential for the proper assembly with pre-LSUs. As mentioned above, the NOC-motif seems to be important for this.
Additionally, the possible involvement of the loop (encompassing helix Hn+9), which reaches close to LSU domain III (Figure 38) has been analyzed in more detail (see section 4.2.3). The results indicate that the loop might be indeed important for association of Noc3p with pre-LSUs (Figure 39). Significantly lower amounts of 27SB pre-rRNA were co-purified by Noc3p implying loop substitutions of Noc1p and Noc4p as well as for full truncation of the helix. Interestingly, truncation of resulted in higher levels of co-purified 27SB pre-rRNA and 7S pre-rRNA thus indicating a release defect of Noc3p in this situation (Figure 39, C, lane 11).
Finally, the N-terminus of Noc3p, which is not resolved in current structures (Figure 25) has been truncated (Figure 40). As shown in Figure 41, neither any N-terminal truncation seems to be important for the recruitment of Noc3p, leaving the possible folding mutants ΔNt-180 and ΔNt-240 out of consideration. However, truncation within the unresolved part up to 131 amino acids from the N-terminus seem to affect the release of Noc3p.

It remains however unclear, whether and to which extent the binding to pre-LSUs containing 27SB pre-rRNA is mediated by Noc3p or by Noc2p, respectively. Earlier studies on conditional expression mutants of Noc2p and Noc3p implying genomically encoded TAP fusion proteins of Noc3p and Noc2p, respectively, indicated that the contact of Noc2p/Noc3p to pre-ribosomes is predominantly established by Noc3p and stabilized by Noc2p (Bachelor Thesis Fabian Teubl, 2013). Moreover, the findings suggested, that Noc2p potentially needs Noc3p to bind to pre-ribosomes incorporating 27SB pre-rRNA.
Regarding the situation for Noc4p/Noc5p, it was proposed that Noc4p can bind independently of Noc5p/Nop14 to pre-ribosomes which would suggest that the binding is as well predominantly established by Noc4p (Kühn et al. 2009). However, recent cryo-EM structures on the SSU-processome incorporating the Noc4p/Noc5p complex (Barandun et al. 2017) reveal, that Noc5p possesses a large N- and C-terminal extension, which is entangled within the pre-ribosomal particle (see also figure Figure 27). According to the alignment between Noc2p and Noc5p (Figure 27), Noc2p lacks the N-terminal extension but both contains a homologous C-terminal part which might be in close contact with pre-LSU elements.

It is furthermore unclear, whether Noc2p leaves the particle after association with Noc1p and re-enters the pre-LSU with Noc3p or if Noc2p stays constantly associated and solely Noc1p gets exchanged by Noc3p.

Low co-purification of 27SB pre-rRNA, but high levels of $27SA_2$ pre-rRNA upon depletion of Noc3p (Figure 41) might indicate that, in this situation, Noc2p co-purifies solely pre-ribosomes of an earlier maturation state. In fact, Noc2p co-purifies higher amounts of $27SA_2$ pre-rRNA under depletion of Noc3p than in the wild type situation (quantification not shown). Possibly, Noc2p cannot associate with pre-ribosomes containing 27SB pre-rRNA without the presence of Noc3p and stays therefore assembled in these earlier particles. Otherwise, Noc2p would be continuously associated with pre-LSUs, in which pre-rRNA processing from $27SA_2$ pre-rRNA further occurs, over several pre-rRNA intermediates (see 3.3.2), to 27SB pre-rRNA and Noc3p can associate. Moreover, Noc1p and Rrp5p, which build a stable complex with Noc2p, are also present in these early pre-ribosomes, containing $27SA_2$ pre-rRNA, and are released upon transition of $27SA_2$ to $27SA_3$ and subsequent removal of ITS1 sequences (Hierlmeier et al. 2012). Therefore, it seems more likely, that Noc2p leaves the pre-ribosomes together with Noc1p and Rrp5p and re-enters pre-LSUs at an intermediate maturation state with Noc3p.

Residual levels of co-purified 27SB pre-rRNA by Noc2p under depletion of Noc3p (Figure 41, A, lane 4) might indicate that Noc2p can associate with pre-ribosomes to a little extent, independently of the presence of its interacting partner Noc3p. On the other side, these low 27SB levels might as well come from residual wild-type Noc3p, still present in the cell after its depletion. Finally, depletion of Pol5p affects the composition of Noc2p-associated pre-ribosomes, but in contrast, the two proteins have not been found in one particle (Braun et al. 2020).

For the findings discussed in this chapter, it might be meaningful, that Noc2p leaves the pre-ribosome together with Noc1p and Rrp5p and re-enters particles upon interaction with Noc3p.

6 Material and Methods

6.1 Material

6.1.1 Yeast Strains

For each strain generated during this study, two biological replicates were generated and achieved in the yeast database, respectively. However, if two replicates were available only “clone1” was used for the respective analysis. “Clone2” serves as backup for false positive strains or for reproducing the obtained results.

Y	Name	Genotype	Origin
206	BY4741	his31, leu20, met150, ura30	Euroscarf Wt-Stamm
777	pGAL-NOC3	ade2-1, can1-100, his3-200, leu2-3,112, trp1-1, ura3-1, Ylr002c::HIS3	Noc3-shuffle derivate
927	pGAL-RPL10	his3-1, leu2-0, ura3-0, Y LR075w::kanMX4	From Y815 (Milkereit, Philipp)
928	pGAL-RPL23	his3-1, leu2-0, ura3-0, YBL087c::HIS3, YER117w::kanMX4	Of Y854 (Milkereit, Philipp)
930	pGAL-RPL34	his3-1, leu2-0, ura3-0, YIL052c::HIS3, YER056c-a::kanMX4	Of Y858 (Milkereit, Philipp)
931	pGAL-RPL16	his3-1, leu2-0, ura3-0, YNL069c::kanMX4, YIL133c::HIS3	From Y868 (Milkereit, Philipp)
933	pGAL-RPL1	his3-1, leu2-0, ura3-0, YGL135W::kanMX4, YPL220w::HIS3	From Y898 (Milkereit, Philipp)
965	pGAL-RPL2	his3-1, leu2-0, ura3-0, YIL018w::kanMX4, YFR031c-a::HIS3	From Y964 (Milkereit, Philipp)
966	pGAL-RPL3	his3-1, leu2-0, ura3-0, YOR063w::kanMX4	From Y901 (Milkereit, Philipp)
1026	pGAL-RPL25	his3-1, leu2-0, ura3-0, YOL127w::kanMX4	Y990 transformed with K865 (pGal-RPL25) (Milkereit, Philipp)
1082	pGal-RPL27	his3-1, leu2-0, ura3-0, YDR471w::HIS3MX6, YHR010w::kanMX4	Of Y1067 (Milkereit, Philipp)
1092	pGAL-RPL5	his3-1, leu2-0, ura3-0, YPL131w::kanMX4	Y861 transformed with K852, selected on FOA (Milkereit, Philipp)

Y	Name	Genotype	Origin
1094	pGAL-RPL35	his3-1, leu2-0, ura3-0, YDL191w::kanMX4, YDL136w::HIS3	Y1002 transformed with K857 (Milkereit, Philipp)
1097	pGAL-RPL8B	his3D1, leu2D0, met15D0/MET15, lys2D0/LYS2, ura3D0, YHL033c::HIS3MX6, YLL045c::kanMX4	Y1045 transformed with K882, selected on FOA (Milkereit, Philipp)
1099	pGAL-RPL19B	his3D1, leu2D0, MET15, ura3D0, LYS2, YBR084c-a::HIS3MX6, YBL027w::kanMX4	Y1050 transformed with K884, selected on FOA (Milkereit, Philipp)
1100	pGAL-RPL21A	his3D1, leu2D0, met15D0/MET15, ura3D0, lys2D0/LYS2, YBR191w::HIS3MX6, YPL079w::kanMX4	Y1054 transformed with K885, selected on FOA (Milkereit, Philipp)
1101	pGAL-RPL40A	his3D1, leu2D0, met15D0/MET15, ura3D0, YIL148w::HIS3MX6, YKR094c::kanMX4	Y1058 transformed with K887, selected on FOA (Milkereit, Philipp)
1102	pGAL-RPL32	his3-1, leu2-0, ura3-0, YBL092w::kanMX4	Y1085 transformed with K880, selected on FOA (Milkereit, Philipp)
1103	pGAL-RPL43A	his3D1, leu2D0, lys2D0, ura3D0, YJR094w-a::HIS3MX6, YPR043w::kanMX4	Y1089 transformed with K881, selected on FOA (Milkereit, Philipp)
1607	pGAL-RPL7 JW 8423	ura3-52, trp1-d101, lys2-801, his3-d200, leu2-d1, rpl7b::kanmx6, GAL-3HA-RPL7A (TRP1)	From Jelena Jakovljenic, Woolford lab
1640	Noc2-1 Rrp5HA Noc3-Myc	MAT alpha, ura3, his3, leu2, noc2-1, RRP5-HA3-hphNT1, NOC3-Myc9-natNT2	Y23, Rrp5 tagged with 3xHA (hph-NT1) (template pYM24, primer #287/#288), Noc3 tagged with 9xMyc (natNT2) (template pYm21, primer #1901/#1902) (Thomas Hierlmeier)
1656	Noc2 Shuffle Rrp5-HA3, Noc3-Myc9	ade2-1, can1-100, his3-200, leu2-3,112, trp1-1, ura3-1, 206w-::his3, Rrp5-HA3 (kanMX), Noc3-Myc9 (nat-NT2)	Strain Y19 (Y773), Rrp5 tagged with 3xHA (kanMX) (template pYM1 #36, primer #287/#288), Noc3 tagged with 9xMyc (natNT2) (template pYM21, primer #1901/#1902) (Thomas Hierlmeier)
2601	Noc3-TAP	his3-1, leu2-0, met15-0, ura3--0, NOC3::Noc3-TAP/klURA3	Y206 transformed with PCR (oligos 170/171) of pBS1539 (Milkereit Philipp)

Y	Name	Genotype	Origin
2852	BY4742 NOC3-TAP	his3-1, leu2-0, ura3-0, lys2-0, YLR002C-TAP, (Kl URA3)	Y92 transformed with PCR (oligos 3670/3671) of pBS1539, URA3 selected, western positive (Ohmayer, Uli)
2940	pGal-NOC3 NOC2-TAP	ade2-1, can1-100, his3-200, leu2-3,112, trp1-1, ura3-1, Ylr002c::HIS3, NOC2-TAP-kanMX	Y777 transformed with PCR (oligos 908/909) of pYM13 (K1890), TRP1 selected, western positive (Fabian Teubl)
3104	pGAL-RPL9A NOC3-TAP	his3-1, leu2-0, lys2-0/LYS2, ura3-0, met15-0/MET15, YNL067w::kanMX4, YGL147c::HIS3MX6, YLR002C-TAP, (Kl URA3)	Y1098 transformed with PCR (oligos 3670/3671) of pBS1539, URA3 selected, western positive (Ohmayer, Uli)
3333	pGAL-RPL23 Noc3-TAP	his3-1, leu2-0, ura3-0, YBL087c::HIS3, YER117w::kanMX4, NOC3::NOC3-TAP, (kl.URA3)	Y928 transformed with PCR (oligos 3670/3671) of pBS1539, URA3 selected, western positive (Fabian Teubl)
3335	pGAL-RPL25 Noc3-TAP	his3-1, leu2-0, ura3-0, YOL127w::kanMX4, NOC3::NOC3-TAP, (kl.URA3)	Y1026 transformed with PCR (oligos 3670/3671) of pBS1539, URA3 selected, western positive (Fabian Teubl)
3337	pGAL-RPL8B Noc3-TAP	his3D1, leu2D0, met15D0/MET15, lys2D0/LYS2, ura3D0, YHL033c::HIS3MX6, YLL045c::kanMX4, NOC3::NOC3-TAP, (kl.URA3)	Y1097 transformed with PCR (oligos 3670/3671) of pBS1539, URA3 selected, western positive (Fabian Teubl)
3339	pGAL-RPL16 Noc3-TAP	his3-1, leu2-0, ura3-0, YNL069c::kanMX4, YIL133c::HIS3, NOC3::NOC3-TAP, (kl.URA3)	Y931 transformed with PCR (oligos 3670/3671) of pBS1539, URA3 selected, western positive (Fabian Teubl)
3341	pGAL-RPL32 Noc3-TAP	his3-1, leu2-0, ura3-0, YBL092w::kanMX4, NOC3::NOC3-TAP, (kl.URA3)	Y1102 transformed with PCR (oligos 3670/3671) of pBS1539, URA3 selected, western positive (Fabian Teubl)
3343	pGAL-RPL34 Noc3-TAP	his3-1, leu2-0, ura3-0, YIL052c::HIS3, YER056c-a::kanMX4, NOC3::NOC3-TAP, (kl.URA3)	Y930 transformed with PCR (oligos 3670/3671) of pBS1539, URA3 selected, western positive (Fabian Teubl)
3419	pGal-RPL27 Noc3-TAP	his3-1, leu2-0, ura3-0, YDR471w::HIS3MX6, YHR010w::kanMX4, NOC3::NOC3_TAP, (klURA3)	Y1082 transformed with PCR (oligos 3670/3671) of pBS1539, URA3 selected, western positive (Fabian Teubl)

Y	Name	Genotype	Origin
3421	pGAL-RPL35 Noc3-TAP	his3-1, leu2-0, ura3-0, YDL191w::kanMX4, YDL136w::HIS3, NOC3::NOC3_TAP, (klURA3)	Y1094 transformed with PCR (oligos 3670/3671) of pBS1539, URA3 selected, western positive (Fabian Teubl)
3433	NOC3-MNase_FLAG	his3-1, leu2-0, ura3-0, lys2-0, NOC3::NOC3_MNase, (Kl URA3)	Y206 transformed with PCR (oligos 3670/3671) of K2372, URA3 selected, western positive (Fabian Teubl)
3449	NOC3-3xFLAG	his3-1, leu2-0, ura3-0, lys2-0, NOC3::NOC3_3xFLAG, (Kl URA3)	Y206 transformed with PCR (oligos 3670/3671) of K2373, URA3 selected, western positive (Fabian Teubl)
3781	pGAL-RPL2 Noc3-TAP	his3-1, leu2-0, ura3-0, YIL018w::kanMX4, YFR031c-a::HIS3, NOC3::NOC3-TAP (kl.URA3)	This study, Y965 transformed with PCR (oligos 3670/3671) of pBs1539, URA3 selected, western positive (Fabian Teubl)
3783	pGAL-RPL5 Noc3-TAP	his3-1, leu2-0, ura3-0, YPL131w::kanMX4, NOC3::NOC3-TAP (kl.URA3)	This study, Y1092 transformed with PCR (oligos 3670/3671) of pBs1539, URA3 selected, western positive (Fabian Teubl)
3785	pGAL-RPL43A Noc3-TAP	his3D1, leu2D0, lys2D0, ura3D0, YJR094w-a::HIS3MX6, YPR043w::kanMX4, NOC3::NOC3-TAP (kl.URA3)	This study, Y1103 transformed with PCR (oligos 3670/3671) of pBs1539, URA3 selected, western positive (Fabian Teubl)
3798	pGAL-RPL25 NOC3-MNase_3x-Flag	his3-1, leu2-0, ura3-0, YOL127w::kanMX4, NOC3::NOC3_MNAse (Kl URA3)	This study, Y1026 transformed with PCR (oligos 3670/3671) of K2372, URA3 selected, FLAG-western positive (Fabian Teubl)
3800	pGAL-RPL27A NOC3-MNase_3x-Flag	his3-1, leu2-0, ura3-0, YDR471w::HIS3MX6, YHR010w::kanMX4, NOC3::NOC3_MNAse (Kl URA3)	This study, Y1082 transformed with PCR (oligos 3670/3671) of K2372, URA3 selected, FLAG-western positive (Fabian Teubl)
3802	pGAL-RPL34 NOC3-MNase_3x-Flag	his3-1, leu2-0, ura3-0, YIL052c::HIS3, YER056c-a::kanMX4, NOC3::NOC3_MNAse (Kl URA3)	This study, Y930 transformed with PCR (oligos 3670/3671) of K2372, URA3 selected, FLAG-western positive (Fabian Teubl)
3804	pGAL-RPL35A NOC3-MNase_3x-Flag	his3-1, leu2-0, ura3-0, YDL191w::kanMX4, YDL136w::HIS3, NOC3::NOC3_MNAse (Kl URA3)	This study, Y1094 transformed with PCR (oligos 3670/3671) of K2372, URA3 selected, FLAG-western positive (Fabian Teubl)

Y	Name	Genotype	Origin
3806	pGAL-RPL2 NOC3-MNase_3x-Flag	his3-1, leu2-0, ura3-0, YIL018w::kanMX4, YFR031c-a::HIS3, NOC3::NOC3_MNAse (Kl URA3)	This study, Y965 transformed with PCR (oligos 3670/3671) of K2372, URA3 selected, FLAG-western positive (Fabian Teubl)
3808	pGAL-RPL5 NOC3-MNase_3x-Flag	his3-1, leu2-0, ura3-0, YPL131w::kanMX4, NOC3::NOC3_MNAse (Kl URA3)	This study, Y1092 transformed with PCR (oligos 3670/3671) of K2372, URA3 selected, FLAG-western positive (Fabian Teubl)
3810	pGAL-RPL43A NOC3-MNase_3x-Flag	his3D1, leu2D0, lys2D0, ura3D0, YJR094w-a::HIS3MX6, YPR043w::kanMX4, NOC3::NOC3_MNAse (Kl URA3)	This study, Y1103 transformed with PCR (oligos 3670/3671) of K2372, URA3 selected, FLAG-western positive (Fabian Teubl)
3982	pGAL-RPL7 NOC3-TAP	ura3-52, trp1-d101, lys2-801, his3-d200, leu2-d1, rpl7b::kanmx6, GAL-3HA-RPL7A (TRP1)	This study, Y1607 transformed with PCR (oligos 3670/3671) of pBs1539, URA3 selected, western positive (Fabian Teubl)
3984	pGAL-RPL21A NOC3-TAP	his3D1, leu2D0, met15D0/MET15, ura3D0, lys2D0/LYS2, YBR191w::HIS3MX6, YPL079w::kanMX4	This study, Y1100 transformed with PCR (oligos 3670/3671) of pBs1539, URA3 selected, western positive (Fabian Teubl)
4021	pGAL-RPL10 Noc3-TAP	his3-1, leu2-0 ura3-0, YBL087c::HIS3, YER117w::kanMX4, NOC3::NOC3-TAP (kl.URA3)	This study, Y927 transformed with PCR (oligos 3670/3671) of pBs1539, URA3 selected, western positive (Fabian Teubl)
4023	pGAL-RPL1 Noc3-TAP	his3-1, leu2-0, ura3-0, YBL087c::HIS3, YER117w::kanMX4, NOC3::NOC3-TAP (kl.URA3)	This study, Y933 transformed with PCR (oligos 3670/3671) of pBs1539, URA3 selected, western positive (Fabian Teubl)
4025	pGAL-RPL19B Noc3-TAP	his3-1, leu2-0, ura3-0, YBL087c::HIS3, YER117w::kanMX4, NOC3::NOC3-TAP (kl.URA3)	This study, Y1099 transformed with PCR (oligos 3670/3671) of pBs1539, URA3 selected, western positive (Fabian Teubl)
4027	pGAL-RPL40A Noc3-TAP	his3-1, leu2-0, ura3-0, YBL087c::HIS3, YER117w::kanMX4, NOC3::NOC3-TAP (kl.URA3)	This study, Y1101 transformed with PCR (oligos 3670/3671) of pBs1539, URA3 selected, western positive (Fabian Teubl)
4029	pGAL-RPL3 Noc3-TAP	his3-1, leu2-0, ura3-0, YBL087c::HIS3, YER117w::kanMX4, NOC3::NOC3-TAP (kl.URA3)	This study, Y966 transformed with PCR (oligos 3670/3671) of pBs1539, URA3 selected, western positive (Fabian Teubl)

Y	Name	Genotype	Origin
4167	pGal-rpL25 Noc3_Nt_MNase	his3-1, leu2-0, ura3-0, YOL127w::kanMX, YLR002C_Nt-MNase (HygR)	This study, Y1026 transformed with PCR (oligos 4317/4318) of K2515, URA3 selected, FLAG-western positive (Fabian Teubl)
4169	pGal-rpL27 Noc3_Nt_MNase	his3-1, leu2-0, ura3-0, YDR471w::HIS3MX6, YHR010w::kanMX4X, YLR002C_Nt-MNase (HygR)	This study, Y1082 transformed with PCR (oligos 4317/4318) of K2515, URA3 selected, FLAG-western positive (Fabian Teubl)
4171	pGal-rpL34 Noc3_Nt_MNase	his3-1, leu2-0, ura3-0, YIL052c::HIS3, YER056c-a::kanMX4, YLR002C_Nt-MNase (HygR)	This study, Y930 transformed with PCR (oligos 4317/4318) of K2515, URA3 selected, FLAG-western positive (Fabian Teubl)
4173	pGal-rpL35 Noc3_Nt_MNase	his3-1, leu2-0, ura3-0, YDL191w::kanMX4, YDL136w::HIS3, YLR002C_Nt-MNase (HygR)	This study, Y1094 transformed with PCR (oligos 4317/4318) of K2515, URA3 selected, FLAG-western positive (Fabian Teubl)
4175	pGal-rpL19B Noc3_Nt_MNase	his3D1, leu2D0, MET15, ura3D0, LYS2, YBR084c-a::HIS3MX6, YBL027w::kanMX4, YLR002C_Nt-MNase (HygR)	This study, Y1099 transformed with PCR (oligos 4317/4318) of K2515, URA3 selected, FLAG-western positive (Fabian Teubl)
4177	pGal-rpL2 Noc3_Nt_MNase	his3-1, leu2-0, ura3-0, YIL018w::kanMX4, YFR031c-a::HIS3, YLR002C_Nt-MNase (HygR)	This study, Y965 transformed with PCR (oligos 4317/4318) of K2515, URA3 selected, FLAG-western positive (Fabian Teubl)
4179	pGal-rpL5 Noc3_Nt_MNase	his3-1, leu2-0, ura3-0, YPL131w::kanMX4, YLR002C_Nt-MNase (HygR)	This study, Y1092 transformed with PCR (oligos 4317/4318) of K2515, URA3 selected, FLAG-western positive (Fabian Teubl)
4181	pGal-rpL43 Noc3_Nt_MNase	his3D1, leu2D0, lys2D0, ura3D0, YJR094w-a::HIS3MX6, YPR043w::kanMX4, YLR002C_Nt-MNase (HygR)	This study, Y1103 transformed with PCR (oligos 4317/4318) of K2515, URA3 selected, FLAG-western positive (Fabian Teubl)

Table 1: Yeast strains used in this study

6.1.2 Plasmids

Data base number	Name	Features	Origin
V17	pNOPPA1	For Nt-Prot A- fusion proteins under Nop1-promoter, no termination element	CEN6 ARSH4 ORI(E.Coli)

Data base number	Name	Features	Origin
V97	pBS1539	C-terminal integration cassette: TAP-Tag, URA3	ORI (E.Coli)
K520	YEplac195-RPS28prom	RPS28 Promoter for constitutive expression	Ori (E.Coli) 2u (yeast)
K792	YEplac195 pRPS28 FLAG modified	Constitutive pRPS28 promotor, N-terminal Flag-tag	Ori (E.Coli) 2u (yeast)
K944	YEp-pRPS28-FLAG-RPL34	rpL34B full length under pRPS28 control (constitutive expression), N-terminal Flag-tag, amplified via cDNA (no insert!), complements lethal phenotype	Ori (E.Coli) 2u (yeast)
K1019	pNOPPA-Noc2-FL	Constitutive expression of deletion constructs of Noc2 with Prot A-tag in yeast, Test for complementation and interaction	CEN6 ARSH4 ORI(E.Coli)
K1020	pNOPPA-Noc2-delta1	Constitutive expression of deletion constructs of Noc2 with Prot A-tag in yeast, domain 1 with AA 1-43 lacks	CEN6 ARSH4 ORI(E.Coli)
K1021	pNOPPA-Noc2-delta1,2	Constitutive expression of deletion constructs of Noc2 with Prot A-tag in yeast, domains 1+2 with AA1-115 lack	CEN6 ARSH4 ORI(E.Coli)
K1022	pNOPPA-Noc2-delta1-3	Constitutive expression of deletion constructs of Noc2 with Prot A-tag in yeast, domains 1-3 with AA 1-243 lack	CEN6 ARSH4 ORI(E.Coli)
K1023	pNOPPA-Noc2-delta 1-4	Constitutive expression of deletion constructs of Noc2 with Prot A-tag in yeast, domains 1-4 with AA 1-377 lack	CEN6 ARSH4 ORI(E.Coli)
K1024	pNOPPA-Noc2-delta6,7	Constitutive expression of deletion constructs of Noc2 with Prot A-tag in yeast, domains 6+7 with AA534-710 lack	CEN6 ARSH4 ORI(E.Coli)
K1025	pNOPPA-Noc2-delta5-7	Constitutive expression of deletion constructs of Noc2 with Prot A-tag in yeast, domains 5-7 with AA 378-710 lack	CEN6 ARSH4 ORI(E.Coli)
K1026	pNOPPA-Noc2-delta4-7	Constitutive expression of deletion constructs of Noc2 with Prot A-tag in yeast, domains 4-7 with AA 244-710 lack	CEN6 ARSH4 ORI(E.Coli)
K1027	pNOPPA-Noc2-delta2	Constitutive expression of deletion constructs of Noc2 with Prot A-tag in yeast, domain 2 with AA 44-115 lacks	CEN6 ARSH4 ORI(E.Coli)
K1135	pNOPPA-Noc2-delta3	Constitutive expression of deletion constructs of Noc2 with Prot A-tag in yeast, domain 3 with AA 116-243 lacks	CEN6 ARSH4 ORI(E.Coli)
K1136	pNOPPA-Noc2-delta4	Constitutive expression of deletion constructs of Noc2 with Prot A-tag in yeast, domain 4 with AA 244-377 lacks	CEN6 ARSH4 ORI(E.Coli)

Data base number	Name	Features	Origin
K1137	pNOPPA-Noc2-delta5	Constitutive expression of deletion constructs of Noc2 with Prot A-tag in yeast, domain 5 with AA 378-533 lacks	CEN6 ARSH4 ORI(E.Coli)
K1138	pNOPPA-Noc2-delta6	Constitutive expression of deletion constructs of Noc2 with Prot A-tag in yeast, domain 6 with AA 534-659 lacks	CEN6 ARSH4 ORI(E.Coli)
K1139	pNOPPA-Noc2-delta7	Constitutive expression of deletion constructs of Noc2 with Prot A-tag in yeast, domain 7 with AA 660-710 lacks	CEN6 ARSH4 ORI(E.Coli)
K2372	pBS1539-MNase-3xFLAG	C-terminal integration cassette: SNAP-Tag followed by 3x FLAG-Tag URA3; compatible with cellzome primers	ORI (E.Coli)
K2373	pBS1539-3xFLAG	C-terminal integration cassette: 3x FLAg-TAG URA3	ORI (E.Coli)
K2450	pRPS28_RPL8_Flag	Constitutive expression of rpL8, C-terminal Flag-tag	Ori (E.Coli) 2u (yeast)
K2453	pRPS28_Flag	No ORF, only Flag-tag	Ori (E.Coli) 2u (yeast)
K2515	Nt-TAG_pRPS28-3xFLAg-MNase	For genomic N-terminal integration; hygromycin cassette (Tef promotor + Hygromycin resistance + TCyc1 terminator), then pRPS28 – 3x-Flag – MNase – 2xHA linker	Ori (E.Coli) 2u (yeast)
K2709	pGEMT_Noc3p_deltaN 1-131	Noc3 with N-terminally truncated AA 1-131 in pGEMT	Ori (E.Coli)
K2710	pRPS28_Noc3p_deltaN 1-131_Ct-FLAG	Noc3 under control of pRPS28-promotor (constitutive expression), AA 1-131 lacking, C-terminal Flag-tag	Ori (E.Coli) 2u (yeast)
K2734	Noc3_Full	Noc3 Full length sequence in commercially available TOPO-Vector	Ori (E.Coli)
K2735	Noc3_Delta50	Noc3 with 50 AS deleted from N-terminus in commercially available TOPO-Vector	Ori (E.Coli)
K2736	Noc3_Delta100	Noc3 with 100 AS deleted from N-terminus in commercially available TOPO-Vector	Ori (E.Coli)
K2737	Noc3_Delta131	Noc3 with 131 AS deleted from N-terminus in commercially available TOPO-Vector	Ori (E.Coli)
K2738	Noc3_Delta180	Noc3 with 180 AS deleted from N-terminus in commercially available TOPO-Vector	Ori (E.Coli)
K2739	Noc3_Delta240	Noc3 with 240 AS deleted from N-terminus in commercially available TOPO-Vector	Ori (E.Coli)
K2740	Noc3_Delta305	Noc3 with 305 AS deleted from N-terminus in commercially available TOPO-Vector	Ori (E.Coli)

Data base number	Name	Features	Origin
K2741	pRPS28_Noc3_Full_Flag	Noc3 Full length sequence under control of pRPS28-promotor (constitutively expressed), C-terminal FLAG-Tag	Ori (E.Coli) 2u (yeast)
K2742	pRPS28_Noc3_Delta 50_Flag	Noc3 with 50 AA deleted from N-terminus under pRPS28-promotor (constitutively expressed), C-terminal FLAG-Tag	Ori (E.Coli) 2u (yeast)
K2743	pRPS28_Noc3_Delta 100_Flag	Noc3 with 100 AA deleted from N-terminus under pRPS28-promotor (constitutively expressed), C-terminal FLAG-Tag	Ori (E.Coli) 2u (yeast)
K2744	pRPS28_Noc3_Delta 131_Flag	Noc3 with 131 AA deleted from N-terminus under pRPS28-promotor (constitutively expressed), C-terminal FLAG-Tag	Ori (E.Coli) 2u (yeast)
K2745	pRPS28_Noc3_Delta 180_Flag	Noc3 with 180 AA deleted from N-terminus under pRPS28-promotor (constitutively expressed), C-terminal FLAG-Tag	Ori (E.Coli) 2u (yeast)
K2746	pRPS28_Noc3_Delta 240_Flag	Noc3 with 240 AA deleted from N-terminus under pRPS28-promotor (constitutively expressed), C-terminal FLAG-Tag	Ori (E.Coli) 2u (yeast)
K2747	pRPS28_Noc3_Delta 305_Flag	Noc3 with 305 AA deleted from N-terminus under pRPS28-promotor (constitutively expressed), C-terminal FLAG-Tag	Ori (E.Coli) 2u (yeast)
K2748	Noc3fragment_altered_ Codons	Eurofins gene fragment: Noc3 fragment ORF 1-1445, flanking T7 promotor (5´) and SP6 promotor (3´) for PCR amplification; additional 5´-KpnI	
K2749	pRPS28_Noc3_altered _Codons_Flag	Noc3 under control of pRPS28-promotor (constitutive expression). Bases 753 and 1350 in ORF modified for introducing BamHI- and XhoI-restriction sites, C-terminal Flag-tag	Ori (E.Coli) 2u (yeast)
K2761	pRPS28_RPL34B_Full _Flag	RPL34B Full length sequence under control of pRPS28-promotor (constitutively expressed), N-terminal FLAG-Tag	Ori (E.Coli) 2u (yeast)
K2762	pRPS28_RPL34B_d19 _Flag	RPL34B with deleted AS1- 19 from the N-terminus under control of pRPS28-promotor (constitutively expressed), N-terminal FLAG-Tag	Ori (E.Coli) 2u (yeast)
K2763	pRPS28_RPL34B_d34 _Flag	RPL34B with deleted AS1- 34 from the N-terminus under control of pRPS28-promotor (constitutively expressed), N-terminal FLAG-Tag	Ori (E.Coli) 2u (yeast)
K2764	pRPS28_RPL34B_d47 _Flag	RPL34B with deleted AS1- 47 from the N-terminus under control of pRPS28-promotor	Ori (E.Coli) 2u (yeast)

Data base number	Name	Features	Origin
		(constitutively expressed), N-terminal FLAG-Tag	
K2765	pRPS28_RPL34B_d57_Flag	RPL34B with deleted AS1- 57 from the N-terminus under control of pRPS28-promotor (constitutively expressed), N-terminal FLAG-Tag	Ori (E.Coli) 2u (yeast)
K2766	pRPS28_RPL34B_d70_Flag	RPL34B with deleted AS1- 70 from the N-terminus under control of pRPS28-promotor (constitutively expressed), N-terminal FLAG-Tag	Ori (E.Coli) 2u (yeast)
K2767	pRPS28_RPL34B_Full	RPL34B with full length sequence under control of pRPS28-promotor (constitutively expressed), NO Flag-Tag!	Ori (E.Coli) 2u (yeast)
K2768	pRPS28_RPL34B_d19	RPL34B with deleted AS1-19 from the N-terminus under control of pRPS28-promotor (constitutively expressed), NO Flag-Tag!	Ori (E.Coli) 2u (yeast)
K2769	pRPS28_RPL34B_d34	RPL34B with deleted AS1-34 from the N-terminus under control of pRPS28-promotor (constitutively expressed), NO Flag-Tag!	Ori (E.Coli) 2u (yeast)
K2770	pRPS28_RPL34B_d47	RPL34B with deleted AS1-47 from the N-terminus under control of pRPS28-promotor (constitutively expressed), NO Flag-Tag!	Ori (E.Coli) 2u (yeast)
K2771	pRPS28_RPL34B_d57	RPL34B with deleted AS1-57 from the N-terminus under control of pRPS28-promotor (constitutively expressed), NO Flag-Tag!	Ori (E.Coli) 2u (yeast)
K2772	pRPS28_RPL34B_d70	RPL34B with deleted AS1-70 from the N-terminus under control of pRPS28-promotor (constitutively expressed), NO Flag-Tag!	Ori (E.Coli) 2u (yeast)
K2773	pRPS28_RPL34B_d81	RPL34B with deleted AS1-81 from the N-terminus under control of pRPS28-promotor (constitutively expressed), NO Flag-Tag!	Ori (E.Coli) 2u (yeast)
K2775	pRPS28_RPL34B_NoCt	RPL34B with deleted AS82-Cterminus under control of pRPS28-promotor (constitutively expressed), NO Flag-Tag!	Ori (E.Coli) 2u (yeast)
K2776	Noc3_Noc1Loop	Eurofins complex gene synthesis: homologous sequences of Noc1 based on structure analysis of Noc3´s loop	Ori (E.Coli) 2u (yeast)
K2777	Noc3_Noc4Loop	Eurofins gene fragment: homologous sequences of Noc4 based on structure analysis of Noc3´s loop	Ori (E.Coli) 2u (yeast)
K2778	Noc3_ShortLoop	Eurofins complex gene synthesis, Based on structure analysis Noc3´s loop shortened by 2/3	Ori (E.Coli) 2u (yeast)

Data base number	Name	Features	Origin
K2779	Noc3_NoLoop_Linker	Eurofins gene fragment: Based on structure analysis Noc3´s loop deleted and replaced by a LGGGS linker sequence	Ori (E.Coli) 2u (yeast)
K2780	pRPS28_Noc3_Loop Noc1_Flag	Noc3 under control of pRPS28-promotor (constitutively expressed), C-terminal FLAG-Tag, Loop of Noc3 replaced by Sequences of Noc1p	Ori (E.Coli) 2u (yeast)
K2781	pRPS28_Noc3_Loop Noc4_Flag	Noc3 under control of pRPS28-promotor (constitutively expressed), C-terminal FLAG-Tag, Loop of Noc3 replaced by Sequences of Noc4p	Ori (E.Coli) 2u (yeast)
K2782	pRPS28_Noc3_Short Loop_Flag	Noc3 under control of pRPS28-promotor (constitutively expressed), C-terminal FLAG-Tag, Loop of Noc3 shortened by 2/3	Ori (E.Coli) 2u (yeast)
K2783	pRPS28_Noc3_NoLoop_Linker_Flag	Noc3 under control of pRPS28-promotor (constitutively expressed), C-terminal FLAG-Tag, Loop of Noc3 deleted and replaced by the linker sequence LGGGS	Ori (E.Coli) 2u (yeast)
K2841	pRPS28_RPL34B_d81_Flag	RPL34B with deleted AA1- 81 from the N-terminus under control of pRPS28-promotor (constitutively expressed), N-terminal FLAG-Tag	Ori (E.Coli) 2u (yeast)
K2842	pRPS28_RPL34B_NoCt_Flag	RPL34B with deleted AA82-Cterminus under control of pRPS28-promotor (constitutively expressed), N-terminal FLAG-Tag	Ori (E.Coli) 2u (yeast)
K2843	pRPS28_Noc3_d598_Flag	Noc3 truncated from AA598-Cterminus under control of pRPS28- romotor (constitutively expressed), C-terminal Flag-Tag	Ori (E.Coli) 2u (yeast)
K2844	pRPS28_Noc3_d633_Flag	Noc3 truncated from AA633-Cterminus under control of pRPS28- romotor (constitutively expressed), C-terminal Flag-Tag	Ori (E.Coli) 2u (yeast)
K2845	pRPS28_Noc3_d646_Flag	Noc3 truncated from AA646-Cterminus under control of pRPS28- romotor (constitutively expressed), C-terminal Flag-Tag	Ori (E.Coli) 2u (yeast)
K2846	pRPS28_Noc3_d658_Flag	Noc3 truncated from AA658-Cterminus under control of pRPS28- romotor (constitutively expressed), C-terminal Flag-Tag	Ori (E.Coli) 2u (yeast)

Table 2: Plasmids used in this study

6.1.3 Oligonucleotides

6.1.3.1 Primer for PCR amplification and sequencing

Oligo	Name	Sequence (5´ -> 3´)
	M13-21/M13	TGTAAAACGACGGCCAG
	M13-R/M13r	CAGGAAACAGCTATGAC
3670	NOC3-TAP_fw	AAAGCATTATTGTCCTGTAGTTACAAAGGGGCTACGCTCTCTATCATC TAGATCTAAAGAGTGTTCTAAATCCATGGAAAAGAGAAG
3671	NOC3-TAP_rev	ACTCGACACGGCAAAAATGATTGGCTAACGATAATCGTGGCTCTTTA TATACTTAATATATAGGATCTAGTACGACTCACTATAGGG
4259	K245*_remov_FLAG_fw	AGCTTTGACTGGGAAAACGAGCTCTTACTGCA
4260	K245*_remov_FLAG_rev	GTAAGAGCTCGTTTTCCCAGTCAA
4317	Noc3_NtermTag_Up	ACTTGGCATTTTATGTCTTCAATCATAAGAGTATAATTCCGGGATAAA AGCTGGAGATATCATAGTAATAGACATGGAGGCCCAGA
4318	Noc3_NtermTag-Do	GGATGAGCCTTTTGCGC
4478	NOC3_deltaN1-131_fw	AAAAAAGGTACCATGGAAAAAATTCTGCAACTAAAAGAA
4479	NOC3-FLAG_rev	ACTTAATGGTAAGGAACAACAA
4500	Noc3_Full_fw	AAAAAAGGTACCATGGCTAAGAGAAATAGATCTCA
4501	Noc3_Delta50_fw	AAAAAAGGTACCATGTGGGATGAAGAAGAACAGG
4502	Noc3_Delta100_fw	AAAAAAGGTACCATGGAAGACGAAGACTCTAATGAC
4503	Delta180_fw	AAAAAAGGTACCATGTTGGTCCCCGTGTTTAA
4504	Noc3_Delta240_fw	AAAAAAGGTACCATG GCTGCTCCTATACAGGTT
4505	Noc3_Delta305_fw	AAAAAAGGTACCATG GAAGAGGGCTCAATATCATTC
4559	BamHI, Volllänge RPL34	GATCGGATCCATGGCTCAACGTGTTACTTTCA
4560	BamHI, dann ATG, dann ab AS20 in RPL34	GATCGGATCCATGATCAAGGTTGTTAAGACCC
4561	BamHI, dann ATG, dann ab AS35 in RPL34	GATCGGATCCATGGTTAAGAAGTTGGCTACTAGAC
4562	BamHI, dann ATG, dann ab AS48 in RPL34	GATCGGATCCATGGGTAGCGCTCTACAAGGTATTTCCA
4563	BamHI, dann ATG, dann ab AS58 in RPL34	GATCGGATCCATGAGACCAAGACAATACGC
4564	BamHI, dann ATG, dann ab AS71 in RPL34	GATCGGATCCATGACTGTTTCCAGAGCTTAC
4565	BamHI, dann ATG, dann ab AS82 in RPL34	GATCGGATCCATGGCCAACTGTGTCAAG
4566	RPL34_Rev	GATCCTGCAGTTATTTCTTAGACTTCTTTTCAGACTTCTTAG
4698	RPL34_NoCt_Rev	GATCCTGCAGTTAACATCTGGAACCACCGTAAG
4699	Noc3_ALL_KpnI_fw	GATC GGTACC ATGGCTAAGAGAAATAGATCTCAA
4700	Noc3_ab_Y598_del_rev	GATC CTGCAG TCTATTCATTAATTTATCAATAAATTTAAGAATGG
4701	Noc3_ab_L633_del_rev	GATC CTGCAG GGTTGCTGCCTCTGG
4702	Noc3_ab_V646_del_rev	GATC CTGCAG AGGACAATAATGCTTTTCAAGAAG
4703	Noc3_ab_S658_del_rev	GATC CTGCAG TCTAGATGATAGAGAGCGTAGC

Table 3: Primer for PCR amplification and sequencing used in this study

6.1.3.2 Primer for primer extension analyses

Oligo	Name	Sequence (5´ -> 3´)
710	M1, Pos. +3144 25SrRNA	TGGAGCAAAGAAATCACCGC
1862	25S_r	GCGCTTGGTTGAATTTCTTC
1888	25S-DomII_rev	CTACTACCACCAAGATCTGCACTA
1892	25S-DomIV_rev	TGCCAAGCCCGTTCCCTTGGCTGT
1896	25S-DomVI_rev	ACAAATCAGACAACAAAGGCTTAA
3037	O3073 25S+1257	GCGGATTCCGACTTCCATGGC
3439	25S-1784-1803-Re	GGATTTTCACGGGCCGTCAC
3853	300bp 3´of 5´25S	CCACTTAGAGCTGCATTCCCA
3910	ITS2 nt223	TGAGGTCAAACTTTAAGAAC
4239	25SrRNA+2748	TTTCATGGTTTGTATTCACAC
4240	25SrRNA+1664	CGCCGACGTCTCCACATTCAG
4241	25SrRNA+2141	AATTAGACAGTCAGATTCCCC
4243	25SrRNA+1002	TCGCTTTACCTCATAAAACTG
4480	25S rRNA+2621	CCCAGCCAAACTCCCCACCTG
4567	25S rRNA+1923	GTAGTGAGGGCCTTGGTCAGA

Table 4: Primer for primer extension analyses used in this study

6.1.3.3 Probes for northern Blotting

Oligo	Name	Sequence (5´ -> 3´)
205	O2-18S	CATGGCTTAATCTTTGAGAC
207	o4-A2/A3	TGTTACCTCTGGGCCC
209	O6-5.8	TTTCGCTGCGTTCTTCATC
210	o7-E/C2	GGCCAGCAATTTCAAGTTA
212	o9-25S	CTCCGCTTATTGATATGC
1819	Ext_ITS1_2	GTAAAAGCTCTCATGCTCTTGCC
1862	25S_r	GCGCTTGGTTGAATTTCTTC
1888	25S-DomII_rev	CTACTACCACCAAGATCTGCACTA
1892	25S-DomIV_rev	TGCCAAGCCCGTTCCCTTGGCTGT
2474	5S-rDNA	TTAACTACAGTTGATCGG
3439	25S-1784-1803-Re	GGATTTTCACGGGCCGTCAC
4170	25S rRNA+2050	TCTACAACAAGGCACGCAAG
4171	25S rRNA+2140	GACAGTCAGATTCCCCTTGT

Table 5: Primer for northern Blotting used in this study

6.1.4 Antibodies (used for western blotting)

Antibody	Species	Dilution	Origin
α-Myc (9E10)	mouse	1:2000	E. Kremmer
α-Flag (3F10)	rat	1:1250	Sigma-Aldrich
α-Tubulin	rat	1:1000	Abcam
α-mouse IgG + (H+L) (peroxidase conjugated)	rabbit	1:5000	Jackson IR/Dianova
α-rat IgG (H+L) (peroxidase conjugated)	goat	1:5000	Jackson IR/Dianova
α-PAP (peroxidase anti-peroxidase)	rabbit	1:5000	Sigma-Aldrich

Table 6: Antibodies used in this study

6.1.5 Chemicals

Chemicals were purchased at the highest available purity from Sigma-Aldrich, Merck, Fluka, Roth or J.T.Baker, except agarose electrophoresis grade (Invitrogen), bromine phenol blue (Serva), Ficoll (Serva) G418/Geneticin (Gibco), 5-FOA (Toronto Research Chemicals), milk powder (Sukofin), Tris ultrapure (USB Corporation) and Tween 20 (Serva). Isotope labeled compounds were purchased from Hartmann Analytic (γ^{32}P-ATP). Ingredients for growth media were purchased from BD Biosciences (Bacto Agar, Bacto Peptone, Bacto Tryptone and Bacto Yeast Extract), Q-Biogene, Bio101, Inc. or Sunrise Science Products (Complete supplement mixtures (CSM), Yeast nitrogen base (YNB), amino acids, adenine) and Sigma-Aldrich (D(+)-glucose, D(+)-galactose, amino acids and uracil).

6.1.6 Media and buffers

If not stated otherwise, all media and solutions have been prepared in water which was purified with an Elga Purelab Ultra device to a resistivity of 18.2 MΩ-cm and total organic content of less than five parts per billion. The pH values were measured at room temperature.

Media	Composition
YPD (yeast extract, peptone, dextrose)	1% (w/v) yeast extract 2% (w/v) peptone 2% (w/v) glucose
YPDA (YPD plus adenine)	YPD + 100 mg/l adenine
YPG (yeast extract, peptone, galactose)	1% (w/v) yeast extract 2% (w/v) peptone 2% (w/v) galactose
YPGA (YPG plus adenine)	YPG + 100 mg/l adenine

Media	Composition
SCD (synthetic complex dextrose)	0.67% (w/v) YNB + nitrogen 0.0062% (w/v) CSM-his-leu-trp 2% (w/v) glucose + 20 mg/L L-histidine + 100 mg/L L-leucine + 50 mg/L L-tryptophan
SCD-URA (SCD minus uracil)	0.67% (w/v) YNB + nitrogen 0.0062% (w/v) CSM-his-leu-ura 2% (w/v) glucose + 20 mg/L L-histidine + 100 mg/L L-leucine
SCDA-URA (SCD minus uracil, plus adenine)	SCD-URA +100 mg/l adenine
SCD-LEU (SCD minus leucin)	0.67% (w/v) YNB + nitrogen 0.0062% (w/v) CSM-his-leu-ura 2% (w/v) glucose + 20 mg/L L-histidine + 100 mg/L L-uracil
SCD-LEU + FOA (SCD minus leucin, plus 5´-FOA)	SCD-LEU + 0.4 % (w/v) 5´-FOA
SCDA-LEU (SCD minus leucin, plus adenine)	SCD-LEU + 100 mg/l adenine
SCG (Synthetic complex galactose)	0.67% (w/v) YNB + nitrogen 0.0062% (w/v) CSM-his-leu-trp 2% (w/v) galactose + 20 mg/L L-histidine + 100 mg/L L-leucine + 50 mg/L L-tryptophan
SCG-URA (SCG minus uracil)	0.67% (w/v) YNB + nitrogen 0.0062% (w/v) CSM-his-leu-ura 2% (w/v) galactose + 20 mg/L L-histidine + 100 mg/L L-leucine
SCGA-URA (SCG minus uracil, plus adenine)	SCG-URA + 100 mg/l adenine
SCG-LEU (SCG minus leucin)	0.67% (w/v) YNB + nitrogen 0.0062% (w/v) CSM-his-leu-ura 2% (w/v) galactose + 20 mg/L L-histidine + 100 mg/L L-uracil
SCGA-LEU (SCG minus leucin, plus adenine)	SCG-LEU + 100 mg/l adenine

Media	Composition
LB (lysogeny broth)	1% (w/v) tryptone 0.5% (w/v) yeast extract 0.5 g/L NaCl
LB_{Amp}	LB + 100 µg/ml ampicillin
SOB (super optimal broth)	2 % (w/v) tryptone 0.5 % (w/v) yeast extract 0.5 g/l NaCl 0.19 g/l KCl 2.03 g/l $MgCl_2$ x 6xH_2O pH 7.0 using NaOH

Table 7: Media used in this study

All media were autoclaved for 20 minutes at 121 °C and subsequently stored at room temperature. For plates 2% (w/v) agar was added to the medium before autoclaving. Antibiotics were added as stock solutions (see 6.1.6) or added as powder to the autoclaved medium after cooling down to ~60 °C. Working concentrations were 100 µg/mL for ampicillin, 300 µg/ml for hygromycin B and 0.4 % (w/v) for 5´-FOA. The finished plates were stored at 4 °C. Plates supplemented with hygromycin B were stored at 4 °C in the dark.

Buffer	Ingredients	Concentration
10 x TBS (western blot)	Tris NaCl pH 7.4 with NaOH	1 M 9% (w/v)
1 x TBST (western blot)	Tris NaCl Tween20 pH 7.4 with NaOH	0.1 M 0.9% (w/v) 0.05% (v/v)
4 x lower Tris (SDS-PAGE)	Tris SDS pH 8.8 with HCl	1.5 M 0.4% (w/v)
4 x upper Tris (SDS-PAGE)	Tris SDS Bromphenol blue pH 6.8 with HCl	0.5 M 0.4% (w/v)
HU buffer	Tris pH 6.8 SDS EDTA pH 8.0 β-Mercaptoethanol Urea Bromphenol blue	0.2 M 5% (w/v) 1 mM 0.21 M 8 M

Buffer	Ingredients	Concentration
10 x electrophoresis buffer (SDS-PAGE)	Tris Glycine SDS	0.25 M 1.92 M 1% (w/v)
Transfer buffer (western blot)	Tris Glycine Methanol SDS	24 mM 192 mM 20% (v/v) 0.05 % (w/v)
Strip buffer (western blot)	SDS β-Mercaptoethanol Tris pH 6.7	2% (w/v) 100 mM 62.5 mM
Poinceau staining solution	Poinceau S HOAc	0.5% (w/v) 1% (v/v)
Coomassie staining solution	Coomassie Brilliant Blue R Methanol HOAc	0.1 (w/v) 0.2 45 % (v/v) 0.3 10 % (v/v)
10 x DNA loading buffer	Tris-HCl pH 8.0 EDTA pH 8.0 Glycerol Bromphenol blue	4 mM 0.4 mM 60% (v/v)
100 x Protease inhibitors (PIs)	Benzamidine PMSF Solvent: ethanol Storage temperature -20 °C	0.2 M 0.1 M
5 x TBE buffer	Tris Boric acid EDTA pH 8.0	445 mM 445 mM 10 mM
AE buffer	NaOAc pH 5.3 EDTA pH 8.0	50 mM 10 mM
RNA solubilization buffer (for agarose gel samples)	Formamide (deionized) Formaldehyde MOPS buffer Storage temperature -20 °C	50% (v/v) 8% (v/v) 1 x
RNA loading buffer (for agarose gel samples)	Glycerol EDTA Xylencyanol Bromphenol blue	50% (v/v) 10 mM
RNA solubilization buffer (for acryl amid gel samples)	Formamide (deionized) TBE Check pH, should be 7.0 Xylencyanol Bromphenol blue	80% (v/v) 0.1 x
2 x Primer extension (PEX) loading buffer	Formamide (deionized) EDTA pH 8.0, Bromphenol blue, Xylene cyanol	95 % (v/v) 20 mM

Buffer	Ingredients	Concentration
1 x PEX loading buffer	2 x PEX loading buffer Water	50 % (v/v) 50 % (v/v)
20 x taurine buffer	Tris Taurine EDTA	1.78 M 0.58 M 10 mM
20 x SSC	NaCl Tri-sodium-citrate dihydrate pH 7.0 with HCl	3 M 0.3 M
10 x MOPS buffer	Sodium acetate trihydrate MOPS EDTA pH 8.0 pH 7.0 with NaOH	20 mM 0.2 M 10 mM
RNA pre-hybridization buffer	Formamid SSC SDS Denhard´s solution	50% (v/v) 5 x 0.5% (w/v) 5 x
50 x Denhard´s solution	Ficoll (Typ 400) Polyvinylpyrrolidone (average MW: 40000 g/mol) BSA (Fraction V)	10 mg/l 10 mg/l 10 mg/l
Buffer A100/200 +	Tris-HCl pH 8.0 KCl $Mg(OAc)_2$ Protease inhibitors	20 mM 100/200 mM 5 mM 1x
Buffer AG 100 +	Tris-HCl pH 8.0 KCl $Mg(OAc)_2$ EGTA/KOH Protease inhibitors	20 mM 100 mM 5 mM 5 mM 1 x
Buffer A100/200 + +T/T	Tris-HCl pH 8.0 KCl Mg(OAc)2 Protease inhibitors Triton X-100 Tween 20	20 mM 100/200 mM 5 mM 1x 0.5% (v/v) 0.1% (v/v)
Buffer AG100 + +T/T	Tris-HCl pH 8.0 KCl Mg(OAc)2 EGTA/KOH Protease inhibitors Triton X-100 Tween 20	20 mM 100/200 mM 5 mM 5 mM 1x 0.5% (v/v) 0.1% (v/v)
Buffer AC	NH4OAc MgCl2 pH 7.4 with NaOAc	100 mM 0.1 mM

Buffer	Ingredients	Concentration
Bufer MB	Solvent: buffer A100+ Triton X-100 Tween 20	 0.5% (v/v) 0.1% (v/v)
Buffer AH	NH4	20 M
TELit	Lithium acetate Tris-HCl pH 8.0 EDTA pH 8.0 with HOAc	100 mM 10 mM 1 mM
LitSorb	Sorbitol Solvent: TELit Sterile filtration	1 M
LitPEG	Polyethylene glycol (PEG 3350), solvent: TELit Sterile filtration	40% (w/v)
Tfb-I	KAc $MnCl_2$ KCl Glycerol pH 5.8 with 0.2 M HOAc sterile filtration	30 mM 50 mM 100 mM 15 % (v/v)
Tfb-II	MOPS $CaCl_2$ KCl Glycerol pH 7.0 with 1M NaOH sterile filtration	10 mM 75 mM 10 mM 15 % (v/v)
Buffer TE	Tris-HCl pH 8.0 EDTA pH 8-0	10 mM 1 mM
Buffer IR	Tris-HCl pH 8.0 EDTA pH 8.0	50 mM 20 mM
Spheroblast buffer	Sorbitol EDTA pH 8.0	0.9 M 0.1 M
Pretreatment solution (denaturating protein extraction)	β-Mercaptoethanol NaOH	7.5% (v/v) 1.85 M
TCA	Trichlor acetic acid	55% (w/v)
Ampicillin stock solution	Ampicillin Storage temperature -20 °C	100 mg/ml
Kanamycin stock solution	Kanamycin Storage temperature -20 °C	50 mg/ml
Hygromycin B stock solution	Hygromycin B Storage temperature 4 °C	300 mg/ml
DTT stock solution	DTT (dithiothreitol) store at -20°C	1 M

Table 8: Buffers used in this study

6.1.7 Kits

Kit	Origin
Herculase II Fusion enzyme	Agilent
SuperScript III® Reverse transcriptase	Invitrogen
HiPure Plasmid Midiprep Kit	Invitrogen
Monarch PCR & DNA cleanup kit	NEB
peqGOLD Plasmid Miniprep Kit	Peqlab
Roche BM Chemiluminescence Western Blotting Substrate (POD)	Merck
Thermo Sequenase Cycle Sequencing Kit	Affimetrix
QIAEX II gel extraction Kit	Qiagen
QIAquick PCR Purification Kit	Qiagen

Table 9: Kits used in this study

6.1.8 Enzymes

Enzyme	Origin
Herculase II Fusion DNA Polymerase	Agilent
Proteinase K	Sigma Aldrich
Taq DNA Polymerase	New England Biolabs
Restriction Endonucleases	New England Biolabs
RNase A (20 mg/ml)	Invitrogen
RNasin® Plus RNase Inhibitor	Promega
Superscript III ® Reverse Transcriptase	Invitrogen
T4 DNA Ligase	New England Biolabs
T4 Polynucleotide Kinase	New England Biolabs
Thermo Sequenase DNA Polymerase	Thermo Fisher Scientific
Zymolyase T100	MP Biomedicals

Table 10: Enzymes used in this study

6.1.9 Consumables

Material	Origin
100 bp DNA ladder	New England Biolabs
1kb DNA ladder	New England Biolabs
6x DNA Loading Dye	New England Biolabs
96-well Plates	Sarstedt
Agarose Electrophoresis Grade	Invitrogen
Anti-FLAG M2 Affinity Gel	Sigma Aldrich
Blotting paper MN 827 B	Millipore
BSA Solution (10 mg/ml stock)	New England Biolabs

Material	Origin
BM Chemiluminescence Blotting Substrate (POD)	Merck
ColorPlus Prestained Protein Marker, Broad Range (7-175 kDa)	New England Biolabs
Color Prestained Protein Standard, Broad Range (11–245 kDa)	New England Bioloabs
Coomassie Brilliant Blue	Bio-Rad
dNTPs Mix (25 mM each)	Agilent Technologies
Extra Thick Blot Paper	Bio-Rad
Falcon Tubes (15/50 ml)	Sarstedt
Glass beads (Ø 0,75-1mm)	Roth
Glycogen (5 mg/ml)	Ambion
Filter Paper 3 mm	Whatman
Gel Slick^{TM} Solution	Lonza
Gene pulser cuvettes	Bio-Rad
Glass Beads (0.75-1 mm)	Roth
Glycogen (5 mg/ml)	Ambion
IgG Sepharose TM 6 Fast Flow	GE Healthcare
Inoculation Loops (1 µl)	Sarstedt
Low Binding Micro Tubes 1.5 ml	Sarstedt
Micro Bio-Spin 6 Columns	Bio-Rad
Membrane Immobilon-P OVDF 0,45 µm	Millipore
Membrane Positive TM	MPB Biomedicals
Milk powder	Sukofin
MobiCol microspin column	MoBiTec
NuPAGETM 4-12% Bis-Tris Gel	Invitrogen
Parafilm	Pechiney Plastic Packaging
Pipette Tips (10-1000 µl)	Sarstedt
Pipettes (2-50 ml)	Sarstedt
Poly-Prep Chromatography columns (10 ml)	Bio-Rad
Precision Wipes (11x21 cm)	Kimberly-Clark
Protein Assay ”Dye Reagent Concentrate”	Bio-Rad
Reaction tubes (1,5 ml/2,0 ml)	Sarstedt
Salmon Sperm DNA (10 mg/ml)	Invitrogen
SYBR Safe DNA Gel Stain	Invitrogen
Ultima Gold Liquid Scintillation Cocktail	Perkin Elmer
γ-[32P]-ATP	Hartmann Analytic

Table 11: Consumables used in this study

6.1.10 Equipment

Device	Manufacturer
1600TR Liquid Scintilation Analyzer	Packard
4800 Proteomics Analyzer MALDI-TOF/TOF	Applied Biosystems
-80 °C freezer (Ultra Low)	Sanyo
Avanti J-26 XP centrifuge	Beckman Coulter
Avanti J-26S XP Centrifuge	Beckman Coulter
BAS Cassette 2040	Fujifilm
BAS-III Imaging Plate (32P)	Fujifilm
C4i centrifuge	Jouan
Centrifuge 16R Megafuge refrigerated	Heraeus
Centrifuge T-324	Kontron Instruments
Biofuge fresco refrigerated tabletop centrifuge	Hereaus
Biofuge Pico tabletop centrifuge	Hereaus
Biofuge Primo	Heraeus
Centrifuge 5415	Eppendorf
Centrifuge 5425	Eppendorf
Contamination Monitor LB 147	Berthold Technologies
Digital-pH-Meter	Knick
Easypet 3	Eppendorf
Electrophoresis system model 45-2010-i	Peqlab Biotechnologie GmbH
Electrophoresis Power Supply-EPS 301	Ge Healthcare
Eppendorf Xplorer® multichannel pipette	Eppendorf
Eraser	Raytest
FLA-3000 phosphor imager	Fujifilm
Gel Documentation System	Intas
LAS-3000 chemiluminescence imager	Fujifilm
Gel Max transilluminator	Intas
Fluo-Link	Vilber Lourmat
Gene Power Supply GPS 200/400	Pharmacia
Hybridisation oven	Peqlab Biotechnologie GmbH
HB-100 Hybridizer Hybridization oven	UVP
Hybridisation tubes	Bachofer, Rettberg
IKA-Vibrax VXR	IKA
Incubators	Memmert
Incubators	Infors
Magnetic Stirrer + Heater MR Hei-Standarf	Heidolph
Megafuge 16R	Thermo Scientific
Microwave	
NanoDrop ND-1000 spectrophotometer	Peqlab Biotechnologie GmbH
PCR Sprint thermocycler	Hybaid
PCR Sprint Thermo	Electron Coorporation
Phosphoimager Screens	Fujifilm

Device	Manufacturer
Power Pac 3000 power supplies	Bio-Rad
Power Supply E443	Consort
Precellys Evolution with Cryolys	Bertin Instruments
Scale EW600-2M	Kern
Scale MC1	Sartorius
Special Accuracy Weighing Machine	Sartorius
Shake incubators Multitron/Minitron	Infors
Tabletop Centrifuge	Sarstedt
Thermomixer compact	Eppendorf
Thermomixer F.1.5	Eppendorf
Trans-Blot SD Semi-Dry Transfer Cell	Bio-Rad
Typhoon FLA-9500	GE Healthcare
Ultimate 3000 NanoHPLC	LC Packings (Dionex)
Vortex Mixer	Heidolph
Water System (ELGA)	Purelab

Table 12: Equipment used in this study

6.1.11 Software

Software	Producer
Acrobat Reader V11	Adobe
Adobe Illustrator CS3	Adobe
Citavi	Swiss Academic Software
Discovery Studio 4.0 Client	Accelrys
Image Reader LAS-3000 Control Software	Fujifilm
Intas GelDoc	Intas
Jalview	Free Software Foundation (FSF)
Microsoft Office 365	Microsoft
Multi Gauge V3.0	Fujifilm
NanoDrop ND-1000 Operating Software	Peqlab Biotechnologies GmbH
Photoshop CS3	Adobe
Putty	Simon Tatham
Relion-3.0	SciLifeLab
SnapGene® Viewer	GSL Biotech
Typhoon FLA 9500 Control Software	GE Healthcare
UCSF Chimera	RBVI
UCSF ChimeraX version 0.96	RBVI
VectorNTI	Invitrogen
WinSCP	Martin Prikyl
Xming	Colin Harrison

Table 13: Software used in this study

6.2 Methods

6.2.1 Work with Saccharomyces cerevisiae

6.2.1.1 Cultivation and harvest of yeast strains

Strains of yeast Saccharomyces cerevisiae were cultivated using standard microbiological methods (Amberg et al., 2005). Liquid strains were grown in the appropriate medium (see section 6.1.6) and incubated at 30 °C (24 °C for temperature sensitive strains), shaking, unless stated otherwise. The cell growth was monitored measuring the optical density at 600 nm (OD_{600}). Cells from liquid cultures were harvested at 6000 x rpm for 8 minutes at room temperature. Resulting pellets were dissolved in ice cold water, transferred in 50 ml falcon tubes and centrifuged at ~ 3500 rpm for 3 minutes at 4 °C. For the cultivation on solid agar plates containing the appropriate medium, single colonies or small aliquots of glycerol stocks or fluid cultures were streaked out using sterile disposable inoculation loops in order to obtain colonies derived from single yeast cells. Plates were incubated upside down at the appropriate temperatures for 1-5 days. Short or long-term storage of the yeast strains was accomplished by keeping the agar plates or fluid cultures in small culture tubes at 4 °C. For long term storage see section 6.2.1.8.

6.2.1.2 Preparation of competent yeast cells

50 mL of an exponentially growing yeast strain (OD_{600} ~0.5-0.8) were harvested by centrifugation for 5 min at 4000 rpm and RT. The cells were first washed with 25 mL H_2O, then with 5 mL LitSorb and subsequently resuspended in 360 µL LitSorb. 40 µL of Salmon sperm DNA, which was previously incubated for 10 min at 99 °C and immediately chilled on ice, were added to the cell suspension as carrier DNA. After mixing, 50 µL aliquots were transferred into 0.5 mL tubes and stored at -80 °C.

6.2.1.3 Transformation of competent yeast cells

An aliquot (50 µl) of the respective competent yeast strain was thawed on ice. The DNA to be transformed (100 ng for Plasmids, 5-10 µg of linear DNA for genomic integration) was added to the sample and mixed. After addition of 6 volumes of LitPEG, the suspension was mixed thoroughly and incubated for at least 30 min (30 min – 3 h) at RT. Subsequently, sterile DMSO (1/9 of the total volume) was added followed by an incubation for 15 min at 42 °C (heat shock). The suspension was centrifuged for 3 min at 2000 rpm and RT. If selection on antibiotic resistance was required, the cells were resuspended in 100 µl YPD(A) or YPG(A) and incubated at 30 °C (24 °C for temperature sensitive strains), shaking for 2-3 generation times to allow the expression of the marker before plating on the respective selection media (see 6.1.6). For selection for auxotrophic markers (e.g. *LEU2, URA3*), the cells were resuspended in 80 µL sterile H_2O, plated directly on SCD(A) or SCG(A) lacking the corresponding amino acid agar plates and stored at the appropriate temperature for 2-4 days. Since

selection for antibiotic resistances often results in a high number of transient transformants, single colonies were anew streaked out on fresh selection media to identify positive clones.

6.2.1.4 Generation of yeast strains expressing epitope tag fusion proteins

Yeast strains expressing endogenously encoded FLAG-tag or TAP-tag fusion proteins were constructed of PCR based tagging cassettes and homologous recombination as widely used and described (Knop et al., 1999; Puig et al., 2001). Different auxotrophy markers were encoded on the PCR fragment for a subsequent selection of the growing clones. The plasmids and oligonucleotides used are listed in sections 6.1.2 and 6.1.3 respectively. Resulting strains are listed in 6.1.1.

6.2.1.5 Purification of genomic DNA from yeast

Note: The following centrifugation steps were conducted at full speed in a table-top centrifuge and room temperature, if not stated otherwise.

A yeast culture was grown over night in 10 ml of its respective growth medium. Cells were harvested by centrifugation and resuspended in 500 µl H_2O. Cells were sedimented again and resuspended in 600 µl spheroblast buffer. 4 µl zymolyase T100 (2 % w/v in H_2O) was added and incubated for 30 min at 37 °C. The spheroblasts were sedimented in a tabletop centrifuge. The supernatant was discarded and the spheroblast pellet was resuspended in 500 µl buffer IR supplemented with 100 µl 10 % SDS (w/v) and vigorously mixed by vortexing. The sample was incubated for 15 min at 65 °C and subsequently cooled down for 2 min at room temperature. 170 µl of 5 M KOAc were added and the sample was kept on ice for 5 min. After centrifugation the supernatant was transferred into a new reaction tube and again centrifuged. The remaining supernatant was transferred into a new reaction tube and 500 µl isopropanol were added. Precipitation of nucleic acids was performed by incubating the sample for 5 min at room temperature. After centrifugation for 5 min, the supernatant was discarded and the pellet was washed with 300 µl 70 % EtOH. The sample was anew centrifuged and the supernatant was completely removed. The nucleic acid pellet was air-dried at room temperature to remove all remnants of ethanol. The pellet was dissolved in 100 µl buffer TE and dissolved for 30 min at 37 °C, shaking.

6.2.1.6 Growth kinetic analysis of yeast strains

Cultures of the yeast strains to be tested were grown to OD_{600} ~ 0.5 - 0.8. From these exponential growing cultures fresh cultures were inoculated to OD_{600} = 0.1 in the appropriate medium and growth was monitored at the desired temperature by measuring the OD_{600} mostly in 1 or 2 h intervals. Since the strains were always kept in the exponential growth phase (OD_{600} ~ 0.1-0.8) by dilution with the respective medium, the dilution factor had to be taken into consideration for the calculation of the growth kinetics.

For estimating generation times of different strains simultaneously, an automated procedure using small volumes of yeast cultures (Ohmayer et al., 2012) was applied. Therefore, the yeast strains of interest were grown overnight in the respective medium and then diluted to an OD_{600} of 0.08 in 0.2 ml of the respective fresh medium in a covered sterile 96 well plate. Cells were incubated at 30 °C in a TECAN infinite F500 reader with measurements taken in kinetic cycle mode (shaking for 30 seconds per cycle in orbital shaking mode with an amplitude of 5 mm, wait time of 30 sec and measurement of the OD_{612}; total cycle length: 15 min). Usually, growth was monitored over 96 cycles, from which generation times were estimated during logarithmic growth phase of the strains.

6.2.1.7 Spot test analysis of yeast strains

Overnight cultures of yeast strains to be tested were diluted in sterile H_2O to an OD_{600} of 0.1. 5 µl of this cell suspension and of serial 1:10, 1:100, 1:1000, 1:10000, 1:100000 dilutions were plated on the appropriate test plates (section 6.1.6). For easier handling an Eppendorf Xplorer® multichannel pipette was used which allowed to simultaneously work with up to eight strains.

6.2.1.8 Long term storage of yeast strains

2 mL of an overnight culture of the respective yeast strain which had to be stored were mixed with 1 mL sterile 50 % (v/v) glycerol and separated into two aliquots in order to additionally generate a biological replicate for storage. Glycerol stocks were stored at -80 °C.

6.2.2 Work with E. coli

6.2.2.1 Cultivation of bacterial strains

Liquid cultures were grown in LB medium supplemented with the required antibiotics at 37 °C, shaking. Cell growth was monitored (if necessary) by measuring the optical density at 600 nm (OD_{600}). For cultivation on solid agar plates containing LB medium and the required antibiotics, single colonies or small aliquots of fluid cultures were streaked out using sterile disposable inoculation loops, in order to obtain colonies arising from a single bacterial cell. Plates were incubated upside down at 37 °C for not longer than 1 day. Short-term storage of bacterial strains was accomplished by keeping the agar plates at 4 °C.

6.2.2.2 Preparation of chemical competent bacterial cells

The *E. coli* strain XL1-Blue was used as a host for amplification of plasmid DNA. In order to increase the efficiency of plasmid DNA uptake, competent cells for chemical transformation were prepared. An overnight culture was grown in 30 ml SOB at 37 °C, shaking. A new culture of 200 ml SOB medium was inoculated with the overnight culture at a starting OD_{600} of 0.1. Cells were grown at 37 °C to mid-log phase (OD_{600} ~ 0.4-0.6) and harvested in 50 ml falcon tubes by centrifugation at 4,500 rpm for 10 min

at 4 °C. The *E. coli* pellets were resuspended in 15 ml TfbI and incubated on ice for 20 min. The previous centrifugation step was repeated and the cell pellets were resuspended in 4 ml TfbII and incubated for another 20 min on ice. Finally, the chemical competent cell suspension was split in 50 µl aliquots and stored at -80 °C.

6.2.2.3 Transformation of chemical competent bacterial cells with DNA by heat shock

An aliquot of chemical competent bacterial cells (see above) was thawed on ice. DNA to be transformed (~ 10-200 ng of the respective plasmid or the whole ligation sample) was added. The sample was mixed and incubated for 5 min on ice. After a heat shock for 1 min at 42 °C the sample was immediately chilled on ice for another 2 min. Subsequently, 1 ml LB medium was added to the transformed cells and incubated for regeneration for 30 min at 37 °C, shaking. 100 µl of the cell suspension was directly plated on LB agar plates supplemented with the required antibiotics for selection and incubated overnight at 37 °C. The remaining cell suspension was centrifuged for 3 min at 5,000 rpm and RT. Approximately 800 µl of the supernatant was discarded. The cell pellet was resuspended in the remaining liquid, plated as described above and incubated overnight at 37 °C.

6.2.2.4 Preparation of electric competent bacterial cells

Cells of the *E. coli* strain XL1-Blue were grown as described in 6.2.2.1. The 200 ml SOB main culture was chilled on ice for 15 min and centrifuged for 10 min at 6,000 rpm and 4 °C. To reduce the ionic strength of the cell suspension, cells were washed three times with ice cold sterile H_2O and once with sterile 10 % (v/v) glycerol. The chemical competent cells were resuspended in sterile 10 % (v/v) glycerol, split to 50 µl aliquots and stored at -80 °C.

6.2.2.5 Transformation of electro-competent bacterial cells with DNA by electroporation

An aliquot (50 µL) of electro competent bacterial cells was thawed on ice. DNA to be transformed (~ 5 ng of the respective plasmid or 1-2 µL of a ligation sample) was added and the sample was mixed. After incubation on ice for 5 minutes, the suspension was transferred in a 0,2 cm electroporation cuvette. The transformation was accomplished using the MicroPulser electroporation apparatus, program EC2. Immediately after the pulse, the suspension was dissolved in 1 ml LB, transferred in a 1,5 ml reaction tube and incubated for 1 h of regeneration at 37 °C, shaking. Subsequently, the suspension was split to two 1,5 ml reaction tubes containing 100 µl and 900 µl of the original bacterial suspension, respectively. After centrifugation for 3 minutes at 5,000 rpm, the resulting pellets were dissolved in 80 µl H_2O and plated on solid agar plates containing LB medium supplemented by the required antibiotics. Plates were incubated, as described above, in 37 °C overnight.

6.2.2.6 Purification of plasmid-DNA from E.coli

3-5 ml fluid bacterial cultures were used for isolating plasmid-DNA using the peqGOLD Plasmid Miniprep Kit (Peqlab) according to the manufacturer´s instructions. Optionally, in order to obtain higher amounts of DNA, 50 ml of a fluid culture can be used in combination with the HiPure Plasmid Midiprep Kit of Invitrogen.

6.2.3 Work with DNA

6.2.3.1 Native agarose gel electrophoresis of DNA

Native agarose gel electrophoresis was used to separate DNA fragments. Depending on the fragment size, electrophoresis was performed with gels composed of 1, 1.5 or 2 % (w/v) of agarose, 0.5 x TBE buffer supplemented by 0.1 µg/ml ethidium bromide or the corresponding amount of SYBR safe stain. 0.5 x TBE was used as electrophoresis buffer and gels were run at 120-160 V. For the length determination of the DNA fragments, 0.5 µg of an appropriate DNA standard (1 kb ladder or 100 bp ladder) was used in a concentration of 50 µg/mL in 1 x DNA loading buffer. DNA fragments were visualized by exposing the gel to UV or blue light (245 nm for ethidium brome, 494 nm for SYBR safe).

6.2.3.2 Purification of DNA fragments from agarose gel

DNA fragments of interest were cut out from the agarose gel and eluted using the QIAEX II gel extraction kit (Qiagen), following the instructions provided by the manufacturer.

6.2.3.3 Polymerase chain reaction

The annealing temperatures for all primers used in PCR were estimated with the T_m calculator for oligos (https://www.promega.de/resources/tools/biomath/tm-calculator/), provided by Promega. DNA fragments were amplified using Herculase II fusion DNA polymerase (Agilent) in 50 µL reactions (50-100 ng template plasmid, 0.25 µM of reverse and forward primers, 0.2 mM each dNTP, 5 U Herculase II). Annealing temperatures and amplification times were individually adjusted according to the manufacturer´s manual. Annealing temperatures and amplification times were individually adjusted according to the manufacturer´s manual. 5 % of each PCR was analyzed by agarose gel electrophoresis and subsequently purified with the Qiaquick PCR purification kit (Qiagen) according to the manufacturer´s instructions or precipitated with ethanol for cloning or integration, respectively.

6.2.3.4 Ethanol precipitation of DNA

To precipitate DNA from PCR reactions, 1/10 volume of 10 M LiCl was added to the aqueous PCR product. For precipitation, 2.5 volumes of 100 % ethanol was added. The solution was stored at -20 °C for 30 minutes – 1 hour. DNA was pelleted by centrifugation at 13,000 rpm for 30 minutes – 1 hour at

4 °C. The supernatant was discarded and the resulting pellet was air dried and subsequently dissolved in 0,1 mM Tris/HCl pH 7.0 or H_2O.

6.2.3.5 DNA quantification using UV spectroscopy

The concentration of pure DNA samples was measured using UV spectroscopy at 260 nm (1 OD_{260} = 50 µg/mL) using a NanoDrop ND-1000 spectrophotometer. To determine the contamination with proteins, the absorbance at 280 nm was measured concomitantly. The ratio of =D_{260}/OD_{280} of pure DNA is between 1.8 and 2.0.

6.2.3.6 Digestion of DNA with restriction endonucleases

Defined amounts of DNA fragments were digested with one or more enzymes out of a variety of restriction endonucleases in order to check the presence and correct orientation of inserts or to prepare DNA fragments for cloning. Digestion of DNA was done according to the manufacturer´s instructions. After digestion, DNA fragments were separated on an appropriate agarose gel by electrophoresis and processed as described above.

6.2.3.7 Dephosphorylation of DNA fragments

In order to minimize re-ligation of the target plasmid (“backbone”), which would strongly interfere with efficient ligation of the desired insert DNA into the plasmid, the respective plasmid gets dephosphorylated right after restriction digest. Therefore, digested DNA is incubated in 1 x Antarctic Phosphatase buffer (NEB) with 5 U Antarctic Phosphatase at 37 °C for 1 h, followed by incubation for 5 minutes at 65 °C in order to inactivate the enzyme. The so dephosphorylated plasmid was directly used for further ligation assays.

6.2.3.8 DNA ligation

In order to clone DNA sequences into an appropriate vector, which can be transformed in bacterial cells, the quantity of the respective digested DNA fragments was measured by UV spectroscopy. For ligation, a fivefold molar excess of the DNA insert compared to the vector backbone was incubated in a 10 µl ligation reaction using 400 U T4 DNA ligase (NEB) for 30 minutes at room temperature or 16-20 h at 16 °C overnight. 1 or 10 µl of the ligation reaction was used to transform an aliquot (50 µl) of electro competent or chemical competent bacterial cells, respectively.

6.2.3.9 DNA sequencing and oligonucleotide synthesis

DNA sequencing was performed by the GENEART/Thermo Fischer company and the service of primer synthesis was provided by Eurofins MWG Operon. Obtained sequences were compared to desired sequences using the nucleotide blast tool of the National Center for Biotechnology Information (NCBI).

6.2.4 Work with RNA

6.2.4.1 RNA extraction

RNA extractions were essentially performed as described previously (Schmitt et al., 1990). Samples from which RNA should be extracted (cell pellets, aliquots of cell lysates, affinity purified material) were resuspended or diluted in 500 µL AE buffer and mixed with 500 µL phenol equilibrated in AE buffer and 50 µL 10 % (w/v) SDS. The samples were incubated in a thermomixer at 65 °C, shaking at 1,400 rpm for 7 min and afterwards chilled on ice for ~ 2 min. After centrifugation for 2 min at 13,000 rpm and RT, 3 x 150 µL of the upper, aqueous phase was collected, transferred to 500 µL phenol equilibrated in AE buffer and mixed by vortexing. The samples were again centrifuged for 2 min at 13,000 rpm and RT. 3 x 130 µL of the upper aqueous supernatant were transferred to 500 µL chloroform and mixed by vortexing. The phases were separated by centrifugation for 2 min at 13,000 rpm and RT. 3 x 100 µL were collected in a new 1,5 ml reaction tube and precipitated by addition of 750 µL NaOAc-EtOH mix (composed of 1 volume 3 M NaOAc pH 5.3 and 25 volumes of ethanol). For RNA obtained from affinity purifications 2 µl glycogen (5 mg/ml) were additionally added. The mixture was incubated for at least 30 min at -20 °C. The precipitated RNA was dissolved by pipetting and vortexing in 30 – 60 µl autoclaved milli-Q water and subsequently stored at -20 °C. Prior to use, aliquots of RNA were denatured by incubation for 15 min at 65 °C using the respective buffer for the agarose- or acrylamide/urea- gel system, respectively.

6.2.4.2 Denaturing agarose gel electrophoresis for high molecular weight RNA

Denaturing agarose gel electrophoresis was used to separate RNA species longer than 1,000 bases (18S, 25S and their respective precursors). In this work, electrophoresis was performed with gels composed of 1.2 % (w/v) agarose, 2 % (v/v) formaldehyde and 1 x MOPS buffer (section 6.1.6) containing 0.5 µg/mL ethidium bromide. The electrophoresis buffer was composed of 1 x MOPS buffer and 2% (v/v) formaldehyde. Gels were run for 16 h at 35 V.

6.2.4.3 Denaturing acryl amide gel electrophoresis for low weight molecular RNA

Denaturating acryl amide gel electrophoresis was used to separate RNA species lower than 1,000 bases (5S, 5,8S and their respective precursors). In this work, electrophoresis was routinely performed with gels composed of 6 % (w/v) arcyl amide (acryl amide: bis-acryl amide 37.5:1), 7 M urea and 0.5 x TBE. The electrophoresis buffer was 0.5 x TBE (section 6.1.6). Gels were run for 75-100 min at 150 V.

6.2.4.4 Northern blotting (passive capillary transfer)

Passive capillary transfer was performed for agarose gels. Prior to transfer, the gel was washed once for 5 min in 1 l milli-Q water, once for 20 min in 10 x SSC supplemented with 0,05 M NaOH to partially hydrolyze RNA and twice for 20 min in 10 x SSC, respectively. The positively charged membrane

(Positive™ MPBiomedicals) was equilibrated for 5 min in milli-Q water and at least 5 min in 10 x SSC. Transfer of RNA from the agarose gel onto the membrane was achieved for 6 hours by constant buffer flow from a reservoir through the gel into a stack of pumping paper. Thereby, the RNAs were eluted from the gel and deposited onto the membrane by aid of the buffer stream. After drawing the membrane at room temperature, RNAs were crosslinked by applying 300 mJ of UV light at 254 nm in the Fluo Linker (Vilber Lourmat).

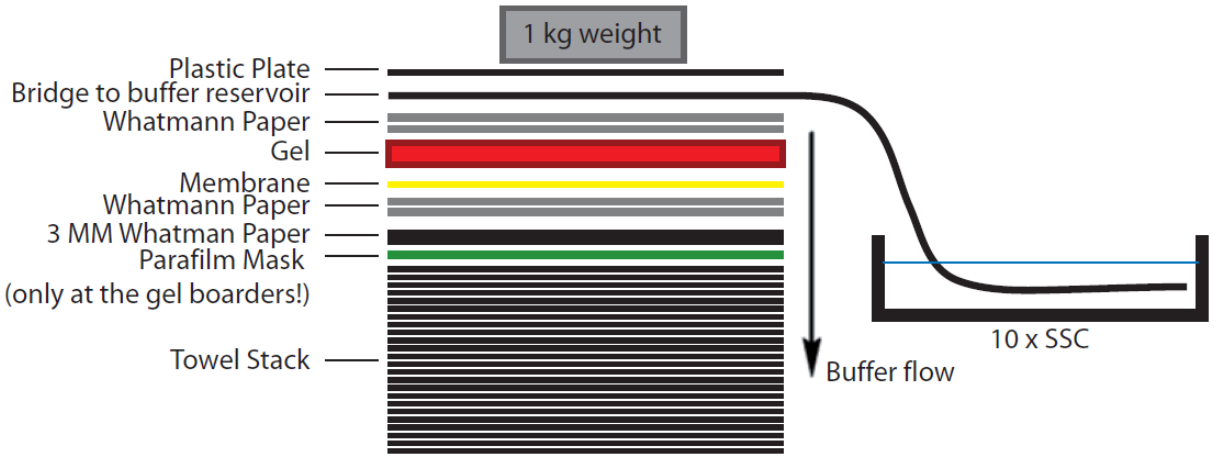

Figure 60: Set-up for capillary transfer of RNA.
In order to obtain a constant buffer flow, a whatman paper reaches from the 10 x SSC buffer reservoir to the top of the gel, separated by two additional whatman papers. On top, a plastic plate and a 1 kg weight provide pressure which guarantees a tight contact between all parts of the blot set-up, thereby preventing the formation of air inclusions. The gel is laid onto the positively charged membrane, followed by two whatman papers and a thick 3 MM whatman paper. The lower part of the set-up consists of a large towel stack which serves as reservoir for the buffer flowing through the gel. Moreover, the storage capacity of the towels results in a constant buffer flow over the whole duration of the experiment. Right on top of the towel stack a frame consisting of one layer of parafilm which is laid at each border of the gel, which inhibits the formation of water bridges and uncontrolled buffer flow past the gel.

6.2.4.5 Northern blot (electro transfer)

RNAs separated by acryl amid gel electrophoresis (section 6.2.4.3) were transferred on positively charged membranes (Positive™ MP Biomedicals) by electro transfer. The transfer was accomplished using 0,5 x TBE (section 6.1.6) as transfer buffer and a wet blotting apparatus (Bio-Rad), applying a voltage of 50 V for 60-90 min. Subsequently, the RNAs were crosslinked to the membrane (after drying at RT) by applying 300 mJ UV light (254 nm) using the Fluo Linker (Vilber Lourmat).

6.2.4.6 Radioactive probe labelling and detection

Different RNA species immobilized on positively charged membranes can be detected using specific DNA probes. Probes used in this work are listed in section 6.1.3.3. The 5´-end of each probe was radioactively labelled with ɣ-P^{32}ATP. 50 pmol of the oligo-probe was incubated with 50 µCi of ɣ-P^{32}ATP (Hartmann Analytik) in 1 x PNK buffer (NEB) and 10 U of T4 Polynucleotide Kinase in a total volume of 15 µL for 45 min at 37 °C. The reaction was stopped by addition of 1 µL 0,5 M EDTA pH 8.0. After

addition of 50 µl H_2O, the labelled probes were separated from non-incorporated ɣ-P^{32}ATP free nucleotides using a size exclusion column (Spin6-Biorad). Incorporated radioactivity was measured by analyzing 1 µl of the particular probe using a scintillation counter (1600TR-Packard). The membranes carrying the respective RNAs were pre-hybridized for at least 3 h at 30 °C on a turning wheel with 15 ml pre-hybridization buffer (section 6.1.6). Prior to the pre-hybridization, blots were damped with 25 ml 6 x SSC in order to prevent soaking of the pre-hybridization buffer. This step allows the use of lower amounts of buffer, resulting in a higher concentration of the respective radioactive labelled probe. Subsequently 1.5 - 3 x 10^7 cpm (depending on the amount of radioactive incorporated ɣ-P^{32}ATP and the half live status of the isotope) of the radioactive labelled probe were added to each blot followed by an incubation for at least 3 h or overnight at 30 °C on a turning wheel. The membranes were pre-washed with 25 ml 2 x SSC followed by a wash step with 25 ml 2 x SSC and 1 x SSC for 15 min, 30 °C on a turning wheel, respectively. Signals were acquired by exposing the membrane to a phosphoimager screen (Fujifilm). The screens were read out depending on the activity of the hybridized membranes after 1-3 days using the FLA-9500 or FLA-5000 phosphor imager (Fujifilm). The obtained data were analyzed with the Multigauge V3.0 software (Fujifilm).

6.2.4.7 Quantification of northern blots with MultiGauge

For quantitative analysis of northern blots, the software program MultiGauge V3.0 (Fujifilm) was used. A square area is positioned over a desired signal, in order to quantitate its signal intensity. Background (horizontally) is detected automatically or can be specified manually. Signals are quantified by integration of the surface area below signal peaks. Values are given as QL (quantum level) or PSL (photo-stimulated luminescence). The PSL value is proportional to the amount of radiation recorded from an image plate. The background has to be subtracted in order to receive meaningful values reflecting the real intensity of any desired signal (PSL-BG). For quantification, the ratio of signal intensities of respective pre-rRNA species can be calculated.

6.2.5 Work with Proteins

6.2.5.1 Determination of protein concentration

Protein concentration was determined using the Bio-Rad Protein Assay which is based on the method by Bradford (Bradford, 1976). 1 µl of a 1:10 dilution of the desired protein sample is mixed with 1 ml protein assay dye after diluting the reagent to an appropriate working concentration following the instructions given by the manufacturer. The protein concentration in µg/µl was estimated by dividing the observed absorbance at 595 nm by the sample volume and multiplying with the factor 230, which was determined using a BSA standard curve and due to the 1:10 dilution of the sample.

6.2.5.2 Denaturing protein extraction with TCA

Yeast cell pellets (1-2 OD_{600}) or a match´s head size of yeast cells were resuspended in 1 ml cold H_2O and mixed with 150 µl pre-treatment solution (section 6.1.6) in order to lyse the cells. After incubation for 15 min on ice, the cell lysate was mixed with 150 µl 55 % TCA (w/v) to precipitate the proteins. Another incubation step on ice was carried out for 10 min. Subsequently the samples were centrifuged at 13,000 rpm and 4 °C. The supernatant was carefully discarded. The obtained protein pellet was dissolved in 40-60 µl HU-buffer (section 6.1.6), neutralized by fumigation with NH_3 vapor and denatured by incubation at 65 °C for 15 min at 1,000 rpm for a subsequent separation by SDS-PAGE.

6.2.5.3 SDS-polyacrylamide gel electrophoresis (SDS-PAGE)

Proteins were separated according to their molecular weight using vertical discontinuous SDS-polyacrylamide gel electrophoresis method by Laemmli (Laemmli, 1970). Depending on the protein size of interest and the purpose, different gel (systems) were used. The discontinuous system used in this work consisted of a lower separating gel, composed of 7.5 %, 10 % or 12 % acrylamide, 375 mM Tris-HCl pH 8.8 and 0.1 % (w/v) SDS and an upper stacking gel composed of 4 % acrylamide, 125 mM Tris-HCl pH 6..8 and 0.1 % SDS. Gels were run for ~ 1,5 h at 50 mA per gel and 180 V in 1 x electrophoresis buffer (section 6.1.6). Molecular weights of the different proteins were estimated using protein markers of known molecular weights (section 6.1.9).

6.2.5.4 Western blot

Proteins separated by SDS-PAGE (section 6.2.5.3) were transferred to a PVDF membrane using a Trans-Blot SD Semi-Dry Transfer Cell (Peqlab Biotchenologie GmbH). The gel and the PVDF membrane which was pretreated with methanol, were placed in the transfer cell between two piles, each consisting of three blotting papers soaked with transfer buffer (section 6.1.6 and 6.1.9). Both the membrane and the blotting papers were pretreated with transfer buffer. Transfer was performed for 1 h at 24 V and 400 mA. If proteins of lower molecular weight (10-40 kDa) should be analyzed, a nitrocellulose membrane was used instead of a PVDF membrane. Due to chemical instability against pure methanol, the nitrocellulose membrane was solely pretreated with transfer buffer. In order to control the transfer prior to immune detection (see below), the membrane was reversibly stained with Ponceau by incubating the membrane for 2 min in Poinceau staining solution and subsequently destained with H_2O until the protein bands were visible.

6.2.5.5 Ponceau S staining after western blotting

In order to visualize protein bands and to check for protein loading and transfer quality after western blotting (see 6.2.5.4), the membranes were stained with Ponceau S (see 6.1.6) for 2 minutes at room

temperature. Destaining was performed with H_2O at room temperature under permanent shaking as required until the protein bands were

6.2.5.6 Detection of proteins by chemiluminescence

To avoid unspecific binding of antibodies, the membrane was blocked with non-related proteins obtained from bovine milk prior to specific immune detection of proteins by incubating the membrane in 5 % (w/v) milk powder in 1 x TBS-T on a shaker for at least 30 min at room temperature or at 4 °C overnight. Antibodies were diluted in an adequate working concentration (section 6.1.4) according to the manufacturer´s instructions in 1 % (w/v) milk powder in 1 x TBS-T. Incubations were performed in 50 ml falcon tubes using 10 ml milk powder solution supplemented with the respective amount of antibodies for 1 h (primary antibodies) or 30 min (secondary antibodies) at RT on a turning wheel. Following each antibody incubation step, the membrane was washed three times with 1 x TBS-T for 10 min on a shaker, respectively. In order to detect specifically bound antibodies, the membrane was incubated for ~ 1 min at RT with 1 ml BM Chemiluminescence Blotting Substrate (POD; Roche), which was prepared according to the manufacturer´s instructions. This reagent contains hydrogen peroxide and a luminal, which is a substrate for the horseradish peroxidase conjugated to the secondary antibody. The light which is emitted during this reaction at the corresponding specific positions on the membrane was detected with a LAS-3000 chemiluminescence imager using Image Reade LAS-3000 V2.2, followed by, if desirable, a quantitative analysis using Multi Gauge V3.0 (Fujifilm). A luminescent marker (phosphorescent window color) was used to label the positions of the lanes and/or color band of the protein marker.

6.2.6 Affinity Purification of RNPs via Epitope Tagged Fusion Proteins

6.2.6.1 Preparation of yeast cell extracts

Frozen cell pellets derived from exponentially growing yeast cultures (usually 0.4 – 1 l) were thawed on ice and washed once with 10 ml of an ice cold appropriate buffer for affinity purification supplemented with 1 x protease inhibitors (section 6.1.6). Cell pellets were weighed and 1.5 ml of cold buffer additionally supplemented with 0.04 U rRNasin/µl was added per 1 gram of cell pellets. 0.8 ml of the resulting cell suspension were added to 1.4 g cold glass beads (Ø 0.75-1 mm) in 2 ml reaction tubes. The cell suspensions were vigorously mixed on a Precellys 24 Tissue Homogenisator (bertin instruments) for 3 x 30 sec at 6,000 rpm with 30 sec pausing, respectively, thereby mechanically disrupting the cells. This procedure was repeated at least once, until an appropriate protein concentration was measured (section 6.2.5.1). During the whole process, the temperature was kept at approximately 4 °C with the aid of a nitrogen cooled Cryolis Cooling Option (bertin instruments). The cell lysate was cleared from cell debris by two centrifugations steps, for 5 and 10 min at 13,000 rpm at

4 °C, respectively. Protein concentration was determined by the Bradford-assay (section 6.2.5.1) which yielded usually 20-50 µg/µl.

6.2.6.2 Affinity purification of (pre)-rRNPs using IgG coupled magnetic beads

Cell extracts were prepared as described in section 6.2.6.1 using buffer A100+ (20 mM Tris-HCl pH 8, 100 mM KCl, 5 mM $Mg(OAc)_2$, 2 mM Benzamidine, 1 mM PMSF; section 6.1.6). Defined volumes of cell extracts corresponding to 250 µg of protein were transferred to 500 µl buffer AE or 40 µl buffer HU as input for northern or western blotting, respectively. The remaining cell extract was adjusted to a final concentration of 0.5 % Triton X-100 and 0.1 % Tween 20 with the appropriate stock solutions. Equal protein amounts of cell lysates were incubated with 100 µl of IgG (rabbit serum, I5006-100MG, Sigma) coupled magnetic beads slurry (1 mm BcMag, FC-102, Bioclone) equilibrated in buffer A100 containing 0.5 % Triton X-100 and 0.1 % Tween 20 for 30 min - 1 hour at 4 °C on a turning wheel. The beads were washed four times with 700 µl cold A100+ + T/T buffer. After the fourth washing step, an aliquot of 20 % (200 µl) of the beads was separated for the analysis of co-purified rRNAs by northern blotting. The remaining beads were washed twice with 1 ml AC buffer to remove salt from the sample. Bound proteins were eluted from the beads twice with freshly prepared 500 mM NH_4OH solution for 20 min at 600 rpm, RT, respectively. Both eluate fractions were pooled and lyophilized overnight. Subsequently the sample was frozen away at –20 °C until ongoing analysis.

6.2.6.3 Affinity purification of pre-ribosomes using IgG coupled sepharose beads

Cell extracts were prepared as described in section 6.2.6.1 using buffer A100 +(20 mM Tris-HCl pH 8, 100 mM KCl, 5 mM $Mg(OAc)_2$, 2 mM Benzamidine, 1 mM PMSF; section 6.1.6). Defined volumes of cell extracts corresponding to 250 µg of protein were transferred to 500 µl buffer AE or 40 µl buffer HU as input for northern or western blotting, respectively. The remaining cell extract was adjusted to a final concentration of 0.5 % Triton X-100 and 0.1 % Tween 20 with the appropriate stock solutions. Equal protein amounts of cell lysates were incubated with 200 µl of IgG sepharose slurry (GE Healthcare, 52-2082-00 AH) equilibrated in buffer A100+ +T/T for 30-60 min at 4 °C on a turning wheel. The beads were transferred to 15 ml Biorad chromatography columns (section 6.1.9) and washed twice with 2 ml and once with 10 ml cold A100+ +T/T. Beads were resuspended in 1 ml A100 and transferred to a 1.5 ml reaction tube. An aliquot of 20 % (200 µl) of the beads was separated into a mobicol column for the analysis of purified bait protein by western blotting and immune detection (sections 6.2.5.4 and 6.2.5.6). After a brief centrifugation step at 2,000 rpm and 4 °C for 2 min, 40 µl buffer HU was added and the samples were, together with the input samples for western analysis incubated for 15 min at 65 °C. The western eluate for the affinity purified fraction was recovered by centrifugation for 2 min 2,000 rpm into 1.5 ml reaction tubes. Both input and affinity purified probes for western analysis were subsequently frozen at -20 °C. The remaining 80 % of the affinity purified fraction were centrifuged for

2 min at 2,000 rpm and 4 °C. The supernatant was discarded and the beads were resuspended in 500 µl buffer AE and as well frozen at -20 °C until ongoing analysis.

6.2.6.4 Affinity purification of pre-RNPs using anti-FLAG antibody coupled sepharose beads

Cell extracts were prepared as described in section 6.2.6.1 using buffer A100+ (20 mM Tris-HCl pH 8, 100 mM KCl, 5 mM $Mg(OAc)_2$, 2 mM Benzamidine, 1 mM PMSF; section 6.1.6). Defined volumes of cell extracts corresponding to 250 µg of protein were transferred to 500 µl buffer AE or 40 µl buffer HU as input for northern or western blotting, respectively. The remaining cell extract was adjusted to a final concentration of 0.5 % Triton X-100 and 0.1 % Tween 20 with the appropriate stock solutions. Equal protein amounts of cell lysates were incubated with 200 µl Anti-FLAG M2 affinity gel slurry equilibrated in buffer AG100+ +T/T. The beads were transferred to a 15 ml chromatography column and washed twice with 2 ml and once with 10 ml cold AG100+ +T/T. Beads were resuspended in 1.0 ml A100+, whereof an aliquot of 20 % (200 µl) was separated to a new 1.5 ml reaction tube for analysis of the purified bait protein by western blotting and immune detection (sections 6.2.5.4 and 6.2.5.6). After a quick centrifugation step for 1 min at 800 rpm and 4 °C, the supernatant was discarded and 40 µl buffer HU was added to the samples. They were incubated together with the input samples for western analysis for 15 min at 65 °C. The input samples were frozen at -20 °C. The samples of the affinity purified fraction were centrifuged for 5 min at 13,000 rpm and RT. The supernatant (= western eluate) was transferred to new 1.5 ml reaction tubes and frozen at – 20°C until ongoing analysis.

6.2.7 Local tertiary structure probing by MNase fusion proteins

6.2.7.1 Yeast strains / generation

All *Saccharomyces cervisiae* strains used for structure probing originate from BY4741 6.1.1 (MATa his3Δ1 leu2Δ0 ura3Δ0). N- or C-terminal MNase-3x-FLAG fusions to Noc3p were introduced via homologous recombination (section 6.2.1.4) of the respective PCR-amplified tagging cassette (section 6.2.3.3).

6.2.7.2 Affinity purification and subsequent MNase digest of pre-RNPs

Cellular extracts were prepared as described in section 6.2.6.1using buffer AG100+ (20 mM Tris-HCl pH 8.0, 100 mM KCl, 5 mM $Mg(OAc)_2$, 5 mM EGTA/KOH pH 8.0, 2 mM Benzamidine, 1 mM PMSF; section 6.1.6). MNase structure probing was performed with strains that include MNase fused to Noc3p, additionally equipped with a 3x-FLAG tag. For this, the experimental procedure for input sample taking, preparation and performance of affinity purification using anti-FLAG M2 affinity gel and subsequent washing steps is identical as described in section 6.2.6.4. , however, all steps were performed with buffer supplemented with 5 mM EGTA/KOH pH 8.0 (section 6.1.6). After washing, the

beads were resuspended in 1.0 ml AG100+, whereof an aliquot of 20 % (200 µl) was separated to a new 1.5 ml reaction tube for analysis of the purified bait protein by western blotting and immune detection (sections 6.2.5.4 and 6.2.5.6).

The remaining bead suspension was split to equal volumes in two 1.5 ml reaction tubes. After a gentle centrifugation step for 1 min at 800 rpm and 4 °C, the volumes were lowered to 200 µl, respectively. MNase was activated in one of the two samples by incubation at 16 °C for 15 min in the presence of 8 mM $CaCl_2$. To stop the reaction, the sample was adjusted to 5 mM EGTA. The second sample was treated with the equal amount of water and incubated as well (untreated control). Both samples were filled to a total volume of 500 µl with buffer AE.

Depending on the experimental setup, it is not necessary to split the bead suspension after affinity purification, if one of the strains to be analyzed expresses the Noc3p-FLAG fusion but lacks the MNase and can therefore serve as "untreated control". In this case, each sample has to be treated with $CaCl_2$.

6.2.7.3 Primer extension

Primer extension employs a reverse transcription reaction in order to determine the 5´-end of RNA molecules. Reactions were performed in a PCR cycler with integrated lid heating, P^{32}-labelled antisense oligos (section 6.2.4.6) and RNA dissolved in H_2O received from affinity purification assays (section 6.2.6). The RNA concentration was measured with a NanoDrop ND-1000 spectrophotometer device and subsequently adjusted to a concentration of 100 ng/µl. 2.5 µl of the RNA template, 10 mM dNTPs and 2 µl of the P^{32}-labelled oligo were mixed and filled with water to a total volume of 13 µl. After incubation for 5 min at 65 °C, in order to denature the RNA, 7 µl of a master mix consisting of 4 µl 5 x First Strand Buffer (Invitrogen), 1 µl 0.1 M DTT (Invitrogen), 40 U rRNasin (Promega) for each reaction and 1 µl Superscript III Reverse Transcriptase (Invitrogen) were added to each tube. Oligonucleotide annealing and reverse transcription was performed for 90 min at 46 °C. To stop the reaction and to degrade template RNA, 2.5 µl 1 M NaOH and 0.5 µl 0,5 M EDTA pH 8.0 were added followed by an incubation for 30 min at 56 °C. To precipitate the obtained cDNA, 2.5 µl 1 M HCl, 2 µl glycogen (5 mg/ml, Ambion), 12.5 µl 7.4M NH_4AC and 100 µl 100 % EtOH were added and the samples were stored at -20 °C overnight. The precipitation mix was centrifuged for at least 30 min at 4 °C and 13,000 rpm. The supernatant was carefully discarded. If necessary, the samples were anew centrifuged for 1 min at 4 °C and 13,000 rpm and the remaining precipitation mix was discarded. The pellet was dried for 3 min at 80 °C in the opened reaction tube and subsequently dissolved in 10 µl 1 x primer extension loading buffer. Prior to loading onto the gel, samples were heated for 3 min at 75 °C and immediately chilled on ice.

6.2.7.4 Sequencing reaction

Sequencing was performed with the vector pT11 (K375, section 6.1.2) that contains the sequence information of the genomic rDNA locus of *Saccharomyces cerevisiae*. Therefore, the 5´-ends of reverse transcribed rRNAs (section6.2.7.3) derived from MNase-structure probing assays (section 6.2.7.2) can be mapped both onto the sequence as well as on its corresponding structure.

The sequencing reaction was performed using the Thermo Sequenase Cycle Sequencing Kit (Affimetrix). 4 µl of each ddNTP termination mix were placed in separate 0.5 ml reaction tubes. A master mix containing 2 µl reaction buffer, 2 µl labelled primer (section 6.2.4.6), 1 µl pT11 (K375, 2.8 µg/µl), 2µl Thermo Sequenase and 10.5 µl water was prepared. 4 µl of the master mix were transferred to each reaction tube containing either the ddATP, ddGTP, ddTTP or the ddCTP termination mix. Sequencing was performed in a fifty-fold cycle PCR assay with the following settings: Melting for 30 sec at 94 °C, annealing for 30 sec at 55 °C, elongation for 60 sec at 72 °C. Subsequently the temperature was lowered down to 4 °C. To stop the reaction, 4 µl stop solution which additionally contains glycerol and dye for gel electrophoresis were added to each reaction tube. Before loading onto the gel, the samples were heated for 3 min at 75 °C and immediately chilled on ice.

6.2.7.5 Gel electrophoresis for low molecular weight DNA

In order to map stops in primer extension reactions to their sequence position within the rRNA, cDNAs (section 6.2.7.3) as well as their corresponding sequencing reaction (section 6.2.7.4) had to be size separated with an appropriate gel system. For this purpose, sequencing gels composed of 6 % (v/v) acryl amide, 0.3 % (v/v) bisacryl amide, 7 M urea and 1 x taurine buffer (section 6.1.6) were used.

Depending on the cDNA size range that aimed to be resolved, gels were run using the Sequi-Gen GT Sequencing Cell device (Bio-Rad) for 1-2 h at 70 W and temperature controlled to a maximum threshold of 50 °C.

After electrophoresis, the gel was cooled at 4 °C for 1h, transferred to a filter paper (Rotilabor Filterbogen Type 601) and dried for 1.5 h at 80 °C and vacuum environment. Radioactive signal detection was subsequently accomplished as described in section 6.2.4.6.

7 References

Adams, Cynthia C.; Jakovljevic, Jelena; Roman, Judibelle; Harnpicharnchai, Piyanun; Woolford, John L. (2002): Saccharomyces cerevisiae nucleolar protein Nop7p is necessary for biogenesis of 60S ribosomal subunits. In: *RNA* 8 (2), S. 150–165. DOI: 10.1017/s1355838202010026.

Allmang, C.; Henry, Y.; Wood, H.; Morrissey, J. P.; Petfalski, E.; Tollervey, D. (1996): Recognition of cleavage site A(2) in the yeast pre-rRNA. In: *RNA* 2 (1), S. 51–62.

Allmang, C.; Mitchell, P.; Petfalski, E.; Tollervey, D. (2000a): Degradation of ribosomal RNA precursors by the exosome. In: *Nucleic Acids Research* 28 (8), S. 1684–1691. DOI: 10.1093/nar/28.8.1684.

Allmang, C.; Tollervey, D. (1998): The role of the 3' external transcribed spacer in yeast pre-rRNA processing. In: *Journal of molecular biology* 278 (1), S. 67–78. DOI: 10.1006/jmbi.1998.1693.

Allmang, Christine; Mitchell, Philip; Petfalski, Elisabeth; Tollervey, David (2000b): Degradation of ribosomal {RNA} precursors by the exosome. In: *Nucleic Acids Research* 28 (8), 1684--1691. Online verfügbar unter http://www.ncbi.nlm.nih.gov/pmc/articles/PMC102825/, zuletzt geprüft am 05.12.2012.

Altvater, Martin; Chang, Yiming; Melnik, Andre; Occhipinti, Laura; Schütz, Sabina; Rothenbusch, Ute et al. (2012): Targeted proteomics reveals compositional dynamics of 60S pre-ribosomes after nuclear export. In: *Molecular systems biology* 8, S. 628. DOI: 10.1038/msb.2012.63.

Andersen, Christian B. F.; Becker, Thomas; Blau, Michael; Anand, Monika; Halic, Mario; Balar, Bharvi et al. (2006): Structure of eEF3 and the mechanism of transfer RNA release from the E-site. In: *Nature* 443 (7112), S. 663–668. DOI: 10.1038/nature05126.

Anderson, Susan J.; Sikes, Martha L.; Zhang, Yinfeng; French, Sarah L.; Salgia, Shilpa; Beyer, Ann L. et al. (2011): The transcription elongation factor Spt5 influences transcription by RNA polymerase I positively and negatively. In: *The Journal of biological chemistry* 286 (21), S. 18816–18824. DOI: 10.1074/jbc.M110.202101.

Anfinsen, Christian B.; Cuatrecasas, Pedro; Taniuchi, Hiroshi (1971): 8 Staphylococcal Nuclease, Chemical Properties and Catalysis. In: Hydrolysis, Bd. 4: Elsevier (The Enzymes), S. 177–204.

Armache, Jean-Paul; Anger, Andreas M.; Márquez, Viter; Franckenberg, Sibylle; Fröhlich, Thomas; Villa, Elizabeth et al. (2013): Promiscuous behaviour of archaeal ribosomal proteins: implications for eukaryotic ribosome evolution. In: *Nucleic Acids Research* 41 (2), S. 1284–1293. DOI: 10.1093/nar/gks1259.

Asano, Nozomi; Kato, Koji; Nakamura, Akiyoshi; Komoda, Keisuke; Tanaka, Isao; Yao, Min (2015): Structural and functional analysis of the Rpf2-Rrs1 complex in ribosome biogenesis. In: *Nucleic Acids Research* 43 (9), S. 4746–4757. DOI: 10.1093/nar/gkv305.

Babiano, Reyes; Badis, Gwenael; Saveanu, Cosmin; Namane, Abdelkader; Doyen, Antonia; Díaz-Quintana, Antonio et al. (2013): Yeast ribosomal protein L7 and its homologue Rlp7 are simultaneously present at distinct sites on pre-60S ribosomal particles. In: *Nucleic Acids Research* 41 (20), S. 9461–9470. DOI: 10.1093/nar/gkt726.

Babl, Virginia; Stöckl, Ulrike; Tschochner, Herbert; Milkereit, Philipp; Griesenbeck, Joachim (2015): Chromatin Endogenous Cleavage (ChEC) as a Method to Quantify Protein Interaction with Genomic DNA in Saccharomyces cerevisiae. In: *Methods in molecular biology (Clifton, N.J.)* 1334, S. 219–232. DOI: 10.1007/978-1-4939-2877-4_14.

Ban, N.; Nissen, P.; Hansen, J.; Moore, P. B.; Steitz, T. A. (2000): The complete atomic structure of the large ribosomal subunit at 2.4 {A} resolution. In: *Science (New York, N.Y.)* 289 (5481), 905--920.

Barandun, Jonas; Chaker-Margot, Malik; Hunziker, Mirjam; Molloy, Kelly R.; Chait, Brian T.; Klinge, Sebastian (2017): The complete structure of the small-subunit processome. In: *Nature Structural & Molecular Biology* 24 (11), S. 944–953. DOI: 10.1038/nsmb.3472.

Barandun, Jonas; Hunziker, Mirjam; Klinge, Sebastian (2018): Assembly and structure of the SSU processome-a nucleolar precursor of the small ribosomal subunit. In: *Current Opinion in Structural Biology* 49, S. 85–93. DOI: 10.1016/j.sbi.2018.01.008.

Barrio-Garcia, Clara; Thoms, Matthias; Flemming, Dirk; Kater, Lukas; Berninghausen, Otto; Baßler, Jochen et al. (2016): Architecture of the Rix1-Rea1 checkpoint machinery during pre-60S-ribosome remodeling. In: *Nature Structural & Molecular Biology* 23 (1), S. 37–44. DOI: 10.1038/nsmb.3132.

Baßler, Jochen; Ahmed, Yasar Luqman; Kallas, Martina; Kornprobst, Markus; Calviño, Fabiola R.; Gnädig, Marén et al. (2017): Interaction network of the ribosome assembly machinery from a eukaryotic thermophile. In: *Protein science : a publication of the Protein Society* 26 (2), S. 327–342. DOI: 10.1002/pro.3085.

Bassler, Jochen; Kallas, Martina; Pertschy, Brigitte; Ulbrich, Cornelia; Thoms, Matthias; Hurt, Ed (2010): The {AAA}-{ATPase} {Rea}1 drives removal of biogenesis factors during multiple stages of 60S ribosome assembly. In: *Molecular cell* 38 (5), 712--721. DOI: 10.1016/j.molcel.2010.05.024.

Baudin-Baillieu, Agnès; Fabret, Céline; Liang, Xue-hai; Piekna-Przybylska, Dorota; Fournier, Maurille J.; Rousset, Jean-Pierre (2009): Nucleotide modifications in three functionally important regions of the Saccharomyces cerevisiae ribosome affect translation accuracy. In: *Nucleic Acids Research* 37 (22), S. 7665–7677. DOI: 10.1093/nar/gkp816.

Baxter-Roshek, Jennifer L.; Petrov, Alexey N.; Dinman, Jonathan D. (2007): Optimization of ribosome structure and function by rRNA base modification. In: *PloS one* 2 (1), e174. DOI: 10.1371/journal.pone.0000174.

Beltrame, M.; Tollervey, D. (1992): Identification and functional analysis of two U3 binding sites on yeast pre-ribosomal RNA. In: *The EMBO journal* 11 (4), S. 1531–1542.

Beltrame, M.; Tollervey, D. (1995): Base pairing between {U}3 and the pre-ribosomal {RNA} is required for 18S {rRNA} synthesis. In: *The EMBO journal* 14 (17), 4350--4356.

Ben-Shem, Adam; Garreau de Loubresse, Nicolas; Melnikov, Sergey; Jenner, Lasse; Yusupova, Gulnara; Yusupov, Marat (2011): The structure of the eukaryotic ribosome at 3.0 Å resolution. In: *Science (New York, N.Y.)* 334 (6062), 1524--1529. DOI: 10.1126/science.1212642.

Ben-Shem, Adam; Jenner, Lasse; Yusupova, Gulnara; Yusupov, Marat (2010): Crystal structure of the eukaryotic ribosome. In: *Science (New York, N.Y.)* 330 (6008), 1203--1209. DOI: 10.1126/science.1194294.

Bernstein, Jade; Patterson, Dimeka N.; Wilson, Gerald M.; Toth, Eric A. (2008): Characterization of the essential activities of Saccharomyces cerevisiae Mtr4p, a 3'-5' helicase partner of the nuclear exosome. In: *Journal of Biological Chemistry* 283 (8), S. 4930–4942. DOI: 10.1074/jbc.M706677200.

Bernstein, Kara A.; Gallagher, Jennifer E. G.; Mitchell, Brianna M.; Granneman, Sander; Baserga, Susan J. (2004): The small-subunit processome is a ribosome assembly intermediate. In: *Eukaryotic Cell* 3 (6), 1619--1626. DOI: 10.1128/EC.3.6.1619-1626.2004.

Biedka, Stephanie; Micic, Jelena; Wilson, Daniel; Brown, Hailey; Diorio-Toth, Luke; Woolford, John L. (2018): Hierarchical recruitment of ribosomal proteins and assembly factors remodels nucleolar pre-60S ribosomes. In: *The Journal of Cell Biology* 217 (7), S. 2503–2518. DOI: 10.1083/jcb.201711037.

Biedka, Stephanie; Wu, Shan; LaPeruta, Amber J.; Gao, Ning; Woolford, John L. (2017): Insights into remodeling events during eukaryotic large ribosomal subunit assembly provided by high resolution cryo-EM structures. In: *RNA biology* 14 (10), S. 1306–1313. DOI: 10.1080/15476286.2017.1297914.

Billy, E.; Wegierski, T.; Nasr, F.; Filipowicz, W. (2000): Rcl1p, the yeast protein similar to the RNA 3'-phosphate cyclase, associates with U3 snoRNP and is required for 18S rRNA biogenesis. In: *The EMBO journal* 19 (9), S. 2115–2126. DOI: 10.1093/emboj/19.9.2115.

Bleichert, Franziska; Granneman, Sander; Osheim, Yvonne N.; Beyer, Ann L.; Baserga, Susan J. (2006): The PINc domain protein Utp24, a putative nuclease, is required for the early cleavage steps in 18S rRNA maturation. In: *Proceedings of the National Academy of Sciences of the United States of America* 103 (25), S. 9464–9469. DOI: 10.1073/pnas.0603673103.

Bohnsack, Markus T.; Kos, Martin; Tollervey, David (2008): Quantitative analysis of snoRNA association with pre-ribosomes and release of snR30 by Rok1 helicase. In: *EMBO reports* 9 (12), S. 1230–1236. DOI: 10.1038/embor.2008.184.

Boissier, Fanny; Schmidt, Christina Maria; Linnemann, Jan; Fribourg, Sébastien; Perez-Fernandez, Jorge (2017): Pwp2 mediates UTP-B assembly via two structurally independent domains. In: *Scientific reports* 7 (1), S. 3169. DOI: 10.1038/s41598-017-03034-y.

Bradatsch, Bettina; Leidig, Christoph; Granneman, Sander; Gnädig, Marén; Tollervey, David; Böttcher, Bettina et al. (2012): Structure of the pre-60S ribosomal subunit with nuclear export factor {Arx}1 bound at the exit tunnel. In: *Nature structural \& molecular biology* 19 (12), 1234--1241. DOI: 10.1038/nsmb.2438.

Brand, R. C.; Klootwijk, J.; van Steenbergen, T. J.; Kok, A. J. de; Planta, R. J. (1977): Secondary methylation of yeast ribosomal precursor {RNA}. In: *European journal of biochemistry / FEBS* 75 (1), 311--318.

Braun, Christina M.; Hackert, Philipp; Schmid, Catharina E.; Bohnsack, Markus T.; Bohnsack, Katherine E.; Perez-Fernandez, Jorge (2020): Pol5 is required for recycling of small subunit biogenesis factors and for formation of the peptide exit tunnel of the large ribosomal subunit. In: *Nucleic Acids Research* 48 (1), S. 405–420. DOI: 10.1093/nar/gkz1079.

Briggs, M. W.; Burkard, K. T.; Butler, J. S. (1998): Rrp6p, the yeast homologue of the human PM-Scl 100-kDa autoantigen, is essential for efficient 5.8 S rRNA 3' end formation. In: *Journal of Biological Chemistry* 273 (21), S. 13255–13263. DOI: 10.1074/jbc.273.21.13255.

Burlacu, Elena; Lackmann, Fredrik; Aguilar, Lisbeth-Carolina; Belikov, Sergey; van Nues, Rob; Trahan, Christian et al. (2017): High-throughput RNA structure probing reveals critical folding events during early 60S ribosome assembly in yeast. In: *Nature communications* 8 (1), S. 714. DOI: 10.1038/s41467-017-00761-8.

Bussiere, Cyril; Hashem, Yaser; Arora, Sucheta; Frank, Joachim; Johnson, Arlen W. (2012): Integrity of the P-site is probed during maturation of the 60S ribosomal subunit. In: *The Journal of Cell Biology* 197 (6), S. 747–759. DOI: 10.1083/jcb.201112131.

Calviño, Fabiola R.; Kharde, Satyavati; Ori, Alessandro; Hendricks, Astrid; Wild, Klemens; Kressler, Dieter et al. (2015): Symportin 1 chaperones 5S RNP assembly during ribosome biogenesis by occupying an essential rRNA-binding site. In: *Nature communications* 6, S. 6510. DOI: 10.1038/ncomms7510.

Carroni, Marta; Saibil, Helen R. (2016): Cryo electron microscopy to determine the structure of macromolecular complexes. In: *Methods (San Diego, Calif.)* 95, S. 78–85. DOI: 10.1016/j.ymeth.2015.11.023.

Carter, A. P.; Clemons, W. M.; Brodersen, D. E.; Morgan-Warren, R. J.; Wimberly, B. T.; Ramakrishnan, V. (2000): Functional insights from the structure of the 30S ribosomal subunit and its interactions with antibiotics. In: *Nature* 407 (6802), 340--348. DOI: 10.1038/35030019.

Cavaillé, J.; Nicoloso, M.; Bachellerie, J. P. (1996): Targeted ribose methylation of {RNA} in vivo directed by tailored antisense {RNA} guides. In: *Nature* 383 (6602), 732--735. DOI: 10.1038/383732a0.

Cech, T. R. (2000): Structural biology. {The} ribosome is a ribozyme. In: *Science (New York, N.Y.)* 289 (5481), 878--879.

Cepeda, Leidy Paola P.; Bagatelli, Felipe F. M.; Santos, Renata M.; Santos, Marlon D. M.; Nogueira, Fabio C. S.; Oliveira, Carla C. (2019): The ribosome assembly factor Nop53 controls association of the RNA exosome with pre-60S particles in yeast. In: *The Journal of biological chemistry* 294 (50), S. 19365–19380. DOI: 10.1074/jbc.RA119.010193.

Chaker-Margot, Malik (2018): Assembly of the small ribosomal subunit in yeast: mechanism and regulation. In: *RNA (New York, N.Y.)* 24 (7), S. 881–891. DOI: 10.1261/rna.066985.118.

Chaker-Margot, Malik; Barandun, Jonas; Hunziker, Mirjam; Klinge, Sebastian (2017): Architecture of the yeast small subunit processome. In: *Science (New York, N.Y.)* 355 (6321). DOI: 10.1126/science.aal1880.

Chaker-Margot, Malik; Hunziker, Mirjam; Barandun, Jonas; Dill, Brian D.; Klinge, Sebastian (2015): Stage-specific assembly events of the 6-MDa small-subunit processome initiate eukaryotic ribosome biogenesis. In: *Nature Structural & Molecular Biology* 22 (11), S. 920–923. DOI: 10.1038/nsmb.3111.

Chaker-Margot, Malik; Klinge, Sebastian (2019): Assembly and early maturation of large subunit precursors. In: *RNA (New York, N.Y.)* 25 (4), S. 465–471. DOI: 10.1261/rna.069799.118.

Chen, Wu; Xie, Zhensheng; Yang, Fuquan; Ye, Keqiong (2017): Stepwise assembly of the earliest precursors of large ribosomal subunits in yeast. In: *Nucleic Acids Research* 45 (11), S. 6837–6847. DOI: 10.1093/nar/gkx254.

Choe, S. Y.; Schultz, M. C.; Reeder, R. H. (1992): In vitro definition of the yeast RNA polymerase I promoter. In: *Nucleic Acids Research* 20 (2), S. 279–285. DOI: 10.1093/nar/20.2.279.

Chu, S.; Archer, R. H.; Zengel, J. M.; Lindahl, L. (1994a): The {RNA} of {RNase} {MRP} is required for normal processing of ribosomal {RNA}. In: *Proceedings of the National Academy of Sciences of the United States of America* 91 (2), 659--663.

Chu, S.; Archer, R. H.; Zengel, J. M.; Lindahl, L. (1994b): The RNA of RNase MRP is required for normal processing of ribosomal RNA. In: *Proceedings of the National Academy of Sciences of the United States of America* 91 (2), S. 659–663. DOI: 10.1073/pnas.91.2.659.

Coleman, Annette W. (2015): Nuclear rRNA transcript processing versus internal transcribed spacer secondary structure. In: *Trends in genetics : TIG* 31 (3), S. 157–163. DOI: 10.1016/j.tig.2015.01.002.

Collins, Jason C.; Ghalei, Homa; Doherty, Joanne R.; Huang, Haina; Culver, Rebecca N.; Karbstein, Katrin (2018): Ribosome biogenesis factor Ltv1 chaperones the assembly of the small subunit head. In: *The Journal of Cell Biology* 217 (12), S. 4141–4154. DOI: 10.1083/jcb.201804163.

Costello, Joe L.; Stead, Jonathan A.; Feigenbutz, Monika; Jones, Rebecca M.; Mitchell, Phil (2011): The C-terminal region of the exosome-associated protein Rrp47 is specifically required for box C/D small nucleolar RNA 3'-maturation. In: *The Journal of biological chemistry* 286 (6), S. 4535–4543. DOI: 10.1074/jbc.M110.162826.

Côté, Colette A.; Greer, Chris L.; Peculis, Brenda A. (2002): Dynamic conformational model for the role of ITS2 in pre-rRNA processing in yeast. In: *RNA* 8 (6), S. 786–797. DOI: 10.1017/s1355838202023063.

Davis, Joseph H.; Tan, Yong Zi; Carragher, Bridget; Potter, Clinton S.; Lyumkis, Dmitry; Williamson, James R. (2016): Modular Assembly of the Bacterial Large Ribosomal Subunit. In: *Cell* 167 (6), 1610-1622.e15. DOI: 10.1016/j.cell.2016.11.020.

Delan-Forino, Clémentine; Spanos, Christos; Rappsilber, Juri; Tollervey, David (2020): Substrate specificity of the TRAMP nuclear surveillance complexes. In: *Nature communications* 11 (1), S. 3122. DOI: 10.1038/s41467-020-16965-4.

DELEY, J. (1964): SEDIMENTATION COEFFICIENTS OF YEAST RIBOSOMES. In: *Journal of general microbiology* 37, S. 153–156. DOI: 10.1099/00221287-37-1-153.

Delprato, Anna; Al Kadri, Yasmine; Pérébaskine, Natacha; Monfoulet, Cécile; Henry, Yves; Henras, Anthony K.; Fribourg, Sébastien (2014): Crucial role of the Rcl1p-Bms1p interaction for yeast pre-ribosomal RNA processing. In: *Nucleic Acids Research* 42 (15), S. 10161–10172. DOI: 10.1093/nar/gku682.

Dembowski, Jill A.; Kuo, Benjamin; Woolford, John L. (2013a): Has1 regulates consecutive maturation and processing steps for assembly of 60S ribosomal subunits. In: *Nucleic Acids Research* 41 (16), S. 7889–7904. DOI: 10.1093/nar/gkt545.

Dembowski, Jill A.; Ramesh, Madhumitha; McManus, C. Joel; Woolford, John L. (2013b): Identification of the binding site of Rlp7 on assembling 60S ribosomal subunits in Saccharomyces cerevisiae. In: *RNA (New York, N.Y.)* 19 (12), S. 1639–1647. DOI: 10.1261/rna.041194.113.

Demoinet, Emilie; Jacquier, Alain; Lutfalla, Georges; Fromont-Racine, Micheline (2007): The Hsp40 chaperone Jjj1 is required for the nucleo-cytoplasmic recycling of preribosomal factors in Saccharomyces cerevisiae. In: *RNA* 13 (9), S. 1570–1581. DOI: 10.1261/rna.585007.

Dever, Thomas E.; Kinzy, Terri Goss; Pavitt, Graham D. (2016): Mechanism and Regulation of Protein Synthesis in Saccharomyces cerevisiae. In: *Genetics* 203 (1), S. 65–107. DOI: 10.1534/genetics.115.186221.

Dez, Christophe; Froment, Carine; Noaillac-Depeyre, Jacqueline; Monsarrat, Bernard; Caizergues-Ferrer, Michèle; Henry, Yves (2004): Npa1p, a component of very early pre-60S ribosomal particles, associates with a subset of small nucleolar {RNPs} required for peptidyl transferase center modification. In: *Molecular and cellular biology* 24 (14), 6324--6337. DOI: 10.1128/MCB.24.14.6324-6337.2004.

Dez, Christophe; Houseley, Jonathan; Tollervey, David (2006): Surveillance of nuclear-restricted pre-ribosomes within a subnucleolar region of {Saccharomyces} cerevisiae. In: *The EMBO journal* 25 (7), 1534--1546. DOI: 10.1038/sj.emboj.7601035.

Diaconu, Mihaela; Kothe, Ute; Schlünzen, Frank; Fischer, Niels; Harms, Jörg M.; Tonevitsky, Alexander G. et al. (2005): Structural {Basis} for the {Function} of the {Ribosomal} {L}7/12 {Stalk} in {Factor} {Binding} and {GTPase} {Activation}. In: *Cell* 121 (7), 991--1004. DOI: 10.1016/j.cell.2005.04.015.

Dieci, Giorgio; Fiorino, Gloria; Castelnuovo, Manuele; Teichmann, Martin; Pagano, Aldo (2007): The expanding RNA polymerase III transcriptome. In: *Trends in genetics : TIG* 23 (12), S. 614–622. DOI: 10.1016/j.tig.2007.09.001.

Dingwall, C.; Lomonossoff, G. P.; Laskey, R. A. (1981): High sequence specificity of micrococcal nuclease. In: *Nucleic Acids Research* 9 (12), S. 2659–2673. DOI: 10.1093/nar/9.12.2659.

Dinman, Jonathan D. (2005): 5S rRNA: Structure and Function from Head to Toe. In: *International journal of biomedical science : IJBS* 1 (1), S. 2–7.

Dlakić, Mensur; Tollervey, David (2004): The {Noc} proteins involved in ribosome synthesis and export contain divergent {HEAT} repeats. In: *RNA* 10 (3), 351--354. DOI: 10.1261/rna.5184704.

Dosil, Mercedes; Bustelo, Xosé R. (2004): Functional characterization of {Pwp}2, a {WD} family protein essential for the assembly of the 90 {S} pre-ribosomal particle. In: *Journal of Biological Chemistry* 279 (36), 37385--37397. DOI: 10.1074/jbc.M404909200.

Dragon, François; Gallagher, Jennifer E. G.; Compagnone-Post, Patricia A.; Mitchell, Brianna M.; Porwancher, Kara A.; Wehner, Karen A. et al. (2002): A large nucleolar {U}3 ribonucleoprotein

required for 18S ribosomal {RNA} biogenesis. In: *Nature* 417 (6892), 967--970. DOI: 10.1038/nature00769.

Dunbar, David A.; Dragon, François; Lee, Sarah J.; Baserga, Susan J. (2000): A nucleolar protein related to ribosomal protein {L}7 is required for an early step in large ribosomal subunit biogenesis. In: *Proceedings of the National Academy of Sciences of the United States of America* 97 (24), 13027--13032. DOI: 10.1073/pnas.97.24.13027.

Dutca, Laura M.; Gallagher, Jennifer E. G.; Baserga, Susan J. (2011): The initial {U}3 {snoRNA}:pre-{rRNA} base pairing interaction required for pre-18S {rRNA} folding revealed by in vivo chemical probing. In: *Nucleic Acids Research* 39 (12), 5164--5180. DOI: 10.1093/nar/gkr044.

Ehresmann, C.; Baudin, F.; Mougel, M.; Romby, P.; Ebel, J. P.; Ehresmann, B. (1987): Probing the structure of RNAs in solution. In: *Nucleic Acids Research* 15 (22), S. 9109–9128. DOI: 10.1093/nar/15.22.9109.

Elela, Sherif Abou; Igel, Haller; Ares, Manuel (1996): RNase III Cleaves Eukaryotic Preribosomal RNA at a U3 snoRNP-Dependent Site. In: *Cell* 85 (1), S. 115–124. DOI: 10.1016/S0092-8674(00)81087-9.

Endo, Y.; Mitsui, K.; Motizuki, M.; Tsurugi, K. (1987): The mechanism of action of ricin and related toxic lectins on eukaryotic ribosomes. The site and the characteristics of the modification in 28 S ribosomal RNA caused by the toxins. In: *Journal of Biological Chemistry* 262 (12), S. 5908–5912.

Endo, Y.; Wool, I. G. (1982): The site of action of alpha-sarcin on eukaryotic ribosomes. The sequence at the alpha-sarcin cleavage site in 28 S ribosomal ribonucleic acid. In: *Journal of Biological Chemistry* 257 (15), S. 9054–9060.

Engel, Christoph; Sainsbury, Sarah; Cheung, Alan C.; Kostrewa, Dirk; Cramer, Patrick (2013): RNA polymerase I structure and transcription regulation. In: *Nature* 502 (7473), S. 650–655. DOI: 10.1038/nature12712.

Eppens, N. A.; Rensen, S.; Granneman, S.; Raué, H. A.; Venema, J. (1999): The roles of {Rrp}5p in the synthesis of yeast 18S and 5.8S {rRNA} can be functionally and physically separated. In: *RNA* 5 (6), 779--793. Online verfügbar unter http://www.ncbi.nlm.nih.gov/pubmed/10376877, zuletzt geprüft am 11.05.2012.

Espinar-Marchena, Francisco J.; Babiano, Reyes; Cruz, Jesús (2017): Placeholder factors in ribosome biogenesis: please, pave my way. In: *Microbial cell (Graz, Austria)* 4 (5), S. 144–168. DOI: 10.15698/mic2017.05.572.

Faber, Alex W.; van Dijk, Marie; Raué, Hendrik A.; Vos, Jan C. (2002): Ngl2p is a {Ccr}4p-like {RNA} nuclease essential for the final step in 3'-end processing of 5.8S {rRNA} in {Saccharomyces} cerevisiae. In: *RNA* 8 (9), 1095--1101. Online verfügbar unter http://rnajournal.cshlp.org.ubproxy.ub.uni-heidelberg.de/content/8/9/1095, zuletzt geprüft am 30.11.2012.

Faber, Alex W.; Vos, Harmjan R.; Vos, Jan C.; Raué, Hendrik A. (2006): 5'-end formation of yeast 5.8SL {rRNA} is an endonucleolytic event. In: *Biochemical and biophysical research communications* 345 (2), 796--802. DOI: 10.1016/j.bbrc.2006.04.166.

Falk, Sebastian; Tants, Jan-Niklas; Basquin, Jerôme; Thoms, Matthias; Hurt, Ed; Sattler, Michael; Conti, Elena (2017): Structural insights into the interaction of the nuclear exosome helicase Mtr4 with the preribosomal protein Nop53. In: *RNA (New York, N.Y.)* 23 (12), S. 1780–1787. DOI: 10.1261/rna.062901.117.

FANG, FENG; PHILLIPS, SEASSON; BUTLER, J. SCOTT (2005): Rat1p and {Rai}1p function with the nuclear exosome in the processing and degradation of {rRNA} precursors. In: *RNA* 11 (10), 1571--1578. DOI: 10.1261/rna.2900205.

Fatica, Alessandro; Oeffinger, Marlene; Dlakić, Mensur; Tollervey, David (2003a): Nob1p {Is} {Required} for {Cleavage} of the 3′ {End} of 18S {rRNA}. In: *Molecular and cellular biology* 23 (5), 1798--1807. DOI: 10.1128/MCB.23.5.1798-1807.2003.

Fatica, Alessandro; Oeffinger, Marlene; Tollervey, David; BOZZONI, IRENE (2003b): Cic1p/{Nsa}3p is required for synthesis and nuclear export of 60S ribosomal subunits. In: *RNA* 9 (12), 1431--1436. DOI: 10.1261/rna.5130503.

Fayet-Lebaron, Eléonore; Atzorn, Vera; Henry, Yves; Kiss, Tamás (2009): 18S {rRNA} processing requires base pairings of {snR}30 {H}/{ACA} {snoRNA} to eukaryote-specific 18S sequences. In: *The EMBO journal* 28 (9), 1260--1270. DOI: 10.1038/emboj.2009.79.

Fernández-Tornero, Carlos; Moreno-Morcillo, María; Rashid, Umar J.; Taylor, Nicholas M. I.; Ruiz, Federico M.; Gruene, Tim et al. (2013): Crystal structure of the 14-subunit RNA polymerase I. In: *Nature* 502 (7473), S. 644–649. DOI: 10.1038/nature12636.

Ferreira-Cerca, Sébastien; Kiburu, Irene; Thomson, Emma; LaRonde, Nicole; Hurt, Ed (2014): Dominant Rio1 kinase/ATPase catalytic mutant induces trapping of late pre-40S biogenesis factors in 80S-like ribosomes. In: *Nucleic Acids Research* 42 (13), S. 8635–8647. DOI: 10.1093/nar/gku542.

Ferreira-Cerca, Sébastien; Pöll, Gisela; Gleizes, Pierre-Emmanuel; Tschochner, Herbert; Milkereit, Philipp (2005): Roles of eukaryotic ribosomal proteins in maturation and transport of pre-18S {rRNA} and ribosome function. In: *Molecular cell* 20 (2), 263--275. DOI: 10.1016/j.molcel.2005.09.005.

Ferreira-Cerca, Sébastien; Pöll, Gisela; Kühn, Holger; Neueder, Andreas; Jakob, Steffen; Tschochner, Herbert; Milkereit, Philipp (2007): Analysis of the in vivo assembly pathway of eukaryotic 40S ribosomal proteins. In: *Molecular cell* 28 (3), 446--457. DOI: 10.1016/j.molcel.2007.09.029.

Ferreira-Cerca, Sébastien; Sagar, Vatsala; Schäfer, Thorsten; Diop, Momar; Wesseling, Anne-Maria; Lu, Haiyun et al. (2012): ATPase-dependent role of the atypical kinase Rio2 on the evolving pre-40S ribosomal subunit. In: *Nature Structural & Molecular Biology* 19 (12), S. 1316–1323. DOI: 10.1038/nsmb.2403.

Fournier, M. J.; Maxwell, E. S. (1993): The nucleolar {snRNAs}: catching up with the spliceosomal {snRNAs}. In: *Trends in biochemical sciences* 18 (4), 131--135.

Francisco-Velilla, Rosario; Remacha, Miguel; Ballesta, Juan P. G. (2013): Carboxy terminal modifications of the P0 protein reveal alternative mechanisms of nuclear ribosomal stalk assembly. In: *Nucleic Acids Research* 41 (18), S. 8628–8636. DOI: 10.1093/nar/gkt637.

Frank, J.; Agrawal, R. K. (2000): A ratchet-like inter-subunit reorganization of the ribosome during translocation. In: *Nature* 406 (6793), S. 318–322. DOI: 10.1038/35018597.

Fraser, Christopher S. (2015): Quantitative studies of mRNA recruitment to the eukaryotic ribosome. In: *Biochimie* 114, S. 58–71. DOI: 10.1016/j.biochi.2015.02.017.

French, Sarah L.; Osheim, Yvonne N.; Cioci, Francesco; Nomura, Masayasu; Beyer, Ann L. (2003): In {Exponentially} {Growing} {Saccharomyces} cerevisiae {Cells}, {rRNA} {Synthesis} {Is} {Determined} by the {Summed} {RNA} {Polymerase} {I} {Loading} {Rate} {Rather} than by the {Number} of {Active} {Genes}. In: *Molecular and cellular biology* 23 (5), 1558--1568. DOI: 10.1128/MCB.23.5.1558-1568.2003.

Fromm, Lisa; Falk, Sebastian; Flemming, Dirk; Schuller, Jan Michael; Thoms, Matthias; Conti, Elena; Hurt, Ed (2017): Reconstitution of the complete pathway of ITS2 processing at the pre-ribosome. In: *Nature communications* 8 (1), S. 1787. DOI: 10.1038/s41467-017-01786-9.

Fujii, Kotaro; Susanto, Teodorus Theo; Saurabh, Saumya; Barna, Maria (2018): Decoding the Function of Expansion Segments in Ribosomes. In: *Molecular cell* 72 (6), 1013-1020.e6. DOI: 10.1016/j.molcel.2018.11.023.

Gadal, O.; Strauss, D.; Kessl, J.; Trumpower, B.; Tollervey, D.; Hurt, E. (2001): Nuclear export of 60s ribosomal subunits depends on {Xpo}1p and requires a nuclear export sequence-containing factor, {Nmd}3p, that associates with the large subunit protein {Rpl}10p. In: *Molecular and cellular biology* 21 (10), 3405--3415. DOI: 10.1128/MCB.21.10.3405-3415.2001.

Gadal, Olivier; Labarre, Sylvie; Boschiero, Claire; Thuriaux, Pierre (2002): Hmo1, an {HMG}-box protein, belongs to the yeast ribosomal {DNA} transcription system. In: *The EMBO journal* 21 (20), 5498--5507.

Galardi, Silvia; Fatica, Alessandro; Bachi, Angela; Scaloni, Andrea; Presutti, Carlo; BOZZONI, IRENE (2002): Purified box C/D snoRNPs are able to reproduce site-specific 2'-O-methylation of target RNA in vitro. In: *Molecular and cellular biology* 22 (19), S. 6663–6668. DOI: 10.1128/MCB.22.19.6663-6668.2002.

Gallagher, Jennifer E. G. (2019): Proteins and RNA sequences required for the transition of the t-Utp complex into the SSU processome. In: *FEMS yeast research* 19 (1). DOI: 10.1093/femsyr/foy120.

Gallagher, Jennifer E. G.; Dunbar, David A.; Granneman, Sander; Mitchell, Brianna M.; Osheim, Yvonne; Beyer, Ann L.; Baserga, Susan J. (2004): RNA} polymerase {I} transcription and pre-{rRNA} processing are linked by specific {SSU} processome components. In: *Genes \& development* 18 (20), 2506--2517. DOI: 10.1101/gad.1226604.

Gamalinda, Michael; Jakovljevic, Jelena; Babiano, Reyes; Talkish, Jason; La Cruz, Jesús de; Woolford, John L. (2012): Yeast polypeptide exit tunnel ribosomal proteins L17, L35 and L37 are necessary to recruit late-assembling factors required for 27SB pre-rRNA processing. In: *Nucleic Acids Research* 41 (3), S. 1965–1983. DOI: 10.1093/nar/gks1272.

Gamalinda, Michael; Ohmayer, Uli; Jakovljevic, Jelena; Kumcuoglu, Beril; Woolford, Joshua; Mbom, Bertrade et al. (2014): A hierarchical model for assembly of eukaryotic 60S ribosomal subunit domains. In: *Genes & development* 28 (2), S. 198–210. DOI: 10.1101/gad.228825.113.

Gamalinda, Michael; Woolford, John L. (2014): Deletion of L4 domains reveals insights into the importance of ribosomal protein extensions in eukaryotic ribosome assembly. In: *RNA (New York, N.Y.)* 20 (11), S. 1725–1731. DOI: 10.1261/rna.046649.114.

Ganot, P.; Bortolin, M. L.; Kiss, T. (1997): Site-specific pseudouridine formation in preribosomal {RNA} is guided by small nucleolar {RNAs}. In: *Cell* 89 (5), 799--809.

Gasse, Lisa; Flemming, Dirk; Hurt, Ed (2015): Coordinated Ribosomal ITS2 RNA Processing by the Las1 Complex Integrating Endonuclease, Polynucleotide Kinase, and Exonuclease Activities. In: *Molecular cell* 60 (5), S. 808–815. DOI: 10.1016/j.molcel.2015.10.021.

Geerlings, T. H.; Vos, J. C.; Raué, H. A. (2000): The final step in the formation of 25S {rRNA} in {Saccharomyces} cerevisiae is performed by 5'--{\textgreater}3' exonucleases. In: *RNA* 6 (12), 1698--1703.

Gelperin, D.; Horton, L.; Beckman, J.; Hensold, J.; Lemmon, S. K. (2001): Bms1p, a novel GTP-binding protein, and the related Tsr1p are required for distinct steps of 40S ribosome biogenesis in yeast. In: *RNA* 7 (9), S. 1268–1283. DOI: 10.1017/s1355838201013073.

Gerbi, Susan A. (1996): Expansion segments: regions of variable size that interrupt the universal core secondary structure of ribosomal RNA. In: *Ribosomal RNA—Structure, evolution, processing, and function in protein synthesis*, S. 71–87.

Gérczei, Tímea; Correll, Carl C. (2004): Imp3p and {Imp}4p mediate formation of essential {U}3–precursor {rRNA} (pre-{rRNA}) duplexes, possibly to recruit the small subunit processome to the pre-{rRNA}. In: *Proceedings of the National Academy of Sciences of the United States of America* 101 (43), 15301--15306. DOI: 10.1073/pnas.0406819101.

Gérczei, Tímea; Shah, Binal N.; Manzo, Anthony J.; Walter, Nils G.; Correll, Carl C. (2009): RNA} chaperones stimulate formation and yield of the {U}3 {snoRNA}-pre-{rRNA} duplexes needed for eukaryotic ribosome biogenesis. In: *Journal of molecular biology* 390 (5), 991--1006. DOI: 10.1016/j.jmb.2009.05.072.

Ghalei, Homa; Schaub, Franz X.; Doherty, Joanne R.; Noguchi, Yoshihiko; Roush, William R.; Cleveland, John L. et al. (2015): Hrr25/CK1δ-directed release of Ltv1 from pre-40S ribosomes is necessary for ribosome assembly and cell growth. In: *The Journal of Cell Biology* 208 (6), S. 745–759. DOI: 10.1083/jcb.201409056.

Gómez Ramos, Lizzette M.; Smeekens, Johanna M.; Kovacs, Nicholas A.; Bowman, Jessica C.; Wartell, Roger M.; Wu, Ronghu; Williams, Loren Dean (2016): Yeast rRNA Expansion Segments: Folding and Function. In: *Journal of molecular biology* 428 (20), S. 4048–4059. DOI: 10.1016/j.jmb.2016.08.008.

Gongadze, G. M. (2011): 5S rRNA and ribosome. In: *Biochemistry. Biokhimiia* 76 (13), S. 1450–1464. DOI: 10.1134/S0006297911130062.

González, Asier; Hall, Michael N. (2017): Nutrient sensing and TOR signaling in yeast and mammals. In: *The EMBO journal* 36 (4), S. 397–408. DOI: 10.15252/embj.201696010.

Granato, Daniela C.; Gonzales, Fernando A.; Luz, Juliana S.; Cassiola, Flávia; Machado-Santelli, Glaucia M.; Oliveira, Carla C. (2005): Nop53p, an essential nucleolar protein that interacts with Nop17p and

Nip7p, is required for pre-rRNA processing in Saccharomyces cerevisiae. In: *The FEBS journal* 272 (17), S. 4450–4463. DOI: 10.1111/j.1742-4658.2005.04861.x.

Granato, Daniela C.; Machado-Santelli, Glaucia M.; Oliveira, Carla C. (2008): Nop53p interacts with 5.8S {rRNA} co-transcriptionally, and regulates processing of pre-{rRNA} by the exosome. In: *The FEBS journal* 275 (16), 4164--4178. DOI: 10.1111/j.1742-4658.2008.06565.x.

Grandi, Paola; Rybin, Vladimir; Bassler, Jochen; Petfalski, Elisabeth; Strauss, Daniela; Marzioch, Martina et al. (2002): 90S pre-ribosomes include the 35S pre-{rRNA}, the {U}3 {snoRNP}, and 40S subunit processing factors but predominantly lack 60S synthesis factors. In: *Molecular cell* 10 (1), 105--115. Online verfügbar unter http://www.ncbi.nlm.nih.gov/pubmed/12150911, zuletzt geprüft am 11.05.2012.

Granneman, Sander; Bernstein, Kara A.; Bleichert, Franziska; Baserga, Susan J. (2006): Comprehensive mutational analysis of yeast DEXD/H box RNA helicases required for small ribosomal subunit synthesis. In: *Molecular and cellular biology* 26 (4), S. 1183–1194. DOI: 10.1128/MCB.26.4.1183-1194.2006.

Granneman, Sander; Gallagher, Jennifer E. G.; Vogelzangs, Judith; Horstman, Wendy; van Venrooij, Walther J.; Baserga, Susan J.; Pruijn, Ger J. M. (2003): The human Imp3 and Imp4 proteins form a ternary complex with hMpp10, which only interacts with the U3 snoRNA in 60-80S ribonucleoprotein complexes. In: *Nucleic Acids Research* 31 (7), S. 1877–1887. DOI: 10.1093/nar/gkg300.

Granneman, Sander; Petfalski, Elisabeth; Swiatkowska, Agata; Tollervey, David (2010): Cracking pre-40S ribosomal subunit structure by systematic analyses of {RNA}-protein cross-linking. In: *The EMBO journal* 29 (12), 2026--2036. DOI: 10.1038/emboj.2010.86.

Granneman, Sander; Petfalski, Elisabeth; Tollervey, David (2011): A cluster of ribosome synthesis factors regulate pre-{rRNA} folding and 5.8S {rRNA} maturation by the {Rat}1 exonuclease. In: *The EMBO journal* 30 (19), 4006--4019. DOI: 10.1038/emboj.2011.256.

Greber, Basil J.; Boehringer, Daniel; Montellese, Christian; Ban, Nenad (2012): Cryo-{EM} structures of {Arx}1 and maturation factors {Rei}1 and {Jjj}1 bound to the 60S ribosomal subunit. In: *Nature structural \& molecular biology* 19 (12), 1228--1233. DOI: 10.1038/nsmb.2425.

Greber, Basil Johannes; Gerhardy, Stefan; Leitner, Alexander; Leibundgut, Marc; Salem, Michèle; Boehringer, Daniel et al. (2016): Insertion of the Biogenesis Factor Rei1 Probes the Ribosomal Tunnel during 60S Maturation. In: *Cell* 164 (1-2), S. 91–102. DOI: 10.1016/j.cell.2015.11.027.

Grünberg, Sebastian; Zentner, Gabriel E. (2017): Genome-wide Mapping of Protein-DNA Interactions with ChEC-seq in Saccharomyces cerevisiae. In: *Journal of visualized experiments : JoVE* (124). DOI: 10.3791/55836.

Gualerzi, Claudio O.; Pon, Cynthia L. (2015): Initiation of mRNA translation in bacteria: structural and dynamic aspects. In: *Cellular and molecular life sciences : CMLS* 72 (22), S. 4341–4367. DOI: 10.1007/s00018-015-2010-3.

Hall, Daniel B.; Wade, Joseph T.; Struhl, Kevin (2006): An HMG protein, Hmo1, associates with promoters of many ribosomal protein genes and throughout the rRNA gene locus in Saccharomyces

cerevisiae. In: *Molecular and cellular biology* 26 (9), S. 3672–3679. DOI: 10.1128/MCB.26.9.3672-3679.2006.

Harms, J.; Schluenzen, F.; Zarivach, R.; Bashan, A.; Gat, S.; Agmon, I. et al. (2001): High resolution structure of the large ribosomal subunit from a mesophilic eubacterium. In: *Cell* 107 (5), S. 679–688. DOI: 10.1016/s0092-8674(01)00546-3.

Hedges, John; West, Matthew; Johnson, Arlen W. (2005): Release of the export adapter, Nmd3p, from the 60S ribosomal subunit requires Rpl10p and the cytoplasmic GTPase Lsg1p. In: *The EMBO journal* 24 (3), S. 567–579. DOI: 10.1038/sj.emboj.7600547.

Henry, Y.; Wood, H.; Morrissey, J. P.; Petfalski, E.; Kearsey, S.; Tollervey, D. (1994): The 5' end of yeast 5.8S {rRNA} is generated by exonucleases from an upstream cleavage site. In: *The EMBO journal* 13 (10), 2452--2463.

Hernandez-Verdun, Danièle; Roussel, Pascal; Thiry, Marc; Sirri, Valentina; Lafontaine, Denis L. J. (2010): The nucleolus: structure/function relationship in {RNA} metabolism. In: *Wiley Interdisciplinary Reviews: RNA* 1 (3), 415--431. DOI: 10.1002/wrna.39.

Heuer, André; Thomson, Emma; Schmidt, Christian; Berninghausen, Otto; Becker, Thomas; Hurt, Ed; Beckmann, Roland (2017): Cryo-EM structure of a late pre-40S ribosomal subunit from Saccharomyces cerevisiae. In: *eLife* 6. DOI: 10.7554/eLife.30189.

Hierlmeier, Thomas; Merl, Juliane; Sauert, Martina; Perez-Fernandez, Jorge; Schultz, Patrick; Bruckmann, Astrid et al. (2012): Rrp5p, {Noc}1p and {Noc}2p form a protein module which is part of early large ribosomal subunit precursors in {S}. cerevisiae. In: *Nucleic Acids Research*. DOI: 10.1093/nar/gks1056.

Hinnebusch, Alan G. (2014): The scanning mechanism of eukaryotic translation initiation. In: *Annual Review of Biochemistry* 83, S. 779–812. DOI: 10.1146/annurev-biochem-060713-035802.

Hinnebusch, Alan G. (2017): Structural Insights into the Mechanism of Scanning and Start Codon Recognition in Eukaryotic Translation Initiation. In: *Trends in biochemical sciences* 42 (8), S. 589–611. DOI: 10.1016/j.tibs.2017.03.004.

Hitchen, J.; Ivakine, E.; Melekhovets, Y. F.; Lalev, A.; Nazar, R. N. (1997): Structural features in the 3' external transcribed spacer affecting intragenic processing of yeast rRNA. In: *Journal of molecular biology* 274 (4), S. 481–490. DOI: 10.1006/jmbi.1997.1376.

Ho, Jennifer Hei-Ngam; Kallstrom, George; Johnson, Arlen W. (2000): Nmd3p {Is} a {Crm}1p-{Dependent} {Adapter} {Protein} for {Nuclear} {Export} of the {Large} {Ribosomal} {Subunit}. In: *The Journal of Cell Biology* 151 (5), 1057--1066. DOI: 10.1083/jcb.151.5.1057.

Hoareau-Aveilla, Coralie; Fayet-Lebaron, Eléonore; Jády, Beáta E.; Henras, Anthony K.; Kiss, Tamás (2012): Utp23p is required for dissociation of {snR}30 small nucleolar {RNP} from preribosomal particles. In: *Nucleic Acids Research* 40 (8), 3641--3652. DOI: 10.1093/nar/gkr1213.

Hong, B.; Brockenbrough, J. S.; Wu, P.; Aris, J. P. (1997): Nop2p is required for pre-rRNA processing and 60S ribosome subunit synthesis in yeast. In: *Molecular and cellular biology* 17 (1), S. 378–388. DOI: 10.1128/mcb.17.1.378.

Horn, Darryl M.; Mason, Saundra L.; Karbstein, Katrin (2011): Rcl1 {Protein}, a {Novel} {Nuclease} for 18 {S} {Ribosomal} {RNA} {Production}. In: *Journal of Biological Chemistry* 286 (39), 34082--34087. DOI: 10.1074/jbc.M111.268649.

Horsey, Edward W.; Jakovljevic, Jelena; Miles, Tiffany D.; Harnpicharnchai, Piyanun; Woolford, John L. (2004): Role of the yeast Rrp1 protein in the dynamics of pre-ribosome maturation. In: *RNA* 10 (5), S. 813–827. DOI: 10.1261/rna.5255804.

Houseley, Jonathan; Tollervey, David (2009): The many pathways of {RNA} degradation. In: *Cell* 136 (4), 763--776. DOI: 10.1016/j.cell.2009.01.019.

Hsiao, Chiaolong; Mohan, Srividya; Kalahar, Benson K.; Williams, Loren Dean (2009): Peeling the onion: ribosomes are ancient molecular fossils. In: *Molecular biology and evolution* 26 (11), S. 2415–2425. DOI: 10.1093/molbev/msp163.

Hughes, J. M. (1996): Functional base-pairing interaction between highly conserved elements of {U}3 small nucleolar {RNA} and the small ribosomal subunit {RNA}. In: *Journal of molecular biology* 259 (4), 645--654. DOI: 10.1006/jmbi.1996.0346.

Hughes, J. M.; Ares, M. (1991): Depletion of U3 small nucleolar RNA inhibits cleavage in the 5' external transcribed spacer of yeast pre-ribosomal RNA and impairs formation of 18S ribosomal RNA. In: *The EMBO journal* 10 (13), S. 4231–4239.

Hung, Nai-Jung; Johnson, Arlen W. (2006): Nuclear {Recycling} of the {Pre}-60S {Ribosomal} {Subunit}-{Associated} {Factor} {Arx}1 {Depends} on {Rei}1 in {Saccharomyces} cerevisiae. In: *Molecular and cellular biology* 26 (10), 3718--3727. DOI: 10.1128/MCB.26.10.3718-3727.2006.

Hung, Nai-Jung; Lo, Kai-Yin; Patel, Samir S.; Helmke, Kara; Johnson, Arlen W. (2008): Arx1 {Is} a {Nuclear} {Export} {Receptor} for the 60S {Ribosomal} {Subunit} in {Yeast}. In: *Molecular Biology of the Cell* 19 (2), 735--744. DOI: 10.1091/mbc.E07-09-0968.

Hunziker, Mirjam; Barandun, Jonas; Petfalski, Elisabeth; Tan, Dongyan; Delan-Forino, Clémentine; Molloy, Kelly R. et al. (2016): UtpA and UtpB chaperone nascent pre-ribosomal RNA and U3 snoRNA to initiate eukaryotic ribosome assembly. In: *Nature communications* 7, S. 12090. DOI: 10.1038/ncomms12090.

Ide, Satoru; Miyazaki, Takaaki; Maki, Hisaji; Kobayashi, Takehiko (2010): Abundance of ribosomal {RNA} gene copies maintains genome integrity. In: *Science (New York, N.Y.)* 327 (5966), 693--696. DOI: 10.1126/science.1179044.

Jackson, Richard J.; Hellen, Christopher U. T.; Pestova, Tatyana V. (2010): The mechanism of eukaryotic translation initiation and principles of its regulation. In: *Nature reviews. Molecular cell biology* 11 (2), 113--127. DOI: 10.1038/nrm2838.

Jakob, Steffen; Ohmayer, Uli; Neueder, Andreas; Hierlmeier, Thomas; Perez-Fernandez, Jorge; Hochmuth, Eduard et al. (2012): Interrelationships between yeast ribosomal protein assembly events and transient ribosome biogenesis factors interactions in early pre-ribosomes. In: *PloS one* 7 (3), e32552. DOI: 10.1371/journal.pone.0032552.

Jakovljevic, Jelena; Ohmayer, Uli; Gamalinda, Michael; Talkish, Jason; Alexander, Lisa; Linnemann, Jan et al. (2012): Ribosomal proteins {L}7 and {L}8 function in concert with six {A}$_3$ assembly factors to propagate assembly of domains {I} and {II} of 25S {rRNA} in yeast 60S ribosomal subunits. In: *RNA (New York, N.Y.)* 18 (10), 1805--1822. DOI: 10.1261/rna.032540.112.

Jeeninga, R. E.; van Delft, Y.; Graaff-Vincent, M. de; Dirks-Mulder, A.; Venema, J.; Raué, H. A. (1997): Variable regions V13 and V3 of Saccharomyces cerevisiae contain structural features essential for normal biogenesis and stability of 5.8S and 25S rRNA. In: *RNA* 3 (5), S. 476–488.

Jia, Huijue; Wang, Xuying; Anderson, James T.; Jankowsky, Eckhard (2012): RNA unwinding by the Trf4/Air2/Mtr4 polyadenylation (TRAMP) complex. In: *Proceedings of the National Academy of Sciences of the United States of America* 109 (19), S. 7292–7297. DOI: 10.1073/pnas.1201085109.

Jia, Huijue; Wang, Xuying; Liu, Fei; Guenther, Ulf-Peter; Srinivasan, Sukanya; Anderson, James T.; Jankowsky, Eckhard (2011): The RNA helicase Mtr4p modulates polyadenylation in the TRAMP complex. In: *Cell* 145 (6), S. 890–901. DOI: 10.1016/j.cell.2011.05.010.

Joseph, N.; Krauskopf, E.; Vera, M. I.; Michot, B. (1999): Ribosomal internal transcribed spacer 2 (ITS2) exhibits a common core of secondary structure in vertebrates and yeast. In: *Nucleic Acids Research* 27 (23), S. 4533–4540. DOI: 10.1093/nar/27.23.4533.

Kappel, Lisa; Loibl, Mathias; Zisser, Gertrude; Klein, Isabella; Fruhmann, Gernot; Gruber, Christof et al. (2012): Rlp24 activates the {AAA}-{ATPase} {Drg}1 to initiate cytoplasmic pre-60S maturation. In: *The Journal of Cell Biology* 199 (5), 771--782. DOI: 10.1083/jcb.201205021.

Kater, Lukas; Mitterer, Valentin; Thoms, Matthias; Cheng, Jingdong; Berninghausen, Otto; Beckmann, Roland; Hurt, Ed (2020): Construction of the Central Protuberance and L1 Stalk during 60S Subunit Biogenesis. In: *Molecular cell*. DOI: 10.1016/j.molcel.2020.06.032.

Kater, Lukas; Thoms, Matthias; Barrio-Garcia, Clara; Cheng, Jingdong; Ismail, Sherif; Ahmed, Yasar Luqman et al. (2017): Visualizing the Assembly Pathway of Nucleolar Pre-60S Ribosomes. In: *Cell* 171 (7), 1599-1610.e14. DOI: 10.1016/j.cell.2017.11.039.

Keener, J.; Dodd, J. A.; Lalo, D.; Nomura, M. (1997): Histones {H}3 and {H}4 are components of upstream activation factor required for the high-level transcription of yeast {rDNA} by {RNA} polymerase {I}. In: *Proceedings of the National Academy of Sciences of the United States of America* 94 (25), 13458--13462.

Keener, J.; Josaitis, C. A.; Dodd, J. A.; Nomura, M. (1998): Reconstitution of yeast RNA polymerase I transcription in vitro from purified components. TATA-binding protein is not required for basal transcription. In: *Journal of Biological Chemistry* 273 (50), S. 33795–33802. DOI: 10.1074/jbc.273.50.33795.

Kemmler, Stefan; Occhipinti, Laura; Veisu, Maria; Panse, Vikram Govind (2009): Yvh1 is required for a late maturation step in the 60S biogenesis pathway. In: *The Journal of Cell Biology* 186 (6), 863--880. DOI: 10.1083/jcb.200904111.

Kertesz, Michael; Wan, Yue; Mazor, Elad; Rinn, John L.; Nutter, Robert C.; Chang, Howard Y.; Segal, Eran (2010): Genome-wide measurement of RNA secondary structure in yeast. In: *Nature* 467 (7311), S. 103–107. DOI: 10.1038/nature09322.

Keys, D. A.; Lee, B. S.; Dodd, J. A.; Nguyen, T. T.; Vu, L.; Fantino, E. et al. (1996): Multiprotein transcription factor {UAF} interacts with the upstream element of the yeast {RNA} polymerase {I} promoter and forms a stable preinitiation complex. In: *Genes \& development* 10 (7), 887--903.

Keys, D. A.; Vu, L.; Steffan, J. S.; Dodd, J. A.; Yamamoto, R. T.; Nogi, Y.; Nomura, M. (1994): RRN}6 and {RRN}7 encode subunits of a multiprotein complex essential for the initiation of {rDNA} transcription by {RNA} polymerase {I} in {Saccharomyces} cerevisiae. In: *Genes \& development* 8 (19), 2349--2362.

Kharde, Satyavati; Calviño, Fabiola R.; Gumiero, Andrea; Wild, Klemens; Sinning, Irmgard (2015): The structure of Rpf2-Rrs1 explains its role in ribosome biogenesis. In: *Nucleic Acids Research* 43 (14), S. 7083–7095. DOI: 10.1093/nar/gkv640.

Khoshnevis, Sohail; Askenasy, Isabel; Johnson, Matthew C.; Dattolo, Maria D.; Young-Erdos, Crystal L.; Stroupe, M. Elizabeth; Karbstein, Katrin (2016): The DEAD-box Protein Rok1 Orchestrates 40S and 60S Ribosome Assembly by Promoting the Release of Rrp5 from Pre-40S Ribosomes to Allow for 60S Maturation. In: *PLoS biology* 14 (6), e1002480. DOI: 10.1371/journal.pbio.1002480.

Khoshnevis, Sohail; Liu, Xin; Dattolo, Maria D.; Karbstein, Katrin (2019): Rrp5 establishes a checkpoint for 60S assembly during 40S maturation. In: *RNA (New York, N.Y.)* 25 (9), S. 1164–1176. DOI: 10.1261/rna.071225.119.

King, Thomas H.; Liu, Ben; McCully, Ryan R.; Fournier, Maurille J. (2003): Ribosome structure and activity are altered in cells lacking {snoRNPs} that form pseudouridines in the peptidyl transferase center. In: *Molecular cell* 11 (2), 425--435.

Kiparisov, Sergey; Petrov, Alexey; Meskauskas, Arturas; Sergiev, Petr V.; Dontsova, Olga A.; Dinman, Jonathan D. (2005): Structural and functional analysis of 5S rRNA in Saccharomyces cerevisiae. In: *Molecular genetics and genomics : MGG* 274 (3), S. 235–247. DOI: 10.1007/s00438-005-0020-9.

Kiss-László, Zsuzsanna; Henry, Yves; Bachellerie, Jean-Pierre; Caizergues-Ferrer, Michèle; Kiss, Tamás (1996): Site-Specific Ribose Methylation of Preribosomal RNA: A Novel Function for Small Nucleolar RNAs. In: *Cell* 85 (7), S. 1077–1088. DOI: 10.1016/S0092-8674(00)81308-2.

Klingauf-Nerurkar, Purnima; Gillet, Ludovic C.; Portugal-Calisto, Daniela; Oborská-Oplová, Michaela; Jäger, Martin; Schubert, Olga T. et al. (2020): The GTPase Nog1 co-ordinates the assembly, maturation and quality control of distant ribosomal functional centers. In: *eLife* 9. DOI: 10.7554/eLife.52474.

Klinge, Sebastian; Voigts-Hoffmann, Felix; Leibundgut, Marc; Arpagaus, Sofia; Ban, Nenad (2011): Crystal structure of the eukaryotic 60S ribosomal subunit in complex with initiation factor 6. In: *Science (New York, N.Y.)* 334 (6058), S. 941–948. DOI: 10.1126/science.1211204.

Klinge, Sebastian; Woolford, John L. (2019): Ribosome assembly coming into focus. In: *Nature Reviews Molecular Cell Biology* 20 (2), S. 116. DOI: 10.1038/s41580-018-0078-y.

Komoda, Taeko; Sato, Neuza S.; Phelps, Steven S.; Namba, Naoki; Joseph, Simpson; Suzuki, Tsutomu (2006): The A-site finger in 23 S rRNA acts as a functional attenuator for translocation. In: *Journal of Biological Chemistry* 281 (43), S. 32303–32309. DOI: 10.1074/jbc.M607058200.

Konikkat, Salini; Woolford, John L. (2017): Principles of 60S ribosomal subunit assembly emerging from recent studies in yeast. In: *The Biochemical journal* 474 (2), S. 195–214. DOI: 10.1042/BCJ20160516.

Kos, Martin; Tollervey, David (2005): The Putative RNA Helicase Dbp4p Is Required for Release of the U14 snoRNA from Preribosomes in Saccharomyces cerevisiae. In: *Molecular cell* 20 (1), S. 53–64. DOI: 10.1016/j.molcel.2005.08.022.

Kos, Martin; Tollervey, David (2010): Yeast pre-{rRNA} processing and modification occur cotranscriptionally. In: *Molecular cell* 37 (6), 809--820. DOI: 10.1016/j.molcel.2010.02.024.

Kos-Braun, Isabelle C.; Jung, Ilona; Koš, Martin (2017): Tor1 and CK2 kinases control a switch between alternative ribosome biogenesis pathways in a growth-dependent manner. In: *PLoS biology* 15 (3), e2000245. DOI: 10.1371/journal.pbio.2000245.

Kressler, Dieter; Bange, Gert; Ogawa, Yutaka; Stjepanovic, Goran; Bradatsch, Bettina; Pratte, Dagmar et al. (2012): Synchronizing nuclear import of ribosomal proteins with ribosome assembly. In: *Science (New York, N.Y.)* 338 (6107), S. 666–671. DOI: 10.1126/science.1226960.

Kressler, Dieter; Hurt, Ed; Baßler, Jochen (2017): A Puzzle of Life: Crafting Ribosomal Subunits. In: *Trends in biochemical sciences* 42 (8), S. 640–654. DOI: 10.1016/j.tibs.2017.05.005.

Kressler, Dieter; Roser, Daniela; Pertschy, Brigitte; Hurt, Ed (2008): The {AAA} {ATPase} {Rix}7 powers progression of ribosome biogenesis by stripping {Nsa}1 from pre-60S particles. In: *The Journal of Cell Biology* 181 (6), 935--944. DOI: 10.1083/jcb.200801181.

Krogan, Nevan J.; Peng, Wen-Tao; Cagney, Gerard; Robinson, Mark D.; Haw, Robin; Zhong, Gouqing et al. (2004): High-definition macromolecular composition of yeast {RNA}-processing complexes. In: *Molecular cell* 13 (2), 225--239. Online verfügbar unter http://www.ncbi.nlm.nih.gov/pubmed/14759368, zuletzt geprüft am 11.05.2012.

Kubota, Miles; Tran, Catherine; Spitale, Robert C. (2015): Progress and challenges for chemical probing of RNA structure inside living cells. In: *Nature chemical biology* 11 (12), S. 933–941. DOI: 10.1038/nchembio.1958.

Kudla, Grzegorz; Granneman, Sander; Hahn, Daniela; Beggs, Jean D.; Tollervey, David (2011): Cross-linking, ligation, and sequencing of hybrids reveals {RNA}-{RNA} interactions in yeast. In: *Proceedings of the National Academy of Sciences of the United States of America* 108 (24), 10010--10015. DOI: 10.1073/pnas.1017386108.

Kufel, J.; Dichtl, B.; Tollervey, D. (1999): Yeast Rnt1p is required for cleavage of the pre-ribosomal RNA in the 3' ETS but not the 5' ETS. In: *RNA* 5 (7), S. 909–917. DOI: 10.1017/s135583829999026x.

Kühlbrandt, Werner (2014): Biochemistry. The resolution revolution. In: *Science (New York, N.Y.)* 343 (6178), S. 1443–1444. DOI: 10.1126/science.1251652.

Kühn, Holger; Hierlmeier, Thomas; Merl, Juliane; Jakob, Steffen; Aguissa-Touré, Almass-Houd; Milkereit, Philipp; Tschochner, Herbert (2009): The {Noc}-domain containing {C}-terminus of {Noc}4p mediates both formation of the {Noc}4p-{Nop}14p submodule and its incorporation into the {SSU} processome. In: *PloS one* 4 (12), e8370. DOI: 10.1371/journal.pone.0008370.

Kulkens, T.; Riggs, D. L.; Heck, J. D.; Planta, R. J.; Nomura, M. (1991): The yeast {RNA} polymerase {I} promoter: ribosomal {DNA} sequences involved in transcription initiation and complex formation in vitro. In: *Nucleic Acids Research* 19 (19), 5363--5370.

Kwok, Chun Kit; Tang, Yin; Assmann, Sarah M.; Bevilacqua, Philip C. (2015): The RNA structurome: transcriptome-wide structure probing with next-generation sequencing. In: *Trends in biochemical sciences* 40 (4), S. 221–232. DOI: 10.1016/j.tibs.2015.02.005.

La Cruz, J. de; Kressler, D.; Tollervey, D.; Linder, P. (1998): Dob1p (Mtr4p) is a putative ATP-dependent RNA helicase required for the 3' end formation of 5.8S rRNA in Saccharomyces cerevisiae. In: *The EMBO journal* 17 (4), S. 1128–1140. DOI: 10.1093/emboj/17.4.1128.

La Cruz, Jesus de; Karbstein, Katrin; Woolford, John L. (2015): Functions of ribosomal proteins in assembly of eukaryotic ribosomes in vivo. In: *Annual Review of Biochemistry* 84, S. 93–129. DOI: 10.1146/annurev-biochem-060614-033917.

La Cruz, Jesús de; Gómez-Herreros, Fernando; Rodríguez-Galán, Olga; Begley, Victoria; La Cruz Muñoz-Centeno, María de; Chávez, Sebastián (2018): Feedback regulation of ribosome assembly. In: *Current genetics* 64 (2), S. 393–404. DOI: 10.1007/s00294-017-0764-x.

La Cruz, Jesús de; Lacombe, Thierry; Deloche, Olivier; Linder, Patrick; Kressler, Dieter (2004): The putative RNA helicase Dbp6p functionally interacts with Rpl3p, Nop8p and the novel trans-acting Factor Rsa3p during biogenesis of 60S ribosomal subunits in Saccharomyces cerevisiae. In: *Genetics* 166 (4), S. 1687–1699. DOI: 10.1534/genetics.166.4.1687.

LaCava, John; Houseley, Jonathan; Saveanu, Cosmin; Petfalski, Elisabeth; Thompson, Elizabeth; Jacquier, Alain; Tollervey, David (2005): RNA} {Degradation} by the {Exosome} {Is} {Promoted} by a {Nuclear} {Polyadenylation} {Complex}. In: *Cell* 121 (5), 713--724. DOI: 10.1016/j.cell.2005.04.029.

Lackmann, Fredrik; Belikov, Sergey; Burlacu, Elena; Granneman, Sander; Wieslander, Lars (2018): Maturation of the 90S pre-ribosome requires Mrd1 dependent U3 snoRNA and 35S pre-rRNA structural rearrangements. In: *Nucleic Acids Research* 46 (7), S. 3692–3706. DOI: 10.1093/nar/gky036.

Lafontaine, D. L.; Bousquet-Antonelli, C.; Henry, Y.; Caizergues-Ferrer, M.; Tollervey, D. (1998): The box H + ACA snoRNAs carry Cbf5p, the putative rRNA pseudouridine synthase. In: *Genes \& development* 12 (4), S. 527–537. DOI: 10.1101/gad.12.4.527.

Lalo, D.; Steffan, J. S.; Dodd, J. A.; Nomura, M. (1996): RRN}11 encodes the third subunit of the complex containing {Rrn}6p and {Rrn}7p that is essential for the initiation of {rDNA} transcription by yeast {RNA} polymerase {I}. In: *Journal of Biological Chemistry* 271 (35), 21062--21067.

Lamanna, Allison C.; Karbstein, Katrin (2009): Nob1 binds the single-stranded cleavage site {D} at the 3'-end of 18S {rRNA} with its {PIN} domain. In: *Proceedings of the National Academy of Sciences of the United States of America* 106 (34), 14259--14264. DOI: 10.1073/pnas.0905403106.

Lebaron, Simon; Schneider, Claudia; van Nues, Robert W.; Swiatkowska, Agata; Walsh, Dietrich; Böttcher, Bettina et al. (2012): Proofreading of pre-40S ribosome maturation by a translation initiation factor and 60S subunits. In: *Nature structural \& molecular biology* 19 (8), 744--753. DOI: 10.1038/nsmb.2308.

Lebaron, Simon; Segerstolpe, Asa; French, Sarah L.; Dudnakova, Tatiana; Lima Alves, Flavia de; Granneman, Sander et al. (2013): Rrp5 binding at multiple sites coordinates pre-rRNA processing and assembly. In: *Molecular cell* 52 (5), S. 707–719. DOI: 10.1016/j.molcel.2013.10.017.

Lebreton, Alice; Rousselle, Jean-Claude; Lenormand, Pascal; Namane, Abdelkader; Jacquier, Alain; Fromont-Racine, Micheline; Saveanu, Cosmin (2008a): 60S ribosomal subunit assembly dynamics defined by semi-quantitative mass spectrometry of purified complexes. In: *Nucleic Acids Research* 36 (15), 4988--4999. DOI: 10.1093/nar/gkn469.

Lebreton, Alice; Tomecki, Rafal; Dziembowski, Andrzej; Séraphin, Bertrand (2008b): Endonucleolytic {RNA} cleavage by a eukaryotic exosome. In: *Nature* 456 (7224), 993--996. DOI: 10.1038/nature07480.

Lee, S. J.; Baserga, S. J. (1999): Imp3p and Imp4p, two specific components of the U3 small nucleolar ribonucleoprotein that are essential for pre-18S rRNA processing. In: *Molecular and cellular biology* 19 (8), S. 5441–5452. DOI: 10.1128/mcb.19.8.5441.

Léger-Silvestre, I.; Trumtel, S.; Noaillac-Depeyre, J.; Gas, N. (1999): Functional compartmentalization of the nucleus in the budding yeast {Saccharomyces} cerevisiae. In: *Chromosoma* 108 (2), 103--113.

Leidig, Christoph; Thoms, Matthias; Holdermann, Iris; Bradatsch, Bettina; Berninghausen, Otto; Bange, Gert et al. (2014): 60S ribosome biogenesis requires rotation of the 5S ribonucleoprotein particle. In: *Nature communications* 5, S. 3491. DOI: 10.1038/ncomms4491.

Li, H. D.; Zagorski, J.; Fournier, M. J. (1990): Depletion of {U}14 small nuclear {RNA} ({snR}128) disrupts production of 18S {rRNA} in {Saccharomyces} cerevisiae. In: *Molecular and cellular biology* 10 (3), 1145--1152.

Liang, W. Q.; Fournier, M. J. (1995): U14 base-pairs with 18S {rRNA}: a novel {snoRNA} interaction required for {rRNA} processing. In: *Genes \& development* 9 (19), 2433--2443.

Liang, Xiaomeng; Zuo, Mei-Qing; Zhang, Yunyang; Li, Ningning; Ma, Chengying; Dong, Meng-Qiu; Gao, Ning (2020): Structural snapshots of human pre-60S ribosomal particles before and after nuclear export. In: *Nature communications* 11 (1), S. 3542. DOI: 10.1038/s41467-020-17237-x.

Liang, Xue-hai; Liu, Qing; Fournier, Maurille J. (2007): rRNA} modifications in an intersubunit bridge of the ribosome strongly affect both ribosome biogenesis and activity. In: *Molecular cell* 28 (6), 965--977. DOI: 10.1016/j.molcel.2007.10.012.

Liang, Xue-hai; Liu, Qing; Fournier, Maurille J. (2009): Loss of {rRNA} modifications in the decoding center of the ribosome impairs translation and strongly delays pre-{rRNA} processing. In: *RNA* 15 (9), 1716--1728. DOI: 10.1261/rna.1724409.

Lin, C. W.; Moorefield, B.; Payne, J.; Aprikian, P.; Mitomo, K.; Reeder, R. H. (1996): A novel 66-kilodalton protein complexes with Rrn6, Rrn7, and TATA-binding protein to promote polymerase I transcription initiation in Saccharomyces cerevisiae. In: *Molecular and cellular biology* 16 (11), S. 6436–6443. DOI: 10.1128/mcb.16.11.6436.

Lin, Jinzhong; Lu, Jing; Feng, Yingang; Sun, Mengyi; Ye, Keqiong (2013): An RNA-binding complex involved in ribosome biogenesis contains a protein with homology to tRNA CCA-adding enzyme. In: *PLoS biology* 11 (10), e1001669. DOI: 10.1371/journal.pbio.1001669.

Lindahl, L.; Archer, R. H.; Zengel, J. M. (1992): A new rRNA processing mutant of Saccharomyces cerevisiae. In: *Nucleic Acids Research* 20 (2), S. 295–301. DOI: 10.1093/nar/20.2.295.

Linnemann, Jan; Pöll, Gisela; Jakob, Steffen; Ferreira-Cerca, Sébastien; Griesenbeck, Joachim; Tschochner, Herbert; Milkereit, Philipp (2019): Impact of two neighbouring ribosomal protein clusters on biogenesis factor binding and assembly of yeast late small ribosomal subunit precursors. In: *PloS one* 14 (1), e0203415. DOI: 10.1371/journal.pone.0203415.

Liu, Quansheng; Greimann, Jaclyn C.; Lima, Christopher D. (2006): Reconstitution, activities, and structure of the eukaryotic RNA exosome. In: *Cell* 127 (6), S. 1223–1237. DOI: 10.1016/j.cell.2006.10.037.

Lo, Kai-Yin; Li, Zhihua; Bussiere, Cyril; Bresson, Stefan; Marcotte, Edward M.; Johnson, Arlen W. (2010): Defining the pathway of cytoplasmic maturation of the 60S ribosomal subunit. In: *Molecular cell* 39 (2), 196--208. DOI: 10.1016/j.molcel.2010.06.018.

Lo, Kai-Yin; Li, Zhihua; Wang, Feng; Marcotte, Edward M.; Johnson, Arlen W. (2009): Ribosome stalk assembly requires the dual-specificity phosphatase {Yvh}1 for the exchange of {Mrt}4 with {P}0. In: *The Journal of Cell Biology* 186 (6), 849--862. DOI: 10.1083/jcb.200904110.

Long, Eric O.; Dawid, Igor B. (1980): Repeated {Genes} in {Eukaryotes}. In: *Annual Review of Biochemistry* 49 (1), 727--764. DOI: 10.1146/annurev.bi.49.070180.003455.

Luviano, Axel; Cruz-Castañeda, Roberto; Sánchez-Puig, Nuria; García-Hernández, Enrique (2019): Cooperative energetic effects elicited by the yeast Shwachman-Diamond syndrome protein (Sdo1) and guanine nucleotides modulate the complex conformational landscape of the elongation factor-like 1 (Efl1) GTPase. In: *Biophysical chemistry* 247, S. 13–24. DOI: 10.1016/j.bpc.2019.02.003.

Lygerou, Z.; Allmang, C.; Tollervey, D.; Séraphin, B. (1996): Accurate processing of a eukaryotic precursor ribosomal {RNA} by ribonuclease {MRP} in vitro. In: *Science (New York, N.Y.)* 272 (5259), 268--270.

Ma, Chengying; Wu, Shan; Li, Ningning; Chen, Yan; Yan, Kaige; Li, Zhifei et al. (2017): Structural snapshot of cytoplasmic pre-60S ribosomal particles bound by Nmd3, Lsg1, Tif6 and Reh1. In: *Nature Structural & Molecular Biology* 24 (3), S. 214–220. DOI: 10.1038/nsmb.3364.

Madru, Clément; Lebaron, Simon; Blaud, Magali; Delbos, Lila; Pipoli, Juliana; Pasmant, Eric et al. (2015): Chaperoning 5S RNA assembly. In: *Genes & development* 29 (13), S. 1432–1446. DOI: 10.1101/gad.260349.115.

Malyutin, Andrey G.; Musalgaonkar, Sharmishtha; Patchett, Stephanie; Frank, Joachim; Johnson, Arlen W. (2017): Nmd3 is a structural mimic of eIF5A, and activates the cpGTPase Lsg1 during 60S ribosome biogenesis. In: *The EMBO journal* 36 (7), S. 854–868. DOI: 10.15252/embj.201696012.

Marmier-Gourrier, Nathalie; Cléry, Antoine; Schlotter, Florence; Senty-Ségault, Véronique; Branlant, Christiane (2011): A second base pair interaction between U3 small nucleolar RNA and the 5'-ETS

region is required for early cleavage of the yeast pre-ribosomal RNA. In: *Nucleic Acids Research* 39 (22), S. 9731–9745. DOI: 10.1093/nar/gkr675.

Matsuo, Yoshitaka; Granneman, Sander; Thoms, Matthias; Manikas, Rizos-Georgios; Tollervey, David; Hurt, Ed (2014): Coupled GTPase and remodelling ATPase activities form a checkpoint for ribosome export. In: *Nature* 505 (7481), S. 112–116. DOI: 10.1038/nature12731.

McCann, Kathleen L.; Charette, J. Michael; Vincent, Nicholas G.; Baserga, Susan J. (2015): A protein interaction map of the LSU processome. In: *Genes & development* 29 (8), S. 862–875. DOI: 10.1101/gad.256370.114.

McCaughan, Urszula M.; Jayachandran, Uma; Shchepachev, Vadim; Chen, Zhuo Angel; Rappsilber, Juri; Tollervey, David; Cook, Atlanta G. (2016): Pre-40S ribosome biogenesis factor Tsr1 is an inactive structural mimic of translational GTPases. In: *Nature communications* 7, S. 11789. DOI: 10.1038/ncomms11789.

McMahon, Aoife C.; Rahman, Reazur; Jin, Hua; Shen, James L.; Fieldsend, Allegra; Luo, Weifei; Rosbash, Michael (2016): TRIBE: Hijacking an RNA-Editing Enzyme to Identify Cell-Specific Targets of RNA-Binding Proteins. In: *Cell* 165 (3), S. 742–753. DOI: 10.1016/j.cell.2016.03.007.

Melnikov, Sergey; Ben-Shem, Adam; Garreau de Loubresse, Nicolas; Jenner, Lasse; Yusupova, Gulnara; Yusupov, Marat (2012): One core, two shells: bacterial and eukaryotic ribosomes. In: *Nature Structural & Molecular Biology* 19 (6), S. 560–567. DOI: 10.1038/nsmb.2313.

Méreau, A.; Fournier, R.; Grégoire, A.; Mougin, A.; Fabrizio, P.; Lührmann, R.; Branlant, C. (1997): An in vivo and in vitro structure-function analysis of the {Saccharomyces} cerevisiae {U}3A {snoRNP}: protein-{RNA} contacts and base-pair interaction with the pre-ribosomal {RNA}. In: *Journal of molecular biology* 273 (3), 552--571. DOI: 10.1006/jmbi.1997.1320.

Merz, Katharina; Hondele, Maria; Goetze, Hannah; Gmelch, Katharina; Stoeckl, Ulrike; Griesenbeck, Joachim (2008): Actively transcribed {rRNA} genes in {S}. cerevisiae are organized in a specialized chromatin associated with the high-mobility group protein {Hmo}1 and are largely devoid of histone molecules. In: *Genes \& development* 22 (9), 1190--1204. DOI: 10.1101/gad.466908.

Meyer, Alison E.; Hoover, Lindsey A.; Craig, Elizabeth A. (2010): The {Cytosolic} {J}-protein, {Jjj}1, and {Rei}1 {Function} in the {Removal} of the {Pre}-60 {S} {Subunit} {Factor} {Arx}1. In: *Journal of Biological Chemistry* 285 (2), 961--968. DOI: 10.1074/jbc.M109.038349.

Meyer, Alison E.; Hung, Nai-Jung; Yang, Peizhen; Johnson, Arlen W.; Craig, Elizabeth A. (2007): The specialized cytosolic J-protein, Jjj1, functions in 60S ribosomal subunit biogenesis. In: *Proceedings of the National Academy of Sciences of the United States of America* 104 (5), S. 1558–1563. DOI: 10.1073/pnas.0610704104.

Miles, Tiffany D.; Jakovljevic, Jelena; Horsey, Edward W.; Harnpicharnchai, Piyanun; Tang, Lan; Woolford, Jr, John L (2005): Ytm1, {Nop}7, and {Erb}1 form a complex necessary for maturation of yeast 66S preribosomes. In: *Molecular and cellular biology* 25 (23), 10419--10432. DOI: 10.1128/MCB.25.23.10419-10432.2005.

Milkereit, P.; Gadal, O.; Podtelejnikov, A.; Trumtel, S.; Gas, N.; Petfalski, E. et al. (2001): Maturation and intranuclear transport of pre-ribosomes requires {Noc} proteins. In: *Cell* 105 (4), 499--509. Online verfügbar unter http://www.ncbi.nlm.nih.gov/pubmed/11371346, zuletzt geprüft am 11.05.2012.

Milkereit, P.; Tschochner, H. (1998): A specialized form of {RNA} polymerase {I}, essential for initiation and growth-dependent regulation of {rRNA} synthesis, is disrupted during transcription. In: *The EMBO journal* 17 (13), 3692--3703. DOI: 10.1093/emboj/17.13.3692.

Milkereit, Philipp; Strauss, Daniela; Bassler, Jochen; Gadal, Olivier; Kühn, Holger; Schütz, Sylvia et al. (2003): A {Noc} complex specifically involved in the formation and nuclear export of ribosomal 40 {S} subunits. In: *Journal of Biological Chemistry* 278 (6), 4072--4081. DOI: 10.1074/jbc.M208898200.

Miller, O. L.; Beatty, Barbara R. (1969): Visualization of {Nucleolar} {Genes}. In: *Science (New York, N.Y.)* 164 (3882), 955--957. DOI: 10.1126/science.164.3882.955.

Mitchell, David; Assmann, Sarah M.; Bevilacqua, Philip C. (2019): Probing RNA structure in vivo. In: *Current Opinion in Structural Biology* 59, S. 151–158. DOI: 10.1016/j.sbi.2019.07.008.

Mitchell, P.; Petfalski, E.; Tollervey, D. (1996): The 3' end of yeast 5.8S rRNA is generated by an exonuclease processing mechanism. In: *Genes \& development* 10 (4), S. 502–513. DOI: 10.1101/gad.10.4.502.

Mitterer, Valentin; Murat, Guillaume; Réty, Stéphane; Blaud, Magali; Delbos, Lila; Stanborough, Tamsyn et al. (2016): Sequential domain assembly of ribosomal protein S3 drives 40S subunit maturation. In: *Nature communications* 7, S. 10336. DOI: 10.1038/ncomms10336.

Mitterer, Valentin; Shayan, Ramtin; Ferreira-Cerca, Sébastien; Murat, Guillaume; Enne, Tanja; Rinaldi, Dana et al. (2019): Conformational proofreading of distant 40S ribosomal subunit maturation events by a long-range communication mechanism. In: *Nature communications* 10 (1), S. 2754. DOI: 10.1038/s41467-019-10678-z.

Montgomery, Tho S. H. (1898): Comparative cytological studies, with especial regard to the morphology of the nucleolus. In: *J. Morphol.* 15 (2), S. 265–582. DOI: 10.1002/jmor.1050150204.

Morrissey, J. P.; Tollervey, D. (1993): Yeast {snR}30 is a small nucleolar {RNA} required for 18S {rRNA} synthesis. In: *Molecular and cellular biology* 13 (4), 2469--2477. Online verfügbar unter http://www.ncbi.nlm.nih.gov/pmc/articles/PMC359567/, zuletzt geprüft am 14.12.2012.

Mougey, E. B.; O'Reilly, M.; Osheim, Y.; Miller, O. L.; Beyer, A.; Sollner-Webb, B. (1993): The terminal balls characteristic of eukaryotic rRNA transcription units in chromatin spreads are rRNA processing complexes. In: *Genes \& development* 7 (8), S. 1609–1619. DOI: 10.1101/gad.7.8.1609.

Musalgaonkar, Sharmishtha; Black, Joshua J.; Johnson, Arlen W. (2019): The L1 stalk is required for efficient export of nascent large ribosomal subunits in yeast. In: *RNA (New York, N.Y.)* 25 (11), S. 1549–1560. DOI: 10.1261/rna.071811.119.

Musters, W.; Knol, J.; Maas, P.; Dekker, A. F.; van Heerikhuizen, H.; Planta, R. J. (1989): Linker scanning of the yeast {RNA} polymerase {I} promoter. In: *Nucleic Acids Research* 17 (23), 9661--9678.

Nariai, Masanobu; Tanaka, Tomohisa; Okada, Takafumi; Shirai, Chiharu; Horigome, Chihiro; Mizuta, Keiko (2005): Synergistic defect in 60S ribosomal subunit assembly caused by a mutation of Rrs1p, a ribosomal protein L11-binding protein, and 3'-extension of 5S rRNA in Saccharomyces cerevisiae. In: *Nucleic Acids Research* 33 (14), S. 4553–4562. DOI: 10.1093/nar/gki772.

Németh, Attila; Perez-Fernandez, Jorge; Merkl, Philipp; Hamperl, Stephan; Gerber, Jochen; Griesenbeck, Joachim; Tschochner, Herbert (2013): RNA polymerase I termination: Where is the end? In: *Biochimica et biophysica acta* 1829 (3-4), S. 306–317. DOI: 10.1016/j.bbagrm.2012.10.007.

Nerurkar, Purnima; Altvater, Martin; Gerhardy, Stefan; Schütz, Sabina; Fischer, Ute; Weirich, Christine; Panse, Vikram Govind (2015): Eukaryotic Ribosome Assembly and Nuclear Export. In: *International review of cell and molecular biology* 319, S. 107–140. DOI: 10.1016/bs.ircmb.2015.07.002.

Nerurkar, Purnima; Gillet, Ludovic; Pena, Cohue; Schubert, Olga T.; Altvater, Martin; Chang, Yiming et al. (2018): The GTPase Nog1 couples polypeptide exit tunnel quality control with ribosomal stalk assembly.

Neyer, Simon; Kunz, Michael; Geiss, Christian; Hantsche, Merle; Hodirnau, Victor-Valentin; Seybert, Anja et al. (2016): Structure of RNA polymerase I transcribing ribosomal DNA genes. In: *Nature* 540 (7634), S. 607–610. DOI: 10.1038/nature20561.

Ni, J.; Tien, A. L.; Fournier, M. J. (1997): Small nucleolar {RNAs} direct site-specific synthesis of pseudouridine in ribosomal {RNA}. In: *Cell* 89 (4), 565--573.

Nissen, P.; Hansen, J.; Ban, N.; Moore, P. B.; Steitz, T. A. (2000): The structural basis of ribosome activity in peptide bond synthesis. In: *Science (New York, N.Y.)* 289 (5481), S. 920–930. DOI: 10.1126/science.289.5481.920.

Oeffinger, Marlene; Leung, Anthony; Lamond, Angus; Tollervey, David; Lueng, Anthony (2002): Yeast {Pescadillo} is required for multiple activities during 60S ribosomal subunit synthesis. In: *RNA* 8 (5), 626--636. Online verfügbar unter http://www.ncbi.nlm.nih.gov/pubmed/12022229, zuletzt geprüft am 11.05.2012.

Oeffinger, Marlene; Tollervey, David (2003): Yeast {Nop}15p is an {RNA}-binding protein required for pre-{rRNA} processing and cytokinesis. In: *The EMBO journal* 22 (24), 6573--6583. DOI: 10.1093/emboj/cdg616.

Oeffinger, Marlene; Zenklusen, Daniel; Ferguson, Angelica; Wei, Karen E.; El Hage, Aziz; Tollervey, David et al. (2009): Rrp17p is a eukaryotic exonuclease required for 5' end processing of {Pre}-60S ribosomal {RNA}. In: *Molecular cell* 36 (5), 768--781. DOI: 10.1016/j.molcel.2009.11.011.

Ohmayer, Uli; Gamalinda, Michael; Sauert, Martina; Ossowski, Julius; Pöll, Gisela; Linnemann, Jan et al. (2013): Studies on the Assembly Characteristics of Large Subunit Ribosomal Proteins in S. cerevisae. In: *PloS one* 8 (7). DOI: 10.1371/journal.pone.0068412.

Ohmayer, Uli; Gil-Hernández, Álvaro; Sauert, Martina; Martín-Marcos, Pilar; Tamame, Mercedes; Tschochner, Herbert et al. (2015): Studies on the Coordination of Ribosomal Protein Assembly Events Involved in Processing and Stabilization of Yeast Early Large Ribosomal Subunit Precursors. In: *PloS one* 10 (12), e0143768. DOI: 10.1371/journal.pone.0143768.

Ohmayer, Uli; Perez-Fernandez, Jorge; Hierlmeier, Thomas; Pöll, Gisela; Williams, Lydia; Griesenbeck, Joachim et al. (2012): Local tertiary structure probing of ribonucleoprotein particles by nuclease fusion proteins. In: *PloS one* 7 (8), e42449. DOI: 10.1371/journal.pone.0042449.

Ohmayer, Uli (2014): Studies on the assembly process of large subunit ribosomal proteins in *S. cerevisiae*. PhD Thesis

Osheim, Yvonne N.; French, Sarah L.; Keck, Kristin M.; Champion, Erica A.; Spasov, Krasimir; Dragon, François et al. (2004): Pre-18S ribosomal {RNA} is structurally compacted into the {SSU} processome prior to being cleaved from nascent transcripts in {Saccharomyces} cerevisiae. In: *Molecular cell* 16 (6), 943--954. DOI: 10.1016/j.molcel.2004.11.031.

Parker, Melissa D.; Collins, Jason C.; Korona, Boguslawa; Ghalei, Homa; Karbstein, Katrin (2019): A kinase-dependent checkpoint prevents escape of immature ribosomes into the translating pool. In: *PLoS biology* 17 (12), e3000329. DOI: 10.1371/journal.pbio.3000329.

Parnell, K. Mark; Bass, Brenda L. (2009): Functional redundancy of yeast proteins Reh1 and Rei1 in cytoplasmic 60S subunit maturation. In: *Molecular and cellular biology* 29 (14), S. 4014–4023. DOI: 10.1128/MCB.01582-08.

Peattie, D. A.; Gilbert, W. (1980): Chemical probes for higher-order structure in RNA. In: *Proceedings of the National Academy of Sciences of the United States of America* 77 (8), S. 4679–4682. DOI: 10.1073/pnas.77.8.4679.

Peña, Cohue; Hurt, Ed; Panse, Vikram Govind (2017): Eukaryotic ribosome assembly, transport and quality control. In: *Nature Structural & Molecular Biology* 24 (9), S. 689–699. DOI: 10.1038/nsmb.3454.

Penev, Petar I.; Fakhretaha-Aval, Sara; Patel, Vaishnavi J.; Cannone, Jamie J.; Gutell, Robin R.; Petrov, Anton S. et al. (2019): Supersized ribosomal RNA expansion segments in Asgard archaea (41).

Pérez-Fernández, Jorge; Martín-Marcos, Pilar; Dosil, Mercedes (2011): Elucidation of the assembly events required for the recruitment of {Utp}20, {Imp}4 and {Bms}1 onto nascent pre-ribosomes. In: *Nucleic Acids Research* 39 (18), 8105--8121. DOI: 10.1093/nar/gkr508.

Pérez-Fernández, Jorge; Román, Angel; Las Rivas, Javier de; Bustelo, Xosé R.; Dosil, Mercedes (2007): The 90S preribosome is a multimodular structure that is assembled through a hierarchical mechanism. In: *Molecular and cellular biology* 27 (15), 5414--5429. DOI: 10.1128/MCB.00380-07.

Pertschy, Brigitte; Saveanu, Cosmin; Zisser, Gertrude; Lebreton, Alice; Tengg, Martin; Jacquier, Alain et al. (2007): Cytoplasmic recycling of 60S preribosomal factors depends on the AAA protein Drg1. In: *Molecular and cellular biology* 27 (19), S. 6581–6592. DOI: 10.1128/MCB.00668-07.

Pertschy, Brigitte; Schneider, Claudia; Gnädig, Marén; Schäfer, Thorsten; Tollervey, David; Hurt, Ed (2009): RNA} helicase {Prp}43 and its co-factor {Pfa}1 promote 20 to 18 {S} {rRNA} processing catalyzed by the endonuclease {Nob}1. In: *The Journal of biological chemistry* 284 (50), 35079--35091. DOI: 10.1074/jbc.M109.040774.

Pestov, D. G.; Stockelman, M. G.; Strezoska, Z.; Lau, L. F. (2001): ERB1, the yeast homolog of mammalian Bop1, is an essential gene required for maturation of the 25S and 5.8S ribosomal RNAs. In: *Nucleic Acids Research* 29 (17), S. 3621–3630. DOI: 10.1093/nar/29.17.3621.

Petes, T. D. (1979): Yeast ribosomal DNA genes are located on chromosome XII. In: *Proceedings of the National Academy of Sciences of the United States of America* 76 (1), S. 410–414. DOI: 10.1073/pnas.76.1.410.

Petes, T. D.; Botstein, D. (1977): Simple Mendelian inheritance of the reiterated ribosomal DNA of yeast. In: *Proceedings of the National Academy of Sciences of the United States of America* 74 (11), S. 5091–5095. DOI: 10.1073/pnas.74.11.5091.

Peyroche, G.; Milkereit, P.; Bischler, N.; Tschochner, H.; Schultz, P.; Sentenac, A. et al. (2000): The recruitment of {RNA} polymerase {I} on {rDNA} is mediated by the interaction of the {A}43 subunit with {Rrn}3. In: *The EMBO journal* 19 (20), 5473--5482. DOI: 10.1093/emboj/19.20.5473.

Philippsen, Peter; Thomas, Marjorie; Kramer, Richard A.; Davis, Ronald W. (1978): Unique arrangement of coding sequences for 5 S, 5.8 S, 18 S and 25 S ribosomal RNA in Saccharomyces cerevisiae as determined by R-loop and hybridization analysis. In: *Journal of molecular biology* 123 (3), S. 387–404. DOI: 10.1016/0022-2836(78)90086-4.

Pilsl, Michael; Engel, Christoph (2020): Structural basis of RNA polymerase I pre-initiation complex formation and promoter melting. In: *Nature communications* 11 (1), S. 1206. DOI: 10.1038/s41467-020-15052-y.

Pöll, Gisela; Braun, Tobias; Jakovljevic, Jelena; Neueder, Andreas; Jakob, Steffen; Woolford, Jr, John L et al. (2009): rRNA} maturation in yeast cells depleted of large ribosomal subunit proteins. In: *PloS one* 4 (12), e8249. DOI: 10.1371/journal.pone.0008249.

Pöll, Gisela; Müller, Christian; Bodden, Malena; Teubl, Fabian; Eichner, Norbert; Lehmann, Gerhard et al. (2017): Structural transitions during large ribosomal subunit maturation analyzed by tethered nuclease structure probing in S. cerevisiae. In: *PloS one* 12 (7), e0179405. DOI: 10.1371/journal.pone.0179405.

Rabl, Julius; Leibundgut, Marc; Ataide, Sandro F.; Haag, Andrea; Ban, Nenad (2011): Crystal structure of the eukaryotic 40S ribosomal subunit in complex with initiation factor 1. In: *Science (New York, N.Y.)* 331 (6018), S. 730–736. DOI: 10.1126/science.1198308.

Ramesh, Madhumitha; Woolford, John L. (2016): Eukaryote-specific rRNA expansion segments function in ribosome biogenesis. In: *RNA (New York, N.Y.)* 22 (8), S. 1153–1162. DOI: 10.1261/rna.056705.116.

Raška, Ivan; Shaw, Peter J.; Cmarko, Dušan (2006): Structure and function of the nucleolus in the spotlight. In: *Current opinion in cell biology* 18 (3), 325--334. DOI: 10.1016/j.ceb.2006.04.008.

Reeves, Raymond (1984): Transcriptionally active chromatin. In: *Biochimica et Biophysica Acta (BBA) - Gene Structure and Expression* 782 (4), S. 343–393. DOI: 10.1016/0167-4781(84)90044-7.

Retèl, J.; van den Bos, R. C.; Planta, R. J. (1969): Characteristics of the methylation in vivo of ribosomal RNA in yeast. In: *Biochimica et Biophysica Acta (BBA) - Nucleic Acids and Protein Synthesis* 195 (2), S. 370–380. DOI: 10.1016/0005-2787(69)90643-1.

Richard B. Roberts (Hg.) (1958): Microsomal Particles and Protein Synthesis. First Symposium of the Biophysical Society. Unter Mitarbeit von Richard B. Roberts. Massachusetts Institute of Technology, 5.-6.8.

Rigaut, G.; Shevchenko, A.; Rutz, B.; Wilm, M.; Mann, M.; Séraphin, B. (1999): A generic protein purification method for protein complex characterization and proteome exploration. In: *Nature biotechnology* 17 (10), 1030--1032. DOI: 10.1038/13732.

Rodnina, Marina V. (2016): The ribosome in action: Tuning of translational efficiency and protein folding. In: *Protein science : a publication of the Protein Society* 25 (8), S. 1390–1406. DOI: 10.1002/pro.2950.

Rodríguez-Galán, Olga; García-Gómez, Juan J.; Kressler, Dieter; La Cruz, Jesús de (2015): Immature large ribosomal subunits containing the 7S pre-rRNA can engage in translation in Saccharomyces cerevisiae. In: *RNA biology* 12 (8), S. 838–846. DOI: 10.1080/15476286.2015.1058477.

Rodríguez-Galán, Olga; García-Gómez, Juan José; La Cruz, Jesús de (2013): Yeast and human RNA helicases involved in ribosome biogenesis: current status and perspectives. In: *Biochimica et biophysica acta* 1829 (8), S. 775–790. DOI: 10.1016/j.bbagrm.2013.01.007.

Rodríguez-Mateos, María; Abia, David; García-Gómez, Juan J.; Morreale, Antonio; La Cruz, Jesús de; Santos, Cruz et al. (2009a): The amino terminal domain from {Mrt}4 protein can functionally replace the {RNA} binding domain of the ribosomal {P}0 protein. In: *Nucleic Acids Research* 37 (11), 3514--3521. DOI: 10.1093/nar/gkp209.

Rodríguez-Mateos, María; García-Gómez, Juan J.; Francisco-Velilla, Rosario; Remacha, Miguel; La Cruz, Jesús de; Ballesta, Juan P. G. (2009b): Role and dynamics of the ribosomal protein {P}0 and its related trans-acting factor {Mrt}4 during ribosome assembly in {Saccharomyces} cerevisiae. In: *Nucleic Acids Research* 37 (22), 7519--7532. DOI: 10.1093/nar/gkp806.

Rosado, Iván V.; Dez, Christophe; Lebaron, Simon; Caizergues-Ferrer, Michèle; Henry, Yves; La Cruz, Jesús de (2007a): Characterization of {Saccharomyces} cerevisiae {Npa}2p ({Urb}2p) reveals a low-molecular-mass complex containing {Dbp}6p, {Npa}1p ({Urb}1p), {Nop}8p, and {Rsa}3p involved in early steps of 60S ribosomal subunit biogenesis. In: *Molecular and cellular biology* 27 (4), 1207--1221. DOI: 10.1128/MCB.01523-06.

Rosado, Iván V.; Kressler, Dieter; La Cruz, Jesús de (2007b): Functional analysis of Saccharomyces cerevisiae ribosomal protein Rpl3p in ribosome synthesis. In: *Nucleic Acids Research* 35 (12), S. 4203–4213. DOI: 10.1093/nar/gkm388.

Rouskin, Silvi; Zubradt, Meghan; Washietl, Stefan; Kellis, Manolis; Weissman, Jonathan S. (2014): Genome-wide probing of RNA structure reveals active unfolding of mRNA structures in vivo. In: *Nature* 505 (7485), S. 701–705. DOI: 10.1038/nature12894.

Sadian, Yashar; Baudin, Florence; Tafur, Lucas; Murciano, Brice; Wetzel, Rene; Weis, Felix; Müller, Christoph W. (2019): Molecular insight into RNA polymerase I promoter recognition and promoter melting. In: *Nature communications* 10 (1), S. 5543. DOI: 10.1038/s41467-019-13510-w.

Sadian, Yashar; Tafur, Lucas; Kosinski, Jan; Jakobi, Arjen J.; Wetzel, Rene; Buczak, Katarzyna et al. (2017): Structural insights into transcription initiation by yeast RNA polymerase I. In: *The EMBO journal* 36 (18), S. 2698–2709. DOI: 10.15252/embj.201796958.

Sahasranaman, Aarti; Dembowski, Jill; Strahler, John; Andrews, Philip; Maddock, Janine; Woolford, Jr, John L (2011): Assembly of {Saccharomyces} cerevisiae 60S ribosomal subunits: role of factors required for 27S pre-{rRNA} processing. In: *The EMBO journal* 30 (19), 4020--4032. DOI: 10.1038/emboj.2011.338.

Sanghai, Z. A.; Miller, L.; Barandun, J.; Hunziker, M.; Chaker-Margot, M.; Klinge, S. (2018a): Yeast nucleolar pre-60S ribosomal subunit (state 3).

Sanghai, Zahra Assur; Miller, Linamarie; Molloy, Kelly R.; Barandun, Jonas; Hunziker, Mirjam; Chaker-Margot, Malik et al. (2018b): Modular assembly of the nucleolar pre-60S ribosomal subunit. In: *Nature* 556 (7699), S. 126–129. DOI: 10.1038/nature26156.

Santos, Cruz; Ballesta, Juan P. G. (2005): Characterization of the 26S rRNA-binding domain in Saccharomyces cerevisiae ribosomal stalk phosphoprotein P0. In: *Molecular microbiology* 58 (1), S. 217–226. DOI: 10.1111/j.1365-2958.2005.04816.x.

Sardana, Richa; Liu, Xin; Granneman, Sander; Zhu, Jieyi; Gill, Michael; Papoulas, Ophelia et al. (2015): The DEAH-box helicase Dhr1 dissociates U3 from the pre-rRNA to promote formation of the central pseudoknot. In: *PLoS biology* 13 (2), e1002083. DOI: 10.1371/journal.pbio.1002083.

Saveanu, C.; Bienvenu, D.; Namane, A.; Gleizes, P. E.; Gas, N.; Jacquier, A.; Fromont-Racine, M. (2001): Nog2p, a putative {GTPase} associated with pre-60S subunits and required for late 60S maturation steps. In: *The EMBO journal* 20 (22), 6475--6484. DOI: 10.1093/emboj/20.22.6475.

Saveanu, Cosmin; Namane, Abdelkader; Gleizes, Pierre-Emmanuel; Lebreton, Alice; Rousselle, Jean-Claude; Noaillac-Depeyre, Jacqueline et al. (2003): Sequential protein association with nascent 60S ribosomal particles. In: *Molecular and cellular biology* 23 (13), S. 4449–4460. DOI: 10.1128/MCB.23.13.4449-4460.2003.

Scaiola, Alain; Peña, Cohue; Weisser, Melanie; Böhringer, Daniel; Leibundgut, Marc; Klingauf-Nerurkar, Purnima et al. (2018): Structure of a eukaryotic cytoplasmic pre-40S ribosomal subunit. In: *The EMBO journal* 37 (7). DOI: 10.15252/embj.201798499.

Schäfer, Thorsten; Maco, Bohumil; Petfalski, Elisabeth; Tollervey, David; Böttcher, Bettina; Aebi, Ueli; Hurt, Ed (2006): Hrr25-dependent phosphorylation state regulates organization of the pre-40S subunit. In: *Nature* 441 (7093), S. 651–655. DOI: 10.1038/nature04840.

Schäfer, Thorsten; Strauss, Daniela; Petfalski, Elisabeth; Tollervey, David; Hurt, Ed (2003): The path from nucleolar 90S to cytoplasmic 40S pre-ribosomes. In: *The EMBO journal* 22 (6), 1370--1380. DOI: 10.1093/emboj/cdg121.

Schmeing, T. Martin; Ramakrishnan, V. (2009): What recent ribosome structures have revealed about the mechanism of translation. In: *Nature* 461 (7268), 1234--1242. DOI: 10.1038/nature08403.

Schmid, Manfred; Durussel, Thérèse; Laemmli, Ulrich K. (2004): ChIC and ChEC; genomic mapping of chromatin proteins. In: *Molecular cell* 16 (1), S. 147–157. DOI: 10.1016/j.molcel.2004.09.007.

Schmitt, M. E.; Clayton, D. A. (1993): Nuclear {RNase} {MRP} is required for correct processing of pre-5.8S {rRNA} in {Saccharomyces} cerevisiae. In: *Molecular and cellular biology* 13 (12), 7935--7941.

Schneider, D. A.; French, S. L.; Osheim, Y. N.; Bailey, A. O.; Vu, L.; Dodd, J. et al. (2006): RNA} polymerase {II} elongation factors {Spt}4p and {Spt}5p play roles in transcription elongation by {RNA} polymerase {I} and {rRNA} processing. In: *Proceedings of the National Academy of Sciences of the United States of America* 103 (34), 12707--12712. DOI: 10.1073/pnas.0605686103.

Schneider, David A.; Michel, Antje; Sikes, Martha L.; Vu, Loan; Dodd, Jonathan A.; Salgia, Shilpa et al. (2007): Transcription elongation by {RNA} polymerase {I} is linked to efficient {rRNA} processing and ribosome assembly. In: *Molecular cell* 26 (2), 217--229. DOI: 10.1016/j.molcel.2007.04.007.

Schuller, Anthony P.; Green, Rachel (2018): Roadblocks and resolutions in eukaryotic translation. In: *Nature Reviews Molecular Cell Biology* 19 (8), S. 526–541. DOI: 10.1038/s41580-018-0011-4.

Sengupta, Jayati; Bussiere, Cyril; Pallesen, Jesper; West, Matthew; Johnson, Arlen W.; Frank, Joachim (2010): Characterization of the nuclear export adaptor protein {Nmd}3 in association with the 60S ribosomal subunit. In: *The Journal of Cell Biology* 189 (7), 1079--1086. DOI: 10.1083/jcb.201001124.

Sharma, K.; Tollervey, D. (1999): Base pairing between {U}3 small nucleolar {RNA} and the 5' end of 18S {rRNA} is required for pre-{rRNA} processing. In: *Molecular and cellular biology* 19 (9), 6012--6019. Online verfügbar unter http://www.ncbi.nlm.nih.gov/pubmed/10454548, zuletzt geprüft am 25.06.2012.

Sharma, K.; Venema, J.; Tollervey, D. (1999): The 5' end of the 18S rRNA can be positioned from within the mature rRNA. In: *RNA* 5 (5), S. 678–686. DOI: 10.1017/s1355838299990052.

Sharma, Sunny; Lafontaine, Denis L. J. (2015): 'View From A Bridge': A New Perspective on Eukaryotic rRNA Base Modification. In: *Trends in biochemical sciences* 40 (10), S. 560–575. DOI: 10.1016/j.tibs.2015.07.008.

Sharma, Sunny; Watzinger, Peter; Kötter, Peter; Entian, Karl-Dieter (2013): Identification of a novel methyltransferase, Bmt2, responsible for the N-1-methyl-adenosine base modification of 25S rRNA in Saccharomyces cerevisiae. In: *Nucleic Acids Research* 41 (10), S. 5428–5443. DOI: 10.1093/nar/gkt195.

Shimoji, Kaori; Jakovljevic, Jelena; Tsuchihashi, Kanako; Umeki, Yuka; Wan, Kun; Kawasaki, Suzuka et al. (2012): Ebp2 and {Brx}1 function cooperatively in 60S ribosomal subunit assembly in {Saccharomyces} cerevisiae. In: *Nucleic Acids Research* 40 (10), 4574--4588. DOI: 10.1093/nar/gks057.

Shirokikh, Nikolay E.; Preiss, Thomas (2018): Translation initiation by cap-dependent ribosome recruitment: Recent insights and open questions. In: *Wiley Interdisciplinary Reviews: RNA* 9 (4), e1473. DOI: 10.1002/wrna.1473.

Shuai, K.; Warner, J. R. (1991): A temperature sensitive mutant of Saccharomyces cerevisiae defective in pre-rRNA processing. In: *Nucleic Acids Research* 19 (18), S. 5059–5064. DOI: 10.1093/nar/19.18.5059.

Siddiqi, I.; Keener, J.; Vu, L.; Nomura, M. (2001): Role of TATA binding protein (TBP) in yeast ribosomal dna transcription by RNA polymerase I: defects in the dual functions of transcription factor UAF cannot be suppressed by TBP. In: *Molecular and cellular biology* 21 (7), S. 2292–2297. DOI: 10.1128/MCB.21.7.2292-2297.2001.

Siekevitz, Philip (1952): Uptake of {Radioactive} {Alanine} in {Vitro} into the {Proteins} of {Rat} {Liver} {Fractions}. In: *Journal of Biological Chemistry* 195 (2), 549--565. Online verfügbar unter http://www.jbc.org/content/195/2/549, zuletzt geprüft am 14.12.2012.

Sloan, Katherine E.; Bohnsack, Markus T. (2018): Unravelling the Mechanisms of RNA Helicase Regulation. In: *Trends in biochemical sciences* 43 (4), S. 237–250. DOI: 10.1016/j.tibs.2018.02.001.

Sloan, Katherine E.; Warda, Ahmed S.; Sharma, Sunny; Entian, Karl-Dieter; Lafontaine, Denis L. J.; Bohnsack, Markus T. (2017): Tuning the ribosome: The influence of rRNA modification on eukaryotic ribosome biogenesis and function. In: *RNA biology* 14 (9), S. 1138–1152. DOI: 10.1080/15476286.2016.1259781.

Smith, M. W.; Meskauskas, A.; Wang, P.; Sergiev, P. V.; Dinman, J. D. (2001): Saturation mutagenesis of 5S rRNA in Saccharomyces cerevisiae. In: *Molecular and cellular biology* 21 (24), S. 8264–8275. DOI: 10.1128/MCB.21.24.8264-8275.2001.

Smola, Matthew J.; Rice, Greggory M.; Busan, Steven; Siegfried, Nathan A.; Weeks, Kevin M. (2015): Selective 2'-hydroxyl acylation analyzed by primer extension and mutational profiling (SHAPE-MaP) for direct, versatile and accurate RNA structure analysis. In: *Nature protocols* 10 (11), S. 1643–1669. DOI: 10.1038/nprot.2015.103.

Soltanieh, Sahar; Lapensée, Martin; Dragon, François (2014): Nucleolar proteins Bfr2 and Enp2 interact with DEAD-box RNA helicase Dbp4 in two different complexes. In: *Nucleic Acids Research* 42 (5), S. 3194–3206. DOI: 10.1093/nar/gkt1293.

Soltanieh, Sahar; Osheim, Yvonne N.; Spasov, Krasimir; Trahan, Christian; Beyer, Ann L.; Dragon, François (2015): DEAD-box RNA helicase Dbp4 is required for small-subunit processome formation and function. In: *Molecular and cellular biology* 35 (5), S. 816–830. DOI: 10.1128/MCB.01348-14.

Spahn, C. M.; Beckmann, R.; Eswar, N.; Penczek, P. A.; Sali, A.; Blobel, G.; Frank, J. (2001): Structure of the 80S ribosome from {Saccharomyces} cerevisiae--{tRNA}-ribosome and subunit-subunit interactions. In: *Cell* 107 (3), 373--386.

Spahn, Christian M. T.; Gomez-Lorenzo, Maria G.; Grassucci, Robert A.; Jørgensen, Rene; Andersen, Gregers R.; Beckmann, Roland et al. (2004): Domain movements of elongation factor eEF2 and the eukaryotic 80S ribosome facilitate tRNA translocation. In: *The EMBO journal* 23 (5), S. 1008–1019. DOI: 10.1038/sj.emboj.7600102.

Steffan, J. S.; Keys, D. A.; Dodd, J. A.; Nomura, M. (1996): The role of TBP in rDNA transcription by RNA polymerase I in Saccharomyces cerevisiae: TBP is required for upstream activation factor-

dependent recruitment of core factor. In: *Genes \& development* 10 (20), S. 2551–2563. DOI: 10.1101/gad.10.20.2551.

Steffan, J. S.; Keys, D. A.; Vu, L.; Nomura, M. (1998): Interaction of {TATA}-binding protein with upstream activation factor is required for activated transcription of ribosomal {DNA} by {RNA} polymerase {I} in {Saccharomyces} cerevisiae in vivo. In: *Molecular and cellular biology* 18 (7), 3752--3761.

Stern, Seth; Moazed, Danesh; Noller, Harry F. (1988): [33] Structural analysis of RNA using chemical and enzymatic probing monitored by primer extension. In: Ribosomes, Bd. 164: Elsevier (Methods in Enzymology), S. 481–489.

Strunk, Bethany S.; Loucks, Cherisse R.; Su, Min; Vashisth, Harish; Cheng, Shanshan; Schilling, Justin et al. (2011): Ribosome {Assembly} {Factors} {Prevent} {Premature} {Translation} {Initiation} by 40S {Assembly} {Intermediates}. In: *Science (New York, N.Y.)* 333 (6048), 1449--1453. DOI: 10.1126/science.1208245.

Strunk, Bethany S.; Novak, Megan N.; Young, Crystal L.; Karbstein, Katrin (2012): A translation-like cycle is a quality control checkpoint for maturing 40S ribosome subunits. In: *Cell* 150 (1), 111--121. DOI: 10.1016/j.cell.2012.04.044.

Sun, Qi; Zhu, Xing; Qi, Jia; An, Weidong; Lan, Pengfei; Tan, Dan et al. (2017): Molecular architecture of the 90S small subunit pre-ribosome. In: *eLife* 6. DOI: 10.7554/eLife.22086.

Svedberg, The; Fåhraeus, Robin (1926): A NEW METHOD FOR THE DETERMINATION OF THE MOLECULAR WEIGHT OF THE PROTEINS. In: *J. Am. Chem. Soc.* 48 (2), S. 430–438. DOI: 10.1021/ja01413a019.

Sweeney, R.; Chen, L.; Yao, M. C. (1994): An rRNA variable region has an evolutionarily conserved essential role despite sequence divergence. In: *Molecular and cellular biology* 14 (6), S. 4203–4215. DOI: 10.1128/mcb.14.6.4203.

Tafur, Lucas; Sadian, Yashar; Hoffmann, Niklas A.; Jakobi, Arjen J.; Wetzel, Rene; Hagen, Wim J. H. et al. (2016): Molecular Structures of Transcribing RNA Polymerase I. In: *Molecular cell* 64 (6), S. 1135–1143. DOI: 10.1016/j.molcel.2016.11.013.

Talkish, Jason; Campbell, Ian Winsten; Sahasranaman, Aarti; Jakovljevic, Jelena; Woolford, John L. (2014a): Ribosome assembly factors Pwp1 and Nop12 are important for folding of 5.8S rRNA during ribosome biogenesis in Saccharomyces cerevisiae. In: *Molecular and cellular biology* 34 (10), S. 1863–1877. DOI: 10.1128/MCB.01322-13.

Talkish, Jason; May, Gemma; Lin, Yizhu; Woolford, John L.; McManus, C. Joel (2014b): Mod-seq: high-throughput sequencing for chemical probing of RNA structure. In: *RNA (New York, N.Y.)* 20 (5), S. 713–720. DOI: 10.1261/rna.042218.113.

Talkish, Jason; Zhang, Jingyu; Jakovljevic, Jelena; Horsey, Edward W.; Woolford, John L. (2012): Hierarchical recruitment into nascent ribosomes of assembly factors required for 27SB pre-{rRNA} processing in {Saccharomyces} cerevisiae. In: *Nucleic Acids Research* 40 (17), 8646--8661. DOI: 10.1093/nar/gks609.

Tang, Lan; Sahasranaman, Aarti; Jakovljevic, Jelena; Schleifman, Erica; Woolford, John L. (2008): Interactions among {Ytm}1, {Erb}1, and {Nop}7 {Required} for {Assembly} of the {Nop}7-{Subcomplex} in {Yeast} {Preribosomes}. In: *Molecular Biology of the Cell* 19 (7), 2844--2856. DOI: 10.1091/mbc.E07-12-1281.

Teubl, Fabian (2013): Molecular Characterization of the Ribosomal Maturation Factor Noc3p. Bachelor Thesis

Teubl, Fabian (2015): Studien zur Funktion von Noc3p in der Biogenese von Ribosomen der Bäckerhefe. Master Thesis

Thiry, Marc; Lafontaine, Denis L. J. (2005): Birth of a nucleolus: the evolution of nucleolar compartments. In: *Trends in Cell Biology* 15 (4), S. 194–199. DOI: 10.1016/j.tcb.2005.02.007.

Thoms, Matthias; Thomson, Emma; Baßler, Jochen; Gnädig, Marén; Griesel, Sabine; Hurt, Ed (2015): The Exosome Is Recruited to RNA Substrates through Specific Adaptor Proteins. In: *Cell* 162 (5), S. 1029–1038. DOI: 10.1016/j.cell.2015.07.060.

Thomson, Emma; Tollervey, David (2005): Nop53p is required for late 60S ribosome subunit maturation and nuclear export in yeast. In: *RNA* 11 (8), S. 1215–1224. DOI: 10.1261/rna.2720205.

Thomson, Emma; Tollervey, David (2010): The {Final} {Step} in 5.8S {rRNA} {Processing} {Is} {Cytoplasmic} in {Saccharomyces} cerevisiae. In: *Molecular and cellular biology* 30 (4), 976--984. DOI: 10.1128/MCB.01359-09.

Tijerina, Pilar; Mohr, Sabine; Russell, Rick (2007): DMS footprinting of structured RNAs and RNA-protein complexes. In: *Nature protocols* 2 (10), S. 2608–2623. DOI: 10.1038/nprot.2007.380.

Tollervey, David; Lehtonen, Hanna; Jansen, Ralf; Kern, Hildegard; Hurt, Eduard C. (1993): Temperature-sensitive mutations demonstrate roles for yeast fibrillarin in pre-rRNA processing, pre-rRNA methylation, and ribosome assembly. In: *Cell* 72 (3), S. 443–457. DOI: 10.1016/0092-8674(93)90120-f.

Torchet, C.; Jacq, C.; Hermann-Le Denmat, S. (1998): Two mutant forms of the {S}1/{TPR}-containing protein {Rrp}5p affect the 18S {rRNA} synthesis in {Saccharomyces} cerevisiae. In: *RNA* 4 (12), 1636--1652. Online verfügbar unter http://www.ncbi.nlm.nih.gov/pubmed/9848659, zuletzt geprüft am 11.05.2012.

Trapman, J.; Planta, R. J. (1975): Detailed analysis of the ribosomal {RNA} synthesis in yeast. In: *Biochimica et biophysica acta* 414 (2), 115--125. Online verfügbar unter http://www.ncbi.nlm.nih.gov/pubmed/1191704, zuletzt geprüft am 13.01.2012.

Trumtel, S.; Léger-Silvestre, I.; Gleizes, P. E.; Teulières, F.; Gas, N. (2000): Assembly and functional organization of the nucleolus: ultrastructural analysis of Saccharomyces cerevisiae mutants. In: *Molecular Biology of the Cell* 11 (6), S. 2175–2189. DOI: 10.1091/mbc.11.6.2175.

Turowski, Tomasz W.; Lebaron, Simon; Zhang, Elodie; Peil, Lauri; Dudnakova, Tatiana; Petfalski, Elisabeth et al. (2014): Rio1 mediates ATP-dependent final maturation of 40S ribosomal subunits. In: *Nucleic Acids Research* 42 (19), S. 12189–12199. DOI: 10.1093/nar/gku878.

Tutuncuoglu, Beril; Jakovljevic, Jelena; Wu, Shan; Gao, Ning; Woolford, John L. (2016): The N-terminal extension of yeast ribosomal protein L8 is involved in two major remodeling events during late nuclear stages of 60S ribosomal subunit assembly. In: *RNA (New York, N.Y.)* 22 (9), S. 1386–1399. DOI: 10.1261/rna.055798.115.

Udem, S. A.; Warner, J. R. (1972): Ribosomal {RNA} synthesis in {Saccharomyces} cerevisiae. In: *Journal of molecular biology* 65 (2), 227--242. Online verfügbar unter http://www.ncbi.nlm.nih.gov/pubmed/4557192, zuletzt geprüft am 13.01.2012.

Udem, S. A.; Warner, J. R. (1973): The cytoplasmic maturation of a ribosomal precursor ribonucleic acid in yeast. In: *Journal of Biological Chemistry* 248 (4), 1412--1416.

Uetz, P.; Giot, L.; Cagney, G.; Mansfield, T. A.; Judson, R. S.; Knight, J. R. et al. (2000): A comprehensive analysis of protein-protein interactions in Saccharomyces cerevisiae. In: *Nature* 403 (6770), S. 623–627. DOI: 10.1038/35001009.

Ulbrich, Cornelia; Diepholz, Meikel; Bassler, Jochen; Kressler, Dieter; Pertschy, Brigitte; Galani, Kyriaki et al. (2009): Mechanochemical removal of ribosome biogenesis factors from nascent 60S ribosomal subunits. In: *Cell* 138 (5), 911--922. DOI: 10.1016/j.cell.2009.06.045.

Underwood, Jason G.; Uzilov, Andrew V.; Katzman, Sol; Onodera, Courtney S.; Mainzer, Jacob E.; Mathews, David H. et al. (2010): FragSeq: transcriptome-wide RNA structure probing using high-throughput sequencing. In: *Nature methods* 7 (12), S. 995–1001. DOI: 10.1038/nmeth.1529.

van Hoof, A.; Lennertz, P.; Parker, R. (2000): Three conserved members of the {RNase} {D} family have unique and overlapping functions in the processing of 5S, 5.8S, {U}4, {U}5, {RNase} {MRP} and {RNase} {P} {RNAs} in yeast. In: *The EMBO journal* 19 (6), 1357--1365. DOI: 10.1093/emboj/19.6.1357.

van Nues, R. W.; Rientjes, J. M.; van der Sande, C A; Zerp, S. F.; Sluiter, C.; Venema, J. et al. (1994): Separate structural elements within internal transcribed spacer 1 of {Saccharomyces} cerevisiae precursor ribosomal {RNA} direct the formation of 17S and 26S {rRNA}. In: *Nucleic Acids Research* 22 (6), 912--919.

Vanácová, Stepánka; Wolf, Jeannette; Martin, Georges; Blank, Diana; Dettwiler, Sabine; Friedlein, Arno et al. (2005): A new yeast poly({A}) polymerase complex involved in {RNA} quality control. In: *PLoS biology* 3 (6), e189. DOI: 10.1371/journal.pbio.0030189.

Veinot-Drebot, Lela M.; Singer, R. A.; Johnston, G. C. (1988): Rapid initial cleavage of nascent pre-rRNA transcripts in yeast. In: *Journal of molecular biology* 199 (1), S. 107–113. DOI: 10.1016/0022-2836(88)90382-8.

Venema, J.; Henry, Y.; Tollervey, D. (1995): Two distinct recognition signals define the site of endonucleolytic cleavage at the 5'-end of yeast 18S rRNA. In: *The EMBO journal* 14 (19), S. 4883–4892.

Venema, J.; Tollervey, D. (1996): RRP}5 is required for formation of both 18S and 5.8S {rRNA} in yeast. In: *The EMBO journal* 15 (20), 5701--5714. Online verfügbar unter http://www.ncbi.nlm.nih.gov/pubmed/8896463, zuletzt geprüft am 14.05.2012.

Venema, Jaap; Tollervey, David (1995): Processing of pre-ribosomal {RNA} in {Saccharomyces} cerevisiae. In: *Yeast* 11 (16), 1629--1650. DOI: 10.1002/yea.320111607.

Voorhees, Rebecca M.; Ramakrishnan, V. (2013): Structural basis of the translational elongation cycle. In: *Annual Review of Biochemistry* 82, S. 203–236. DOI: 10.1146/annurev-biochem-113009-092313.

Voorhees, Rebecca M.; Schmeing, T. Martin; Kelley, Ann C.; Ramakrishnan, V. (2010): The mechanism for activation of GTP hydrolysis on the ribosome. In: *Science (New York, N.Y.)* 330 (6005), S. 835–838. DOI: 10.1126/science.1194460.

Vos, Harmjan R.; Bax, Ralph; Faber, Alex W.; Vos, Jan C.; Raué, Hendrik A. (2004): U3 {snoRNP} and {Rrp}5p associate independently with {Saccharomyces} cerevisiae 35S pre-{rRNA}, but {Rrp}5p is essential for association of {Rok}1p. In: *Nucleic Acids Research* 32 (19), 5827--5833. DOI: 10.1093/nar/gkh904.

Warner, Jonathan R. (1999): The economics of ribosome biosynthesis in yeast. In: *Trends in biochemical sciences* 24 (11), 437--440. DOI: 10.1016/S0968-0004(99)01460-7.

Watkins, N. J.; Ségault, V.; Charpentier, B.; Nottrott, S.; Fabrizio, P.; Bachi, A. et al. (2000): A common core {RNP} structure shared between the small nucleoar box {C}/{D} {RNPs} and the spliceosomal {U}4 {snRNP}. In: *Cell* 103 (3), 457--466. Online verfügbar unter http://www.ncbi.nlm.nih.gov/pubmed/11081632, zuletzt geprüft am 11.05.2012.

Watkins, Nicholas J.; Bohnsack, Markus T. (2012): The box C/D and H/ACA snoRNPs: key players in the modification, processing and the dynamic folding of ribosomal RNA. In: *Wiley Interdisciplinary Reviews: RNA* 3 (3), S. 397–414. DOI: 10.1002/wrna.117.

Weaver, P. L.; Sun, C.; Chang, T. H. (1997): Dbp3p, a putative RNA helicase in Saccharomyces cerevisiae, is required for efficient pre-rRNA processing predominantly at site A3. In: *Molecular and cellular biology* 17 (3), S. 1354–1365. DOI: 10.1128/mcb.17.3.1354.

Wegierski, T.; Billy, E.; Nasr, F.; Filipowicz, W. (2001): Bms1p, a {G}-domain-containing protein, associates with {Rcl}1p and is required for 18S {rRNA} biogenesis in yeast. In: *RNA* 7 (9), 1254--1267. Online verfügbar unter http://www.ncbi.nlm.nih.gov/pmc/articles/PMC1370170/, zuletzt geprüft am 06.12.2012.

Wehner, Karen A.; Baserga, Susan J. (2002): The σ70-like Motif. In: *Molecular cell* 9 (2), S. 329–339. DOI: 10.1016/S1097-2765(02)00438-0.

Wehner, Karen A.; Gallagher, Jennifer E. G.; Baserga, Susan J. (2002): Components of an interdependent unit within the SSU processome regulate and mediate its activity. In: *Molecular and cellular biology* 22 (20), S. 7258–7267. DOI: 10.1128/MCB.22.20.7258-7267.2002.

Weinmann, R.; Roeder, R. G. (1974): Role of DNA-dependent RNA polymerase 3 in the transcription of the tRNA and 5S RNA genes. In: *Proceedings of the National Academy of Sciences of the United States of America* 71 (5), S. 1790–1794. DOI: 10.1073/pnas.71.5.1790.

Weis, Félix; Giudice, Emmanuel; Churcher, Mark; Jin, Li; Hilcenko, Christine; Wong, Chi C. et al. (2015): Mechanism of eIF6 release from the nascent 60S ribosomal subunit. In: *Nature Structural & Molecular Biology* 22 (11), S. 914–919. DOI: 10.1038/nsmb.3112.

Wells, Graeme R.; Weichmann, Franziska; Colvin, David; Sloan, Katherine E.; Kudla, Grzegorz; Tollervey, David et al. (2016): The PIN domain endonuclease Utp24 cleaves pre-ribosomal RNA at two coupled sites in yeast and humans. In: *Nucleic Acids Research* 44 (11), S. 5399–5409. DOI: 10.1093/nar/gkw213.

Wells, Graeme R.; Weichmann, Franziska; Sloan, Katherine E.; Colvin, David; Watkins, Nicholas J.; Schneider, Claudia (2017): The ribosome biogenesis factor yUtp23/hUTP23 coordinates key interactions in the yeast and human pre-40S particle and hUTP23 contains an essential PIN domain. In: *Nucleic Acids Research* 45 (8), S. 4796–4809. DOI: 10.1093/nar/gkw1344.

Wilson, Daniel N.; Doudna Cate, Jamie H. (2012): The structure and function of the eukaryotic ribosome. In: *Cold Spring Harbor perspectives in biology* 4 (5). DOI: 10.1101/cshperspect.a011536.

Woolford, John L.; Baserga, Susan J. (2013): Ribosome biogenesis in the yeast Saccharomyces cerevisiae. In: *Genetics* 195 (3), S. 643–681. DOI: 10.1534/genetics.113.153197.

Wu, K.; Wu, P.; Aris, J. P. (2001): Nucleolar protein Nop12p participates in synthesis of 25S rRNA in Saccharomyces cerevisiae. In: *Nucleic Acids Research* 29 (14), S. 2938–2949. DOI: 10.1093/nar/29.14.2938.

Wu, Shan; Tutuncuoglu, Beril; Yan, Kaige; Brown, Hailey; Zhang, Yixiao; Tan, Dan et al. (2016): Diverse roles of assembly factors revealed by structures of late nuclear pre-60S ribosomes. In: *Nature* 534 (7605), S. 133–137. DOI: 10.1038/nature17942.

Xia, Yuqiong; Zhang, Ruili; Wang, Zhongliang; Tian, Jie; Chen, Xiaoyuan (2017): Recent advances in high-performance fluorescent and bioluminescent RNA imaging probes. In: *Chemical Society reviews* 46 (10), S. 2824–2843. DOI: 10.1039/c6cs00675b.

Yamamoto, R. T.; Nogi, Y.; Dodd, J. A.; Nomura, M. (1996): RRN}3 gene of {Saccharomyces} cerevisiae encodes an essential {RNA} polymerase {I} transcription factor which interacts with the polymerase independently of {DNA} template. In: *The EMBO journal* 15 (15), 3964--3973.

Yeh, L. C.; Thweatt, R.; Lee, J. C. (1990): Internal transcribed spacer 1 of the yeast precursor ribosomal {RNA}. {Higher} order structure and common structural motifs. In: *Biochemistry* 29 (25), 5911--5918.

Yeh, Lee-Chuan C.; Lee, John C. (1990): Structural analysis of the internal transcribed spacer 2 of the precursor ribosomal RNA from Saccharomyces cerevisiae. In: *Journal of molecular biology* 211 (4), S. 699–712. DOI: 10.1016/0022-2836(90)90071-S.

Young, Crystal L.; Karbstein, Katrin (2011): The roles of {S}1 {RNA}-binding domains in {Rrp}5's interactions with pre-{rRNA}. In: *RNA (New York, N.Y.)* 17 (3), 512--521. DOI: 10.1261/rna.2458811.

Yusupov, M. M.; Yusupova, G. Z.; Baucom, A.; Lieberman, K.; Earnest, T. N.; Cate, J. H.; Noller, H. F. (2001): Crystal structure of the ribosome at 5.5 {A} resolution. In: *Science (New York, N.Y.)* 292 (5518), 883--896. DOI: 10.1126/science.1060089.

Yusupova, Gulnara Zh.; Yusupov, Marat M.; Cate, J.H.D.; Noller, Harry F. (2001): The Path of Messenger RNA through the Ribosome. In: *Cell* 106 (2), S. 233–241. DOI: 10.1016/S0092-8674(01)00435-4.

Zanchin, N. I.; Roberts, P.; DeSilva, A.; Sherman, F.; Goldfarb, D. S. (1997): Saccharomyces cerevisiae {Nip}7p is required for efficient 60S ribosome subunit biogenesis. In: *Molecular and cellular biology* 17 (9), 5001--5015. Online verfügbar unter http://www.ncbi.nlm.nih.gov/pmc/articles/PMC232351/, zuletzt geprüft am 29.12.2012.

Zebarjadian, Y.; King, T.; Fournier, M. J.; Clarke, L.; Carbon, J. (1999): Point mutations in yeast CBF5 can abolish in vivo pseudouridylation of rRNA. In: *Molecular and cellular biology* 19 (11), S. 7461–7472. DOI: 10.1128/mcb.19.11.7461.

Zentner, Gabriel E.; Kasinathan, Sivakanthan; Xin, Beibei; Rohs, Remo; Henikoff, Steven (2015): ChEC-seq kinetics discriminates transcription factor binding sites by DNA sequence and shape in vivo. In: *Nature communications* 6, S. 8733. DOI: 10.1038/ncomms9733.

Zhang, Jingyu; Harnpicharnchai, Piyanun; Jakovljevic, Jelena; Tang, Lan; Guo, Yurong; Oeffinger, Marlene et al. (2007): Assembly factors {Rpf}2 and {Rrs}1 recruit 5S {rRNA} and ribosomal proteins {rpL}5 and {rpL}11 into nascent ribosomes. In: *Genes \& development* 21 (20), 2580--2592. DOI: 10.1101/gad.1569307.

Zhang, Liman; Wu, Chen; Cai, Gaihong; Chen, She; Ye, Keqiong (2016): Stepwise and dynamic assembly of the earliest precursors of small ribosomal subunits in yeast. In: *Genes & development* 30 (6), S. 718–732. DOI: 10.1101/gad.274688.115.

Zhang, Wen; Dunkle, Jack A.; Cate, Jamie H. D. (2009a): Structures of the ribosome in intermediate states of ratcheting. In: *Science (New York, N.Y.)* 325 (5943), S. 1014–1017. DOI: 10.1126/science.1175275.

Zhang, Yinfeng; Sikes, Martha L.; Beyer, Ann L.; Schneider, David A. (2009b): The {Paf}1 complex is required for efficient transcription elongation by {RNA} polymerase {I}. In: *Proceedings of the National Academy of Sciences of the United States of America* 106 (7), 2153--2158. DOI: 10.1073/pnas.0812939106.

Zhang, Yinfeng; Smith, 4th, Archer D; Renfrow, Matthew B.; Schneider, David A. (2010): The {RNA} polymerase-associated factor 1 complex ({Paf}1C) directly increases the elongation rate of {RNA} polymerase {I} and is required for efficient regulation of {rRNA} synthesis. In: *The Journal of biological chemistry* 285 (19), 14152--14159. DOI: 10.1074/jbc.M110.115220.

Zheng, Qi; Ryvkin, Paul; Li, Fan; Dragomir, Isabelle; Valladares, Otto; Yang, Jamie et al. (2010): Genome-wide double-stranded RNA sequencing reveals the functional significance of base-paired RNAs in Arabidopsis. In: *PLoS genetics* 6 (9), e1001141. DOI: 10.1371/journal.pgen.1001141.

Zheng, Shawn Q.; Palovcak, Eugene; Armache, Jean-Paul; Verba, Kliment A.; Cheng, Yifan; Agard, David A. (2017): MotionCor2: anisotropic correction of beam-induced motion for improved cryo-electron microscopy. In: *Nature methods* 14 (4), S. 331–332. DOI: 10.1038/nmeth.4193.

Zhou, Dejian; Zhu, Xing; Zheng, Sanduo; Tan, Dan; Dong, Meng-Qiu; Ye, Keqiong (2019a): Cryo-EM structure of an early precursor of large ribosomal subunit reveals a half-assembled intermediate. In: *Protein & cell* 10 (2), S. 120–130. DOI: 10.1007/s13238-018-0526-7.

Zhou, Yi; Musalgaonkar, Sharmishtha; Johnson, Arlen W.; Taylor, David W. (2019b): Tightly-orchestrated rearrangements govern catalytic center assembly of the ribosome. In: *Nature communications* 10 (1), S. 958. DOI: 10.1038/s41467-019-08880-0.

Ziehler, W. A.; Engelke, D. R. (2001): Probing RNA structure with chemical reagents and enzymes. In: *Current protocols in nucleic acid chemistry* Chapter 6, Unit 6.1. DOI: 10.1002/0471142700.nc0601s00.

8 List of Figures

9 List of Tables

10 Publications and Presentations

Publications

2017 Pöll, Gisela; Müller, Christian; Bodden, Malena; Teubl, Fabian; Eichner, Norbert; Lehmann, Gerhard et al. (2017): **Structural transitions during large ribosomal subunit maturation analyzed by tethered nuclease structure probing in *S. cerevisiae*.** In: *PloS one* 12 (7), e0179405. DOI: 10.1371/journal.pone.0179405.

Presentations

2019 Fabian Teubl, Uli Ohmayer, Thomas Hierlmeier, Jan Linnemann, Gisela Pöll, Joachim Griesenbeck, Herbert Tschochner and Philipp Milkereit
Poster: **Structural and Functional Studies on the Role of Noc3p for Large Ribosomal Subunit Maturation in *Saccharomyces cerevisiae***
1st Munich Yeast Meeting 2019, Germany

2018 Fabian Teubl, Thomas Hierlmeier, Jan Linnemann, Gisela Pöll, Joachim Griesenbeck, Herbert Tschochner and Philipp Milkereit
Poster: **Structural and Functional Studies on the Role of Noc3p for Large Ribosomal Subunit Maturation in *Saccharomyces cerevisiae*.**
The 11th International Conference on Ribosome Synthesis in Orford, Canada

2017 Fabian Teubl, Thomas Hierlmeier, Jan Linnemann, Gisela Pöll, Joachim Griesenbeck, Herbert Tschochner and Philipp Milkereit
Poster: **Structural and Functional Studies on the Role of Noc3p for Large Ribosomal Subunit Maturation in *Saccharomyces cerevisiae.***
SFB960 Conference on "The Biology of RNA-Protein Complexes" in Regensburg, Germany

11 Acknowledgements / Danksagung

Abschließend möchte ich mich noch bei allen bedanken, die zum Gelingen meiner Doktorarbeit beigetragen haben.

Voran bei Dr. Philipp Milkereit, der mich auch schon durch meine Masterarbeit begleitet hat. Danke Philipp, für die interessante Fragestellung und die Möglichkeit weiter an meinem Lieblingsprotein Noc3p zu forschen, um das sich auch schon meine früheren Arbeiten und Praktika gedreht haben. Mit Noc3p gibt es einfach immer wieder etwas Neues zu entdecken, besonders als erstmals eine Struktur publiziert wurde und wir das Protein in seiner vollen Pracht, inklusive seiner langen Extension, bewundern konnten. Du hast mich motiviert hast, alle Ergebnisse stets kritisch zu hinterfragen und jede Möglichkeit zur Interpretation in Betracht zu ziehen. Auch bei der Planung und Durchführung der Experimente, sowie beim Schreiben meiner Arbeit hast Du mir immer **sehr** viel Freiraum gelassen, sodass ich während den Jahren ein hohes Maß an Selbstständigkeit und Eigeninitiative entwickelt habe.

Weiterhin möchte ich mich bei Prof. Dr. Joachim Griesenbeck bedanken, besonders für sein Mentorat während meiner Doktorarbeit, die stetige Unterstützung und die vielen anregenden Diskussionen. Vielen Dank auch dafür, als Erstgutachter meine Doktorarbeit zu bewerten.

Ein besonderer Dank gilt Prof. Dr. Herbert Tschochner dafür, dass ich an seinem Lehrstuhl promovieren durfte. Ich bedanke mich sehr für sein Mentorat während meiner Doktorarbeit und dass er den Vorsitz in meinem Prüfungskomitee übernimmt.

Bei Prof. Dr. Gunter Meister möchte ich mich sehr herzlich bedanken, dass er sich bereit erklärt hat, wie auch schon vor einigen Jahren für meine Masterarbeit, als Zweitgutachter meine Doktorarbeit zu bewerten und so auch Teil meines Prüfungskomitees zu sein.

Bei Prof. Dr. Klaus Grasser bedanke ich mich für die Übernahme der Aufgabe, als Drittprüfer in meinem Prüfungskomitee zu fungieren.

Prof. Dr. Wolfang Seufert möchte ich danken, dass er sich sofort bereit erklärt hat, als Ersatzprüfer in meinem Prüfungskomitee tätig zu sein.

Recht herzlich möchte ich mich auch bei Prof. Dr. Dierk Niessing bedanken, der sofort und ohne Zögern den wichtigen Posten des externen Mentorats für meine Doktorarbeit übernahm.

Ein besonderer Dank gilt dem RIGeL-Team, allen voran Kinga Ay und Karolin Apfel, die mir während meiner gesamten Promotion in allen Fragen rund um das Doktoranden-Dasein und den anfallenden Papierkram stets sehr hilfreich zur Seite standen!

Danke an Ribonoc-Subgruppe, besonders den PIs Sébastien und Jorge, die mir als Ribosomenbiogenese Experten in allen Fragen immer sehr geholfen haben. Danke für stetige Unterstützung, besonders in der Endphase meiner Doktorarbeit und danke für die tolle Zeit!

Ein besonderer Dank gilt dem Modellorganismus der Bäckerhefe *Saccharomyces cerevisiae,* auch liebevoll Yeastie-Boys genannt. Ich wollte von euch stets nur das Beste – eure Ribosomen. Dafür habt ihr euch aufopferungsvoll zur Verfügung gestellt. Ohne euch wäre meine Forschung nicht möglich gewesen. Mit euch konnte man machen, was immer man wollte und meist seid ihr auch so gewachsen wie geplant – mit Ausnahme folgender Stämme: Y3906, Y3908, Y3962, Y3964, Y3974 und Y3976 – vielen Dank für NICHTS (deshalb taucht ihr auch nicht in meiner Arbeit auf)!

Ganz besonders bedanke ich mich bei meinen langjährigen Mitstreitern Christopher (Agent Orange), Christina (Marili Marille) und Robert (Robo), die mich die längste Zeit an der Uni Regensburg begleitet haben. Die Arbeit kann noch so spannend und interessant sein, aber erst die richtigen Kollegen machen es perfekt. Das galt vor allem dann, und das war oft so, wenn wieder etwas nicht funktionierte oder es sonstige Probleme, egal welcher Art, gab. Den Zusammenhalt, den wir untereinander hatten, findet man selten und so hoffe ich, dass wir den Kontakt zueinander niemals verlieren werden! Es war eine wunderschöne Zeit, besonders natürlich, wenn wir privat etwas zusammen unternommen haben – seien es Grillparties, Geburtstagsfeiern oder das alljährliche Gaibodnfest!
Danke an Kati, meine einzige Praktikantin! Du hast es mit mir ausgehalten und bist sogar nach deinem Master zu uns an den Lehrstuhl zur Doktorarbeit gekommen – und obwohl wir nicht in derselben Arbeitsgruppe sind, hast du dennoch die Bürde auf dich genommen und mit mir zusammen ein Methodenpaper geschrieben!
Danke auch an Michael (MJ), der mich zum Bouldern bekehrt hat, dem ich seither mit großer Begeisterung nachgehe.
Danke an Cathili, wir haben viel Zeit im Labor 1 miteinander verbracht. Du bist so eine durchgehend positive und liebe Person und für jeden Schmarrn zu haben!
Besonders freut es mich, dass sich neben Catha auch weitere neue Doktoranden – Sebastian und Nicholas – an unseren Lehrstuhl verirrt haben – führt unsere alten Traditionen und Gepflogenheiten würdig weiter!

Besonders bedanken möchte ich mich bei unserem TA Tobi (Carl-Carsten). Als der Neue im Labor 1 hast du dich bei uns gut eingelebt und bist uns allen sehr wichtig geworden! Dir gebührt allein schon dafür Ehre, dass du täglich unsere vogelwuide Musik geduldet hast (was man nicht von jedem behaupten kann :P)

Danke auch an Gisela, nicht nur für die vielen hilfreichen Tipps und Hilfen rund ums Labor, sondern auch rund um den Garten – und natürlich für die vielen grünen Mitbringsel!

Bei meinen Eltern möchte ich mich auch ganz herzlich bedanken – sowohl für die finanzielle als auch die moralische Unterstützung! Nicht nur während meiner Doktorarbeit, sondern auch während meines ganzen bisherigen Lebens! Ihr habt mir immer alle Freiheiten gelassen das zu machen, was ich wollte, und mir so alle Wege eröffnet.

Zu guter Letzt gilt mein größter Dank meiner Freundin Paulina. Du hast mich immer aufgebaut, wenn ich es am meisten brauchte – und das kam durchaus das ein oder andere Mal vor. Du hast stets zu mir gehalten und bist jederzeit hinter mir gestanden! Tut mir leid, wenn du mich wegen langen Labor- oder Schreibtagen nicht viel gesehen hast, aber gerade dann hast du mir gezeigt was ich an Dir habe!